The Physiological, Pharmacological and Toxicological Roles of Nrf2 in the Kidney

Thesis submitted in accordance with the requirements of

the University of Liverpool for the degree of

Doctor of Philosophy

By

Luke Shelton

March 2015

Declaration

This thesis is the result of my own work. The material contained within this thesis has not been presented, nor is currently being presented, either wholly or in part for any other degree or qualification.

Luke Shelton

This research was conducted in the Department of Molecular and Clinical Pharmacology, The University of Liverpool, UK.

Contents

Acknowledgements

This thesis would quite simply not be possible without the expert guidance and knowledge of my main supervisor Ian Copple. I would also like to thank Kevin Park for the supervision and opportunity to do this PhD; Neil Kitteringham, Roz Jenkins, Adam Lister, Emanuele Ricci, Cliff Rowe and Jo Walsh for their assistance with the work contained in Chapter 2 and Dave McEwan and Niraj Shah for assistance with the work in Chapter 3.

My PhD experience has been made all the more enjoyable by the excellent people (past and present) of Office 2.64. The company of James, Jack, Oisin, Bhav, Mike, Agnes, Jo and Jon has been invaluable and hilarious, and I will miss them when I've gone. Additionally, Anthony, Phil, George, Gibson, Sully, Liam, Ryan, Jamie, Ross, Liz, Monday, Holly, Ali, Hannah, Catherine and Aine from around the Department and University have contributed to how much I have appreciated my time here.

Finally, I'm hugely grateful for the encouragement from my Mum and Dad, whose lifts, money and general reassurance have been treasured.

Publications

Shelton LM, Lister A, Walsh J, Jenkins RE, Wong MHL, Rowe C, Ricci E, Ressel L, Fang Y, Demougin P, Vukojevic V, Goldring CE, Kitteringham NR, Park BK, Odermatt A and Copple IM. Integrated Transcriptomic and Proteomic Analyses Reveal the Role of Nrf2 as a Key Regulator of Homeostatic Processes in the Kidney, *Kidney International* (2015) *in revision*

Copple IM, **Shelton LM**, Walsh J, Kratschmar DV, Lister A, Odermatt A, Goldring CE, Dinkova-Kostova AT, Honda T and Park BK. Chemical Tuning Enhances Both Potency Toward Nrf2 and *in vitro* Therapeutic Index of Triterpenoids, *Toxicological Sciences* (2014)

Shelton LM, Park BK and Copple IM, Role of Nrf2 in Protection Against Acute Kidney Injury. *Kidney International* (2013)

Selected Communications

Shelton LM, Walsh J, Jenkins RE, Kitteringham NR, Park BK and Copple IM, Proteomic analysis reveals vital role of the transcription factor Nrf2 in the regulation of cell defence processes in the mouse kidney, *pA_2 Online: E-Journal of the British Pharmacological Society* (2013)

Abbreviations

ABCC	Multidrug resistance protein (ABC transporter C subfamily)
Acat1	Acetyl-CoA acetyltransferase, mitochondrial
ACN	Acetonitrile
Acot12	Acyl-coenzyme A thioesterase 12
Acox1	Peroxisomal acyl-coenzyme A oxidase 1
Acsm2	Acyl-CoA synthetase medium-chain family member 2
Acy3	Aspartoacylase-3
ADH	Alcohol dehydrogenase
ADR	Adverse drug reaction
Agpat3	1-acyl-glycerol-3-phosphate acyltransferase
AKI	Acute kidney injury
Akr1a1	aldo-keto reductase family 1, member A1 (aldehyde reductase)
ALDH	Aldehyde dehydrogenase
ARE	Antioxidant response element
ATP	Adenosine triphosphate
AVP	Anti-diuretic hormone
BAX	Bcl-2-associated X protein
BCA	Bicinchoninic acid
BNP	B-type natriuretic peptide
BTB	Bric-à-Brac
bZip	Basic leucine zipper
C57/BL6	C57/Black 6 inbred laboratory mice
Cat	Catalase
Cbr1	Carbonyl reductase 1
CD	Concentration of a compound provoking a two-fold increase in ARE8L activity
CDDO	2-cyano-3,12-dioxooleana-1,9(11)-dien-28-oic acid
CDDO-Im	2-cyano-3,12-dioxooleana-1,9-dien-28-imidazolide
CDDO-Me	Methyl 2-cyano-3,12-dioxooleana-1,9(11)dien-28-oate, Bardoxolone methyl
CDF	Difluorinated curcumin
cDNA	Copy DNA
CEX	Cation exchange
CKD	Chronic kidney disease
Coasy	Bifunctional coenzyme A synthase
Cryz	Quinone oxidoreductase
C_T	Cycle threshold
Cul3-Rbx1	Cullin 3-Ring-box-1
CYP	Cytochrome P450
DGR	Double glycine repeat
DLG	Aspartate, leucine, glycine
DICER	Endoribonuclease Dicer
DMF	Dimethyl fumarate
DMSO	Dimethyl sulphoxide
DN	Diabetic nephropathy

dNTPs	Deoxynucleotide triphosphates
Dpys	Dihydropyrimidinase
dT	A short sequence of deoxy-thymine nucleotides
ECGC	Epigallocatechin-3-gallate
eGFR	Estimated glomerular filtration rate
Eif	Eukaryotic initiation factor
Entpd5	Ectonucleoside-triphosphate diphosphohydrolase
Ephx	Epoxide hydrolase
Et_AR	Endothelin receptor A
ETGE	Glutamate, threonine, glycine, glutamate
EtOH	Ethanol
FA	Formic acid
Faah	Fatty-acid amide hydrolase 1
FACS	Fluorescence-activated cell sorting
FAD	Flavin adenine dinucleotide
FDA	Food and drug administration
FDR	False detection rate
FENTA	Ferric nitrilotriacetate
FH	Fumarate hydratase
FSGS	Focal segmental glomerulosclerosis
G6pd	Glucose-6-phosphate dehydrogenase
Gclc	γ-Glutamyl-cysteine ligase, catalytic subunit
Glyctk	Glycerate kinase
Gpx	Glutathione peroxidase
GSH	Reduced glutathione
Gst	Glutathione S-transferases
H4IIE-ARE8L	Rat hepatoma cell line expressing a luciferase reporter regulated by an ARE
HBSS	Hank's buffered saline solution
HEK	Human embryonic kidney cell line
Hepa1c1c7	Mouse hepatoma cell line
HEPES	4-(2-hydroxyethyl)-1-piperazineethanesulphonic acid
HepG2	Human hepatic cancer cell line
Ho-1	Haem oxygenase-1
i.p.	Intraperitoneal
IPA	Ingenuity pathway analysis
IR	Ischaemic reperfusion
iTRAQ	Isobaric tag for relative and absolute quantification
IVR	Intervening region
JAK/STAT	Janus kinase and signal transducer and activator of transcription
kDa	Kilo-Daltons
Keap1	Kelch-like ECH-associated protein 1

Lap3	Leucine aminopeptidase 3
LC50	Concentration of a compound provoking a two-fold decrease in ATP content
mA	MiliAmps
Maf	Proto-oncogene maf
Me1	NADP-dependent malic enzyme
miR	MicroRNA, miRNA
MMTS	Methyl methanethiosulphonate
MOPS	3-(N-morpholino)propanesulphonic acid
MRP	Multidrug resistance proteins
mRNA	Messenger RNA
MS	Mass spectrometry
MS/MS	Tandem mass spectrometry
NADPH	Nicotinamide adenine dinucleotide phosphate
Nampt	Nicotinamide phosphoribosyltransferase
NCCT	Na^+/Cl^- symporter
Neh	Nrf2-ECH homology
NF-E2	Nuclear factor erythroid 2
NF-κB	Nuclear factor kappa-light-chain-enhancer of activated B cells
NHE	Na^+/H^+ antiporter
Nqo1	NADPH: quinone oxidoreductase 1
Nrf2	Nuclear factor (erythroid-derived 2)-like 2, NFE2L2
NSAIDs	Non-steroidal anti-inflammatory drugs
OAT	Organic anion transporter
OATP	Organic anion transporting polypeptide transporter
OCT	Organic cation transporter
OTA	Ochratoxin A
p53	Tumour protein p53
PBS	Phosphate-buffered saline
PCR	Polymerase chain reaction
Pgd	Phosphogluconate dehydrogenase
PI	Propidium iodide
Pipox	Peroxisomal sarcosine oxidase
Pklr	Pyruvate kinase isozymes R/L
Poly(A) tail	Polyadenylated mRNA tail
Por	NADPH--cytochrome P450 reductase
PPARγ	Peroxisome proliferator-activated receptor gamma
Ppia	Peptidylprolyl isomerase A
Prdx	Peroxiredoxin
qRT-PCR	Quantitative real-time polymerase chain reaction
RISC	RNA-induced silencing complex
ROS	Reactive oxygen species
RPS2	Ribosomal protein 2
RT	Reverse transcription

SDS	Sodium dodecylsulphate
SGLT1/2	Na^+ dependent glucose transporter
SKH-1	An immunocompetent hairless laboratory mouse strain
SLC	Solute carrier family
snRNA	Small nuclear RNA
SQSTM1/p62	Sequestosome 1/p62
Srxn	Sulphi redoxin
STS	Staurosporine
SUL	Sulphoraphane
TBS-T	TBS-Tween solution
TGF-β	Transforming growth factor-β
Tkt	Transketolase
TP	Triterpenoid
Trx	Thioredoxin
Txnrd	Thioredoxin reductase
Ugt	UDP-glucuronyltransferases
UTR	Untranslated region
Ugdh	UDP-glucose-6-dehydrogenase

Abstract

Nrf2 is a transcription factor that, under conditions of chemical stress, is able to evade its cytosolic repression and translocate to the nucleus to initiate the transcription of a battery of cytoprotective genes, such as those involved in the detoxication of xenobiotics. Nrf2 has previously been shown to afford protection against chronic and acute renal injury, yet, relatively little is known about the mechanism by which Nrf2 affords this protection, and the extent of its transcriptional roles in the kidney. This thesis seeks to further our understanding of the physiological, pharmacological and toxicological roles of Nrf2 in the kidney.

Using an iTRAQ-based proteomic approach to quantify protein expression levels in the kidneys of $Nrf2^{+/+}$ and $Nrf2^{-/-}$ mice, acutely treated with vehicle or the potent Nrf2 inducer CDDO-Me (3 mg/kg), we demonstrated that 189 proteins were differentially expressed in the $Nrf2^{-/-}$ mouse kidney, compared to $Nrf2^{+/+}$, and 42 proteins were differentially expressed in the CDDO-Me treated $Nrf2^{+/+}$ mouse kidney, compared to vehicle. The key finding was that the kidneys of $Nrf2^{-/-}$ mice are deficient in proteins that mediate cellular redox balance, the metabolism of a range of xenobiotics, and the regulation of core metabolic processes, including energy metabolism and the synthesis and recycling of amino acids. Functional demonstration of a reduction in energy metabolism was demonstrated by assessing total NADPH and GSH, of which $Nrf2^{-/-}$ mouse kidneys had 35% and 30% less than their $Nrf2^{+/+}$ counterparts, respectively. A single acute dose of CDDO-Me failed to augment the expression of proteins, other than Nqo1, that were shown to be regulated by Nrf2 at the basal level in the mouse kidney, however qPCR analysis of these kidneys revealed that CDDO-Me has an effect at the transcriptional level which has not fully translated within the timeframe of this study. In summary, we have provided evidence that Nrf2 regulates the expression of an array of proteins that contribute to cell defence and the maintenance of homeostasis in the kidney, supporting current interest in Nrf2 as a novel therapeutic target in a number of renal diseases.

MicroRNAs are a recently discovered RNA-regulatory element that show promise in their use as biomarkers of physiological and pathological events. In order to provide insight into the microRNAs under Nrf2 control in the kidney, we performed an unbiased microRNA array analysis on kidney homogenates from $Nrf2^{+/+}$ and $Nrf2^{-/-}$ mice, treated with vehicle or CDDO-Me, and then validated several promising microRNA candidates using targeted qPCR analysis. Of particular note are miR-466h-3p, the expression of which was significantly increased in the CDDO-Me treated $Nrf2^{+/+}$ mouse kidney and decreased in the $Nrf2^{-/-}$ mouse kidney, compared to their respective controls, and miR-28c and 144, which were both significantly decreased in the CDDO-Me treated $Nrf2^{+/+}$ mouse kidney, and increased in the $Nrf2^{-}$

$^{/-}$ mouse kidney. This novel analysis represents the first step in characterising the renal Nrf2 microRNA-ome, which could reveal novel mechanisms of Nrf2 function and markers of its activity that could translate to the clinic.

Recent interest in the use of CDDO-Me as a therapeutic intervention for late-stage chronic kidney disease has culminated in a phase III clinical trial (BEACON), which was subsequently terminated due to unforeseen adverse cardiac events, of which the cause has yet to be identified. In order to determine whether the drive to produce more potent Nrf2 inducers has inadvertently led to the generation of inherently more toxic compounds, the relationship between potency towards Nrf2 and toxicity was evaluated for CDDO-Me and related triterpenoids, and other classes of Nrf2 inducer. Using a rat H4IIE-ARE8L luciferase reporter cell line to determine *in vitro* therapeutic indices, it was discovered that within the compounds tested an increase in potency toward Nrf2 of four magnitudes results was associated with an increase in toxicity of only two magnitudes, resulting in a relative increase in *in vitro* safety. This data indicates that it is possible to generate potent Nrf2-inducers that are not inherently toxic, and suggests that therapeutic targeting of Nrf2 continues to hold promise as a novel treatment for a range of diseases.

In summary, by using a proteomic approach we have identified an array of renal Nrf2-regulated proteins that contribute to various cytoprotective and metabolic processes in the kidney, supporting current interest in the therapeutic targeting of Nrf2 as treatment for renal disease. Additionally, the microRNAs under Nrf2 regulation in the kidney have also been identified, and represent the first step in fully characterising the Nrf2 microRNA-ome. Finally, it was shown that the drive to produce more potent Nrf2 inducers has not led to the generation of inherently more toxic compounds; indeed an increase in potency is associated with a relative increase in *in vitro* safety, suggesting that the targeting of Nrf2 is still a promising therapeutic route. Overall, the work presented in this thesis has furthered our understanding of the physiological, pharmacological and toxicological roles of Nrf2 in the kidney.

Chapter 1

General Introduction

Contents

1.1 Introduction

Acute kidney injury (drug-induced toxicity or ischaemic-reperfusion injury) is responsible for approximately 20 % of emergency hospital admissions (Wang *et al.*, 2012), and the incidence of chronic kidney disease (CKD) in Europe is about 135 per 1,000,000 population (Hamer *et al.*, 2006), but accounts for over 2 % of the European healthcare budget (Hamer *et al.*, 2006). The kidney is particularly susceptible to drug-induced oxidative stress (an imbalance of the redox state of the cell provoked by either the induction of the formation of reactive oxygen species (ROS) or the prevention of their removal (Park, 1986)) as a result of its anatomical structure and physiological roles (Perazella, 2009). The transcription factor Nrf2 has previously been shown to afford protection against acute kidney injury (for a review, see (Shelton *et al.*, 2013)) and chronic kidney disease (for a review, see (Ruiz *et al.*, 2013)) in a number of experimental models. Compared to other organs, relatively little is known about the mechanisms by which Nrf2 provides this protection, and the extent of its transcriptional roles in the kidney. Such knowledge would provide insights into disease mechanisms and inform the use of Nrf2-modulating drugs as novel treatments for kidney pathologies. Based on data from animal studies and serendipitous observations from clinical trials (Wu *et al.*, 2011b; Hong *et al.*, 2012), the potent triterpenoid Nrf2 inducer CDDO-Me has recently been investigated as a novel treatment for CKD. However, the toxicological consequences of targeting Nrf2 with chemically reactive drugs have not been fully examined. Such knowledge would inform the design and use of Nrf2 inducers as

novel drugs. To address these research questions, this thesis seeks to determine the physiological, pharmacological and toxicological roles of Nrf2 in the kidney.

1.2 Kidney physiology

The kidney maintains the homeostasis of the body, reabsorbing water, glucose, amino acids and various electrolytes to maintain correct function and pH of the blood (Fig. 1), in addition to regulating waste management via the excretion of water and unwanted solutes.

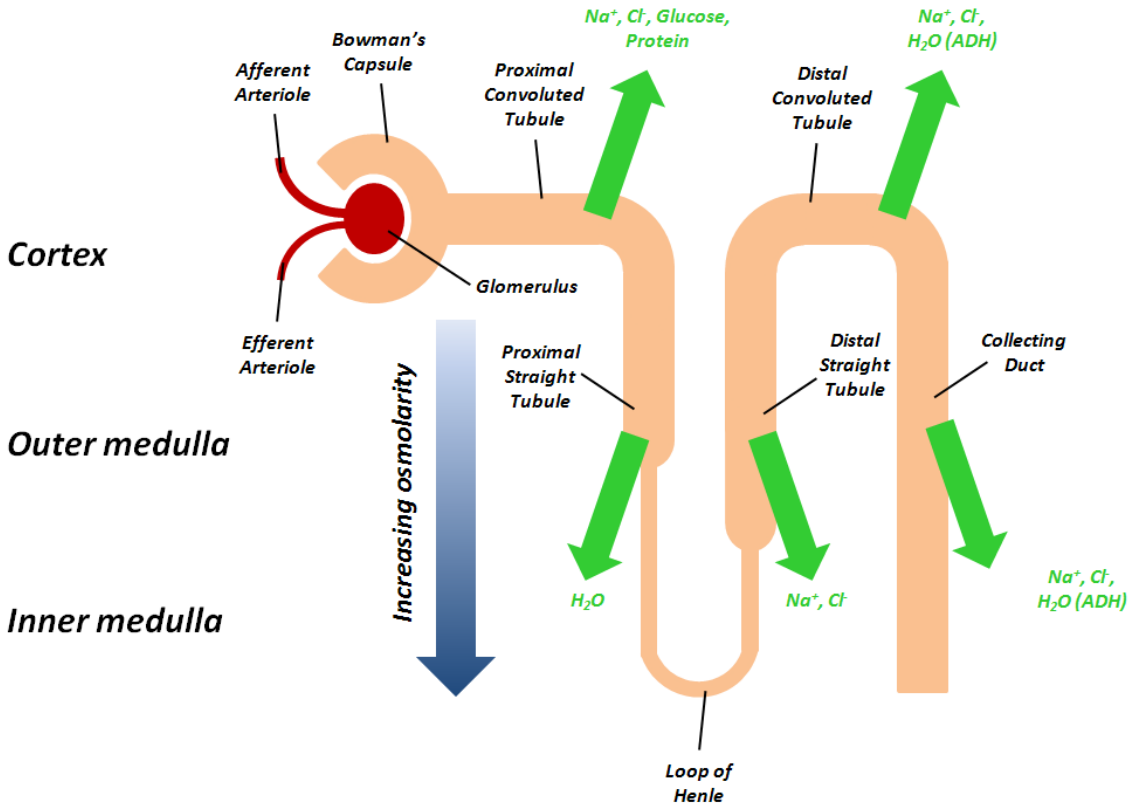

Fig.1: Schematic of a nephron, with major structural areas labelled in black and main reabsorption solutes labelled in green. The filtrate enters the Bowman's capsule, travelling along the proximal convoluted tubule, where the majority of Na^+, Cl^-, glucose and proteins are reabsorped. Due to increasing osmolarity in the medulla, H_2O passively diffuses out of the filtrate along the descending limb of the loop of Henle. The ascending limb is impermeable to H_2O; Na^+ and Cl^- are actively transported out of the filtrate to maintain medullary osmolarity. Na^+ and Cl^- are reabsorped in the distal convoluted tubule, as is H_2O depending on the presence of anti-diuretic hormone (AVP). A similar process occurs along the collecting duct, before the filtrate is passed into the urine.

1.2.1 The glomerulus, Bowman's capsule and proximal tubule

The kidney receives approximately 25% of cardiac output (Lote *et al.*, 1996), which is filtered through the nephron, the functional unit of the kidney (Fig. 1) via afferent and efferent arterioles. The difference in arteriolar diameter between afferent and efferent arterioles causes a heightened pressure in the glomerulus (a modified capillary bed), which, combined with a podocytic apical surface and glomerular hydrostatic pressure allow for the filtration of the solute into the Bowman's capsule, with large proteins being retained. The ultrafiltrate, consisting of water, smaller proteins and various electrolytes (Na^+, K^+, HCO_3^- , etc.) passes into the Bowman's capsule through its podocyte membrane, and into the proximal tubule segment (Fig. 1 and 2). Lined with proximal tubular epithelial cells, the convoluted and straight proximal tubule are responsible for the reabsorption of the majority of the ultrafiltrate (Bokenkamp *et al.*, 2011). Proximal tubular epithelial cells are brush border cells, with microvilli lining the apical surface of the lumen concentrated with various transporters (Fig 2). Proximal tubule cells have a high requirement for ATP due to their dependence on oxidative phosphorylation for energy, and therefore have a relatively high volume of mitochondria (up to 44% by cell volume (Bakris *et al.*, 2009)). The expression of transporters differs between the convoluted and straight proximal tubules (Dominguez *et al.*, 1992; Rodriguez-Mulero *et al.*, 2005), with the majority of glucose and water being reabsorped purely by the proximal convoluted tubule section (Hummel *et al.*, 2011).

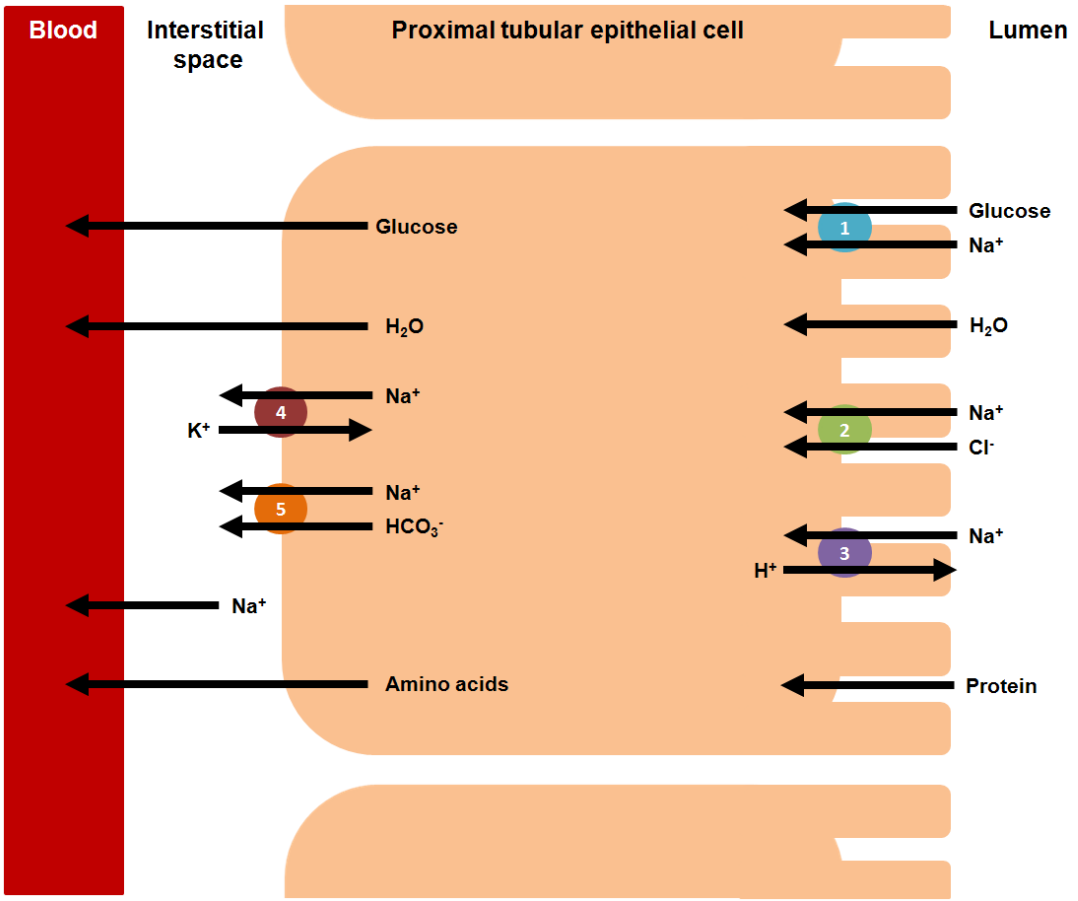

Fig.2: Schematic of proximal convoluted/distal tubule structure. Transport of major components of ultrafiltrate is highlighted. Transporters (with abbreviations and solute carrier (SLC) family) are: (1) Na^+ dependent glucose transporter (SGLT1/2, SLC5), (2) Na^+/Cl^- symporter (NCCT, SLC12), (3) Na^+/H^+ antiporter (NHE, SLC9) (4) Na^+/K^+ ATPase (ATP1), (5) Na^+/HCO_3^- cotransporter (SLC4).

As the filtrate passes along the proximal tubule, the basolateral Na^+/K^+ ATPase drives Na^+ out of the proximal tubule cell, into the interstitial space and the blood, enabling absorption of further Na^+ from the filtrate at the apical pole due to a difference in Na^+ concentration, and a stoichiometrically regulated negatively charged intracellular environment (Nakamura *et al.*, 2014). Transport of Na^+ into the proximal tubule cell from the lumen drives reabsorption of filtrate components

by secondary active transport (Fig. 2, (Bakris *et al.*, 2009)). Water reabsorption in the proximal tubule segment occurs through net diffusion due to differences in osmotic gradient, through aquaporin 1 channels (transmembrane proteins allowing for the osmosis of water (Nielsen *et al.*, 2002)) or through inter-cellular junctions (Greger, 2000; Bakris *et al.*, 2009). Approximately 60-70% of Na^+ and water is reabsorped in the proximal tubule (Greger, 2000).

1.2.2 The loop of Henle

The loop of Henle acts as a counter-current multiplying system to handle urea, achieving a concentration gradient (increasing osmolarity and solute concentration from cortex to inner medulla) in the kidney. The descending limb of the loop of Henle is highly permeable to water via aquaporin 1 (membrane water channel protein), and less so to filtrate ions, so water diffuses out via aquaporins (Fig. 1, (Nielsen *et al.*, 1993)). Urea concentration increases in the medulla along the descending limb, allowing for passive diffusion of water via aquaporins for its duration. The filtrate hence becomes more concentrated. The ascending limb lacks aquaporins, and is highly permeable to Na^+ and Cl^- ions (Nielsen *et al.*, 1993). Na^+, K^+ and Cl^- ions are actively transported into the medullary space along the ascending limb, meaning that the space maintains concentration gradient and continues to allow the diffusion of water into the medulla along the descending limb. Up to 30% of filtered Na^+ is reabsorbed along the ascending limb of the loop of Henle, and at this point most of the total Na^+ in the filtrate has been reabsorbed (Brater, 2000). The filtrate hence becomes more dilute.

1.3.3 The distal tubule and collecting duct

The function of the distal tubule is primarily regulation of ion balance and pH of the filtrate, urine dilution and blood pressure regulation (Eladari *et al.*, 2012). Na^+ ions are reabsorped in the distal tubule through coupled secretion of H^+ and K^+, thereby acidifying the filtrate (Fig. 1) (Dantzler, 2003). Furthermore, the distal tubule is responsible for the secretion of ammonia, creatinine and the products of drug metabolism into the filtrate. Distal tubular epithelial cells lack a brush border and are relatively impermeable to H_2O, however in the presence of AVP secreted from the pituitary gland, aquaporin 2 channels are inserted into the distal tubule, allowing H_2O reabsorption and concentration of the filtrate (Nielsen *et al.*, 2002).

A region of columnar epithelial cells, known as the macula densa, are located close to the afferent and efferent arteriole and glomerulus, and they function to detect and modify Na^+ levels in the filtrate (Ren *et al.*, 2007). In response to elevated Na^+ in the filtrate (potentially due to inefficient reabsorption in the Bowman's capsule and proximal tubule) cells of the macula densa uptake Na^+ via apical $Na^+/K^+/Cl^-$ transporters, and due to consequent change in osmolarity, H_2O diffuses into the cells of the macula densa (Komlosi *et al.*, 2004). The turgidity of the cells induces basolateral adenosine release, which induces afferent arteriolar constriction and efferent arteriolar dilation (Castrop, 2007; Ren *et al.*, 2007), reducing glomerular flow rate and increasing the proportion of Na^+ reabsorped at the Bowman's capsule and proximal tubule.

Finally, the collecting duct is responsible for fine modulation of filtrate osmolarity, chiefly by reabsorbing H_2O and Na^+ (Fig. 1), and additionally bicarbonate and calcium. Similarly to the distal tubule, modulation of H_2O reabsorption is controlled by the release of AVP and subsequent aquaporin insertion and H_2O diffusion into the normally H_2O-impermeable collecting duct in response to dilute urine or reduced blood volume. The filtrate (urine) hence becomes more concentrated entering the ureter.

1.3 Antioxidant mechanisms of the cell

1.3.1 Oxidative stress

Drug induced oxidative stress arises when a drug induces the formation of ROS, or prevents their removal (Park, 1986; Schafer *et al.*, 2001), leading to an imbalance in the redox state of the cell. Indeed, may drugs provoke off-target effects via the generation of ROS (Antoine *et al.*, 2009; Copple *et al.*, 2010a). The kidney is particularly susceptible to oxidative stress due to a relatively hypoxic environment experienced by cells in the loop of Henle, and high metabolic activity demonstrated by cells involved in absorption and secretion (Perazella, 2009).

The majority of systemic ROS are generated by the electron transport chain in the mitochondria (Pieczenik *et al.*, 2007), however under certain conditions, ROS such as superoxide (O_2^-), hydrogen peroxide (H_2O_2), the hydroxyl radical ($^{\bullet}HO$) and others such as peroxynitrite (ONOO-) and organic hydroperoxides (ROOH) are produced, and cause damage to DNA (various lesions, including abasic sites, oxidised bases and strand breaks (Shibutani *et al.*, 1991)), and to proteins (primarily through the oxidation of cysteine residues (Bandyopadhyay *et al.*, 1994)).

1.3.2 The Keap1/Nrf2 antioxidant response pathway

Whilst the repair of oxidative stress-induced damage (for example through DNA base-excision repair or protein degradation) is important for the maintenance of cellular homeostasis, the prevention of such damage also critical. A key mechanism of prevention of oxidative stress-induced damage is the Keap1/Nrf2 antioxidant response pathway, which initiates the transcription of various antioxidant enzymes and proteins in response to oxidative stress.

The key components of the Keap1-Nrf2 pathway are the antioxidant response element (ARE), Nuclear factor (erythroid-derived 2)-like 2 (NFE2L2, Nrf2) and Kelch-like ECH-associated protein 1 (Keap1). The ARE is a cis-acting enhancer motif located in the promoter regions of Nrf2 target genes (Nioi *et al.*, 2003). The ARE was initially identified as an oxidant-responsive promoter element of the detoxicating antioxidant genes glutathione S-transferase A2 (Gsta2) (Rushmore *et al.*, 1990) and NADPH: quinone oxidoreductase 1 (Nqo1) (Favreau *et al.*, 1991). Originally thought to be a conserved 20 bp sequence, based on alignment of the rat Gsta2, Gstp1 and human and rat Nqo1 genes (Wasserman *et al.*, 1997), the ARE is now known to comprise four distinct classes of enhancers with differing consensus sequences and motifs (Hayes *et al.*, 2010), allowing for more dynamic induction and regulation by stressors and transcription factors. Table 1 gives some examples of genes containing the ARE that are known to be regulated by Nrf2.

Category	Gene	Function	Reference
Glutathione metabolism	*γ-Glutamyl-cysteine ligase, catalytic subunit* (*Gclc*)	Rate-limiting enzyme in the synthesis of glutathione, catalyzes the conjugation of L-glutamine and L-cysteine to yield γ-L-glutamyl-L-cysteine	(Chan *et al.*, 2000)
	Glutathione peroxidase (*Gpx*)	Catalyzes the reduction (by glutathione) of H_2O_2 and other hydroperoxides to water	(Banning *et al.*, 2005)
Antioxidants	*Sulphiredoxin* (*Srxn*)	Catalyzes the reduction of oxidized cysteine in peroxiredoxin, maintaining the latter's antioxidant function	(Singh *et al.*, 2009)
	Thioredoxin (*Trx*)	Facilitates the reduction of other proteins by cysteine thiol–disulphide exchange	(Kim *et al.*, 2001)
Iron metabolism	*Ferritin* (*Ft*)	Facilitates storage of iron in a soluble, nontoxic form	(Pietsch *et al.*, 2003)
	Heme oxygenase-1 (*Ho-1*)	Catalyzes the degradation of soluble, toxic heme	(Alam *et al.*, 2003)
Xenobiotic metabolism	*Glutathione S-transferase* (*Gst*)	Catalyzes the conjugation of reduced glutathione to exogenous and endogenous hydrophobic electrophiles	(Hayes *et al.*, 2000)
	NAD(P)H quinone oxidoreductase 1 (*Nqo1*)	Catalyzes the two-electron reduction of quinones to hydroquinones, without the production of radical species	(Dinkova-Kostova *et al.*, 2010a)
	UDP glucuronyl transferase (*Ugt*)	Catalyzes conjugation of lipophilic molecules with glucuronic acid, forming water-soluble and excretable metabolites	(Shelby *et al.*, 2006)
Xenobiotic transport	*Multidrug resistance–associated protein* (*Mrp*)	Organic anion transporter that mediates the cellular export of drugs and other small molecules	(Maher *et al.*, 2005)

Table 1: Examples of Nrf2-regulated genes containing an ARE, from (Shelton *et al.*, 2013).

Nrf2 was first isolated in 1994 in a screen for nuclear factor erythroid 2 (NF-E2) regulating proteins (Moi *et al.*, 1994). Nrf2 is a cap 'n' collar basic leucine zipper (bZip) transcription factor consisting of 605 amino acids (Kim *et al.*, 2012) arranged into six functional Nrf2-ECH homology (Neh) domains (Fig. 3). The Neh1 domain facilitates DNA binding to the ARE (Plafker *et al.*, 2010) and contains the bZip motif responsible for heterodimerisation with small Maf proteins in the nucleus (Plafker *et al.*, 2010). The multifunctional, conserved Neh2 domain contains critical motifs that mediate interaction with Keap1, the cytosolic repressor of Nrf2 (Itoh *et al.*,

1999). The Neh3 (Nioi *et al.*, 2005), 4 (Kim *et al.*, 2012) and 5 (Apopa *et al.*, 2008) domains contain transactivation motifs and are able to interact with co-activator proteins to modulate the cytoprotective signals transduced by Nrf2 (Kim *et al.*, 2012). The Neh6 domain regulates Nrf2 turnover in a Keap1-independent manner (McMahon *et al.*, 2004). The other members of the Nrf transcription factor family, Nrf1 (Chan *et al.*, 1993) and Nrf3 (Kobayashi *et al.*, 1999), share some structural homology with Nrf2, but serve different cellular functions, including the regulation of β-globin gene expression, cellular differentiation and inflammation (Biswas *et al.*, 2010; Chevillard *et al.*, 2011). Moreover, disruption of the Nrf1 gene *in vivo* is embryonically lethal (Biswas *et al.*, 2010), whereas transgenic $Nrf2^{-/-}$ mice grow to adulthood with no acute disease phenotype (Chan *et al.*, 1996). However, Nrf2 deficient mice have a propensity to be more susceptible to toxic insult than their wild type counterparts (Taguchi *et al.*, 2011). Indicative of a role for Nrf2 in modulating sensitivity to inflammation, $Nrf2^{-/-}$ female mice develop autoimmune nephritis late into adulthood (Yoh *et al.*, 2001).

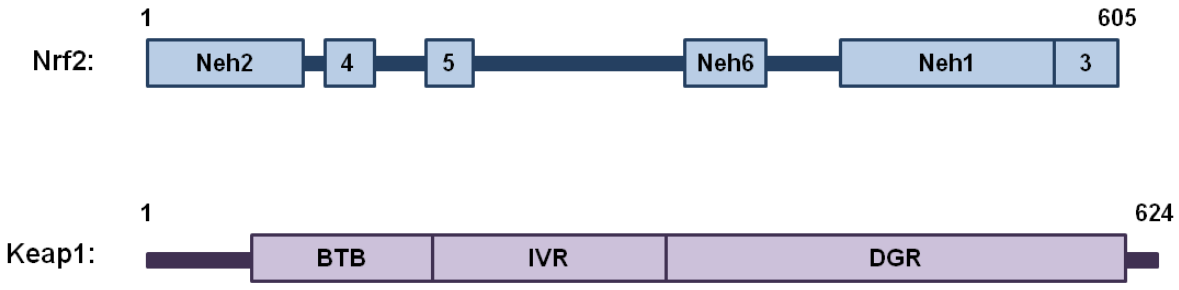

Fig.3: Nrf2 and Keap1 protein domain structure (Copple *et al.*, 2010a).

Keap1, discovered in 1999 (Itoh *et al.*, 1999), is a zinc finger protein comprising of 624 amino acids forming three major functional domains (Copple *et al.*, 2010a; Taguchi *et al.*, 2011) (Fig. 3). The Bric-à-Brac (BTB) domain facilitates homodimerisation and interaction with the Cullin 3-Ring-box-1 (Cul3-Rbx1) ubiquitin E3 ligase complex that enables Keap1 to target Nrf2 for ubiquitination and proteasomal degradation (Kaspar *et al.*, 2010) (Zipper *et al.*, 2002; Tian *et al.*, 2012). The docking of the Cul3-Rbx1 E3 ligase complex to Keap1 is in part regulated by Cys-151 in the BTB domain of the latter; mutation of this cysteine reduces Keap1 affinity for Cul3 without altering its affinity for Nrf2 (Eggler *et al.*, 2009). A cysteine-rich intervening region (IVR) separates the BTB domain from the C-terminal double glycine repeat (DGR) domain, which comprises six kelch repeats that are required for Keap1 binding to the actin cytoskeleton and Nrf2 (Adams *et al.*, 2000).

1.3.2.1 Regulation of the Keap1/Nrf2 pathway

Under normal cellular conditions (i.e. in the absence of overt stress), Nrf2 is sequestered in the cytoplasm by its physical interaction with Keap1 (Fig. 4). Specifically, the Neh2 domain of Nrf2 contains critical ^{29}DLG^{31} and ^{79}ETGE^{82} motifs that permit binding of the transcription factor to the DGR domain of Keap1. The ^{79}ETGE^{82} motif has high affinity for Keap1 (Tong *et al.*, 2006) and directs the recruitment of Nrf2 to the Keap1 complex (Tong *et al.*, 2006). The ^{29}DLG^{31} motif has a lower affinity for Keap1, and is thought to orient Nrf2 in the correct position for Cul3-directed ubiquitination of any combination of seven lysines residues located within the Neh2 domain of the transcription factor (Tong *et al.*, 2007).

Ubiquitination of Nrf2 targets it for proteolysis by the 26S proteasome (Kobayashi *et al.*, 2004) and as a result Nrf2 has a relatively short half-life of 10-30 minutes in the absence of stress (Itoh *et al.*, 2003; McMahon *et al.*, 2003).

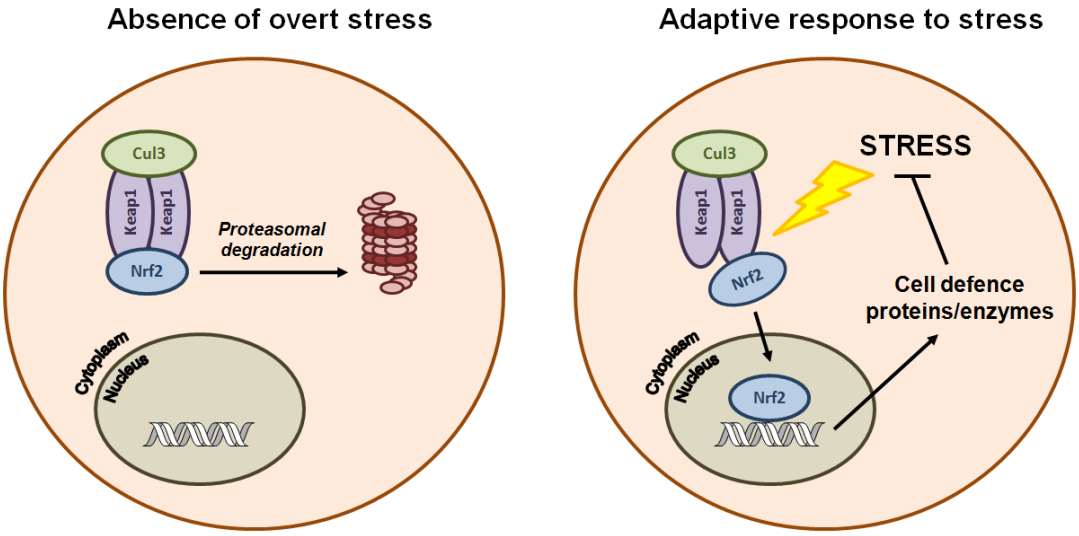

Fig.4: Diagram of Keap1/Nrf2 pathway regulation (from (Shelton *et al.*, 2013)). In the absence of stress, Keap1 constitutively targets Nrf2 for proteasomal degradation. Nrf2 evades Keap1 repression following chemical or oxidative stress, and translocates to the nucleus to induce the transcription of ARE-containing target genes.

In response to an array of cellular insults, Nrf2 evades repression by Keap1, and accumulates within the nucleus via a nuclear localisation signal (Li *et al.*, 2008a). In the nucleus, Nrf2 heterodimerises with small Maf proteins (Blank, 2008), masking the nuclear export signal of Nrf2 (Li *et al.*, 2008b) and facilitating the transactivation of ARE-containing target genes. The molecular trigger for the induction of Nrf2 appears to be underpinned by its phosphorylation (Niture *et al.*, 2009) and/or redox

modification of cysteine residues in Keap1 (Sekhar *et al.*, 2010), of which there are 27 and 25 in the human and mouse proteins, respectively. It is known that mutation of Cys-151, -273 or -288 of mouse Keap1 renders the protein unable to repress Nrf2 or transduce signals for its induction (Zhang *et al.*, 2003; Levonen *et al.*, 2004; Wakabayashi *et al.*, 2004; Zhang *et al.*, 2004; Kobayashi *et al.*, 2006; Yamamoto *et al.*, 2008). These findings indicate that the structural integrity of Keap1 is critical for the efficient regulation of Nrf2 activity, and that the modification of these and other cysteines in Keap1 likely underlies the induction of Nrf2 under conditions of chemical or oxidative stress (Sekhar *et al.*, 2010). In addition, the activity of the Keap1-Nrf2 pathway can be modulated by physical interaction of the complex with SQSTM1/p62, (Copple *et al.*, 2010b; Fan *et al.*, 2010; Jain *et al.*, 2010; Komatsu *et al.*, 2010), which competes with Nrf2 for binding to Keap1, and regulates the degradation of Keap1 (Copple *et al.*, 2010b; Bui *et al.*, 2011), most probably via autophagy (Taguchi *et al.*, 2012).

1.3.2.2 Examples of Nrf2-regulated antioxidant genes and proteins

Genes and proteins regulated by Nrf2 typically function to maintain redox homeostasis. One of the most well-established Nrf2 target genes, Nqo1, is a multifunctional antioxidant enzyme with roles in the two-electron reduction of xenobiotic quinones and of vitamin E quinone and ubiquinone (Ross, 2004) to hydroquinones, preventing the production of ROS intermediates through redox signalling (Dinkova-Kostova *et al.*, 2010a). Nqo1 is robustly regulated by Nrf2 and is often used as a marker of Nrf2 activity (Benson *et al.*, 1980). Catalase functions to

decompose H_2O_2 to H_2O and O_2; deficiency of catalase renders the kidney more susceptible to oxidative stress (Kobayashi *et al.*, 2005) and catalase is known to be regulated by Nrf2 (Zhu *et al.*, 2005). Glutathione (in its reduced form, GSH) is an antioxidant tripeptide containing a thiol group that can detoxify ROS and regulate the nitric oxide cycle (Tirmenstein *et al.*, 2000). GSH also plays an important role in the bioactivation and elimination of various xenobiotics, with conjugation mediated by a family of glutathione S-transferase enzymes (Rushmore *et al.*, 1990; Hayes *et al.*, 2000). The enzymes responsible for the synthesis and conjugation of GSH, namely ɣ-glutamylcysteine ligase, glutathione synthetase, glutathione s-transferases and glutathione reductase are under Nrf2 control (Pietsch *et al.*, 2003; Harvey *et al.*, 2009).

1.3.3 Regulation of Nrf2 by MicroRNAs

1.3.3.1 MicroRNA biology

MicroRNAs (miRNA, miR), which are approximately 21-nucleotides in length (Rana, 2007), are non-coding regulatory elements, responsible for gene silencing and mRNA post-transcriptional regulation. MicroRNAs derive from transcripts that fold back on themselves (Fig. 7) , giving rise to a distinct hairpin structure (Bartel, 2004). These primary miRNA transcripts (pri-miRNA) are processed by DROSHA, a nuclear RNase (Lee *et al.*, 2003), into shorter 70-nucleotide microRNA precursors (pre-miRNA). Following exportation from the nucleus to the cytoplasm by Exportin-5, pre-miRNA are cleaved by DICER (a cystosolic RNase (Filipowicz *et al.*, 2008)) into mature 21 base pair miRNA duplexes. One strand is selected (the other, passenger strand is degraded) for incorporation into the RNA-induced silencing complex (RISC) in a dynamic process that is thought to be due to RISC Argonaute (proteins with RNase activity (Filipowicz *et al.*, 2008)) selection preferences (Okamura *et al.*, 2009; Meijer *et al.*, 2014).

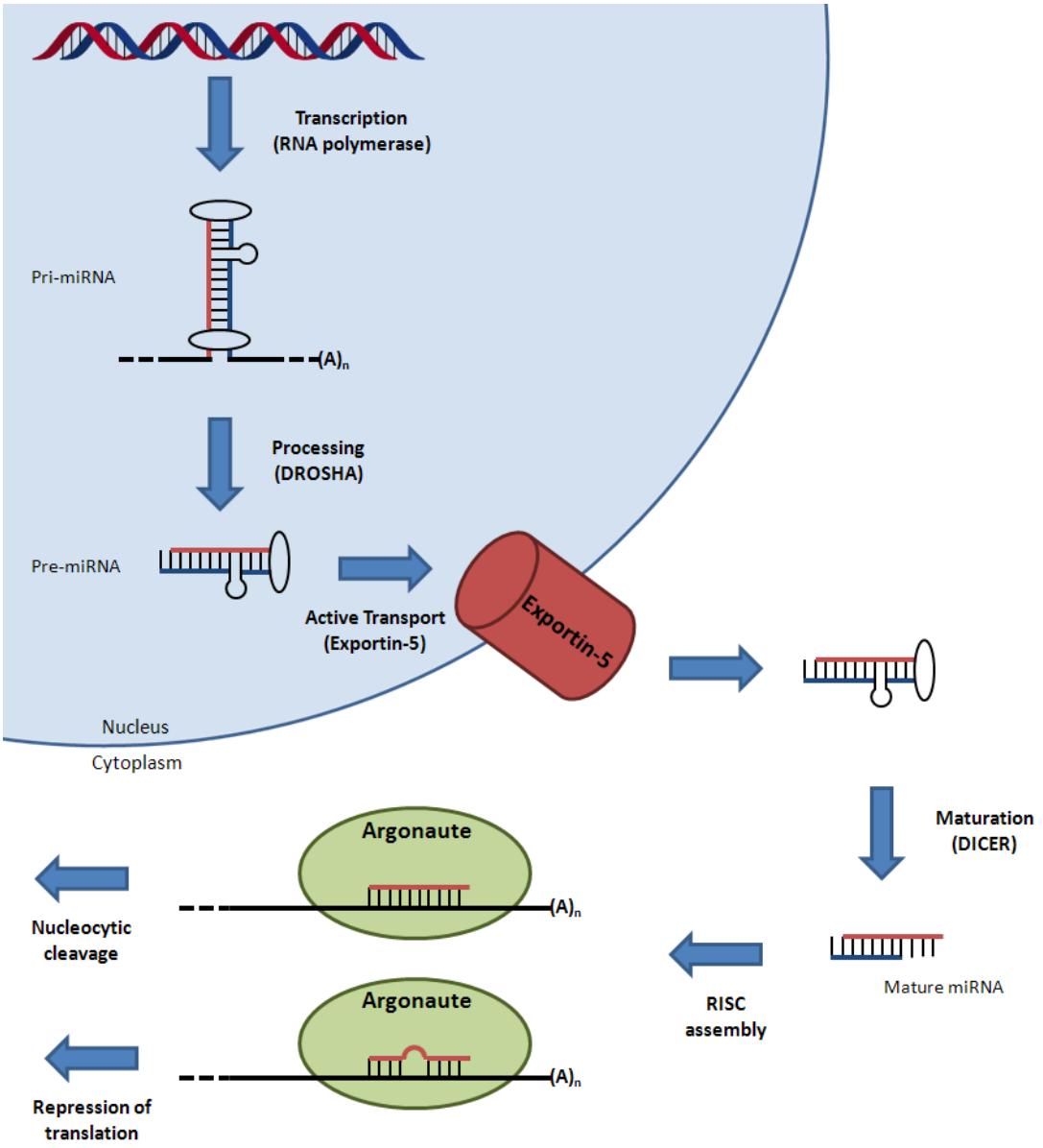

Fig. 7: MicroRNA biogenesis and processing. Adapted from (Filipowicz *et al.*, 2008).

Complimentarity of microRNAs to target mRNA sequences determines the mechanism of translational repression. Animal microRNAs pair with target mRNA imperfectly with partial complimentarity, with rules governing base-pairing derived from bioinformatic analyses including that the first 2 – 7/8 nucleotides of microRNAs (the seed region) have conserved Watson-Crick base pairing with target mRNA, and as such are the primary sequence in determining the target mRNA (Bartel, 2009). Additional rules include that a degree of mismatch must be present in the middle of the microRNA-mRNA duplex (Grimson *et al.*, 2007) and that there should be a reasonable degree of complimentarity of the target mRNA sequence to the 3' sequence of the microRNA (Grimson *et al.*, 2007).

MicroRNA binding sites in mammalian genes tend to be in the 3' untranslated region (UTR, the section of transcript immediately following a translation termination codon) of the target mRNA sequence (Grimson *et al.*, 2007), and multiple sites close to each other act cooperatively (Grimson *et al.*, 2007; Filipowicz *et al.*, 2008). The mechanisms by which microRNA repress translation in animals are varied (Morozova *et al.*, 2012), and include blocking of ribosomal elongation (Nottrott *et al.*, 2006), degradation of nascent peptide (Nottrott *et al.*, 2006), deadenylation of the mRNA poly(A) tail (Wu *et al.*, 2006), microRNA-mediated reorganisation of chromatin structure (Kim *et al.*, 2008) and complete repression of initiation of translation (Filipowicz *et al.*, 2008; Morozova *et al.*, 2012). MicroRNAs display distinct tissue and organ expression patterns (Starkey Lewis *et al.*, 2011), and as such are promising candidates for biomarkers of cellular injury, being

detectable in various biofluids (Starkey Lewis *et al.*, 2011; Starkey Lewis *et al.*, 2012).

1.3.3.2 Nrf2 and microRNAs

At the time of writing, the exact role that Nrf2 plays in the regulation of microRNA expression is unclear, however the action of Exportin-5 is thought to be modulated by cellular redox status (Crampton *et al.*, 2009), indicating that redox changes can alter the biogenesis of microRNAs.

MicroRNAs have been shown to control Nrf2 and Nrf2-regulated gene expression; *in silico* analysis of the Nrf2 gene revealed 85 putative microRNA binding sites (Papp *et al.*, 2012) that could be involved in the downregulation of Nrf2 activity. miR-28 (Yang *et al.*, 2011), 144 (Narasimhan *et al.*, 2012) and 34a (Li *et al.*, 2011b) have all been shown to be involved in the downregulation of Nrf2 in various cell lines. Overexpression of miR-144 was demonstrated to downregulate Nrf2 protein levels in a neuronal cell line (Narasimhan *et al.*, 2012), suggesting a role for microRNA to sensitise cells to oxidative stress. In addition to directly downregulating Nrf2 mRNA, miR-200a targets Keap1 mRNA in breast cancer cells (Eades *et al.*, 2011), indicating that this microRNA is capable of fine-tuning the Nrf2 antioxidant response. There is an implication that Nrf2-regulated genes may be targeted by microRNAs; miR-34a regulates microsomal glutathione S-tranferase 1 expression (Li *et al.*, 2011b), however prior to the work contained in Chapter 3, there was little evidence that modulation of Nrf2 itself modifies microRNA expression.

1.4 Nrf2 in the kidney

Nrf2 expression is primarily localised to the renal cortex (Wu *et al.*, 2011b), which, in the context of the nephron (Fig. 1), is indicative of the necessity for high expression of various antioxidant and xenobiotic defence genes as the filtrate (containing various reactive metabolites) first enters the Bowman's capsule and proximal tubule. Similarly, Keap1 expression is high in the renal cortex compared with glomerular and medullary fractions (Yoshida *et al.*, 2005), likely due to high basal Nrf2 expression. Nrf2-regulated proteins are consequently more localised to the cortex (McBride *et al.*, 2005; Wu *et al.*, 2011b; Reisman *et al.*, 2012).

1.4.1 Role of Nrf2 in protection against acute kidney injury

Acute kidney injury can be defined as an abrupt loss in renal function, via ischaemia or toxic insult. An increasing body of evidence supports a vital physiological role for Nrf2 in the kidney in the regulation of prevention against a number of toxic insults (Copple *et al.*, 2008). The induction of injury following drug treatment remains a significant clinical problem, accounting for the cessation of multiple promising drug targets during development (Choudhury *et al.*, 2006), and as such the requirement for understanding the balance between renal adaptation and susceptibility to toxic insult must be addressed in the context of Nrf2, both in animal and cell-models. Experimentally, Nrf2 induction has been shown to ameliorate acute kidney injury, such as drug-induced toxicity ((Wu *et al.*, 2014a); for a review, see (Shelton *et al.*, 2013)) and ischaemic injury (Liu *et al.*, 2014). However, as yet Nrf2 induction has

not been used to treat acute kidney injury in a clinical setting, likely because more research into Nrf2 induction as a preventative as opposed to a reactive therapy has been performed to date (Zhang, 2013).

1.4.1.1 Renal ischaemic-reperfusion injury

Provoked by the cessation and subsequent re-establishment of blood perfusion, renal ischaemic-reperfusion (IR) injury generates reactive oxygen species via reintroduction of blood to the hypoxic kidney (Leonard *et al.*, 2006), and is responsible for approximately half of all acute kidney injury hospital cases (Star, 1998). Subsequent oxidative stress and inflammation induce tubular atrophy, microvasculature endothelial monolayer disruption and apoptosis (Fig. 6, (Legrand *et al.*, 2008)). Experimental renal IR injury has been found to elevate a number of Nrf2-regulated cell defense genes in wild type mice, but not in the kidneys of $Nrf2^{-/-}$ mice (Leonard *et al.*, 2006; Liu *et al.*, 2009). Pretreatment of $Nrf2^{+/+}$ mice with the small molecule Nrf2 inducers CDDO-Me (Wu *et al.*, 2011b), CDDO-Im (Liu *et al.*, 2014), sulphoraphane (Yoon *et al.*, 2008) and N-acetylcysteine (Liu *et al.*, 2009; Zhang *et al.*, 2014) ameliorates IR injury. The severity of renal IR injury is exacerbated by the loss of Nrf2 (Liu *et al.*, 2009); pre-treating $Nrf2^{-/-}$ mice with GSH, N-acetylcysteine (Liu *et al.*, 2009) and CDDO-Im (Liu *et al.*, 2014) reduces IR injury when compared to untreated $Nrf2^{-/-}$ mice. Therefore, Nrf2 has an important role in protecting the kidney from oxidative stress that underlies the pathogenesis of renal IR injury.

1.4.1.2 Cisplatin nephrotoxicty

The anti-neoplastic agent cisplatin (Fig. 5, 6) is used to treat a diverse range of tumours, including sarcomas and lymphomas (Cooley *et al.*, 1994), though its therapeutic efficacy is limited by its ability to induce proximal tubular cell injury via the induction of oxidative stress and DNA damage (Aleksunes *et al.*, 2010). Cisplatin nephrotoxicity is exacerbated in $Nrf2^{-/-}$ mice, measured by kidney injury biomarkers and histopathology (Aleksunes *et al.*, 2010), whilst the pre-administration of Nrf2 inducers has been shown to inhibit cisplatin-mediated nephrotoxicity in wild type mice. For example, 3*H*-1,2-dithiole-3-thione has been shown to induce Nrf2 expression in mouse renal tubular cells and confer resistance to cisplatin-mediated nephrotoxicity (Park *et al.*, 2008). Furthermore, lycopene (a carotenoid found in tomatoes) mitigates the cytotoxic effects of cisplatin by inducing Nrf2-regulated genes and inhibiting the pro-inflammatory actions of NF-κB (Sahin *et al.*, 2010a). Pre-treatment with the Nrf2-inducing agents epigallocatechin-3-gallate (ECGC) (Sahin *et al.*, 2010b) and CDDO-Im (Aleksunes *et al.*, 2010) has also been shown to lessen cisplatin-induced nephrotoxicity in rodents. In a human renal mesangial cell line, Nrf2 activation by eriodictyol-7-O-glucoside was found to significantly reduce sensitivity to cisplatin toxicity (Hu *et al.*, 2012).

On the other hand, the antioxidant ginsenoside RG3 prevents the cisplatin-induced nuclear accumulation of Nrf2 and subsequent induction of cell defence processes in mice, and is currently being investigated as a method of enhancing the chemotherapeutic efficacy of cisplatin (Lee *et al.*, 2012b). Wistar rats have reduced sensitivity to cisplatin toxicity following treatment with the polyphenol Nrf2 inducer

curcumin and a modified equivalent, difluorinated curcumin (CDF) (Sahin *et al.*, 2014). Additionally, compared to curcumin, CDF reduces the expression of pro-inflammatory renal injury biomarkers to a greater extent (Sahin *et al.*, 2014), suggesting that medicinal chemistry can be used to develop less toxic, second-generation Nrf2-inducing compounds that can enhance the efficacy of (in this instance) chemotherapeutics (for further discussion, see Chapter 4).

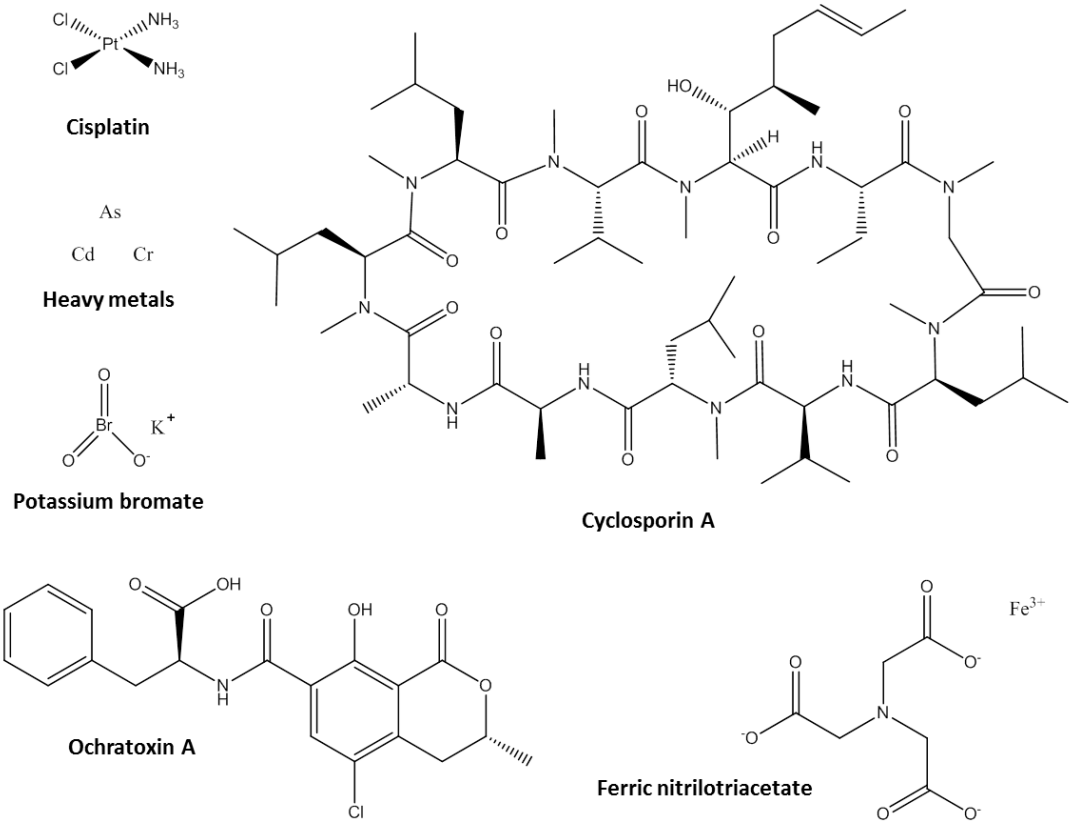

Fig.5: Chemical structures of nephrotoxins that Nrf2 is known to protect against (Shelton *et al.*, 2013).

1.4.1.3 Heavy metal nephrotoxicity

The accumulation of naturally occurring and pollutant-derived heavy metals can lead to environmental damage, as well as multiorgan toxicity and carcinogenesis in humans (Calderon *et al.*, 2003). Nrf2 has been shown to protect against nephrotoxicity induced by numerous heavy metals (Fig. 5), including arsenic (Prabu et al., 2012), chromium (Molina-Jijon et al., 2011), and cadmium (Chen et al., 2009). Indeed, concomitant treatment with the Nrf2-inducing antioxidant silibinin ameliorates sodium arsenite nephrotoxicity in rats (Prabu et al., 2012). In addition, ectopic expression or RNA interference depletion of Nrf2 decreases or increases, respectively, the sensitivity of normal rat kidney epithelial cells to cadmium-induced oxidative stress (Chen et al., 2009), whereas induction of Nrf2 by curcumin lessens the nephrotoxicity of chromium (Molina-Jijon et al., 2011). Therefore, Nrf2 protects against the renal injury caused by numerous heavy metals.

1.4.1.4 Cyclosporin A nephrotoxicity

The immunosuppressant cyclosporin A (Fig. 5) is commonly used to decrease the risk of rejection during organ transplantation, but induces nephrotoxicity via an upregulation of transforming growth factor-β (TGF-β), which promotes epithelial–mesenchymal transition and renal fibrosis (Busauschina *et al.*, 2004). Cyclosporin A provokes upregulation of Nrf2-regulated cell defense genes (Louhelainen *et al.*, 2006; Shin *et al.*, 2010), whereas RNA interference depletion of Nrf2 has a detrimental effect on the viability of renal cells exposed to cyclosporin A *in vitro*

(Shin *et al.*, 2010). Furthermore, sulphoraphane (Shin *et al.*, 2010) and the natural antioxidant lipoic acid (Louhelainen et al., 2006) ameliorate cyclosporin A nephrotoxicity in rodents by inducing Nrf2-mediated cell defense processes.

1.4.1.5 Ochratoxin A nephrotoxicity

The mycotoxin ochratoxin A (OTA, Fig. 5, 6) is carcinogenic and nephrotoxic in rodents, with the latter effect provoked by the generation of oxidative stress and the induction of tubular degradation and renal cortical fibrosis (Petrik *et al.*, 2003) following uptake via OAT1 (Tsuda *et al.*, 1999). Gene expression and protein analysis has indicated that the Nrf2 pathway is downregulated in the kidney of rats fed OTA for up to 12 months (Marin-Kuan *et al.*, 2006; Cavin *et al.*, 2007), as well as in cultured primary renal proximal tubule cells exposed to the mycotoxin (Cavin *et al.*, 2007; Stachurska *et al.*, 2013). It is thought that the inhibited capacity of the Nrf2 pathway to protect against OTA–induced oxidative DNA damage manifests in enhanced cytotoxicity in the kidney (Cavin *et al.*, 2007). In keeping with this concept, adenoviral overexpression of Nrf2 has been shown to inhibit the ability of OTA to induce oxidative stress and TGF-β expression (Stachurska *et al.*, 2013). In addition, pretreatment with the Nrf2 inducers cafestol–kahweol or coumarin ameliorates OTA–induced lipid peroxidation, DNA damage, and cytotoxicity in cultured rat tubular cells (Cavin *et al.*, 2007; Cavin *et al.*, 2009), further indicating a protective role for Nrf2 against ochratoxin A nephrotoxicity.

1.4.1.6 Potassium bromate nephrotoxicity

Potassium bromate is a food additive with nephrotoxic, mutagenic, and carcinogenic side effects. Nephrotoxicity manifests as changes in proximal tubule brush border protein functionality and expression, provoking kidney failure (Ahmad *et al.*, 2012). Human primary proximal tubule cells treated with a sublethal dose of potassium bromate have an enriched Nrf2-regulated gene complement, in addition to elevated expression of genes involved in the glutathione pathway (Limonciel *et al.*, 2012). Furthermore, Nrf2-deficient mice suffer more severe kidney damage as compared with wild-type counterparts, following exposure to potassium bromate (Jaloszynski *et al.*, 2007).

1.4.1.7 Ferric nitrilotriacetate nephrotoxicity

Ferric nitrilotriacetate (FENTA) is used experimentally to induce renal damage via the generation of iron-mediated oxidative stress and subsequent proximal tubular cell necrosis (Umemura *et al.*, 1990). FENTA has been shown to augment the mRNA levels of Nrf2 target genes, including Nqo1, Gclc, and Gstp1/2 in wild-type but not Nrf2-deficient mice (Tanaka *et al.*, 2008). Furthermore, $Nrf2^{-/-}$ mice treated with FENTA display significantly reduced glutathione levels, more severe histopathological necrosis, and increased blood urea nitrogen and serum creatinine levels than wild-type counterparts (Kanki *et al.*, 2008; Tanaka *et al.*, 2008). Importantly, pretreatment of wild-type mice with the Nrf2 inducer CDDO-Me lessens the renal injury provoked by FENTA (Tanaka *et al.*, 2008), demonstrating a protective role for Nrf2 in this form of kidney toxicity.

1.4.2 Role of Nrf2 in protection against chronic kidney disease

The induction of Nrf2 has proven to be protective against pathologies as diverse as neurodegeneration (Yang *et al.*, 2009), diabetes (de Souza *et al.*, 2012) and some types of cancer (Jeong *et al.*, 2006; Jaramillo *et al.*, 2013), with the small molecule Nrf2 inducer dimethyl fumarate recently being licensed for the clinical treatment of multiple sclerosis (Lee *et al.*, 2013). Chronic kidney disease (a progressive loss of renal function) is often initially asymptomatic, but can be determined through the measurement of renal injury biomarkers such as creatinine clearance and proteinuria. Oxidative stress is critical in the mechanistic progression of CKD, inducing inflammation via the activation of NF-κB, which in turn induces further oxidative stress through the production of ROS from activated immune cells (Ruiz *et al.*, 2013). Increased ROS production is present in various animal models of CKD, including 5/6 nephrectomy rats (Aminzadeh *et al.*, 2014) and Imai rats spontaneously developing focal segmental glomerulosclerosis (Kim *et al.*, 2011). Constitutive Nrf2 expression is required for the maintenance of an effective redox balance, however CKD is associated with impaired Nrf2 activity (Kim *et al.*, 2010; Kim *et al.*, 2011; Aminzadeh *et al.*, 2013b). A lack of Nrf2 functionality further contributes to the pathogenesis of CKD, allowing the accumulation of ROS and amplifying NF-κB activation. Targeting the Keap1/Nrf2 pathway to attenuate the progression of CKD is therefore a promising clinical strategy.

1.4.2.1 Renal fibrosis

Tubular and interstitial fibrotic injury (Fig. 6) is associated with the end-stage progression of CKD. The pathogenesis of fibrotic kidney injury is complex, and involves epithelial-to-mesenchymal renal cell transformation mediated via TGF-β signalling, which progresses to tubular atrophy and renal fibrosis (Liu, 2006). Angiotensin II-mediated suppression of Nrf2 in renal epithelial cells stimulates EMT by enhancing the activity of TGF-β, likely due to heightened levels of oxidative stress (Kang *et al.*, 2011). The Nrf2 inducer dimethylfumarate and adenovirus-mediated over-expression of Nrf2 have been shown to decrease alpha-smooth muscle actin, collagen and fibronectin expression in TGF-β -treated rat renal fibroblasts and mesangial cells (Oh *et al.*, 2012), whilst dimethylfumarate also suppresses renal fibrosis in the unilateral ureteral obstruction mouse model (Oh *et al.*, 2012). These findings support a role for Nrf2 in protection against renal fibrosis.

1.4.2.2 Focal segmental glomerulosclerosis

Focal segmental glomerulosclerosis (FSGS, Fig. 6) is a common form of idiopathic nephritic syndrome, characterised by induction of oxidative stress, inflammation and renal fibrosis, and is the leading glomerular disorder causing end-stage CKD (D'Agati *et al.*, 2011). In a mouse model of FSGS, treatment with antroquinolol increases renal Nrf2 activity and causes a corresponding inhibition of NF-κB and TGF-β1 signalling, leading to a decrease in oxidative stress, proteinuria, epithelial

injury and renal dysfunction (Tsai *et al.*, 2011). Therefore, Nrf2 can protect against the deleterious effects of FSGS.

1.4.2.3 Diabetic nephropathy

Diabetic nephropathy (DN) is a chronic disease resulting in kidney hypertrophy, tubular atrophy, interstitial fibrosis and glomerular sclerosis (Ayodele *et al.*, 2004). Diabetes causes over 1 million deaths per year, and cases of DN increased by 150 % between 1994 and 2004 in the US, with similar trends emerging in Europe, Asia and developing countries (Ayodele *et al.*, 2004). In animals treated with streptozotocin, hyperglycaemia-induced DN is associated with renal fibrosis and elevated levels of oxidative stress, which is exacerbated in $Nrf2^{-/-}$ mice (Yoh *et al.*, 2008; Jiang *et al.*, 2010) and ameliorated in rats treated with the proteasomal inhibitor MG132 (Luo *et al.*, 2011), which induces the Nrf2-dependent oxidative stress response by limiting the transcription factor's proteolytic degradation. Furthermore, the Nrf2 inducers sulphoraphane (Zheng *et al.*, 2011), resveratrol (Palsamy *et al.*, 2011) and tert-butylhydroquinone (Li *et al.*, 2011a) reduce renal injury in the streptozotocin-induced DN mouse model by upregulating the expression of cytoprotective genes and downregulating the expression of pro-inflammatory cytokines. Importantly, the protective effect of sulphoraphane is lost in $Nrf2^{-/-}$ mice (Zheng *et al.*, 2011). In the methylglyoxal-induced DN mouse model, both ankaflavin (Lee *et al.*, 2012a) and sulphoraphane (Xue *et al.*, 2008) upregulate Nrf2 target genes and protect against experimental diabetes. Moreover, MG132 induces the expression of catalase, superoxide dismutase and Ho-1, and lessens proteinuria and renal dysfunction, in

the OVE26 mouse model of type 1 diabetes (Cui *et al.*, 2013). Therefore, induction of Nrf2 appears to be a promising strategy for the prevention of DN renal injury (de Haan, 2011).

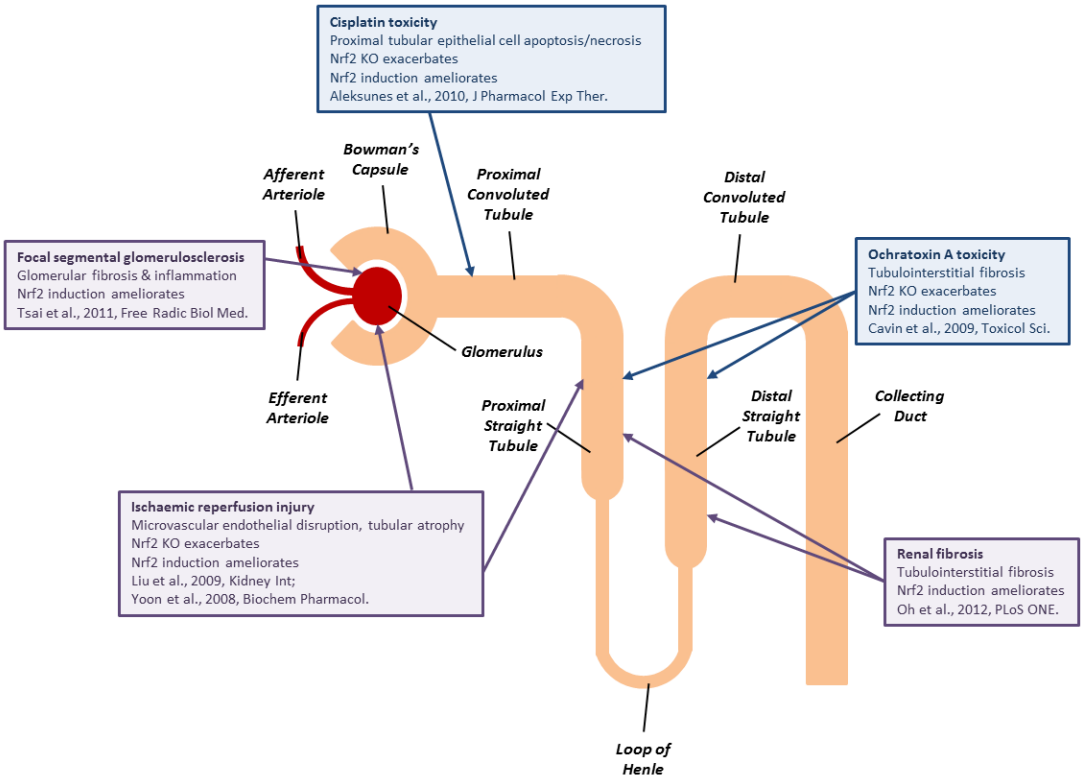

Fig.6: Roles of Nrf2 in protection against various forms of acute and chronic kidney pathology affecting discrete areas of the renal nephron.

1.4.3 Fumarate and renal cell carcinoma

In contrast to CKD, renal cancer is associated with an increase in Nrf2 expression, which allows tumour cells to survive hypoxic conditions (Ooi *et al.*, 2013). Nrf2 has been shown to play a role in the development of renal cancer driven by genetic deficiency of the tumour suppressor gene fumarate hydratase (FH). Indeed, Nrf2 and its target gene battery have been found to be highly expressed in the kidneys of mice in which the renal Fh gene has been conditionally deleted, as well as in type 2 hereditary papillary renal cell carcinoma tissue from patients carrying heterozygous germline Fh mutations (Adam *et al.*, 2011; Ooi *et al.*, 2011). At the chemico-biological level, it has been demonstrated that specific cysteine residues (including Cys-151 and -288) in Keap1 are succinated as a result of the accumulation of fumarate that is associated with deficiency of FH (Adam *et al.*, 2011; Ooi *et al.*, 2011). It is thought that the resulting inactivation of Keap1 allows renal Nrf2 activity to remain unchecked under high fumarate conditions (Adam *et al.*, 2011; Ooi *et al.*, 2011). Somatic (i.e. non-hereditary) papillary renal cell carcinoma is associated with mutation of Nrf2 and Cul3 (Ooi *et al.*, 2013), showing a convergence with hereditary papillary renal cell carcinoma and demonstrating a degree of positive selection of Nrf2 activity by cancerous cells. Therefore, in keeping with a number of reports depicting hyper-activity of Nrf2 in tumours of lung, pancreas, breast and endometrium, amongst others (Taguchi *et al.*, 2011), activation of the Nrf2 pathway by somatic mutation or by a hereditary deficiency of FH can lead to the development of renal cancer.

1.5 CDDO-Me: a potent Nrf2 inducer and novel treatment for CKD

Oleanolic acid is a triterpenoid compound used in Asian medicine with anti-tumorigenic, anti-inflammatory and cytoprotective properties (Shanmugam *et al.*, 2014). Synthesis of structurally similar triterpenoid compounds commenced with the modification of the A and C rings of oleanolic acid, with the resulting compound CDDO (2-cyano-3,12-dioxooleana-1,9(11)-dien-28-oic acid, (Honda *et al.*, 1998)) found to be 400 times more potent than previously designed compounds at preventing the production of nitric oxide in mouse macrophages (Honda *et al.*, 1998).

At nanomolar concentrations, CDDO and its imidazole derivative CDDO-Im (1-[2-cyano-3-,12-dioxooleana-1,9(11)-dien-28-oyl]imidazole) were found to induce HO-1 both *in vitro* (leukaemic and lung carcinoma cells (Liby *et al.*, 2005)) and *in vivo* (the stomach, small intestine, colon, liver, lung, kidney, and heart of CD-1 mice (Liby *et al.*, 2005)). Compared with oltipraz (an Nrf2 inducing dithiolethione (Kwak *et al.*, 2001)), CDDO-Im is 100 times more potent as an inducer of Nrf2 and associated antioxidant and Phase II metabolism genes in the mouse liver (Yates *et al.*, 2006).

Further examination of the capacity of CDDO-Im to induce Nrf2 focussed on the modulation of the ARE-regulated gene Nqo1 following CDDO-Im treatment of mice (Yates *et al.*, 2007). CDDO-Im treatment induced Nqo1 transcripts at very low doses (0.3 µmol/kg), and induced both Nqo1 and Gclc (Glutamine cysteine ligase (catalytic subunit)) genes in a variety of mouse organs, including the liver, lung and kidney (Yates *et al.*, 2007). The methyl ester of CDDO (CDDO-Me, methyl 2-cyano-3,12-dioxooleana-1,9(11)dien-28-oate, also known as bardoxolone methyl) was also

shown to be an extremely potent inducer of Nqo1 in the murine small intestinal mucosa and liver (Yates *et al.*, 2007).

Like its parent compound oleanolic acid, CDDO-Me has apoptotic properties (via the inhibiton of NF-κB activity and JAK/STAT signalling) in cancer cell lines (Ahmad *et al.*, 2006). A phase I first-in-human clinical trial was set up to determine dose-limiting toxicity, maximum tolerated dose and various pharmacokinetic and pharmacodynamic parameters in patients with solid tumours and lymphomas, with a prospective phase II trial to look at efficacy in tumour treatment (Hong *et al.*, 2012). In patients receiving CDDO-Me, Nqo1 mRNA transcripts were found to be increased in PBMCs, and NF-κB levels were reduced in tumour biopsies (Hong *et al.*, 2012). However, an unexpected clinical outcome was an increase in estimated glomerular filtration rate (eGFR, a measure of kidney function, (Hong *et al.*, 2012)). Research has demonstrated that the production of ROS correlates with the progression of CKD (Dounousi *et al.*, 2006), and the Nrf2 pathway is impaired in CKD (Kim *et al.*, 2010). Based on the effect of CDDO-Me on eGFR in this trial, further trials were designed to examine the beneficial effects of CDDO-Me in CKD patients.

A preliminary phase IIa trial was conducted on patients with established moderate to severe diabetic nephropathy (Pergola *et al.*, 2011a). The study was designed to determine appropriate dosing of CDDO-Me to improve kidney function, and as such the key biomarker measured was eGFR, which was improved following CDDO-Me treatment (Pergola *et al.*, 2011a). No major changes in renal injury biomarkers were reported, so a phase IIb trial (BEAM) was conducted (Pergola *et al.*, 2011b). This trial enrolled a larger number of patients with CKD, dosed with either a placebo

or CDDO-Me, and again a significant improvement in eGFR was reported in patients receiving CDDO-Me (Pergola *et al.*, 2011b).

1.6 Summary and aims

Acute kidney injury and chronic kidney disease are a serious clinical burden. Nrf2 has previously been shown to afford protection against both acute kidney injury (Shelton *et al.*, 2013) and chronic kidney disease (Ruiz *et al.*, 2013) in a number of experimental models, and the Nrf2 inducer CDDO-Me as recently been investigated as a novel treatment for CKD (de Zeeuw *et al.*, 2013a). To better understand the physiological, pharmacological and toxicological consequences of targeting Nrf2 in the kidney, this thesis has tested the following hypotheses:

Chapter 2: Nrf2 controls multiple proteins involved in the regulation of homeostatic processes in the kidney.

Through proteomic and targeted analysis of kidney tissue from $Nrf2^{+/+}$ and $Nrf2^{-/-}$ mice treated with the Nrf2 inducer CDDO-Me, it is predicted that the renal genes, proteins and biological processes under Nrf2 control will be defined, providing insights into the physiological roles of Nrf2 in the kidney.

Chapter 3: Nrf2 controls microRNAs in the kidney.

The regulation of Nrf2 expression by microRNAs has been demonstrated in a small number of studies, but information about the regulation of microRNA expression by Nrf2 itself is lacking. Using a transcriptomic approach, it is predicted that microRNAs indicative of Nrf2 activity will be discovered, providing new insights into the biology of the Nrf2 pathway as well as revealing novel transcriptional markers of Nrf2 activity.

Chapter 4: The drive to produce more potent Nrf2-inducing drugs has not led to the development of inherently more toxic molecules.

In order to investigate, based on the adverse events reported in the CDDO-Me 'BEACON' clinical trial (de Zeeuw *et al.*, 2013a), whether the drive to produce more potent Nrf2 inducing compounds has unwittingly lead to the development of more toxic molecules that could provoke off-target effects in patients, the relationship between thiol reactivity (a common feature of many small molecule Nrf2 inducers (Bryan *et al.*, 2013)), potency toward Nrf2 and toxicity has been examined for a series of triterpenoids and second-generation monocyclic and tricyclic Nrf2 inducers, which hold promise as novel drug candidates.

By testing these hypotheses, this thesis seeks to further our understanding of the physiological, pharmacological and toxicological roles of Nrf2 in the kidney.

Chapter 2

Proteomic analysis reveals the role of Nrf2 as a regulator of proteins controlling homeostatic processes in the mouse kidney

Contents

2.1 Introduction

Acute kidney injury (AKI) is a significant clinical problem, with more than 7% of patients developing some form of AKI following admission to hospital (Nash *et al.*, 2002). Furthermore, the kidney is uniquely susceptible to toxic insult, due to a relatively hypoxic environment in the nephron and high metabolic rate (Perazella, 2009). As a result of the renal vasculature being exposed to 25% of resting cardiac output (Lote *et al.*, 1996), the kidney often encounters and concentrates relatively high levels of xenobiotics and their metabolites, of which a number are known to suppress renal function. A key mechanism underlying the nephrotoxicity of many xenobiotics (examples include cisplatin (Aleksunes *et al.*, 2010), ferric nitrilotriacetate (Umemura *et al.*, 1990) and streptozotocin (Jiang *et al.*, 2010)) is their ability to induce the generation of reactive oxygen species (ROS) and consequent oxidative stress (Shelton *et al.*, 2013).

Research in this laboratory has previously provided a detailed insight into the molecular mechanisms by which Nrf2 protects against drug-induced liver injury, by defining the constitutive Nrf2-regulated hepatic proteome (Kitteringham *et al.*, 2010). Using an iTRAQ-based proteomic approach, we demonstrated that the expression of a number of proteins responsible for the detoxification of acetaminophen and other drugs is markedly decreased in the livers of $Nrf2^{-/-}$ mice (Kitteringham *et al.*, 2010), consistent with their enhanced sensitivity to the hepatotoxicty provoked by these compounds (Chan *et al.*, 2001; Enomoto *et al.*, 2001; Copple *et al.*, 2008; Liu *et al.*, 2013). In an extension to this study, we recently defined the biological processes that are sensitive to modulation of Nrf2 in

the liver by detailing the hepatic proteins augmented in $Nrf2^{+/+}$, but not $Nrf2^{-/-}$, mice in response to CDDO-Me (Walsh *et al.*, 2014). This work revealed that CDDO-Me is a highly selective inducer of Nrf2-regulated proteins in the liver, and identified six proteins (cytochrome P4502A5 (Cyp2a5), glutathione-S-transferases Mu 1 (Gstm1) and Mu 3 (Gstm3), ectonucleoside-triphosphate diphosphohydrolase (Entpd5), epoxide hydrolase 1 (Ephx1) and UDP-glucose-6-dehydrogenase (Ugdh)) that were both downregulated in $Nrf2^{-/-}$ mice and upregulated by CDDO-Me in $Nrf2^{+/+}$ mice (Walsh *et al.*, 2014).

Isobaric tag for relative and absolute quantification (iTRAQ)-based proteomics (Thompson *et al.*, 2003; Ross *et al.*, 2004) uses tandem mass spectrometry (MS/MS) to quantify the amount of proteins from different sources in the same experimental run. Isobaric tags of differing masses (but balanced to the same overall mass) are used to stably label digested peptides from up to 8 different samples, which are then combined (Fig. 1A, (Unwin, 2010)).

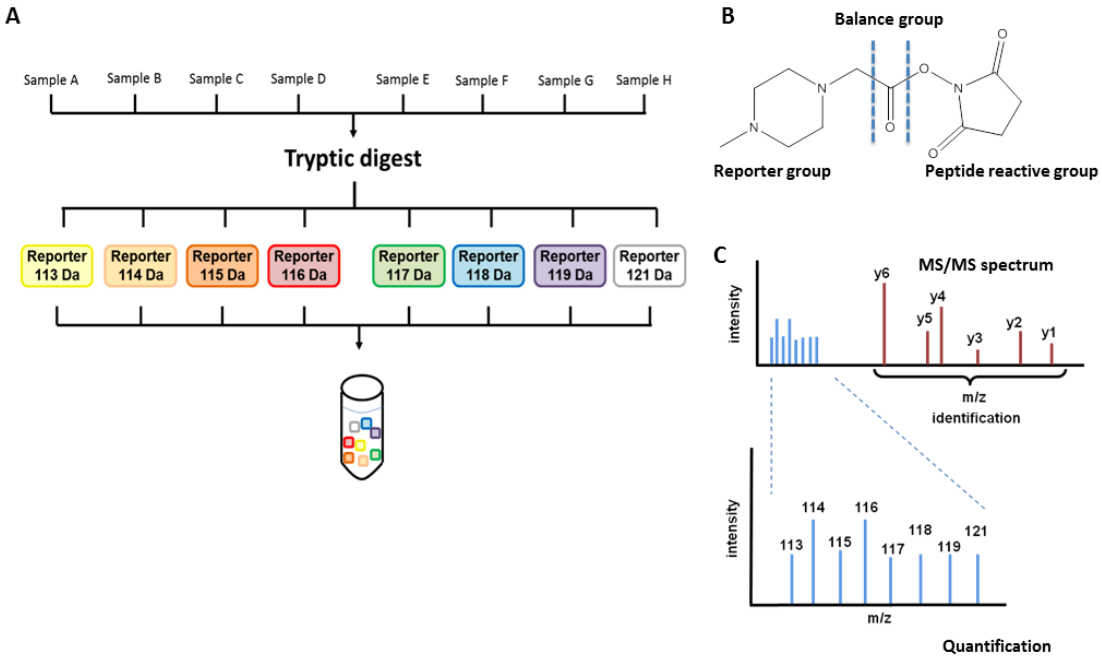

Fig. 1: iTRAQ procedure schematic. (A) Subsequent to a tryptic digest, samples are stably labelled with the iTRAQ labelling reagents (B), and combined for tandem mass spectrometric analysis (MS/MS, C), which allows for the identification and quantification of sample proteins based on isobaric label ratios.

When analysed simultaneously, the first MS trace represents the same peptide from all of the samples at the same mass (Fig. 1B). Collision-induced dissociation facilitates amino acid sequencing (Unwin, 2010), and therefore reveals the peptide identity. The abundance of iTRAQ tag-specific reporter ions, specific to each sample, is also quantified, allowing the relative abundance of the particular peptide in each of the labelled samples (Unwin, 2010) to be determined, relative to a pooled control (Fig. 1B).

Despite multiple studies demonstrating the ability of Nrf2 to protect against nephrotoxic insult in experimental models (Leonard *et al.*, 2006; Yoon *et al.*, 2008; Liu *et al.*, 2009; Wu *et al.*, 2011b; Shelton *et al.*, 2013; Wu *et al.*, 2014a), the underlying biological mechanisms by which Nrf2 protects the kidney are not fully understood. To provide a detailed insight into the biological processes controlled by Nrf2 in the kidney, we have performed iTRAQ-based proteomic analysis of kidney homogenates from $Nrf2^{+/+}$ and $Nrf2^{-/-}$ mice treated with CDDO-Me or DMSO vehicle for 24 h. Some of the content of this chapter has contributed to a manuscript under preparation, "**Shelton et al., Integrated Transcriptomic and Proteomic Analysis Reveals the Role of Nrf2 as a Key Regulator of Homeostatic Processes in the Kidney**".

2.2 Methods

Animals and dosing: Non-fasted male $Nrf2^{+/+}$ and $Nrf2^{-/-}$ mice (C57BL/6 background) of 10-12 weeks of age were used throughout the study. $Nrf2^{-/-}$ mice express a mutant Nrf2 protein that lacks the C-terminal 280 amino acids that constitute the DNA-binding bZip and transactivation domains of the transcription factor, thus rendering it functionally inactive (Itoh *et al.*, 1997; McMahon *et al.*, 2001). The study was conducted according to the Animals (Scientific Procedures) Act 1986 and University of Liverpool local guidelines. Mice were housed at 19-23 °C on a 12 hour light/dark cycle, and given free access to food and water. Six mice of each genotype were administered a single intraperitoneal (i.p.) dose of vehicle (DMSO, 100 µL/mouse) or CDDO-Me (3 mg/kg, (Walsh *et al.*, 2014)), and sacrificed 24 h later by exposure to a rising concentration of CO_2 followed by cardiac puncture. The renal capsule and fat were removed from excised kidneys, which were snap-frozen, along with other organs, and stored at -80 °C. Six samples per treatment group (($Nrf2^{+/+}$ + DMSO, $Nrf2^{-/-}$ + DMSO, $Nrf2^{+/+}$ + CDDO-Me and $Nrf2^{-/-}$ + CDDO-Me) were generated. For the dose-response experiment, two $Nrf2^{+/+}$ mice per treatment group were administered the indicated dose of CDDO-Me (i.p.), and culled after 24 hours. For the time course experiment, four $Nrf2^{+/+}$ mice per treatment group were administered a single i.p. dose of 3 mg/kg CDDO-Me, and culled at the indicated times.

General reagents: Unless otherwise stated, reagents were purchased from Sigma-Aldrich (UK).

Sample preparation: Snap-frozen mouse kidney was cut in half and submerged in 300 µL iTRAQ buffer (0.5 M triethylammonium bicarbonate/0.1 % sodium dodecyl sulphate (SDS)). A metal bead was introduced to the sample, which was subsequently homogenised using the Retsch MM400 homogeniser, at 30/s for 3 minutes. The metal bead was removed and sample subsequently underwent an overnight freeze-thaw cycle at -80 ^{o}C, and sonication (3 x 10 second bursts at 3 µm amplitude). Samples were centrifuged at 12,000 *x g* for 10 minutes at 4 oC, and the supernatant saved and centrifuged again under the same conditions. The resulting sample was diluted by 1/10, and the bicinchoninic acid (BCA) assay was performed to determine protein concentration.

Total protein determination: Protein content was determined using the BCA assay. Briefly, a standard curve was made using Bovine serum albumin in 0.9 % saline, and plated on Nunc 96 well flat bottomed plates. 1, 3 and 5 µL of sample was plated, and 200 µL BCA assay reagent (a ratio of 50:1 bicinchoninic acid solution to copper (II) sulphate (4 % wv/v) solution) was added. Following incubation at 37 ^{o}C for 30 minutes, the plate was read at 570 nM using an MRX microplate reader (Dynex). Resulting values were plotted against the concentration curve to generate µg/µL values.

iTRAQ labelling: 8-plex iTRAQ analysis was performed as described (Walsh *et al*., 2014). Samples were diluted to 100 µg protein in 20 µL iTRAQ buffer, and were denatured and reduced using 2 µL Tris(2-carboxyethyl)phosphine hydrochloride for one hour at 60^{o}C, and sulphydryl groups capped with 1 µL methyl methanethiosulphonate (MMTS) for 10 minutes at room temperature. Four vials of

mass spectrometry grade trypsin were reconstituted in 95 µL ddH_2O, and 10 µL was subsequently added per sample. Samples were briefly vortexed and incubated for 12-16 hours (overnight) at 37^{o}C.

iTRAQ isobaric tag labelling reagents (ABSciex, Massachusetts, USA) were allowed to reach room temperature, and reconstituted with 50 µL high-performance liquid chromatography-grade isopropanol. iTRAQ labelling reagents were combined with samples, and subsequently vortexed, centrifuged, and incubated for 2 hours at room temperature. All 8 samples were then combined, and 0.5 mL of a cation exchange (CEX) buffer (10 mM potassium dihydrogen phosphate/25 % acetonitrile) added. Samples were centrifuged (10,000 RPM for 4 minutes at room temperature) to sediment debris, transferred to a 7 mL bijou and made up to 5 mL with CEX buffer. Concentrated phosphoric acid was used to pH the sample to pH 3. Sample was centrifuged again at 10,000 RPM for 4 minutes at room temperature.

Cation exchange: Cation exchange fractionation was performed using a Polysulphoethyl A strong cation-exchange column (200 × 4.6 mm, 5 mm, 300 Å; Poly LC, Columbia, MD). Fractions of 2 mL were collected and were dried by centrifugation under vacuum (SpeedVac, Eppendorf). Fractions were reconstituted in 1 mL of 0.1 % trifluoro acetic acid (TFA) and were subsequently desalted using a mRP Hi Recovery protein column 4.6 x 50 mm (Agilent) on a Vision Workstation (Applied Biosystems) prior to mass spectrometric analysis.

Mass spectrometric analysis: Desalted fractions were reconstituted in 40 µL 0.1 % formic acid and 5 µL aliquots were delivered into a Triple TOF 5600 (AB Sciex) via an Eksigent NanoUltra cHiPLC System (AB Sciex) mounted with a microfluidic trap and analytical column (15 cm × 75 µm) packed with ChromXP C_{18}–CL 3 µm. A NanoSpray III source was fitted with a 10 µm inner diameter PicoTip emitter (New Objective). The trap column was washed with 2 % acetonitrile (ACN)/0.1 % formic acid (FA) for 10 min at 2 µL/min before switching in-line with the analytical column. A gradient of 2–50 % ACN/0.1 % FA (v/v) over 90 minutes was applied to the column at a flow rate of 300 nL/min. Operating in positive ion mode with survey scans of 250 ms, the instrument used an MS/MS accumulation time of 100 ms for the 25 most intense ions (total cycle time 2.5 seconds). A threshold for triggering MS/MS of 100 counts per second was used, with dynamic exclusion for 12 seconds and rolling collision energy, adjusted for the use of iTRAQ reagent in the Analyst method. Information-dependent acquisition was powered by Analyst TF 1.5.1. software, using mass ranges of 400-1600 atomic mass units (amu) in MS and 100-1400 amu in MS/MS. The instrument was calibrated after every fifth sample using a beta-galactosidase digest.

Protein detection and analysis: Kidney homogenates were analysed over four iTRAQ runs, using two pooled controls per run for normalisation between different experimental runs. Sample allocation to each run was randomised. Ratios for each iTRAQ label were obtained using label 121 as the common denominator. Data were searched using ProteinPilot 4.2 and the Paragon algorithm (AB Sciex) against the latest version of the SwissProt database, with MMTS as a fixed modification of

cysteine residues and biological modifications allowed. The data were also searched against a reversed decoy database and only proteins lying within a 1 % global FDR were included in subsequent analyses. The software R (R-Programming-Environment, 2005) was used to analyse the data, allowing for simultaneous comparisons between multiple treatments using design and contrast matrices via a linear regression model. Mean fold changes were calculated and analysis conducted on the log_2 fold-change values. Raw P values (unpaired T test) were subsequently used to compare expression between the relevant groups ($Nrf2^{+/+}$ + DMSO v $Nrf2^{-/-}$ + DMSO, and $Nrf2^{+/+}$ + DMSO v $Nrf2^{+/+}$ + CDDO-Me). Proteins reported were discovered in at least 4/6 kidney homogenates, with at least a 30 % fold change between groups. Raw P values and a 30% fold change were chosen as opposed to determining exact levels of expression (which is affected by inter-animal variability) to provide insight into hitherto unknown processes regulated by Nrf2 in the kidney.

Pathway analysis: Ingenuity pathway analysis (IPA, Qiagen, UK) was performed to reveal biological pathways perturbed during experimental conditions. Relevant iTRAQ data (proteins, log fold changes and P values) was uploaded to the IPA online database, and subsequent canonical pathways, P value and ratio are reported. Pathways represented by a single gene/protein were excluded for robustness.

Immunoblotting*:* Kidney homogenates (20 µg total protein) were loaded onto NuPAGE 4-12 % Bis Tris Precast gels (Life Technologies, UK) and proteins were subsequently separated using electrophoresis, using the MOPS running buffer (50 mM 3-(N-morpholino)propanesulphonic acid (Fisher Scientific), 50 mM Tris

Base, 0.1% SDS, 1 mM ethylenediaminetetraacetic acid) with the samples separated at 90 V for 10 minutes, then 170 V for 45 minutes. The gel was transferred to a nitrocellulose membrane (Amersham Hybond ECL, GE Healthcare, Buckinghamshire, UK) in a tank containing transfer buffer (192 mM glycine, 25 mM Tris base and 20 % methanol), a rotating stirrer and ice pack. Proteins were transferred to the membrane at a constant current of 230 mA for 60 minutes. Equal loading of protein was ensured using Ponceau red staining, and membranes were blocked for overnight with 10 % milk in TBS-Tween solution. TBS-Tween (TBS-T) solution contains 150 mM NaCl, 3 mM KCl, 25 mM Tris base and 0.1 % Tween-20, pH 7. Membranes were washed several times with TBS-T, and incubated for 3 hours with the indicated primary antibodies (1:4000) in TBS-T containing 2 % milk (Abcam: Nqo1 (ab2346), Gstm (ab53942), Entpd5 (ab92542), Cat (ab16731) and β-actin (ab6276)). Membranes were again washed several times with TBS-T, and incubated for one hour with the appropriate peroxidase-conjugated secondary antibody (1:10,000) in TBS-T containing 2 % milk. Enhanced Chemiluminescence Plus (GE Healthcare) was used to visualise the level of protein-antibody complex; using 2 mL per membrane for one minute. Membranes were dried and exposed to X-Ray film (Amersham hyperfilm) for up to 7 minutes to determine protein expression. X-Ray film was subsequently submerged in 20 % Carestream Kodak autoradiography GBX developer/replenisher for one minute and then washed in water and submerged in Carestream Kodak autoradiography GBS fixer/replenisher for one minute. Densitometry was performed using Quantity One 1D Analysis Software (BioRad). Protein bands were normalised to actin expression.

Mouse kidney RNA isolation: Snap-frozen mouse kidney was cut in half and submerged in QIAzol (Qiagen, UK), 10 µL/mg of tissue, no more than 30 mg total tissue. A metal bead was introduced to the sample, which was subsequently homogenised using the Retsch MM400 homogeniser, at 30 shakes per second for 3 minutes. The metal bead was removed and samples incubated at room temperature for 5 minutes. Chloroform (1/5 total volume) was added, and samples were shaken vigorously for 15 seconds. The samples were incubated at room temperature for 3 minutes, and centrifuged at 12,000 *x g* for 15 minutes at 4 ^{o}C. The upper, aqueous phase was transferred to a new microcentrifuge tube, and 1/2 volume of isopropanol was added. The sample was thoroughly vortexed and incubated at room temperature for 10 minutes. The sample was subsequently centrifuged at 12,000 *x g* for 10 minutes at 4 ^{o}C, and resulting supernatant discarded. The pellet was resuspended in 1 volume of 75 % ethanol, which was then centrifuged at 7,500 *x g* for 5 minutes at room temperature. The supernatant was discarded, and the pellet air dried for no longer than 3 minutes. The pellet was then resuspended in 20 µL RNase-free water.

DNase treatment: DNase treatment was performed on all RNA samples using the Ambion DNA-free^{TM} Kit (Life Technologies, UK). 1/10 volume 10X DNase buffer and 1 µL DNase I were added to the RNA samples, and incubated at 37 ^{o}C for 25 minutes. 1/10 volume DNase Inactivation Reagent (at least 2 µL) was added to samples, and thoroughly mixed. Samples were incubated at room temperature for 2 minutes, and mixed occasionally. Samples were subsequently centrifuged at

10,000 *x g* for 2 minutes at room temperature, and DNase-free RNA removed to new eppendorfs.

RNA quality assessment: RNA quality was assessed using an RNA 600 Nano Kit and 2100 Bioanalyzer (Agilent), according to manufacturer's instructions. Electrodes were decontaminated using RNaseZap, and pre-prepared gel was allowed to reach room temperature (550 µL Agilent RNA 6000 Nano gel matrix had been filtered using spin columns, and prepared into 65 µL aliquots). RNA 6000 Nano dye concentrate was centrifuged for 10 seconds at a low speed, and 1 µL added to the 65 µL aliquot of gel. The dye-gel mixture was vortexed, and stored in the dark until use. This mixture was subsequently centrifuged at 13,000 *x g* for 10 minutes at room temperature, and 9 µL added to the appropriate well of the Nano chip. The chip was pressurised accordingly, and then 9 µL dye-gel mixture was added to the appropriate wells. 5 µL of RNA 6000 Nano marker was added to the appropriate wells of the Nano chip. 1 µL of RNA ladder was added to the Nano chip, followed by 2 µL denatured (70 ^{o}C for 2 minutes) RNA samples. The Nano chip was subsequently vortexed using an IKA vortex mixer at 2400 RPM for 60 seconds, and Nano chip was inserted into the 2100 Bioanalyzer (Agilent). RNA bioanalysis was performed, and resultant mRNA electropherogram analysed using the 2100 expert software (version B.02.02) to produce an RNA integrity number (RIN), of which samples with a RIN of >7 were utilised for reverse transcription to cDNA.

Reverse Transcription of mRNA: RNA samples were reverse-transcribed (RT) to cDNA using the ImProm-II Reverse Transcription System (Promega, UK). RNA was quantified using NanoDrop ND-1000 (Labtech, UK). 1 µg RNA was added to

duplicate 200 µL nuclease-free tubes (Starlab, UK) containing 1 µL Oligo dT primer and dH_2O to make a total volume of 20 µL. Using a GeneAmp PCR 9700 thermal cycler (Life Technologies, UK) the samples were heated to 70 ^{o}C for 5 minutes. A master mix was prepared for reverse transcription, containing 8 µL 5X RT buffer, 6.4 µL 25 mM $MgCl_2$, 1 µL deoxynucleotide triphosphates (dNTPs), 2 µL reverse transcriptase and 2.6 µL dH_2O per sample. To control for aberrant reverse transcription of contaminated samples, a negative reverse transcriptase master mix was prepared, using 8 µL 5X RT buffer, 6.4 µL 25 mM $MgCl_2$ and 5.6 µL dH_2O per sample. Duplicate RNA samples subsequently had 20 µL of either reverse transcription or negative reverse transcription master mix added, and samples were vortexed and centrifuged at 3000 *x g* for 2 minutes at room temperature. The samples were transferred to the thermal cycler and subjected to a run of 5 minutes at 25 ^{o}C, 60 minutes at 42 ^{o}C and 15 minutes at 70 ^{o}C, followed by a 4 ^{o}C hold. cDNA samples were subsequently diluted with 160 µL dH_2O.

qRT-PCR: Primers for Nqo1, Gstm1, Gsta3, Cat, Entpd5, Cbr1, Nampt, Dpys, Slc22a12 and Ppia were purchased from Eurofins (Luxembourg) and diluted to 10 µM (sequences detailed in Table 1). A master mix was prepared using 8.75 µL dH_2O, 0.5 µL forward primer, 0.5 µL reverse primer, 0.25 µL ROX reference dye and 12.5 µL SYBR® Green JumpStart™ *Taq* ReadyMix™. 22.5 µL master mix was added to the appropriate wells of a 96 well PCR plate (Starlab, UK), followed by 2.5 µL cDNA in duplicate. The PCR plate was covered with an adhesive seal, and centrifuged at 2,000 *x g* for 1 minute at room temperature. PCR was performed using the ABI Prism 7000 Sequence Detection system (Applied Biosystems), for 1 cycle at 95 ^{o}C

for 2 minutes, 40 cycles of 95 ^{o}C for 15 seconds and 60 ^{o}C for 1 minute, and then a dissociation curve of 95 ^{o}C for 1 minute, 65 ^{o}C for 2 minutes, 95 ^{o}C to 65 ^{o}C at 2 ^{o}C/minute, and finally a 4 ^{o}C hold. Resultant Gene C_T values were normalised to Peptidylprolyl isomerase A (Ppia) expression (Kim *et al.*, 2014).

Gene	Primer	Sequence
Ppia	Sense	5'-CAAATGCTGGACCAAACACAAACG-3'
	Antisense	5'-GTTCATGCCTTCTTTCACCTTCCC-3'
Nqo1	Sense	5'-AGCGTTCGGTATTACGATCC-3'
	Antisense	5'-AGTACAATCAGGGCTCTTCTCG-3'
Gstm1	Sense	5'-ATACTGGGATACTGGAACGTCC-3'
	Antisense	5'-AGTCAGGGTTGTAACAGAGCAT-3'
Gsta3	Sense	5'-GGTTCCTGGTTTGTTCCTTG-3'
	Antisense	5'-CTATGGGAAGGACATGAAGGAG-3'
Cat	Sense	5'-TGGTTAATGCAGATGGAGAGG-3'
	Antisense	5'-TTGAAAAGATCTCGGAGGCC-3'
Entpd5	Sense	5'-GGGCTACCTCACTTCCTTTG-3'
	Antisense	5'-TCAGTCCCTTTTGCTTCCAG -3'
Cbr1	Sense	5'-ACAACCCGCAGAGCATTC-3'
	Antisense	5'-GTTCGTTTTCATTGTCACCTCTG-3'
Nampt	Sense	5'-GAATGTCTCCTTCGGTTCTGG-3'
	Antisense	5'-TCAGCAACTGGGTCCTTAAAC-3'
Dpys	Sense	5'-TGTGACTATAGCCTGCATGTG-3'
	Antisense	5'-CGGGCAAGGGTTTTCATTTC-3'
Scl22a12	Sense	5'-GAGGGAGACACGTTGACCA -3'
	Antisense	5'-AAGTCCACAATCCCGATGAG-3'

Table 1: Primers used for qRT-PCR analysis of mouse kidney tissue.

Quantification of NADPH content: Determination of NADPH content was performed using NADP/NADPH-Glo^{TM} (Promega). Whole kidney tissue was lysed in a bicarbonate buffer containing 100 mM sodium carbonate, 20 mM sodium bicarbonate, 10 mM nicotinamide, 0.05 % Triton X-100 (Thermo Scientific) and 0.5

% dodecyltrimethylammonium bromide, and subjected to a 1 h freeze-thaw cycle. Protein content was determined as previously described, and lysates were diluted to 1 µg/µL. 50 µL per sample was incubated at 60 ^{o}C for 15 min, room temperature for 10 min, and then 50 µL 0.2 N HCl/0.25 M Trizma base solution was added and gently mixed. 20 µL per reaction was removed to a 96 well white luminescence plate (Grenier Bio-One), and 20 µL NADPH reaction buffer was added. The plate was gently mixed, and luminescence was determined using the Thermo Scientific VarioSkan Flash 3001 device. Data are expressed as a percentage of luminescence in vehicle-treated $Nrf2^{+/+}$ kidney lysates.

Quantification of GSH content: Total GSH was measured using GSH-Glo^{TM} (Promega), essentially as described. Kidney tissues were lysed in PBS containing 2 mM EDTA (160 mg tissue per mL), and subjected to a 1 h freeze-thaw cycle. Samples were subsequently centrifuged at 12,000 RPM for 10 min, and the supernatant was used for the assay. 6.25 µL per sample was loaded onto a 96 well white luminescence plate, followed by 18.75 µL PBS. GSH-Glo reaction buffer was added at a ratio of 1:1, and the plate was incubated for 30 min at room temperature. To detect GSH, 50 µL luciferin detection reagent was added per well, and incubated at room temperature for 2 min before assessing luminescence. Data are expressed as a percentage of luminescence in vehicle-treated $Nrf2^{+/+}$ kidney lysates.

Immunohistochemistry: Whole kidneys from $Nrf2^{+/+}$ mice dosed with DMSO or CDDO-Me (3 mg/kg for 24 hours) and $Nrf2^{-/-}$ mice dosed with DMSO (5 per group) were excised and preserved in 4 % formalin. At the Veterinary Pathology Centre (The University of Liverpool), samples were longitudinally cut and embedded in paraffin. Serial 4 µm-thick sections were cut and placed on polylysine-coated slides, rehydrated through serial passages in solutions at decreasing concentrations of alcohol and moved to TBS-T, before quenching endogenous peroxidase activity through incubation in 0.3 % hydrogen peroxide. Anti-Nqo1 antibody (Sigma HPA007308) was diluted 1:100 and applied overnight at 4 ^{o}C, after blocking non-specific labelling using a 30 minute incubation at room temperature with 20 % normal goat serum. After washing in TBS-T, swine anti-rabbit HRP EnVision^{TM} polymer detection system (K4011, Dako) secondary antibody was used for detection of Nqo1. Negative control staining was performed with normal rabbit serum. After a 30 minute incubation with the antibody, slides were washed with TBS-T, and DAB (3,3-diaminiobenzidine) was added as a chromogen for 10 minutes. Slides were counterstained with Papanicolaou haematoxylin and mounted. For each experimental animal, a maximum of 10 non-overlapping microscopic fields of the cortex (including at least one glomerulus) and 5 fields of the medulla were captured at 100X with a Nikon DS-5Mc camera mounted on a Nikon Eclipse 80i microscope, before automated processing with ImageJ software (NIH). After elaboration of an appropriate plug-in for batch measure, colour channel splitting, application of colour threshold and measurement of percentage of stained area within the microscope fields was consecutively and automatically performed for all

images and all experimental groups. Raw data was analysed in Excel, and an unpaired T-test was used to compare between experimental groups.

2.3 Results

2.3.1 Genetic and pharmacological modulation of Nrf2 in the mouse kidney

In order to verify that the Nrf2 pathway was functional in the kidneys of $Nrf2^{+/+}$ mice and non-functional in $Nrf2^{-/-}$ mice, prior to conducting microarray and iTRAQ analysis, we determined the expression level of the established Nrf2 target Nqo1 by immunoblotting and qPCR in kidney homogenates from both genotypes, 24 h after dosing with vehicle or CDDO-Me (Elangovan *et al.*, 2008). The level of Nqo1 protein (Fig. 2A-B) and mRNA (Fig. 2C) was significantly lower in the kidneys of vehicle-exposed $Nrf2^{-/-}$ mice, compared with $Nrf2^{+/+}$ counterparts, consistent with loss of Nrf2 function. Moreover, whilst the Nrf2 inducer CDDO-Me provoked the induction of Nqo1 24 h after administration to $Nrf2^{+/+}$ mice, this effect was abrogated in $Nrf2^{-/-}$ mice (Fig. 2A-C). These data validate our model of genetic and pharmacological modulation of Nrf2 in the mouse kidney.

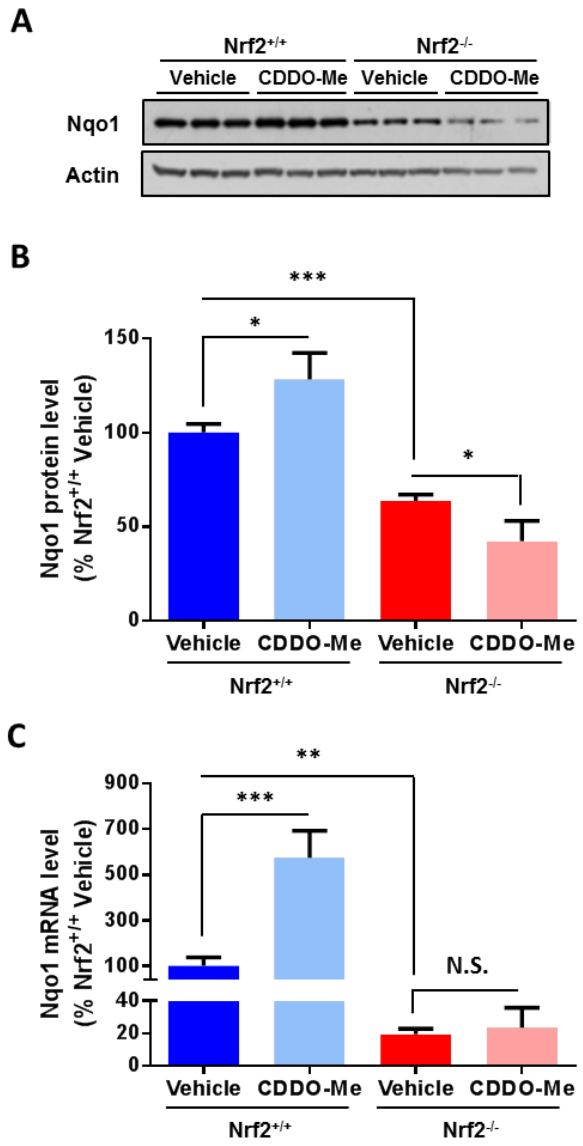

Figure 2: Differential activity of Nrf2 in the kidneys of $Nrf2^{+/+}$ and $Nrf2^{-/-}$ mice. Mice of the indicated genotype were given a single acute i.p. dose of vehicle (DMSO) or CDDO-Me (3 mg/kg). 24 h later, Nqo1 levels were determined by (A-B) immunoblotting and (C) qPCR. (B) Band volumes were quantified by densitometry and normalised against β-actin. (C) Nqo1 mRNA levels were normalised to Ppia. Data analysis represents mean + S.D. of n=6 animals per treatment group. Statistical analysis was performed with an unpaired T test, * $P \leq 0.05$; ** $P \leq 0.01$; *** $P \leq 0.001$ *; N.S.* not-significant.

2.3.2 Definition of the basal Nrf2-regulated renal proteome

To provide a hitherto unparalleled insight into the proteins controlled by Nrf2 in the kidney at the basal level, an iTRAQ-based proteomic analysis was performed on kidney homogenates from $Nrf2^{+/+}$ and $Nrf2^{-/-}$ mice (treated with the vehicle DMSO). This proteomic profiling yielded 3684 unique identifications at a FDR of <1 %. From these, 2655 proteins were shown to be quantifiable in at least four mice from each experimental group. Of these, the expression levels of 108 proteins were shown to be downregulated (Table 2) and 81 upregulated (Table 3) by at least 30 % ($P \leq 0.05$, T test) in whole kidney homogenates of vehicle-treated $Nrf2^{-/-}$ mice compared to their $Nrf2^{+/+}$ counterparts (Fig. 3A). Three of the most substantially down-regulated proteins identified in the iTRAQ analysis, Gstm1 (11.5-fold lower in $Nrf2^{-/-}$ vs. $Nrf2^{+/+}$ mice), Cat (4.3-fold lower) and Entpd5 (2.8-fold lower), were further shown to be expressed at a lower level in the kidneys of $Nrf2^{-/-}$ mice by immunoblotting of tissue homogenates (Fig. 3B-C). Manual interrogation (Fig. 3) and Ingenuity Pathway Analysis (Tables 4-5) of the iTRAQ data sets revealed that a substantial number of targets that were downregulated in the kidneys of $Nrf2^{-/-}$ mice were known to play roles in xenobiotic metabolism (Nqo1, Cyp7b1, Por), the synthesis and conjugation of glutathione (Gstm1, Gclc), and the maintenance of cellular redox balance (Cat, Prdx1). Furthermore, proteins contributing to a number of core metabolic processes, including glycolysis (Tkt, Me1), the supply of NAPDH (Nampt), the synthesis and recycling of amino acids (Acy3, Pipox) and the metabolism of lipids/fatty acids (Acat1, Faah), were found to be expressed at a lower level in the $Nrf2^{-/-}$ kidney (Fig. 4, Tables 4-5).

Accession	Gene symbol	Protein	Peptides	Fold decrease	P value
P10649	Gstm1	Glutathione S-transferase Mu 1	39	11.48	< 0.001
P30115	Gsta3	Glutathione S-transferase A3	9	6.19	< 0.001
P24270	Cat	Catalase	111	4.28	< 0.001
Q6ZQM8	Ugt1a7c	UDP-glucuronosyltransferase 1-7C	35	4.06	< 0.001
Q8QZT1	Acat1	Acetyl-CoA acetyltransferase, mitochondrial	94	3.94	< 0.001
Q64669	Nqo1	NAD(P)H dehydrogenase [quinone] 1	4	3.57	< 0.001
Q8R0Y6	Aldh1l1	Cytosolic 10-formyltetrahydrofolate dehydrogenase	62	3.08	< 0.001
Q60991	Cyp7b1	25-hydroxycholesterol 7-alpha-hydroxylase	8	2.86	< 0.001
P06801	Me1	NADP-dependent malic enzyme	37	2.83	< 0.001
Q9WUZ9	Entpd5	Ectonucleoside triphosphate diphosphohydrolase 5	12	2.75	< 0.001
Q3UNX5	Acsm3	Acyl-coenzyme A synthetase ACSM3, mitochondrial	39	2.74	0.003
Q9EPL9	Acox3	Peroxisomal acyl-coenzyme A oxidase 3	38	2.72	< 0.001
Q9DBE0	Csad	Cysteine sulphinic acid decarboxylase	19	2.68	0.011
Q7TNG8	Ldhd	Probable D-lactate dehydrogenase, mitochondrial	54	2.62	0.009
O08709	Prdx6	Peroxiredoxin-6	20	2.42	0.005
Q9JII6	Akr1a1	Alcohol dehydrogenase [NADP+]	62	2.34	< 0.001
P17563	Selenbp	Selenium-binding protein 1	70	2.24	< 0.001
P32020	Scp2	Non-specific lipid-transfer protein	24	2.18	0.002
Q91XE4	Acy3	Aspartoacylase-3	53	2.17	0.004
Q9R0H0	Acox1	Peroxisomal acyl-coenzyme A oxidase 1	121	2.16	0.005
P02762	Mup6	Major urinary protein 6	13	2.13	0.042
P37040	Por	NADPH--cytochrome P450 reductase	21	2.04	0.012
P16858	Gapdh	Glyceraldehyde-3-phosphate dehydrogenase	90	2.03	0.026
Q8C0I1	Agps	Alkyldihydroxyacetonephosphate synthase, peroxisomal	24	2.00	< 0.001
P34914	Ephx2	Epoxide hydrolase 2	58	2.00	0.005
Q9EQ06	Hsd17b11	Estradiol 17-beta-dehydrogenase 11	23	1.95	0.025
Q9R0Q9	Mpdu1	Mannose-P-dolichol utilization defect 1 protein	2	1.94	0.002

Q8VCN5	Cth	Cystathionine gamma-lyase	16	1.93	0.009
P00329	Adh1	Alcohol dehydrogenase 1	25	1.93	0.007
Q9D826	Pipox	Peroxisomal sarcosine oxidase	38	1.92	0.003
P56395	Cyb5a	Cytochrome b5	30	1.90	0.007
Q80W22	Thnsl1	Threonine synthase-like 2	23	1.89	0.001
P11930	Nudt19	Nucleoside diphosphate-linked moiety X motif 19, mitochondrial	57	1.88	< 0.001
P40142	Tkt	Transketolase	51	1.84	0.006
Q64462	Cyp4b1	Cytochrome P450 4B1	62	1.84	0.008
P97494	Gclc	Glutamate--cysteine ligase catalytic subunit	17	1.82	0.001
P28665	Mug1	Murinoglobulin-1	36	1.82	< 0.001
P10639	Txn	Thioredoxin	10	1.81	0.019
Q7TNE1	-	CaiB/baiF CoA-transferase family protein C7orf10 homolog	12	1.81	0.003
O70475	Ugdh	UDP-glucose 6-dehydrogenase	11	1.81	0.001
Q8R1G2	Cmbl	Carboxymethylenebutenolidase homolog	15	1.80	0.048
P51855	Gss	Glutathione synthetase	23	1.80	< 0.001
P35700	Prdx1	Peroxiredoxin-1	27	1.80	0.016
Q8BH00	Aldh8a1	Aldehyde dehydrogenase family 8 member A1	49	1.79	0.010
Q9DB29	Iah1	Isoamyl acetate-hydrolyzing esterase 1 homolog	14	1.79	< 0.001
Q9JLF6	Tgm1	Protein-glutamine gamma-glutamyltransferase K	9	1.78	0.004
P62960	Ybx1	Nuclease-sensitive element-binding protein 1	21	1.78	0.014
P47738	Aldh2	Aldehyde dehydrogenase, mitochondrial	72	1.76	0.010
Q8K0L3	Acsm2	Acyl-coenzyme A synthetase ACSM2, mitochondrial	175	1.74	0.010
P09103	P4hb	Protein disulphide-isomerase	48	1.71	0.024
Q8BWM0	Ptges2	Prostaglandin E synthase 2	10	1.69	0.002
P51660	Hsd17b4	Peroxisomal multifunctional enzyme type 2	50	1.67	0.002
P68372	Tubb4b	Tubulin beta-4B chain	57	1.67	0.005
Q9DBK0	Acot12	Acyl-coenzyme A thioesterase 12	9	1.65	0.015
Q99KQ4	Nampt	Nicotinamide phosphoribosyltransferase	17	1.64	0.008

Q64442	Sord	Sorbitol dehydrogenase	32	1.63	0.045
P47199	Cryz	Quinone oxidoreductase	50	1.61	0.036
Q8VCT4	Ces3	Carboxylesterase 3	34	1.59	0.049
Q60759	Gcdh	Glutaryl-CoA dehydrogenase, mitochondrial	27	1.58	0.015
O08914	Faah	Fatty-acid amide hydrolase 1	7	1.57	0.007
P97447	Fhl1	Four and a half LIM domains protein 1	6	1.57	0.027
Q9QXZ6	Oatp1a1	Solute carrier organic anion transporter family member 1A1	5	1.55	0.011
P28271	Aco1	Cytoplasmic aconitate hydratase	48	1.54	0.006
Q91WC0	Setd3	Histone-lysine N-methyltransferase setd3	3	1.53	0.039
Q91WS0	Cisd1	CDGSH iron-sulphur domain-containing protein 1	14	1.53	0.003
Q9DBL7	Coasy	Bifunctional coenzyme A synthase	11	1.53	0.017
Q9DCD0	Pgd	6-phosphogluconate dehydrogenase, decarboxylating	17	1.53	0.023
Q9EQF5	Dpys	Dihydropyrimidinase	4	1.52	0.038
P11499	Hsp90ab1	Heat shock protein HSP 90-beta	68	1.52	0.049
P10126	Eef1a1	Elongation factor 1-alpha 1	75	1.51	0.022
Q921S7	Mrpl37	39S ribosomal protein L37, mitochondrial	5	1.51	0.046
O55125	Nipsnap1	Protein NipSnap homolog 1	9	1.51	0.014
Q8BH86	-	UPF0317 protein C14orf159 homolog, mitochondrial	25	1.49	0.010
Q9CPY7	Lap3	Cytosol aminopeptidase	59	1.48	0.036
Q78JT3	Haao	3-hydroxyanthranilate 3,4-dioxygenase	16	1.47	0.010
P23953	Ces1c	Carboxylesterase 1C	17	1.47	0.026
O09174	Amacr	Alpha-methylacyl-CoA racemase	32	1.46	0.027
Q9CY58	Serbp1	Plasminogen activator inhibitor 1 RNA-binding protein	2	1.46	0.002
Q99JW2	Acy1	Aminoacylase-1	16	1.46	0.044
Q9DBG6	Rpn2	Dolichyl-diphosphooligosaccharide—protein glycosyltransferase	33	1.45	0.030
P25444	Rps2	40S ribosomal protein S2	11	1.45	0.003
P58252	Eef2	Elongation factor 2	61	1.44	0.014
P30412	Ppic	Peptidyl-prolyl cis-trans isomerase C	5	1.43	0.007

Q8CFZ5	Slc22a12	Solute carrier family 22 member 12	8	1.43	0.021
Q00612	G6pdx	Glucose-6-phosphate 1-dehydrogenase X	8	1.41	0.047
Q8C1E7	Tmem120a	Transmembrane protein 120A	2	1.41	0.001
Q8VDJ3	Hdlbp	Vigilin	20	1.39	0.027
Q9CYH2	Fam213a	Redox-regulatory protein FAM213A	7	1.38	0.003
Q8BWF0	Aldh5a1	Succinate-semialdehyde dehydrogenase, mitochondrial	13	1.36	0.029
Q6NZJ6	Eif4g1	Eukaryotic translation initiation factor 4 gamma 1	11	1.36	0.031
Q80XN0	Bdh1	D-beta-hydroxybutyrate dehydrogenase, mitochondrial	23	1.35	0.009
Q8R146	Apeh	Acylamino-acid-releasing enzyme	21	1.35	0.028
P62918	Rpl8	60S ribosomal protein L8	7	1.34	0.035
Q8VC69	Slc22a6	Solute carrier family 22 member 6	5	1.33	0.001
Q8BGD9	Eif4b	Eukaryotic translation initiation factor 4B	3	1.33	0.011
Q9D517	Agpat3	1-acyl-sn-glycerol-3-phosphate acyltransferase gamma	6	1.33	0.006
Q80U72	Scrib	Protein scribble homolog	3	1.32	0.043
P50172	Hsd11b1	Corticosteroid 11-beta-dehydrogenase isozyme 1	8	1.31	0.027
P62889	Rpl30	60S ribosomal protein L30	5	1.31	0.012
Q91WL5	Cyp4a12a	Cytochrome P450 4A12A	9	1.31	0.035
Q8R050	Gstp1	Eukaryotic peptide chain release factor GTP-binding subunit ERF3A	4	1.31	0.047
Q9CQ92	Fis1	Mitochondrial fission 1 protein	4	1.31	0.043
P23116	Eif3a	Eukaryotic translation initiation factor 3 subunit A	13	1.31	0.028
Q9CZU3	Skiv2l2	Superkiller viralicidic activity 2-like 2	5	1.30	0.041
Q8QZY2	Glyctk	Glycerate kinase	13	1.30	0.035

Table 2: Proteins down-regulated in the kidneys of $Nrf2^{-/-}$ mice. The expression levels of 108 proteins were found to be decreased by at least 30 % ($P \leq 0.05$) in the kidneys of $Nrf2^{-/-}$ mice. Proteins are ordered by fold decrease in expression in $Nrf2^{-/-}$ compared with $Nrf2^{+/+}$ mice (n=4-6 animals per group). The average number of peptides used for quantification across all iTRAQ runs is shown for each protein.

Accession	Gene symbol	Protein	Peptides	Fold increase	P value
O88833	Cyp4a10	Cytochrome P450 4A10	10	2.65	0.003
Q9QYR9	Acot2	Acyl-coenzyme A thioesterase 2, mitochondrial	33	2.56	< 0.001
Q9WVM8	Aadat	Kynurenine/alpha-aminoadipateaminotransferase	39	2.23	< 0.001
Q9NYQ2	Hao2	Hydroxyacid oxidase 2	9	2.09	0.004
Q9CR51	Atp6v1g1	V-type proton ATPase subunit G 1	5	2.02	0.003
P62806	Hist4h4	Histone H4	39	1.98	0.023
P16406	Enpep	Glutamyl aminopeptidase	18	1.97	< 0.001
Q05793	Hspg2	Basement membrane-specific heparan sulphate proteoglycan core	28	1.94	0.001
Q99K48	Nono	Non-POU domain-containing octamer-binding protein	8	1.93	0.009
P11404	Fabp3	Fatty acid-binding protein, heart	9	1.92	0.003
Q8BWT1	Acaa2	3-ketoacyl-CoA thiolase, mitochondrial	57	1.90	0.034
P12658	Calb1	Calbindin	30	1.87	0.034
P57780	Actn4	Alpha-actinin-4	100	1.85	< 0.001
Q60953	Pml	Protein PML	2	1.85	0.044
P53657	Pklr	Pyruvate kinase isozymes R/L	10	1.84	0.015
Q920R6	Atp6v0a4	V-type proton ATPase 116 kDa subunit a isoform 4	22	1.82	0.015
O55137	Acot1	Acyl-coenzyme A thioesterase 1	21	1.81	0.010
P56135	Atp5j2	ATP synthase subunit f, mitochondrial	5	1.79	0.005
O35409	Folh1	Glutamate carboxypeptidase 2	10	1.79	0.004
P09242	Alpl	Alkaline phosphatase, tissue-nonspecific isozyme	20	1.74	< 0.001
P10493	Nid1	Nidogen-1	3	1.72	0.018
P60710	Actb	Actin, cytoplasmic 1	158	1.72	0.046
Q91VW3	Sh3bgrl3	SH3 domain-binding glutamic acid-rich-like protein 3	5	1.70	0.046
Q9DBN5	Lonp2	Lon protease homolog 2, peroxisomal	6	1.67	0.015
Q9JIL4	Pdzk1	Na(+)/H(+) exchange regulatory cofactor NHE-RF3	61	1.67	< 0.001
Q62261	Sptbn1	Spectrin beta chain, non-erythrocytic 1	148	1.67	< 0.001
Q9D687	Slc6a19	Sodium-dependent neutral amino acid transporter B(0)AT1	4	1.64	0.001

Q7TPR4	Actn1	Alpha-actinin-1	53	1.63	0.003
Q62418	Dbnl	Drebrin-like protein	4	1.62	0.037
Q9D964	Gatm	Glycine amidinotransferase, mitochondrial	45	1.62	0.046
Q9JLB4	Cubn	Cubilin	42	1.62	0.028
P16546	Sptan1	Spectrin alpha chain, non-erythrocytic 1	191	1.61	0.002
Q8BMS1	Hadha	Trifunctional enzyme subunit alpha, mitochondrial	67	1.61	0.003
Q9D0K2	Oxct1	Succinyl-CoA:3-ketoacid-coenzyme A transferase 1	67	1.60	0.014
Q9DCJ9	Npl	N-acetylneuraminate lyase	11	1.59	0.021
O35598	Adam10	Disintegrin and metalloproteinase domain-containing protein 10	2	1.58	0.017
P28843	Dpp4	Dipeptidyl peptidase 4	7	1.58	< 0.001
Q9QXT0	Cnpy2	Protein canopy homolog 2	5	1.57	0.027
P29758	Oat	Ornithine aminotransferase, mitochondrial	17	1.54	0.023
Q9CQI6	Cotl1	Coactosin-like protein	8	1.54	0.005
Q80X90	Flnb	Filamin-B	72	1.53	< 0.001
Q61767	Hsd3b4	3 beta-hydroxysteroid dehydrogenase type 4	16	1.53	0.008
Q2TPA8	Hsdl2	Hydroxysteroid dehydrogenase-like protein 2	14	1.52	0.023
Q9CZU6	Cs	Citrate synthase, mitochondrial	38	1.52	0.002
Q9QWR8	Naga	Alpha-N-acetylgalactosaminidase	3	1.51	0.030
O88502	Pde8a	cAMP-specific and IBMX-insensitive 3',5'-cyclic phosphodiesterase	1	1.51	0.026
P24527	Lta4h	Leukotriene A-4 hydrolase	15	1.51	0.008
Q9Z0E8	Slc22a5	Solute carrier family 22 member 5	2	1.50	0.023
P11276	Fn1	Fibronectin	11	1.49	0.023
Q8VDD5	Myh9	Myosin-9	178	1.48	0.009
Q62468	Vil1	Villin-1	69	1.46	0.009
Q91YI0	Asl	Argininosuccinate lyase	29	1.46	0.011
Q9CQJ8	Ndufb9	NADH dehydrogenase [ubiquinone] 1 beta subcomplex subunit 9	12	1.45	0.026
P10852	Slc3a2	4F2 cell-surface antigen heavy chain	15	1.44	0.021
P55264	Adk	Adenosine kinase	10	1.43	0.043

P13634	Ca1	Carbonic anhydrase 1	10	1.43	0.027
P10922	H1f0	Histone H1.0	9	1.43	0.035
Q8BH59	Slc25a12	Calcium-binding mitochondrial carrier protein Aralar1	34	1.41	0.005
P48962	Slc25a4	ADP/ATP translocase 1	50	1.41	0.044
Q99MR8	Mccc1	Methylcrotonoyl-CoA carboxylase subunit alpha, mitochondrial	40	1.39	0.005
P41438	Slc19a1	Folate transporter 1	2	1.38	0.043
Q9DAW9	Cnn3	Calponin-3	4	1.38	0.027
Q8BVE3	Atp6v1h	V-type proton ATPase subunit H	26	1.36	0.019
B2RXS4	Plxnb2	Plexin-B2	6	1.36	0.013
Q68FD5	Cltc	Clathrin heavy chain 1	170	1.35	0.048
Q7TSV4	Pgm2	Phosphoglucomutase-2	5	1.35	0.018
P47809	Map2k3	Dual specificity mitogen-activated protein kinase kinase 4	2	1.34	0.048
P14824	Anxa6	Annexin A6	25	1.34	0.028
Q9EPU0	Upf1	Regulator of nonsense transcripts 1	8	1.33	0.045
Q64727	Vcl	Vinculin	51	1.33	0.010
P07356	Anxa2	Annexin A2	20	1.32	0.008
Q9DCS3	Mecr	Trans-2-enoyl-CoA reductase, mitochondrial	11	1.32	0.027
Q9EPC1	Parva	Alpha-parvin	8	1.31	0.008
Q61879	Myh10	Myosin-10	61	1.31	0.001
Q61702	Itih1	Inter-alpha-trypsin inhibitor heavy chain H1	3	1.31	0.048
P25976	Ubtf	Nucleolar transcription factor 1	2	1.31	0.050
O35343	Kpna3	Importin subunit alpha-4	6	1.30	0.044
Q8JZV7	Amdhd2	Putative N-acetylglucosamine-6-phosphate deacetylase	7	1.30	0.038
Q9QUM9	Psma6	Proteasome subunit alpha type-6	8	1.30	0.033

Table 3: Proteins up-regulated in the kidneys of $Nrf2^{-/-}$ mice. The expression levels of 81 proteins were found to be increased by at least 30 % ($P \leq 0.05$) in the kidneys of $Nrf2^{-/-}$ mice. Proteins are ordered by fold increase in expression in $Nrf2^{-/-}$ compared with $Nrf2^{+/+}$ mice (n=4-6 animals per group). The average number of peptides used for quantification across all iTRAQ runs is shown for each protein.

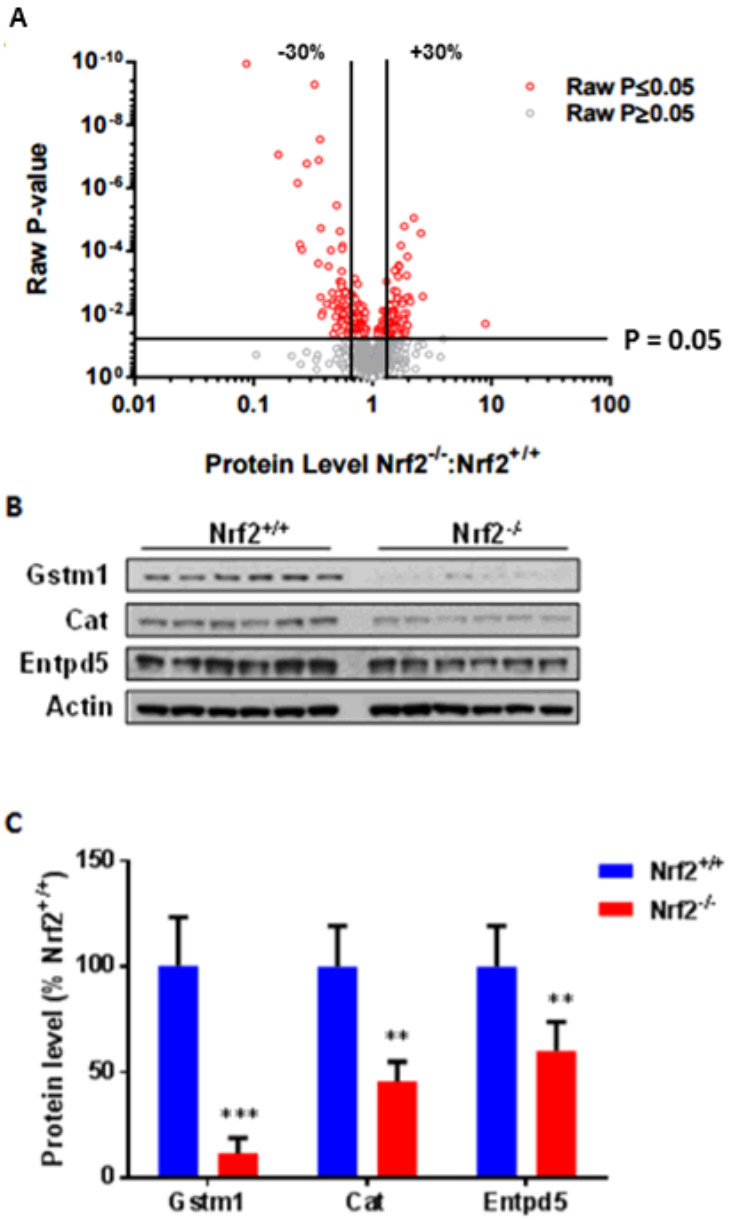

Fig. 3: Basal Nrf2-regulated renal proteome. (A) Volcano plot depicting differentially expressed proteins in the kidneys of $Nrf2^{-/-}$ mice, compared with $Nrf2^{+/+}$ counterparts. Each point represents a single protein. Proteins shown to be differentially expressed (at least ± 30 % change, P ≤ 0.05) are defined in Tables 1 and 2. (B-C) Immunoblot validation of Gstm1, Cat and Entpd5 as proteins with decreased expression in the kidneys of $Nrf2^{-/-}$ mice. (C) Gstm1, Cat and Entpd5 band volumes were quantified by densitometry and normalised to β-actin. Data represent mean + S.D. of n=6 animals per group. Statistical analysis was performed with an unpaired t test; ** $P \leq 0.01$, *** $P \leq 0.001$.

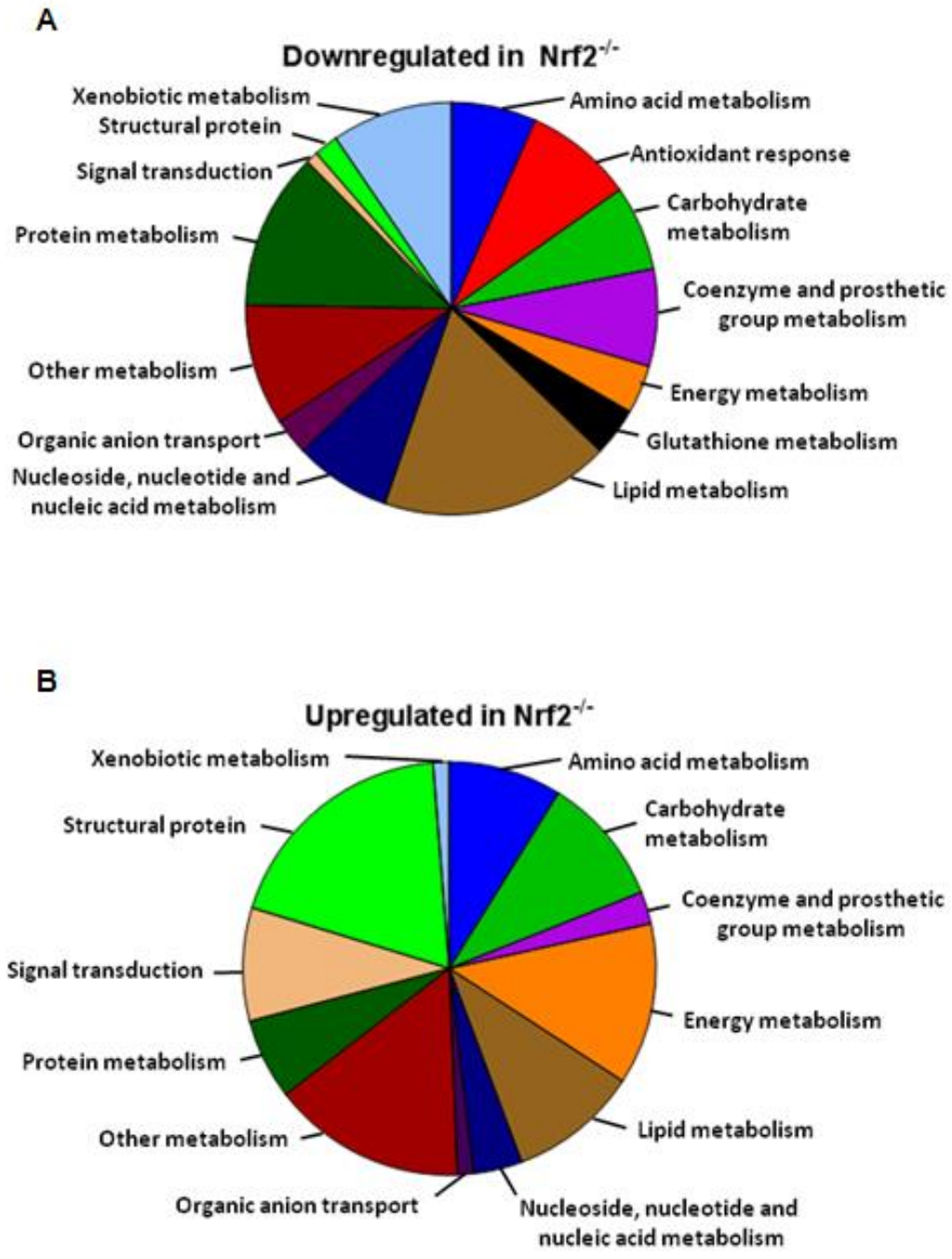

Fig. 4: Manual interrogation of proteins identified in basal iTRAQ study allowed for classification of major biological processes shown to be sensitive to transgenic loss of Nrf2 in the kidney. Proteins that were significantly (A) downregulated (n=108) or (B) upregulated (n=81) in the kidneys of $Nrf2^{-/-}$ mice were functionally categorised according to the UniProt database.

Canonical Pathway	P Value	Ratio	Molecules
Xenobiotic Metabolism Signaling	<0.001	0.04	Gsta3, Gstm1, Abcc2, Nqo1, Aldh8, Gclc, Aldh9a1, Aldh1l1, Ces1, Hsp90ab1, Ugt1a7c, Cat, Aldh5a1
Tryptophan Degradation III (Eukaryotic)	<0.001	0.20	Haao, Acat1, Hsd17b4, Gcdh
NRF2-mediated Oxidative Stress Response	<0.001	0.04	Gsta3, Gstm1, Akr1a1, Prdx1, Abcc2, Cat, Nqo1, Gclc, Txn, Gclm
Aryl Hydrocarbon Receptor Signaling	<0.001	0.05	Gsta3, Aldh1l1, Gstm1, Hsp90ab1, Nqo1, Aldh8a1, Acox3, Aldh5a1, Aldh9a1
Pentose Phosphate Pathway	<0.001	0.30	Pgd, Tkt, G6pd
LPS/IL-1 Mediated Inhibition of RXR Function	<0.001	0.04	Gsta3, Aldh1l1, Gstm1, Acox1, Abcc2, Cat, Aldh8a1, Acox3, Aldh5a1, Aldh9a1
Glutaryl-CoA Degradation	<0.001	0.27	Acat1, Hsd17b4, Gcdh
Glutathione Biosynthesis	<0.001	0.67	Gclc, Gclm, Gss
Serotonin Degradation	<0.001	0.09	Aldh2, Akr1a1, Ugt1a7c, Adh1c, Aldh9a1
Pentose Phosphate Pathway, Oxidative Branch	<0.001	0.50	Pgd, G6pd
Triacylglycerol Degradation	<0.001	0.13	Faah, Ces1, Prdx6
Superoxide Radicals Degradation	0.001	0.33	Cat, Nqo1
Ethanol Degradation II	0.001	0.11	Aldh2, Akr1a1, Adh1c, Aldh9a1
Noradrenaline and Adrenaline Degradation	0.001	0.10	Aldh2, Akr1a1, Adh1c, Aldh9a1
Ketolysis	0.001	0.25	Bdh1, Acat1
Estrogen Biosynthesis	0.001	0.09	Por, Cyp4b1, Hsd17b4
Ketogenesis	0.002	0.20	Bdh1, Acat1
γ-glutamyl Cycle	0.002	0.18	Gclc, Gclm, Gss
Nicotine Degradation III	0.002	0.07	Por, Cyp4b1, Ugt1a7c
Melatonin Degradation I	0.002	0.07	Por, Cyp4b1, Ugt1a7c
Bile Acid Biosynthesis, Neutral Pathway	0.002	0.17	Amacr, Scp2
Superpathway of Melatonin Degradation	0.003	0.07	Por, Cyp4b1, Ugt1a7c
EIF2 Signaling	0.003	0.03	Rpl8, Rps2, Rpl30, Eif3a, Eif4g1, Rpl10a
Nicotine Degradation II	0.004	0.06	Por, Cyp4b1, Ugt1a7c
Tryptophan Degradation X (Mammalian)	0.005	0.12	Aldh2, Akr1a1, Aldh9a1
Ethanol Degradation IV	0.005	0.11	Aldh2, cat, Aldh9a1

Hypoxia Signaling in the Cardiovascular System	0.007	0.05	P4hb, Hsp90a1, Nqo1
Bupropion Degradation	0.008	0.09	Por, Cyp4b1
Gluconeogenesis I	0.008	0.09	Gapdh, Me1
Glutathione-mediated Detoxification	0.008	0.09	Gsta3, Gstm1
Acetone Degradation I (to Methylglyoxal)	0.008	0.09	Por, Cyp4b1
Retinoate Biosynthesis I	0.015	0.06	Aldh8a1, Adh1c
mTOR Signaling	0.021	0.02	Rps2, Eif3a, Eif4g1, Eif4b

Table 4: Biological processes downregulated in the kidneys of $Nrf2^{-/-}$ mice. Proteins identified in the iTRAQ analysis as being expressed at a lower level in the kidneys of $Nrf2^{-/-}$ mice were categorised using Ingenuity Pathway Analysis. Ratio represents the number of proteins in the dataset as a proportion of the total number of proteins comprising each pathway. Proteins populating the highlighted pathways are listed under 'Molecules'.

Canonical Pathway	P value	Ratio	Molecules
ILK Signaling	<0.001	0.05	Map2k4, Flnb, Myh10, TgfB1l1, Parva, Fn1, Myh9, Flna, Actb, Actn4, Actn1
Paxillin Signaling	<0.001	0.06	Map2k4, Parva, Actb, Itga1, Vcl, Actn4, Actn1
Actin Cytoskeleton Signaling	<0.001	0.03	Myh10, Actr2, Fn1, Myh9, Flna, Actb, Mylk, Vcl, Actn4, Actn1
Epithelial Adherens Junction Signaling	<0.001	0.04	Myh10, Actr2, Myh9, Actb, Vcl, Actn4, Actn1
Sertoli Cell-Sertoli Cell Junction Signaling	<0.001	0.03	Map2k4, Sptbn1, Actb, Sptan1, Actn4, Acnt1
Arginine Biosynthesis IV	<0.001	0.40	Oat, Asl
Remodeling: Epithelial Adherens Junctions	<0.001	0.06	Actr2, Actb, Vcl, Actn4, Actn1
Integrin Signaling	<0.001	0.03	Map2k4, Actr2, Parva, Actb, Itga1, Mylk, Vcl, Actn4, Actn1
Ketolysis	0.001	0.25	Oxct1, Hadha
Tight Junction Signaling	0.001	0.03	Myh10, Myh9, Actb, Mylk, Sptan1, Vcl
VEGF Signaling	0.001	0.04	Actb, Vcl, Actn4, Actn1
Superpathway of Citrulline Metabolism	0.002	0.14	Oat, Asl
Leukocyte Extravasation Signaling	0.002	0.03	Map2k4, Actb, Itga1, Vcl, Actn4, Actn1
Calpain Protease Regulation (Mechanical)	0.002	0.04	Vcl, Actn4, Actn1
Agrin Interactions Neuromuscular Junction	0.003	0.04	Map2k4, Pklr, Actb, Itga1
Germ Cell-Sertoli Cell Junction Signaling	0.005	0.03	Map2k4, Actb, Actn4, Actn1
Agranulocyte Adhesion and Diapedesis	0.007	0.02	Myh10, Fn1, Myh9, Actb, Itga1
Virus Entry via Endocytic Pathways	0.007	0.03	Flnb, Flna, Actb, Cltc, Itga1
Fatty Acid β-oxidation I	0.008	0.07	Acaa2, Eci1, Hadha
Inhibition of Angiogenesis by TSP1	0.010	0.06	Map2k4, Hspg2
Inhibition of Matrix Metalloproteases	0.012	0.05	Hspg2, Adam10
Cellular Effects of Sildenafil (Viagra)	0.018	0.02	Myh10, Myh9, Actb, Mylk
Induction of Apoptosis by HIV1	0.027	0.03	Map2k4, Slc25a4
Mitochondrial Dysfunction	0.035	0.02	Map2k4, Ndufb9, Ndufs7, Atp5j2, Ndufa3, Dhodh
Caveolar-mediated Endocytosis Signaling	0.040	0.03	Flnb, Flna, Actb, Itga1

Table 5: Biological processes upregulated in the kidneys of $Nrf2^{-/-}$ mice. Proteins identified in the iTRAQ analysis as being expressed at a higher level in the kidneys of $Nrf2^{-/-}$ mice were categorised using Ingenuity Pathway Analysis. Ratio represents the number of proteins in the dataset as a proportion of the total number of proteins comprising each pathway. Proteins populating the highlighted pathways are listed under 'Molecules'.

In order to ensure that the DMSO treatment had no impact on the expression levels of the reported proteins, an independent iTRAQ analysis of kidney homogenates from untreated $Nrf2^{+/+}$ and $Nrf2^{-/-}$ mice (n=6 per genotype) was performed (Fig. 5), which showed excellent agreement with the primary study. It was therefore concluded that the DMSO vehicle had little effect on the expression levels of Nrf2-regulated proteins in the main iTRAQ study (Tables 2-3, Fig 3). Taken together, these data demonstrate the vital role of Nrf2 in regulating the basal expression of proteins that coordinate of homeostatic processes in the kidney.

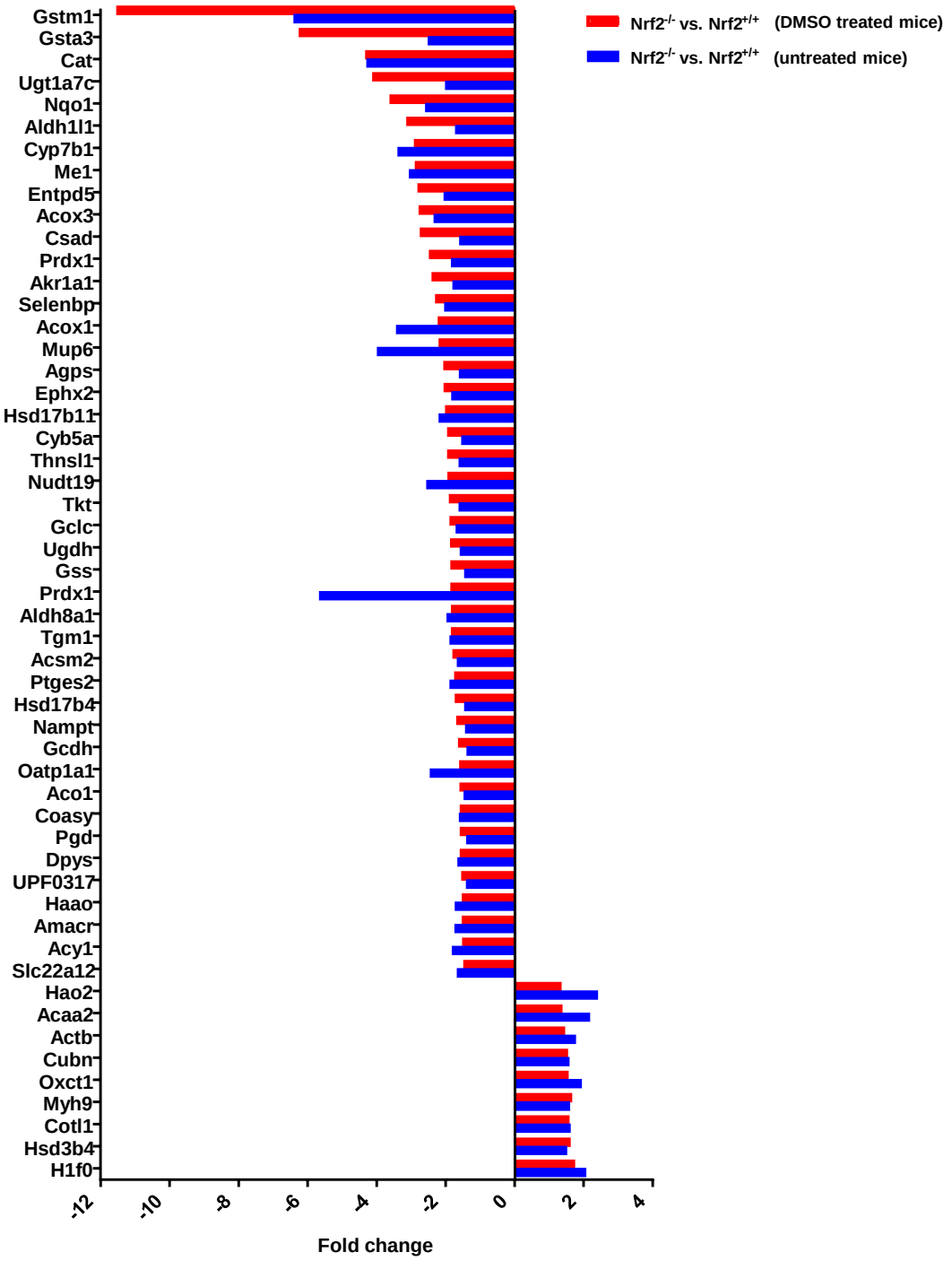

Fig. 5: Comparison of differentially expressed proteins in the kidneys of DMSO treated and untreated Nrf2$^{-/-}$ mice (compared to Nrf2$^{+/+}$). iTRAQ proteomic analysis of kidneys from untreated Nrf2$^{+/+}$ and Nrf2$^{-/-}$ mice was performed to compare the fold change in expression of the indicated proteins (those showing ≥ 50% increase or decrease in expression in the kidneys of vehicle-exposed Nrf2$^{-/-}$ mice) reported in the main data set.

2.3.3 Definition of the CDDO-Me -inducible renal proteome

In light of the recent interest in using the Nrf2 inducer CDDO-Me as a novel treatment for kidney dysfunction (de Zeeuw *et al.*, 2013a), we set out to identify the proteins that were differentially expressed in the kidneys (n=6 per treatment group) of $Nrf2^{+/+}$ mice after dosing with CDDO-Me for 24h (based on the knowledge that 24 h exposure to CDDO-Me (3 mg/kg) elicits an upregulation of Nqo1 in the kidney (Fig. 2), as well as various Nrf2-regulated proteins in the liver (Walsh *et al.*, 2014)). The expression levels of 24 proteins were found to be up-regulated (Table 6), whilst 18 proteins were down-regulated (Table 7), by at least 30 % ($P<0.05$) in animals dosed with CDDO-Me compared with those receiving the vehicle (Fig. 6). Whilst these proteins were not significantly altered by CDDO-Me in $Nrf2^{-/-}$ mice, compared with vehicle control (data not shown), it was notable that, with the exception of Nqo1 (induced 1.4-fold by CDDO-Me, Table 6), none of the 108 proteins that were found to be positively regulated by Nrf2 at the basal level (i.e. their expression was significantly decreased in $Nrf2^{-/-}$ mice compared with $Nrf2^{+/+}$ mice; Table 2) were induced by CDDO-Me under the conditions used. The relatively small number of proteins that were significantly modulated by CDDO-Me in $Nrf2^{+/+}$ mice was reflected in the small number of renal processes that were found to be altered through manual interrogation (Fig. 7A-B) and Ingenuity Pathway Analysis of the iTRAQ data (Tables 8 and 9). Overall, these data suggest that a single dose of CDDO-Me has relatively little effect on the renal expression of proteins that are constitutively regulated by Nrf2 at the basal level.

Accession	Gene	Protein	Peptides	Fold increase	P value
P62858	Rps28	40S ribosomal protein S28	2	2.51	0.012
Q03160	Grb7	Growth factor receptor-bound protein 7	3	1.79	0.009
Q91WK5	Gcsh	Glycine cleavage system H protein, mitochondrial	4	1.74	0.044
Q9DBM2	Ehhadh	Peroxisomal bifunctional enzyme	124	1.66	0.033
P23780	Glb1	Beta-galactosidase	7	1.63	0.031
P50171	Hsd17b8	Estradiol 17-beta-dehydrogenase 8	11	1.60	0.023
Q9DCY0	Keg1	Glycine N-acyltransferase-like protein Keg1	76	1.55	0.014
P42703	Lifr	Leukemia inhibitory factor receptor	2	1.50	0.011
Q8VE95	-	UPF0598 protein C8orf82 homolog	4	1.46	0.029
Q8BU88	Mrpl22	39S ribosomal protein L22, mitochondrial	2	1.44	0.048
P48758	Cbr1	Carbonyl reductase [NADPH] 1	14	1.41	0.009
Q8K010	Oplah	5-oxoprolinase	26	1.40	0.008
Q9JHJ3	-	Lysosomal protein NCU-G1	2	1.40	0.049
Q9Z2J0	Slc23a1	Solute carrier family 23 member 1	9	1.39	0.002
Q60649	Clpb	Caseinolytic peptidase B protein homolog	4	1.39	0.011
Q6PDY2	Ado	2-aminoethanethiol dioxygenase	2	1.38	0.048
Q62219	Tgfb1i1	Transforming growth factor beta-1-induced transcript 1 protein	2	1.36	0.022
Q64669	Nqo1	NAD(P)H dehydrogenase [quinone] 1	4	1.36	0.001
Q9CYW4	Hdhd3	Haloacid dehalogenase-like hydrolase domain-containing protein 3	4	1.34	0.008
Q8BGB2	Ttc7a	Tetratricopeptide repeat protein 7A	3	1.33	0.025
Q99J99	Mpst	3-mercaptopyruvate sulphurtransferase	8	1.33	0.009
Q8R5L3	Vps39	Vam6/Vps39-like protein	2	1.32	0.044
Q3TLP5	Echdc2	Enoyl-CoA hydratase domain-containing protein 2, mitochondrial	20	1.32	0.045
Q9Z0N1	Eif2s3x	Eukaryotic translation initiation factor 2 subunit 3, X-linked	9	1.31	0.028

Table 6: Proteins up-regulated by CDDO-Me in the kidneys of $Nrf2^{+/+}$ mice. The expression levels of 24 proteins were found to be increased by at least 30 % ($P \leq 0.05$) in the kidneys of $Nrf2^{+/+}$ mice following a single i.p. injection of CDDO-Me (3 mg/kg). Proteins are ordered by fold increase in expression in CDDO-Me -exposed compared with vehicle-exposed mice (n=4-6 animals per group). The average number of peptides used for quantification across all iTRAQ runs is shown for each protein. None of the proteins were found to be up-regulated by CDDO-Me in the kidneys of $Nrf2^{-/-}$ mice (data not shown).

Accession	Gene	Protein	Peptides	Fold decrease	P value
Q00623	Apoa1	Apolipoprotein A-I	37	1.81	0.015
Q9D0J8	Ptms	Parathymosin	7	1.75	0.009
Q60692	Psmb6	Proteasome subunit beta type-6	3	1.70	0.045
P26040	Ezr	Ezrin	48	1.57	0.004
Q9D0E1	Hnrnpm	Heterogeneous nuclear ribonucleoprotein M	6	1.56	0.021
P97384	Anxa11	Annexin A11	11	1.48	0.002
Q8BIQ5	Cstf2	Cleavage stimulation factor subunit 2	1	1.39	0.034
P08113	Hsp90b1	Endoplasmin	45	1.38	0.049
Q91WS0	Cisd1	CDGSH iron-sulphur domain-containing protein 1	14	1.38	0.013
Q80UM3	Naa15	N-alpha-acetyltransferase 15, NatA auxiliary subunit	3	1.36	0.026
P19258	Mpv17	Protein Mpv17	3	1.35	0.042
P23116	Eif3a	Eukaryotic translation initiation factor 3 subunit A	13	1.34	0.018
Q8VE97	Srsf2	Serine/arginine-rich splicing factor 4	4	1.34	0.046
Q6P1B1	Xpnpep1	Xaa-Pro aminopeptidase 1	11	1.33	0.012
Q9CY58	Serbp1	Plasminogen activator inhibitor 1 RNA-binding protein	2	1.32	0.009
Q9Z0X1	Aifm1	Apoptosis-inducing factor 1, mitochondrial	38	1.32	0.048
P06151	Ldha	L-lactate dehydrogenase A chain	43	1.32	0.022
P25444	Rps2	40S ribosomal protein S2	21	1.30	0.020

Table 7: Proteins down-regulated by CDDO-Me in the kidneys of $Nrf2^{+/+}$ mice. The expression levels of 18 proteins were found to be decreased by at least 30 % ($P \leq 0.05$) in the kidneys of $Nrf2^{+/+}$ mice following a single i.p. injection of CDDO-Me (3 mg/kg). Proteins are ordered by fold decrease in expression in CDDO-Me -exposed compared with vehicle-exposed mice (n=4-6 animals per group). The average number of peptides used for quantification across all iTRAQ runs is shown for each protein. None of the proteins were found to be down-regulated by CDDO-Me in the kidneys of $Nrf2^{-/-}$ mice (data not shown).

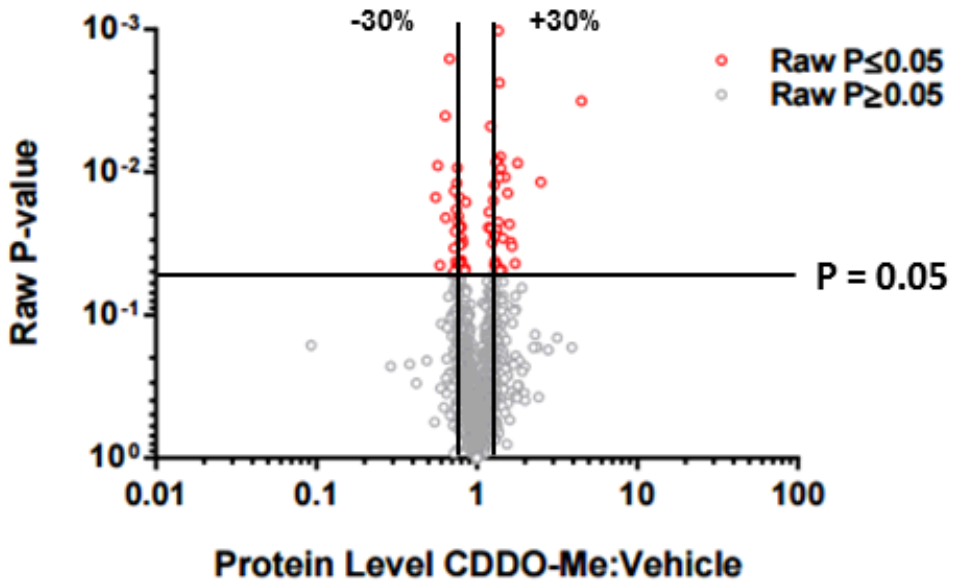

Fig. 6: CDDO-Me-inducible renal proteome. Volcano plot depicting differentially expressed proteins in the kidneys of $Nrf2^{+/+}$ mice 24 h after receiving a single i.p. injection of CDDO-Me (3 mg/kg), compared with vehicle control. Each point represents a single protein. Proteins shown to be differentially expressed (at least ± 30 % change, $P \leq 0.05$) are defined in Tables 5 and 6.

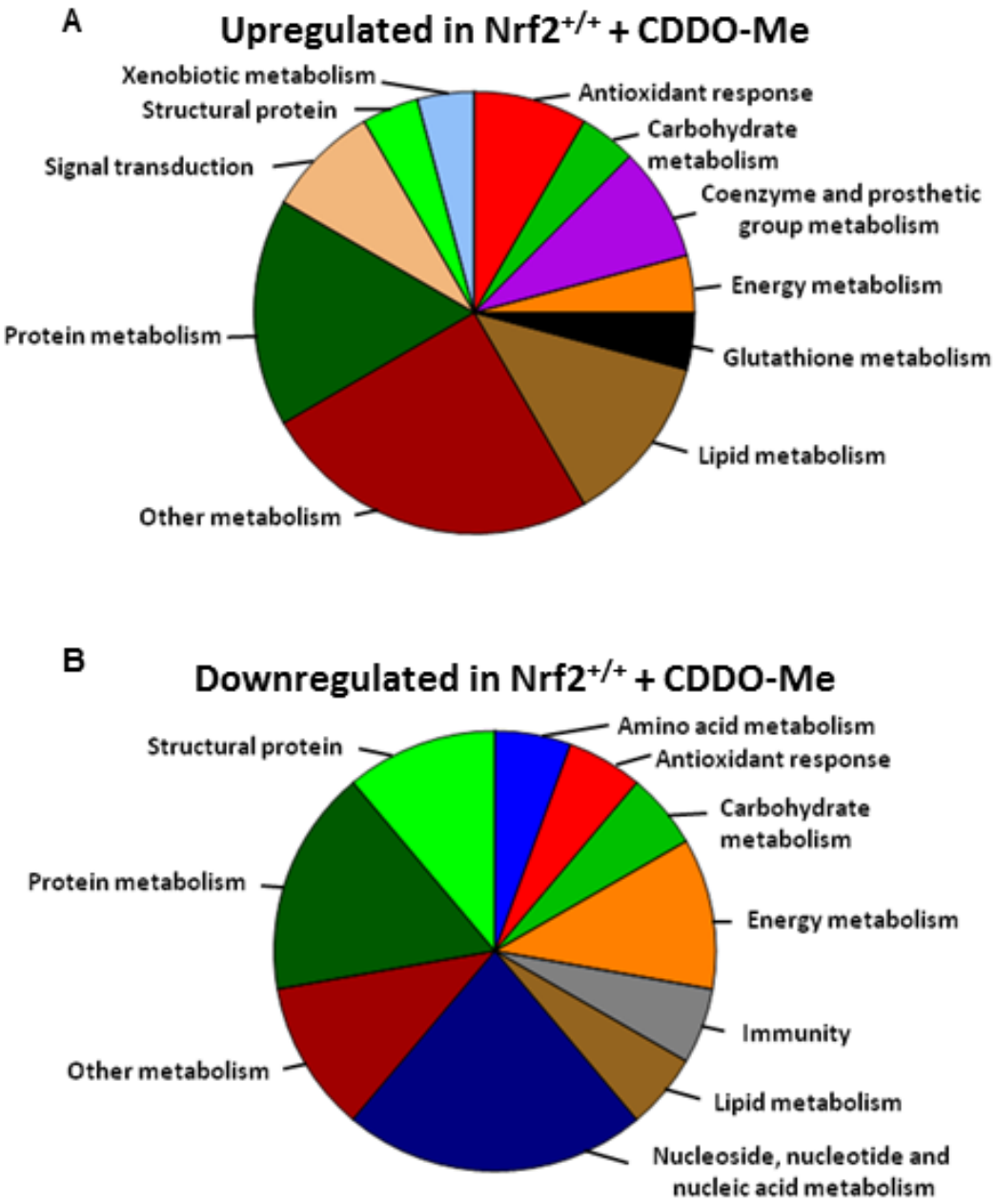

Fig. 7: Major biological processes shown to be sensitive to induction of Nrf2 activity in the kidney. Proteins that were significantly (A) upregulated (n=24) or (B) downregulated (n=18) in the kidneys of $Nrf2^{+/+}$ mice exposed to CDDO-Me ere functionally categorised according to the UniProt database.

Canonical Pathway	P value	Ratio	Molecules
Glutaryl-CoA Degradation	<0.001	0.18	Echdc2, Hsd17b8
Tryptophan Degradation III (Eukaryotic)	<0.001	0.10	Echdc2, Hsd17b8
Fatty Acid β-oxidation I	<0.001	0.07	Echdc2, Hsd17b8
NRF2-mediated Oxidative Stress Response	0.013	0.01	Nqo1, Cbr1
EIF2 Signaling	0.040	0.01	Rps28, Eif2s3

Table 8: Biological processes upregulated by CDDO-Me in the kidneys of $Nrf2^{+/+}$ mice. Proteins identified in the iTRAQ analysis as being expressed at a higher level in the kidneys of CDDO-Me treated $Nrf2^{+/+}$ mice were categorised using Ingenuity Pathway Analysis. Ratio represents the number of proteins in the dataset as a proportion of the total number of proteins comprising each pathway. Proteins populating the highlighted pathways are listed under 'Molecules'

Canonical Pathway	P value	Ratio	Molecules
Hypoxia Signaling, Cardiovascular System	0.002	0.03	Hsp90b1, Ldha
Regulation of eIF4 and p70S6K Signaling	0.009	0.01	Rps2, Eif3a
PPARα/RXRα Activation	0.013	0.01	Hsp90b1, Apoa1, Stat5b
EIF2 Signaling	0.013	0.01	Rps2, Eif3a
mTOR Signaling	0.014	0.01	Rps2, Eif3a

Table 9: Biological processes downregulated by CDDO-Me in the kidneys of $Nrf2^{+/+}$ mice. Proteins identified in the iTRAQ analysis as being expressed at a lower level in the kidneys of CDDO-Me treated $Nrf2^{+/+}$ mice were categorised using Ingenuity Pathway Analysis. Ratio represents the number of proteins in the dataset as a proportion of the total number of proteins comprising each pathway. Proteins populating the highlighted pathways are listed under 'Molecules'**2.**

2.3.4 Validation of CDDO-Me dosing

The data presented in Tables 6-9 and Fig. 6-7 demonstrate that a single dose of CDDO-Me failed to augment the expression of proteins, other than Nqo1, that were shown to be regulated by Nrf2 at the basal level in the mouse kidney. The lack of appreciable induction of Nrf2 signalling by CDDO-Me in this study may be due to the exposure of the animals to a single dose of the compound for a fixed 24 h period, although this previously was found to be sufficient to induce a large number of Nrf2-regulated proteins in the mouse liver (Walsh *et al.*, 2014). It is plausible that the induction of different Nrf2-regulated proteins may proceed under distinct timeframes. Fig. 8 depicts immunoblotting of whole kidney homogenates for known Nrf2-regulated proteins, in an attempt to determine if the selected time period and dose of CDDO-Me used in the iTRAQ analysis (3 mg/kg for 24 hours) was sub-optimal. Mice were treated with a range of doses of CDDO-Me for 24 hours, with appreciable increase in Nqo1 and Gstm1 expression noted following a dose of 3 mg/kg (Fig. 8A-B). Consequently, mice were dosed with 3 mg/kg CDDO-Me for different times, with appreciable induction of Nqo1 at ≥ 24 h being the only statistically significant result (Fig. 8C-D). Therefore, it was determined that, whilst CDDO-Me significantly induces the expression of Nqo1, a single dose of the compound has relatively little effect on the renal expression of proteins that are constitutively regulated by Nrf2 at the basal level.

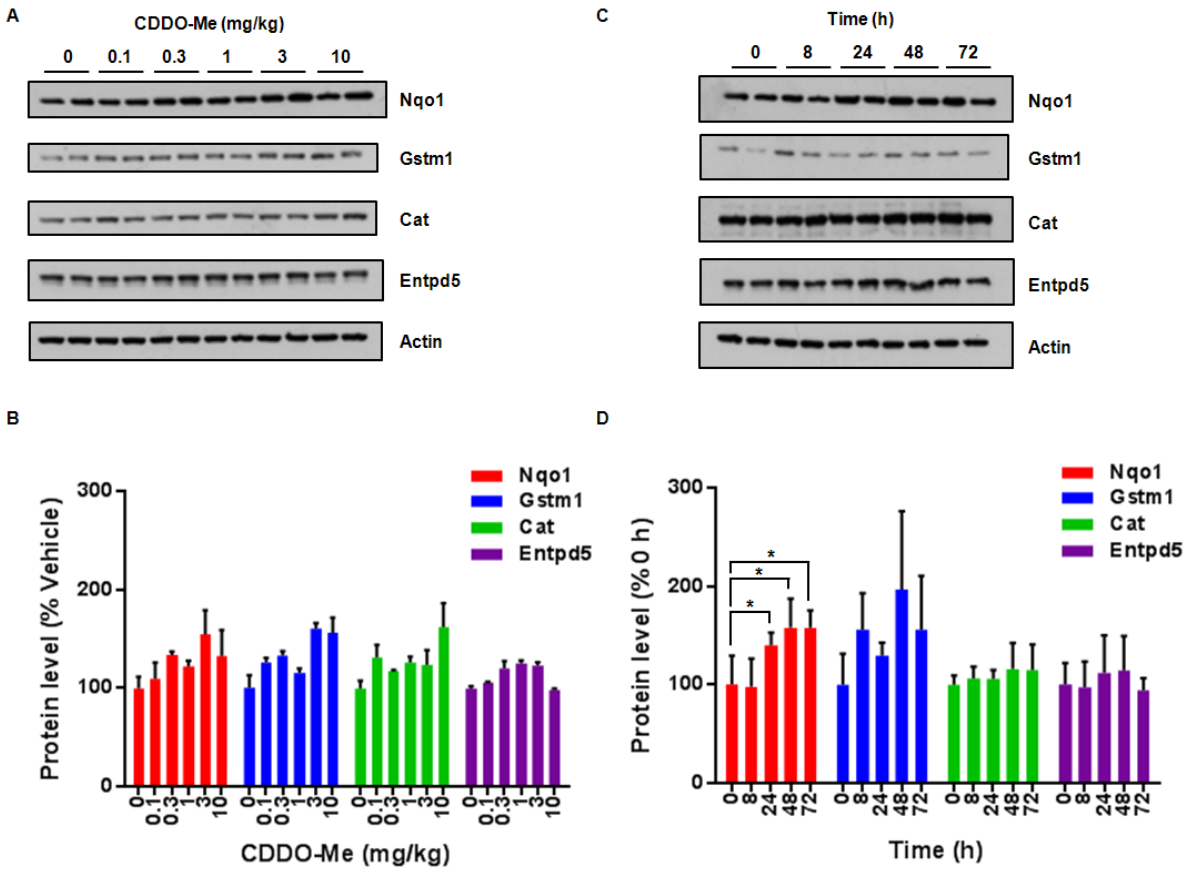

Fig. 8: Validation of CDDO-Me dosing. (A,B) Mice were treated with the indicated doses of CDDO-Me for 24 h, and whole kidney homogenates were probed for Nqo1, Gstm1, Cat, Entpd5 and Actin by immunoblotting. (C,D) Mice were treated with 3 mg/kg CDDO-Me for the indicated times, and whole kidney homogenates were probed as (A,B). Protein band volumes were quantified by densitometry and normalised against β-actin. (A,B) Data represent the mean + S.D. of n=2 animals per group, (C,D) Data represent the mean + S.D. of n=4 animals per group (representative samples from n=2 animals shown). Statistical analysis was performed with an unpaired t test; *, $p \leq 0.05$.

2.3.5 Comparative analysis of the expression of Nrf2-regulated proteins in the kidney and liver

It has been previously determined that CDDO-Me induces the hepatic expression of 6 proteins that are regulated by Nrf2 at the basal level in the mouse liver (Walsh *et al.*, 2014). However, in the mouse kidney only Nqo1 appears to be sensitive to both inhibition and induction of Nrf2 (Tables 2 and 6). To provide insight into why CDDO-Me appears to have relatively little effect on the expression of Nrf2-regulated proteins in the kidney, the basal expression levels of four representative proteins known to be regulated by Nrf2 in the liver (Walsh *et al.*, 2014) and the kidney (Table 2) were analysed by immunoblotting of tissue homogenates from $Nrf2^{+/+}$ mice (Fig. 9). The expression of Nqo1 was found to be 9-fold higher in the kidney than the liver; however Gstm1 expression was over 3-fold lower in the kidney. Additionally, there was no difference in expression of Cat and Entpd5 between the tissues. These data argue against the kidney being less sensitive to pharmacological induction of Nrf2 by CDDO-Me as a result of having a generally high basal level of Nrf2 activity. Therefore, further work is required to define the ability of CDDO-Me to augment Nrf2-regulated processes in the kidney.

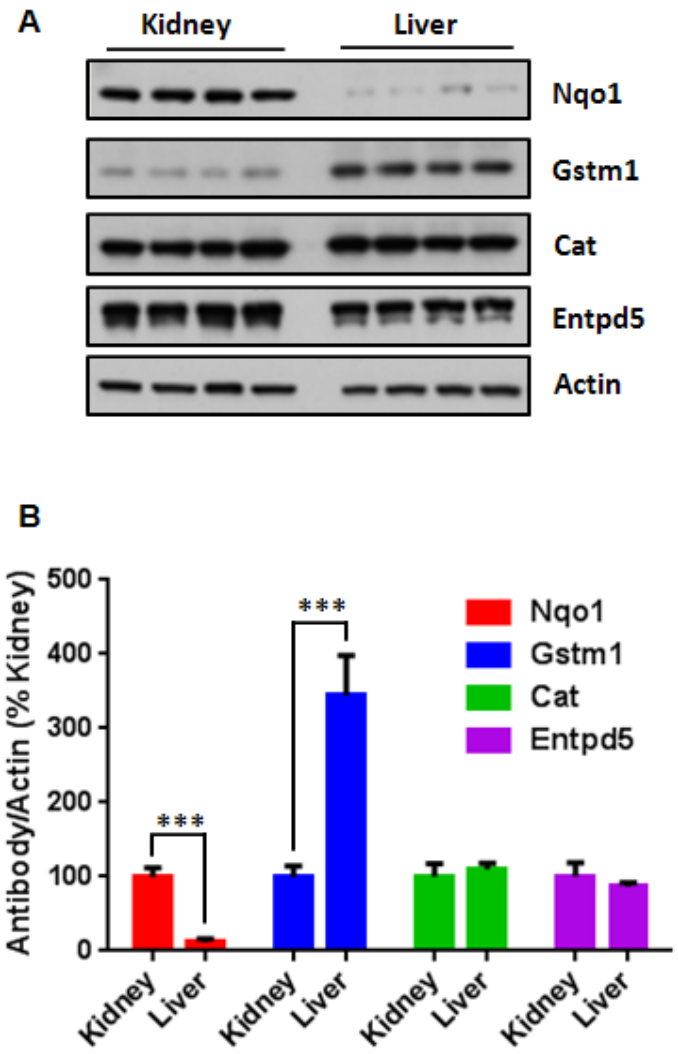

Fig. 9: Basal expression of Nrf2-regulated proteins in the kidneys and livers of $Nrf2^{+/+}$ mice. (A) Nqo1, Gstm1, Cat, Entpd5 and Actin levels were determined by immunoblotting. (B) Protein band volumes were quantified by densitometry and normalised against β-actin, and expressed as % of kidney expression. Data represent mean + S.D. of n=4 animals per group. Statistical analysis was performed with an unpaired t test; ***, $p \leq 0.001$.

2.3.6 Transcriptional regulation of Nrf2-regulated proteins in the kidney

In order to examine the mechanisms behind the lack of appreciable increase in Nrf2-regulated protein expression following CDDO-Me induction, targeted PCR was performed on a panel of genes encoding for proteins that were found to be regulated by Nrf2 at the basal level (Table 2). The differential expression of this sub-set of genes in the kidneys of $Nrf2^{-/-}$, compared to $Nrf2^{+/+}$, mice showed excellent agreement with the iTRAQ data (Fig. 10), but also showed that CDDO-Me has more of a discernible effect on Nrf2-regulated genes at the transcriptional level (Fig. 10). It is likely that the acute dosing regimen used in the study did not allow these transcriptional effects to be translated fully to changes at the protein level (Schwanhausser *et al.*, 2011).

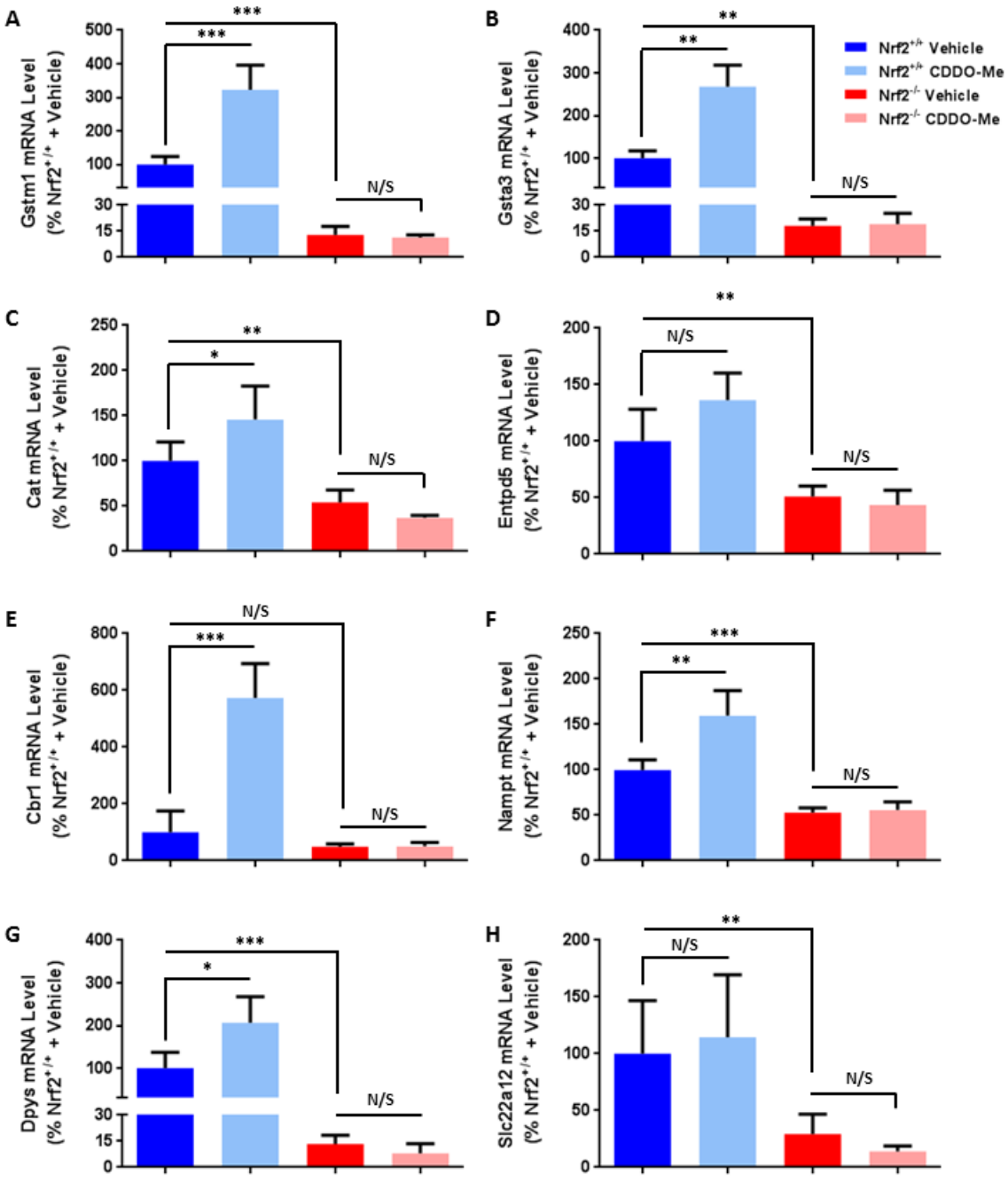

Fig. 10: Genes sensitive to genetic inhibition and/or pharmacological induction of Nrf2 in the mouse kidney. A panel of genes encoding for proteins that were found to be significantly downregulated in the kidneys of $Nrf2^{-/-}$ mice by iTRAQ (Table 2) were chosen for qRT-PCR analysis. Gene expression levels are normalised to Ppia. Data represent mean + S.D. of n=6 animals per group. Statistical analysis of qPCR data was performed with an unpaired t test or Mann-Whitney test, * $P \leq 0.05$; ** $P \leq 0.01$; *** $P \leq 0.001$; *N.S.* non-significant.

2.3.7 Nrf2 regulates the provision of NADPH and GSH in the kidney

Following iTRAQ analysis, it was noted that numerous proteins in the $Nrf2^{-/-}$ mouse were involved in the synthesis and metabolism of both NADPH (Nampt, G6pd, Pgd, etc.) and GSH (Gclc, Gss, Gst, etc.). Whole kidney homogenates were analysed for NADPH content (Fig. 11A), where it was determined that there was a 35 % reduction in total NADPH in kidneys from $Nrf2^{-/-}$ mice compared with $Nrf2^{+/+}$ mice, supporting a role for Nrf2 as a regulator of energy homeostasis highlighted in this and other research ((Wu *et al.*, 2011a). Total GSH was decreased by 30% in the $Nrf2^{-/-}$ mouse kidney compared with $Nrf2^{+/+}$ counterparts (Fig. 11B), reflecting the reduction in expression of proteins involved in GSH metabolism in the $Nrf2^{-/-}$ mouse. No difference in total NADPH or GSH was seen in the kidneys of $Nrf2^{+/+}$ mice treated with CDDO-Me, likely due to the acute dosing regimen of this study.

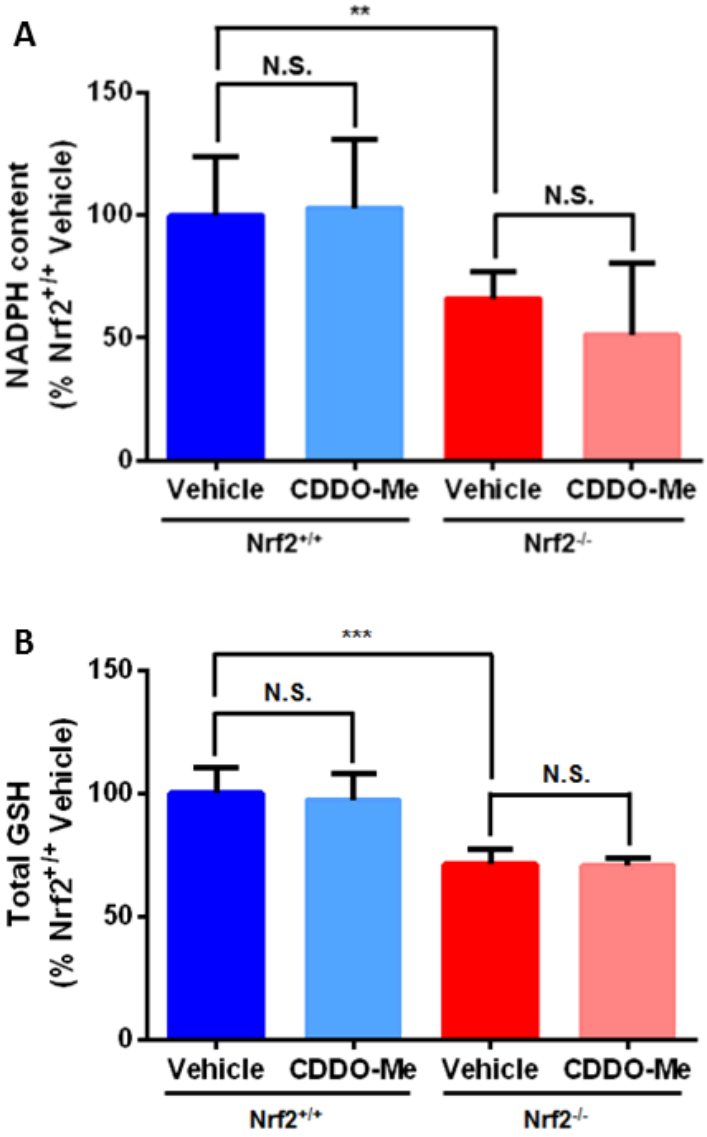

Fig. 11: Quantification of (A) total NADPH and (B) total GSH was performed on kidney lysates from $Nrf2^{+/+}$ or $Nrf2^{-/-}$ mice treated with vehicle (DMSO) or CDDO-Me for 24 h. Both NADPH content and GSH content are expressed as a percentage of vehicle-treated $Nrf2^{+/+}$ mice. Data represent mean + S.D. of n=8 animals per group. Statistical analysis was performed using an unpaired t test; **, $P \leq 0.01$, ***, $P \leq 0.001$, N.S., non-significant.

2.3.8 Histological examination of Nqo1 activity in the kidney

In light of the heterogeneous anatomical nature of the kidney, and to provide a histological insight into the role of Nrf2 in the regulation of renal homeostatic processes, we performed immunohistochemical analyses of kidney tissue from the previous experiments. Given the presence of the non-functional Nrf2 protein in the $Nrf2^{-/-}$ mice (described previously), immunohistochemical staining for Nqo1 was used instead. Consistent with our iTRAQ and qRT-PCR data indicating that Nqo1 is highly sensitive to modulation of Nrf2 activity in the kidney, there was a significant decrease in Nqo1 staining in the renal cortex of $Nrf2^{-/-}$ mice, compared with $Nrf2^{+/+}$ counterparts (Fig. 12). Furthermore, there was a significant increase in Nqo1 staining in the cortex of $Nrf2^{+/+}$ mice in response to CDDO-Me (Fig. 12). Qualitative analysis of the tissue sections indicated that Nqo1 staining was highest in the proximal tubules of these animals, consistent with Nrf2's established role in in the protection of mice against proximal tubule-specific nephrotoxins (Shelton *et al.*, 2013). Nqo1 staining is particularly high within the S3 segment of the proximal tubule, consistent with their known susceptibility to nephrotoxix injury (Aleksunes *et al.*, 2010) and likely requirement for a dynamic Nrf2 response. Taken together, these data further confirm the role of Nrf2 in regulating the renal expression of cytoprotective genes, particularly in the cortex of the mouse kidney.

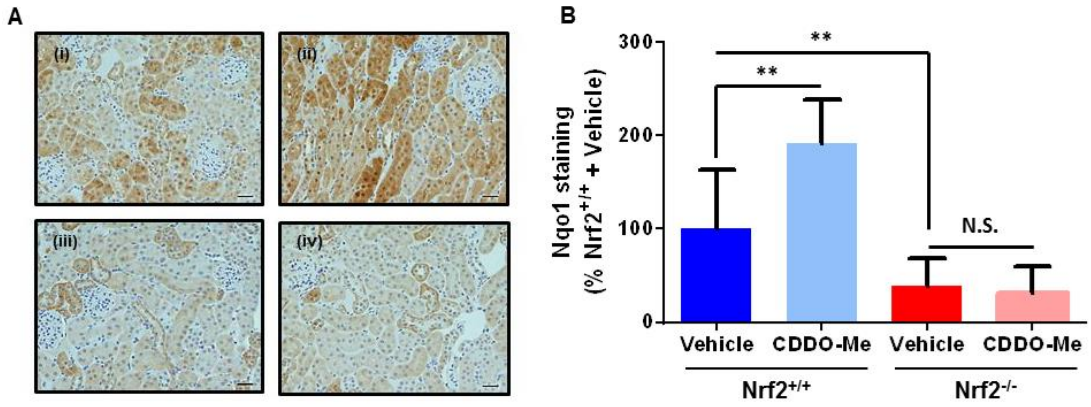

Fig. 12: Histological examination of Nqo1 activity in the kidney. Images in (A) are representative of immunohistochemical staining for Nqo1 in the cortex of $Nrf2^{+/+}$ mice 24 h after receiving a single i.p. injection of (i) DMSO or (ii) CDDO-Me (3 mg/kg), or $Nrf2^{-/-}$ mice 24 h after receiving a single i.p. injection of (iii) DMSO or (iv) CDDO-Me. Scale bars represent 100 µm. Data represent mean + S.D. of n=5 animals per group. Statistical analysis was performed with an unpaired T test, ;, ***, $P \leq 0.01$, N.S. not-significant .

2.4 Discussion

Nrf2 is a critical regulator of mammalian cell defence against various forms of stress (Bryan *et al.*, 2013). As a result, Nrf2 has become an attractive therapeutic target in numerous pathological contexts (Copple, 2012). Indeed, dimethyl fumarate has recently become the first Nrf2-inducing drug to be licensed for clinical use, in patients with relapsing-remitting multiple sclerosis (Lee *et al.*, 2013). A detailed understanding of the biological processes that are modulated by Nrf2 inducers will be critical to the development of such compounds as next-generation drug candidates, yet, aside from focused gene expression analyses (Aleksunes *et al.*, 2010), such studies are noticeably lacking in the kidney, despite an increasing interest in the use of Nrf2 inducers and other antioxidants for the treatment of renal pathologies (Ruiz *et al.*, 2013). In order to address this knowledge gap, we have performed a global proteomic analysis of the battery of proteins that are regulated by Nrf2 in the mouse kidney.

The findings of this study demonstrate that the kidneys of $Nrf2^{-/-}$ mice are deficient in proteins that maintain cellular redox balance, mediate the synthesis and conjugation of glutathione (the effects of which are demonstrated functionally as a decrease in the level of total GSH in the $Nrf2^{-/-}$ mouse kidney, Fig. 11B) and control the metabolism and disposition of a wide range of xenobiotics. Moreover, and consistent with recent reports indicating that Nrf2 regulates core metabolic processes that promote the proliferation of cancer cells (Mitsuishi *et al.*, 2012), as well as hepatic NADPH levels (Wu *et al.*, 2011a), we noted that a substantial proportion of the proteins expressed at a lower level in the kidneys of $Nrf2^{-/-}$ mice,

compared with their $Nrf2^{+/+}$ counterparts, are known to regulate pyruvate metabolism, glycolysis, the supply of NADPH, and the synthesis and recycling of amino acids (Tables 2, 4 and 5). The examination of NADPH supply in renal homogenates from the mice (Fig. 11) confirmed that the reduction in expression of proteins involved in the synthesis and metabolism of NADPH in the $Nrf2^{-/-}$ mouse had an effect on NADPH availability, therefore Nrf2 appears to play an important role in maintaining renal homeostasis by supporting anabolic processes and the provision of cellular fuel.

The decreased activity of the above processes likely contributes to the enhanced susceptibility of $Nrf2^{-/-}$ mice to various renal insults (Shelton *et al.*, 2013). Indeed, it has been shown that Nqo1, shown here to be the protein that is most sensitive to genetic inhibition and pharmacological induction of renal Nrf2 activity, directly protects against cisplatin nephrotoxicity in mice (Gang *et al.*, 2013; Oh *et al.*, 2013). Therefore, modulation of Nrf2 activity may be an attractive strategy for antagonising stresses that are associated with the development of acute kidney injury.

CDDO-Me had shown promise as a novel treatment for chronic kidney disease (Pergola *et al.*, 2011b), until the recent termination of the phase III BEACON trial due to adverse cardiovascular events for which the underlying mechanisms are currently under investigation (de Zeeuw *et al.*, 2013b; Chin *et al.*, 2014b). Whilst CDDO-Me and its analogues have been shown to protect against AKI and enhance Nrf2 signalling in animal models (Tanaka *et al.*, 2008; Aleksunes *et al.*, 2010; Wu *et al.*, 2011b), a role for Nrf2 in the improved estimated glomerular filtration rate

observed in patients has yet to be demonstrated, to our knowledge. In this study, we determined that a single acute exposure to CDDO-Me failed to augment the expression of proteins, other than Nqo1, that were shown to be regulated by Nrf2 at the basal level in the mouse kidney.

Indeed, qRT-PCR analysis of the expression of genes whose proteins found to be regulated by Nrf2 at the basal level suggests that CDDO-Me augments their expression (Fig. 10), however its pharmacodynamic effects were less pronounced at the protein level. The lack of appreciable induction of Nrf2-regulated proteins by CDDO-Me in this study may be due to the exposure of the animals to a single dose of the compound, and that the induction of different Nrf2-regulated proteins may proceed under distinct timeframes (Fig. 8). Therefore, a more detailed validation of the dose and time-dependent response of Nrf2 to CDDO-Me could have improved the design of the current study. Chronic stimulation may be necessary to provoke meaningful changes in the expression of Nrf2-regulated proteins in the kidney, however a recent study has demonstrated only minimal induction of such renal targets in a mouse model of systemic lupus erythematosus, following administration of CDDO-Me (3mg/kg) three times per week for two months (Wu *et al.*, 2014b). It is possible that alternative pharmacological modulators may stimulate renal Nrf2 signalling to a greater degree than CDDO-Me, due to pharmacodynamic and/or -kinetic factors. Therefore, in order to better understand the potential value of Nrf2 inducers as novel treatments for renal disease, further work is required to define the scope of small molecules such as CDDO-Me to augment Nrf2-regulated processes in the human kidney.

We have found that the basal Nrf2-regulated renal proteome (108 proteins with reduced expression levels in $Nrf2^{-/-}$ mice, described here) is larger than the equivalent hepatic proteome (45 proteins (Walsh *et al.*, 2014)), yet only one protein (Nqo1) was found to be sensitive to both inhibition and acute pharmacological induction of Nrf2 in the kidney (Tables 2 and 6), compared with six proteins (Cyp2a5, Gstm3, Gstm1, Entpd5, Udgh and Ephx1) in the liver (Walsh *et al.*, 2014). The qRT-PCR data, however, shows that the expression of Nqo1, Gstm1, Gsta3, Cat, Nampt and Dpys are altered in response to both genetic inhibition and acute pharmacological induction of Nrf2 (Fig. 10), suggesting that CDDO-Me has more of an effect at the transcriptional level, at least within the timeframe of this study. Therefore, whilst this data confirms that CDDO-Me can induce Nrf2-regulated genes in the mouse kidney, further work is required to define its ability to augment Nrf2-regulated proteins in this context.

One limitation of the experimental design of this study is the use, due to technical limitations, of homogenised whole kidney tissues, which, taking into account the heterogenous nature of the cells of the kidney, could have resulted in an effective dilution of the effects of genetic and/or pharmacological modulation of Nrf2 in specific regions of the kidney. It would therefore be of interest to use laser-capture microdissection to isolate specific regions of the kidney in order to examine the regulatory roles of Nrf2 in more detail. Indeed, the mice themselves are a constitutive $Nrf2^{-/-}$ model, so systemic changes are also evident where they might not be in a renal- or proximal tubule-specific $Nrf2^{-/-}$ model.

The tissue specific activity of Nrf2 is further evidenced by examination of the expression profiles of proteins that were recently shown to be sensitive to genetic inhibition or pharmacological induction of Nrf2 in the mouse liver (Walsh *et al.*, 2014). One third of these proteins were found here to be similarly regulated by Nrf2 in the kidney, indicating that whilst there is some overlap in the biological processes Nrf2 controls in discrete organs, there is clearly a degree of tissue specificity in its transcriptional activity. This is exemplified by data from Yates et al demonstrating the differential induction of Nqo1 mRNA in various mouse tissues following a single 6 h exposure to CDDO-Me or its structural analogues (Yates *et al.*, 2007), and the data in Fig. 9.

The exact molecular roles that some of the described proteins play in the regulation of different homeostatic processes in the kidney should be further explored, for example via siRNA knockdown in renal cells. ChIP sequencing of Nrf2-regulated genes has been performed in lymphoid cells treated with sulphoraphane (Chorley *et al.*, 2012), and in $Nrf2^{-/-}$ and $Keap1^{-/-}$ mouse embryonic fibroblasts (Malhotra *et al.*, 2010), and whilst both studies delineate multiple novel targets of Nrf2, they did not use primary (nor renal) tissue, an advantage of this study. ChIP sequencing of renal tissue from the $Nrf2^{+/+}$ and $Nrf2^{-/-}$ mice, treated with CDDO-Me or vehicle, would complement this work to build a full genomic, transcriptomic and proteomic picture of the renal regulatory roles of Nrf2.

Several animal studies have provided evidence for the downregulation of the Nrf2 pathway during the pathogenesis of kidney disease. Indeed, Vaziri and colleagues have observed a higher burden of oxidative stress and a lower level of expression of

Nrf2 and its target genes, linked to an increase in the level of Keap1, in rat models of spontaneous focal glomerulosclerosis (Kim *et al.*, 2011), surgical nephrectomy (Kim *et al.*, 2010) and tubulo-interstitial nephropathy (Aminzadeh *et al.*, 2013a). Furthermore, it has been shown that aged female $Nrf2^{-/-}$ mice develop lupus-like autoimmune nephritis (Yoh *et al.*, 2001), whilst genetic ablation of Nrf2 enhances sensitivity to hyperglycemia-induced renal dysfunction (Yoh *et al.*, 2008). These findings imply that the dysfunction of the Nrf2 pathway, and the resulting impaired capacity to manage levels of oxidative stress, at least partly contributes to the progression of different forms of kidney disease.

In summary, we have provided evidence that Nrf2 regulates the expression of an array of proteins that contribute to cell defence and the maintenance of homeostasis in the kidney. These data support the current interest in Nrf2 as a novel therapeutic target in a number of renal diseases, and provide insight into the means by which Nrf2 protects against acute renal insults.

Chapter 3

Identification of novel Nrf2-regulated microRNAs in the mouse kidney

Contents

3.1 Introduction

MicroRNAs are a recently discovered RNA-regulatory element serving to negatively regulate the expression of genes involved in numerous important cellular processes. MicroRNAs within introns or exons of protein coding genes are transcribed by RNA polymerase II (Lee *et al.*, 2004), whereas microRNAs without sequences in introns or exons are transcribed via RNA polymerase II or III, depending on the presence of the relevant promoter (Bartel, 2004; Zhou *et al.*, 2008; Schanen *et al.*, 2011). MicroRNAs may also participate in regulatory loops to modulate their expression; for example, miR-145 is a pro-apoptotic microRNA dependent on p53 activation, and this activation itself can stimulate miR-145 expression in an apoptosis-promoting loop (Spizzo *et al.*, 2010).

MicroRNA profiles can be both organism-specific and tissue-specific (Starkey Lewis *et al.*, 2011), leading to an interest in their use as biomarkers of physiological and pathological events (Waldman *et al.*, 2008). For example, miR-122, which is highly enriched in hepatocytes, has recently been described as a novel blood-based marker of drug-induced liver injury in mice and humans (Starkey Lewis *et al.*, 2011).

Multiple microRNAs have been implicated in the regulation of Nrf2 expression, including miR-28, which targets the 3'UTR of Nrf2 mRNA in HEK cells to prevent its translation (Yang *et al.*, 2011). Additionally, miR-144 downregulates Nrf2 protein levels when overexpressed in a neuronal cell line (Narasimhan *et al.*, 2012), miR-93 downregulates Nrf2 expression when ectopically expressed in a human breast epithelial cell line (Singh *et al.*, 2013) and the induction of miR-34 results in decreased Nrf2 expression in HEK cells (Li *et al.*, 2011b).

Ochratoxin A (OTA) nephrotoxicity results in reduced Nrf2 expression, and concomitantly induced ROS levels (Stachurska *et al.*, 2013). Further investigation has revealed that OTA-mediated induction of miR-132 downregulates Nrf2 expression in porcine renal proximal tubular cells, whilst inhibition of this microRNA counteracts OTA toxicity (Stachurska *et al.*, 2013).

Research into microRNA-regulation of Nrf2 expression is ongoing (Li *et al.*, 2011b; Narasimhan *et al.*, 2012), however the exact role that Nrf2 itself plays in the regulation of microRNA expression is relatively unexplored. There is data demonstrating the involvement of microRNAs in the regulation of antioxidant genes (Sangokoya *et al.*, 2010). The expression of DICER protein is downregulated by oxidative stress in rat cerebral microvascular endothelial cells (CMVECs) and human trophoblast JAR cells (Wiesen *et al.*, 2009; Ungvari *et al.*, 2013), and upregulated with resveratrol and sulphoraphane treatment in CMVECs (Ungvari *et al.*, 2013). *In silico* analysis revealed the presence of an ARE sequence in the human DICER gene (Ungvari *et al.*, 2013), suggesting its expression to be modulated by redox status, however the functional relevance of this remains unclear, due to the non-specific ribonuclease role of DICER in the biogenesis of microRNA (Vermeulen *et al.*, 2005). Additionally, the action of Exportin-5 is thought to be modulated by cellular redox status (Crampton *et al.*, 2009), indicating that redox changes can alter the biogenesis of microRNAs, which themselves can alter cellular redox status via feedback loops (Cheng *et al.*, 2013).

In order to provide a detailed insight into the microRNAs that are under Nrf2 control in the kidney, we performed an unbiased microRNA array analysis of renal

homogenates from $Nrf2^{+/+}$ and $Nrf2^{-/-}$ mice treated with CDDO-Me or vehicle for 24 h. The data, validated by targeted qPCR analysis in an independent cohort of animals, reveals a novel role for Nrf2 in regulating the expression of selected microRNAs in the kidney, which may have utility as markers of Nrf2 pathway activity.

3.2 Methods

Animals and dosing: Non-fasted $Nrf2^{+/+}$ and $Nrf2^{-/-}$ mice (C57BL/6 background, generation and genotyping described previously (Itoh *et al.*, 1997; McMahon *et al.*, 2001)) of 10-12 weeks of age were used throughout the study, which was conducted according to the Animals (Scientific Procedures) Act 1986 and University of Liverpool local guidelines. Mice were housed at 19-23 °C on a 12 hour light/dark cycle, and given free access to food and water. For microarray and targeted PCR analysis of the primary cohort, five male mice of each genotype were administered a single intraperitoneal (i.p.) dose of vehicle (DMSO, 100 µL/mouse) or CDDO-Me (3 mg/kg), and sacrificed 24 h later by exposure to a rising concentration of CO_2 followed by cardiac puncture. The renal capsule and fat were removed from excised kidneys, which were snap-frozen, along with other organs, and stored at -80 °C. Five samples per treatment group (($Nrf2^{+/+}$ + DMSO, $Nrf2^{-/-}$ + DMSO, $Nrf2^{+/+}$ + CDDO-Me and $Nrf2^{-/-}$ + CDDO-Me) were generated. For the second cohort, six untreated female mice of each genotype were sacrificed as previously described and relevant organs snap-frozen and stored at -80 ^{o}C.

Reagents: Unless indicated, all reagents were purchased from Sigma Aldrich (UK).

Sample preparation for immunoblotting: Frozen kidneys were cut in half, and prepared in iTRAQ buffer, with immunoblotting performed using conditions described in Chapter 2. Primary antibodies (Abcam: Nqo1 (ab2346) and β-actin (ab6276), and secondary antibodies (the appropriate peroxidase-conjugated antibodies) were used as previously described, with immunoblot densitometry

performed using Quantity One 1D Analysis Software (BioRad), normalising to actin expression.

RNA isolation: Kidney RNA was isolated using the mirVana microRNA isolation kit (Life Technologies, UK). Frozen kidneys were cut in half, and wash solutions were prepared by adding the appropriate volumes of EtOH as per the manufacturer's instructions. Samples were weighed, and homogenised in 10 volumes of lysis/binding buffer (i.e. sample weight 30 mg, lysis/binding buffer 300 µL). The homogenate was supplemented with 1/10 lysate volume (i.e. 30 µL) of miRNA homogenate additive, and kept on ice for 10 minutes. The same volume of acid-phenol:chloroform as lysis/binding buffer (i.e. 300 µL) was added, and the sample vortexed for 60 seconds. The sample was then centrifuged at 10,000 *x g* for 5 minutes at room temperature. The aqueous, upper phase was removed from each sample to a new microcentrifuge tube. Room temperature EtOH was added to the sample (1.25 volumes, i.e. 375 µL) which was then dispensed into a filter cartridge loaded onto a collection tube. The tubes were centrifuged at 10,000 *x g* for 15 seconds, and flow-through discarded. 700 µL of miRNA Wash Solution 1 (working solution) was added to the filter compartment of the filter-collection tube, and the tubes centrifuged at 10,000 *x g* for 10 seconds, with the flow-through being discarded. Subsequently, samples were washed twice, each time adding 500 µL miRNA Wash Solution 2/3 (working solution) to the filter compartment, centrifuging at 10,000 *x g* for 10 seconds and discarding the flow through. Samples were centrifuged at 10,000 *x g* for one minute to remove any residual fluid from the filter cartridges, which were then transferred to fresh, labelled collection tubes. 40

µL of 95 ^{o}C dH_2O was applied to the filter, and the filter-collection tubes were centrifuged at maximum speed for 30 seconds to elute total RNA containing microRNAs.

RNA quality assessment: RNA quality was assessed using an RNA 600 Nano Kit and 2100 Bioanalyzer (Agilent), as previously described in Chapter 2. Only samples with a RIN of >6.5 (n=4 per treatment group) were utilised for the microRNA array.

Sample preparation for microRNA array: Samples were prepared for hybridisation to mouse miRNA Microarray System (Agilent, with miRNA Complete Labelling and Hybridisation Kit) at the Centre for Genome Research, University of Liverpool. 100 ng of total RNA was used as the input; and processed according to the manufacturer's instructions. Briefly, both spike-in controls were prepared as specified. 100 ng of RNA (in 2 µL) was added to a 1.5 mL microcentrifuge tube on ice. A Calf Intestinal Alkaline Phosphatase (CIP) master mix was prepared, using 0.4 µL 10X Calf Intestinal Phosphatase Buffer, 1.1 µL diluted Labelling Spike-In Solution and 0.5 µL Calf Intestinal Phosphatase per reaction. 2 µL of this master mix was added to the 1.5 mL microcentrifuge tube containing the RNA, and gently mixed. The sample was then dephosphorylated at 37 ^{o}C for 30 minutes. To denature samples, 2.8 µL DMSO was added, and samples were incubated at 100 ^{o}C for 7 minutes. Samples were immediately transferred to an ice-water bath.

A ligation master mix was prepared, using 1 µL 10X T4 RNA Ligase Buffer, 3 µL Cyanine3-pCp and 0.5 µL T4 RNA Ligase per reaction. 4.5 µL ligation master mix was added to each sample tube, gently mixed and incubated at 16 ^{o}C for 2 hours. Labelled RNA was purified (i.e. DMSO and free Cyanine3-pCp removed) using Micro

Bio-Spin 6 columns (Bio-Rad, UK). Following spin column preparation, 38.7 µL of RNase-free dH_2O was added to the labelled sample. The sample was pipetted onto the prepared spin column gel bed. The microcentrifuge tubes containing the spin columns were then centrifuged for 4 minutes at 1000 *x g*. The columns were discarded, and the flow-through kept on ice. The sample was subsequently dried by centrifugation under a vacuum (SpeedVac, Eppendorf) for approximately 1 hour. Following 10X blocking agent preparation (125 µL H_2O added and mixed), the dried samples were resuspended in 17 µL dH_2O. 1 µL diluted Hyb Spike-In Solution was added to each sample, followed by 4.5 µL 10X blocking agent and 22.5 µL 2X Hi-RPM Hybridisation Buffer and the samples were gently vortexed. Samples were incubated at 100 ^{o}C for 5 minutes, and transferred to a ice water bath for 5 minutes. Samples were subsequently centrifuged at < 1500 RPM for 20 seconds, and the hybridisation assembly prepared.

microRNA array hybridisation and analysis: The miRNA system microarray slides were prepared according to the manufacturer's instructions at the Centre for Genome Research, University of Liverpool. Eight samples per slide were loaded onto prepared arrays, and hybridised at 55 ^{o}C for 20 hours at 20 RPM in a hybridisation oven (Agilent, US). Following hybridisation, the microarray slides were washed using the appropriate wash buffers. The slides were removed from the hybridisation chamber, placed into the slide rack and submerged in Gene Expression Buffer 1 at room temperature for 5 minutes with constant mixing. The slides were subsequently removed and submerged in Gene Expression Buffer 2 at 37 ^{o}C for 5 minutes, again with constant mixing. Slides were inserted into Agilent

slide holders, and read immediately using an Agilent G2505C Microarray Scanner at a resolution of 3 μm. Data was extracted using Agilent Feature Extraction software v11.0.1.1. Differential microRNA expression analysis was conducted using the limma package within the R programming environment (R-Programming-Environment, 2005), enabling simultaneous analysis across multiple treatments and experiments. Raw P values were corrected for the impact of multiple comparisons using the Benjamini-Hochberg procedure, and resultant FDR-adjusted P values were used to compare microRNA expression across the relevant groups ($Nrf2^{+/+}$ + DMSO v $Nrf2^{-/-}$ + DMSO, and $Nrf2^{+/+}$ + DMSO v $Nrf2^{+/+}$ + CDDO-Me). MicroRNAs detected in at least 3/5 samples per treatment group are reported.

Reverse-transcription of total RNA: Reverse-transcription of total RNA to cDNA containing reverse-transcribed microRNAs was accomplished using the miScript II RT kit (Qiagen, UK). 0.5 μg total RNA (quantified using NanoDrop ND-1000 (Labtech, UK)) was added to each reaction well, with dH_2O added to make a total volume of 12 μL. 8 μL of a reverse transcription master mix (containing 4 μL 5x miScript HiFlex buffer, 2 μL 10x nucleics mix and 2 μL reverse transcriptase mix per sample) was added, mixing gently. The plate was centrifuged at < 1600 RPM for 20 seconds, and incubated at 37 ^{o}C for 60 minutes, followed by 95 ^{o}C for 5 minutes. Resultant cDNA samples were diluted by the addition of 140 μL of dH_2O.

qRT-PCR for Nqo1 mRNA: Primers (Table 1) were purchased from EuroFins (Luxembourg). Primers were diluted to a working concentration of 10 μM. Power SYBR Green (Life Technologies, UK) was used for qRT-PCR. A master mix was constructed (10 μL SYBR Green, 2 μL sense primer, 2 μL antisense primer, 4 μL dH_2O

per sample) and 18 µL added to the appropriate well of a 96-well PCR plate (Starlab, UK) in duplicate. 2 µL cDNA was added, and the plate centrifuged for 20 seconds at <1500 RPM. PCR was performed using the ABI Prism 7000 Sequence Detection system (Applied Biosystems), for 1 cycle at 95 ^{o}C for 2 minutes, followed by 40 cycles of 95 ^{o}C for 15 seconds and 60 ^{o}C for 1 minute, and then a dissociation curve of 95 ^{o}C for 1 minute, 65 ^{o}C for 2 minutes, 95 ^{o}C to 65^{o}C at 2 ^{o}C/minute. Resultant Nqo1 C_T values were normalised to Gapdh expression.

Mouse *Gapdh*	Sense	5'-TGTCCGTCGTGGATCTGAC-3'
	Antisense	5'-CCTGCTTCACCACCTTCTTG-3'
Mouse *Nqo1*	Sense	5'-AGCGTTCGGTATTACGATCC-3'
	Antisense	5'-AGTACAATCAGGGCTCTTCTCG-3'

Table 1: qRT-PCR primer sequences for Gapdh and Nqo1.

qRT-PCR for microRNAs: Primers for microRNAs were purchased from Life Technologies (UK), based on their reported FASTA sequences (detailed in Table 2) from miRBase (www.mirbase.org, version 21). Primers were diluted to a working concentration of 10 µM. miScript SYBR Green PCR kit (Qiagen, UK) was used for qRT-PCR. A master mix was constructed (10 µL SYBR Green, 2 µL microRNA primer, 2 µL universal primer, 4 µL dH_2O per sample), and 18 µL was added to the appropriate well of a 96-well PCR plate (Starlab, UK) in duplicate. 2 µL cDNA was then added, and the plate centrifuged for 20 seconds at < 1500 RPM. PCR was performed using the ABI Prism 7000 Sequence Detection system (Applied Biosystems), for 1 cycle at 94 ^{o}C for 10 minutes, followed by 40 cycles of 94 ^{o}C for

15 seconds, 55 ^{o}C for 30 seconds and 70 ^{o}C for 34 seconds. A dissociation curve (95 ^{o}C for 1 minute, 65 ^{o}C for 2 minutes, 95 ^{o}C to 65^{o}C at 2 ^{o}C/minute) was also performed. Resultant values were normalised to U6 snRNA (Corney *et al.*, 2007; Lee *et al.*, 2012c).

Primer	**Sequence**
U6 snRNA	TGGCCCCTGCGCAAGGATG
miR-28c	AGGAGCTCACAGTCTATTGA
miR-34b	AGGCAGTGTAATTAGCTGATTGT
miR-144	GGATATCATCATATACTGTAAGT
miR-146a	TGAGAACTGAATTCCATGGGTT
miR-207	GCTTCTCCTGGCTCTCCTCCCTC
miR-466f-3p	CATACACACACACATACACAC
miR-466h-3p	TACGCACGCACACACACAC
miR-574-3p	CACGCTCATGCACACACCCACA
miR-669p-3p	CATAACATACACACACACACGTAT
miR-1187	TATGTGTGTGTGTATGTGTGTAA
miR-3082	GACAGAGTGTGTGTGTCTGTGT

Table 2: qRT-PCR primer sequences for the indicated microRNAs. The sequence of the universal microRNA primer provided by Qiagen is proprietary information.

3.3 Results

3.3.1 Genetic and pharmacological modulation of Nrf2 in the mouse kidney

Given that Nqo1 was found to be the most sensitive marker of renal Nrf2 activity in the experiments described in Chapter 2, to verify that the Nrf2 pathway was functional in the kidneys of $Nrf2^{+/+}$ mice and non-functional in $Nrf2^{-/-}$ mice, prior to conducting microarray and targeted qRT-PCR microRNA analysis, we determined the expression level of Nqo1 in kidney homogenates from the animals by immunoblotting and qRT-PCR. The level of Nqo1 protein (Fig. 1A-B) and mRNA (Fig. 1C) was significantly lower in the kidneys of vehicle-exposed $Nrf2^{-/-}$ mice, compared with $Nrf2^{+/+}$ counterparts, consistent with loss of Nrf2 function. Moreover, whilst CDDO-Me provoked the induction of Nqo1 24 h after administration to $Nrf2^{+/+}$ mice, this effect was abrogated in $Nrf2^{-/-}$ mice (Fig. 1A-C), validating our model of genetic and pharmacological modulation of Nrf2 in the mouse kidney.

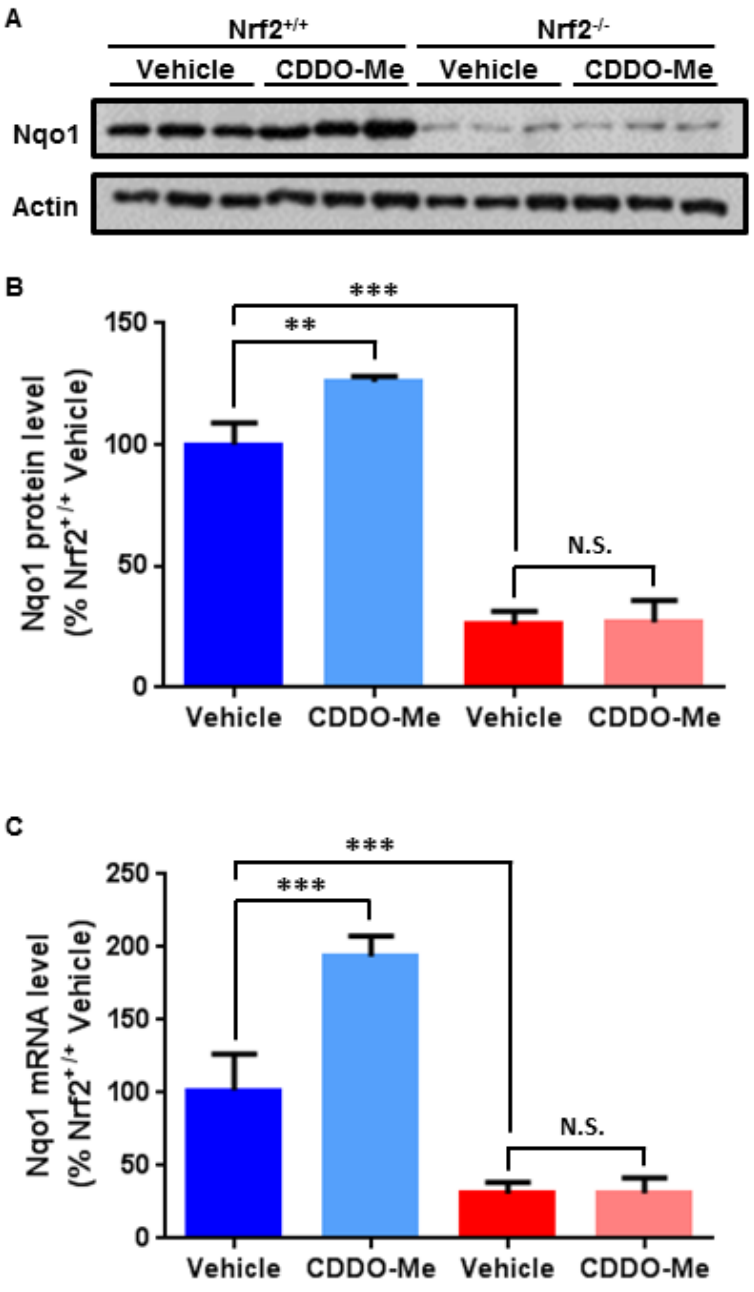

Fig. 1: Differential activity of Nrf2 in the kidneys of $Nrf2^{+/+}$ and $Nrf2^{-/-}$ mice. Mice of the indicated genotype were given a single acute i.p. dose of vehicle (DMSO) or CDDO-Me (3 mg/kg). 24 h later, Nqo1 levels were determined by (A-B) immunoblotting and (C) qPCR. (B) Band volumes were quantified by densitometry and normalised against β-actin. (C) Nqo1 mRNA levels were normalised to Gapdh. Data represent mean + S.D. of n=5 animals per treatment group. Statistical analysis was performed with an unpaired T test, ** $P \leq 0.01$; *** $P \leq 0.001$; *N.S.* not-significant.

3.3.2 Regulation of microRNAs by Nrf2 in the mouse kidney

To provide a detailed insight into the microRNAs controlled by Nrf2 in the kidney at both the basal and inducible levels, a microRNA array was performed on total RNA extracted from $Nrf2^{+/+}$ and $Nrf2^{-/-}$ mice, treated with 3 mg/kg CDDO-Me or the vehicle DMSO for 24 h. Of the 1247 microRNAs for which probes were present on the microarray slides, 427 were detected in the mouse kidney samples. Of these, 50 microRNAs had significantly altered expression in the kidneys of $Nrf2^{-/-}$ mice, compared to $Nrf2^{+/+}$ counterparts (Supplementary Table 1) and 116 had significantly altered expression in the kidneys of CDDO-Me treated $Nrf2^{+/+}$ mice (Supplementary Table 2), compared to those treated with vehicle (Fig. 2). 23 microRNA species were found to be significantly changed in both $Nrf2^{-/-}$ and $Nrf2^{+/+}$ + CDDO-Me kidneys (Table 3), with 2 microRNA species (miR-146a-5p and miR-342-3p) both upregulated in $Nrf2^{-/-}$ and downregulated in $Nrf2^{+/+}$ + CDDO-Me mouse kidneys. No microRNA species were both significantly downregulated in $Nrf2^{-/-}$ and upregulated in CDDO-Me treated $Nrf2^{+/+}$ mouse kidney.

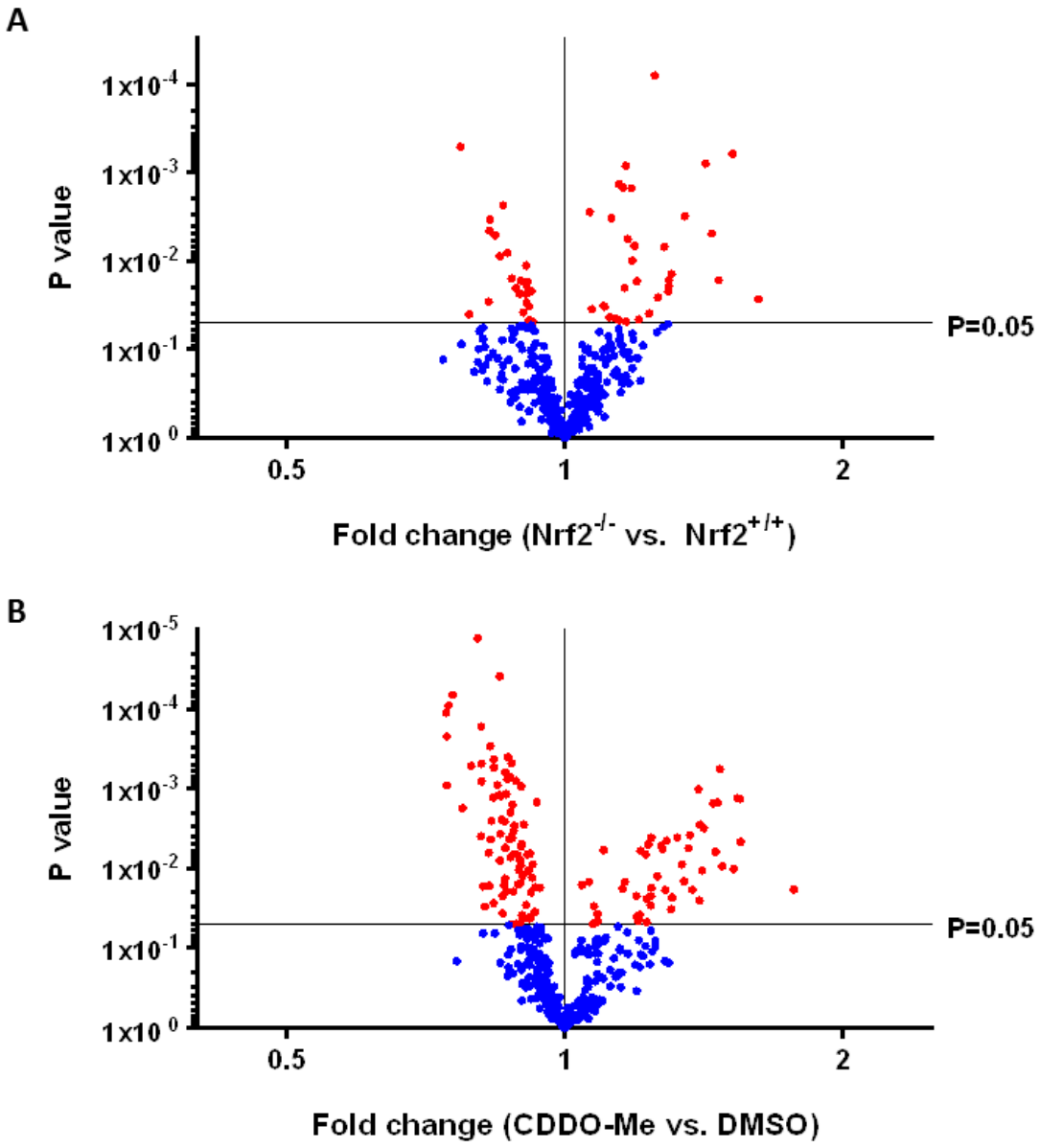

Fig. 2: Volcano plots displaying differentially expressed microRNAs in (A) the kidneys of $Nrf2^{-/-}$ mice, compared to $Nrf2^{+/+}$, and (B) the kidneys of $Nrf2^{+/+}$ mice treated with 3 mg/kg CDDO-Me. microRNAs differentially expressed with a P value of ≤0.05 (red) are reported in Supplementary Tables 1 and 2.

microRNA ID	$Nrf2^{-/-}$ vs. $Nrf2^{+/+}$		CDDO-Me vs. vehicle	
	Fold change	P value	Fold change	P value
miR-146a-5p	1.164	0.001	0.878	0.002
miR-15a-5p	0.916	0.047	0.889	0.007
miR-181b-5p	0.909	0.019	0.897	0.005
miR-195a-5p	0.923	0.048	0.862	0.001
miR-196a-5p	0.886	0.020	0.855	0.002
miR-196b-5p	0.857	0.002	0.877	0.004
miR-203-3p	0.827	0.029	0.837	0.027
miR-20b-5p	0.913	0.048	0.892	0.010
miR-211-3p	1.305	0.014	1.239	0.029
miR-26b-5p	0.909	0.030	0.863	0.001
miR-2861	1.296	0.019	1.366	0.004
miR-296-5p	1.101	0.032	1.085	0.046
miR-29c-5p	0.910	0.017	0.919	0.020
miR-301a-3p	0.894	0.024	0.849	0.001
miR-3102-5p	1.282	0.007	1.272	0.005
miR-322-5p	0.867	0.008	0.874	0.007
miR-335-5p	0.841	0.005	0.879	0.019
miR-342-3p	1.180	0.001	0.916	0.042
miR-3960	1.468	0.016	1.480	0.009
miR-455-5p	0.830	0.003	0.812	0.001
miR-5126	1.296	0.016	1.472	0.001
miR-690	0.902	0.038	0.812	<0.001
miR-9-5p	0.920	0.022	0.745	<0.001

Table 3: MicroRNA species differentially expressed as a result of both genetic inhibition ($Nrf2^{-/-}$) and pharmacological induction (CDDO-Me) of Nrf2 in the mouse kidney ($P \leq 0.05$, n=5).

3.3.3 qRT-PCR validation of Nrf2-regulated microRNAs

Of the 23 microRNA species detailed in Table 3, miR-146a was chosen for targeted qRT-PCR validation of its sensitivity to changes in Nrf2 activity, utilising the knowledge that it has previously been shown to downregulate NF-κB (Taganov *et al.*, 2006). The remaining 21 microRNA species were either upregulated or downregulated in response to both genetic and pharmacological modulation of Nrf2, respectively, and as such are not good candidates as markers of Nrf2 activity. Therefore, based on the reported data in Supplementary Tables 1 and 2, further microRNA species were chosen for targeted qRT-PCR validation of their sensitivity to changes in Nrf2 activity.

MiR-466h-3p (Hunsberger *et al.*, 2012), 574-3p (Alvarez-Mora *et al.*, 2013) and 1187 (Yu *et al.*, 2012) were significantly upregulated in $Nrf2^{+/+}$ mice treated with CDDO-Me, and were chosen based on their reported involvement in cellular stress responses. MiR-34b was significantly downregulated in the CDDO-Me treated $Nrf2^{+/+}$ mouse kidney, and is involved in cancer signalling suppression and stress responses (He *et al.*, 2007; Yamakuchi *et al.*, 2008). miR-28c was also significantly downregulated in the CDDO-Me treated $Nrf2^{-/-}$ mouse kidney, as was miR-144, and both are reported to negatively regulate Nrf2 expression (Sangokoya *et al.*, 2010; Yang *et al.*, 2011). MiR-3082 was chosen as a result of its relatively large increase in expression in the CDDO-Me treated mouse kidney, compared to the vehicle treated. MiR-466f-3p and miR-669p-3p expression was significantly increased in the CDDO-Me treated $Nrf2^{+/+}$ mouse kidney compared with the vehicle (Supplementary Table 2), and was decreased in the $Nrf2^{-/-}$ mouse kidney compared

with the $Nrf2^{+/+}$, but not significantly (P>0.05). Finally, miR-207 was chosen for targeted analysis because its expression was increased in the CDDO-Me treated mouse kidney, and decreased in the $Nrf2^{-/-}$ mouse kidney, compared to controls, but not significantly (P = 0.08 and 0.06, respectively). Total RNA was extracted from kidney homogenates of $Nrf2^{+/+}$ and $Nrf2^{-/-}$ mice, exposed to vehicle or CDDO-Me for 24 hours. This was evaluated for quality, and reverse-transcribed to cDNA for quantification by real-time PCR (Fig. 3).

MiR-28c expression was significantly reduced in the CDDO-Me treated $Nrf2^{+/+}$ mouse kidney (Fig. 3), in agreement with the microRNA array data (Supplementary Table 2). Furthermore, the expression of miR-28c in the kidneys of $Nrf2^{-/-}$ mice treated with CDDO-Me was not different from the vehicle-treated $Nrf2^{-/-}$ mice, suggesting this microRNA species to be regulated by Nrf2. MiR-34b was significantly upregulated in the $Nrf2^{-/-}$ mouse kidney, again consistent with the microRNA array data (Supplementary Table 1). The expression of both miR-144 and miR-146a was significantly increased in the $Nrf2^{-/-}$ mouse kidney, but no significant difference in expression was found in the CDDO-Me treated $Nrf2^{+/+}$ mouse kidney. MiR-466h expression was upregulated in the CDDO-Me treated mouse kidney, in agreement with the microRNA array data (Supplementary Table 2), and this targeted analysis also revealed its expression to be downregulated in the $Nrf2^{-/-}$ mouse kidney (the microRNA array data also showed this, but the difference was not significant). The expression of miR-574-3p was significantly increased in the kidneys of CDDO-Me treated $Nrf2^{+/+}$ mice (Fig. 3), consistent with the microRNA array data (Supplementary Table 2). The expression of miR-574-3p was also

significantly induced in the kidneys of $Nrf2^{-/-}$ mice treated with CDDO-Me, significantly different from the vehicle-treated $Nrf2^{-/-}$ mouse kidney, indicative that this microRNA species may not be under the regulation of Nrf2; rather that it responds to an off-target effect of CDDO-Me signalling.

MiR-1187 expression was not significantly altered in the qPCR (Fig. 3) however it does appear that the expression of this microRNA is reduced somewhat in the $Nrf2^{-/-}$ mouse kidney (Fig. 3). The expression of miR-3082 was significantly reduced in the $Nrf2^{-/-}$ mouse kidney (Fig. 3), and there was no significant difference in expression in the CDDO-Me treated $Nrf2^{+/+}$ mouse kidney, which was not consistent with the microRNA array data (Supplementary Table 2). The expression of miR-466f-3p, miR-207 and miR-669p-3p was not significantly altered in the qPCR (Fig. 3), demonstrating the robustness of the microRNA array data (Fig. 2). On the whole, the microRNA array data was in agreement with the targetted qRT-PCR analysis, validating the altered expression of the selected microRNA species in response to modulation of Nrf2 activity in the mouse kidney.

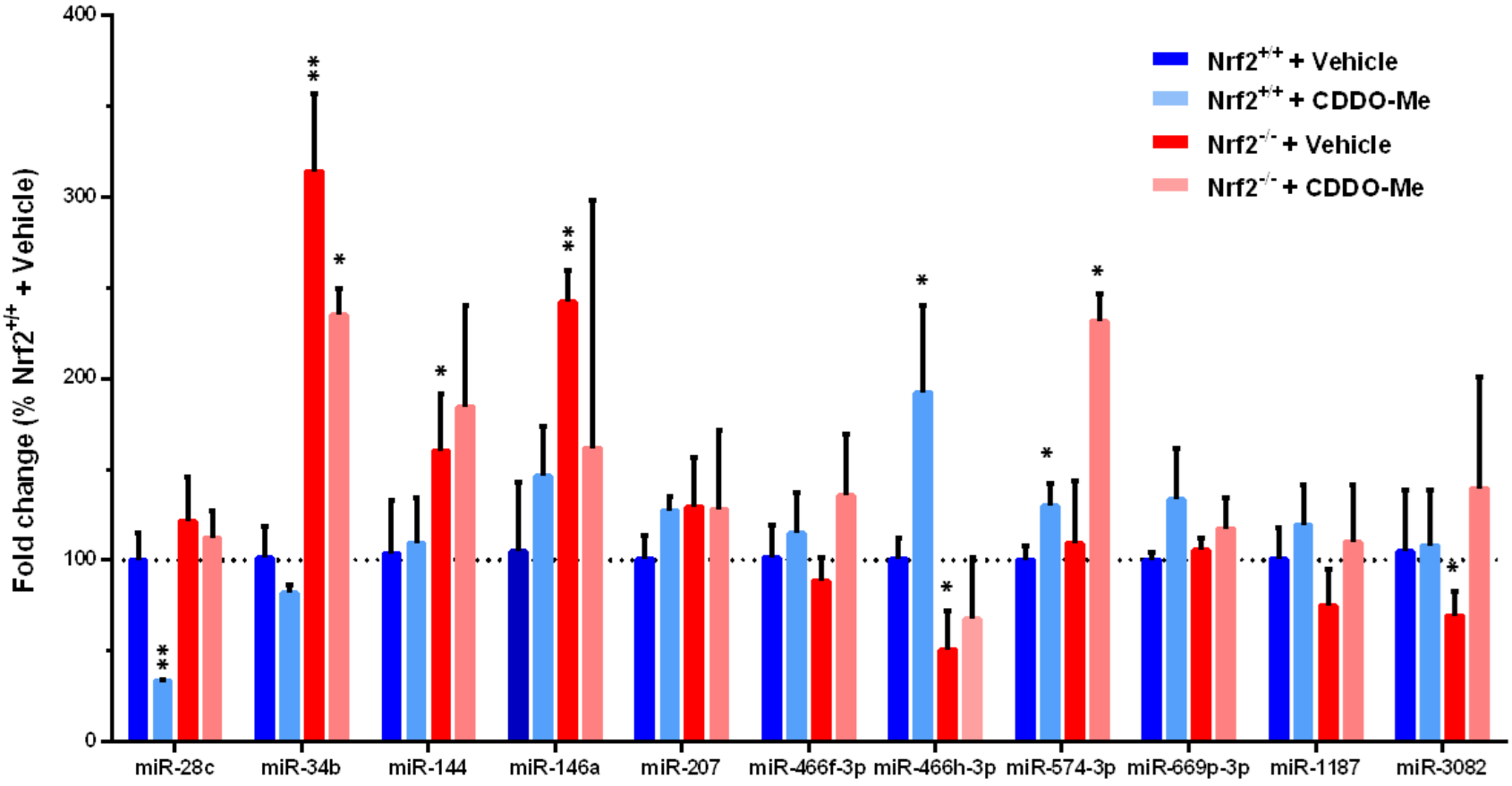

Fig. 3: microRNA species differentially expressed following modulation of Nrf2 activity in the mouse kidney. qRT-PCR was performed on cDNA derived from mouse kidney. Data represents mean and S.D. of n=5 animals per treatment group. Data is normalised to $Nrf2^{+/+}$ + vehicle. Statistical analysis was performed with an unpaired T test, * $P \leq 0.05$, ** $P \leq 0.01$, n=5.

3.3.4 Further validation of selected microRNA responses to modulation of Nrf2 in the female mouse kidney

In order to further validate the differential expression of the panel of microRNAs in response to modulation of Nrf2, a second cohort of animals (female $Nrf2^{+/+}$ and $Nrf2^{-/-}$ mice) were chosen, their kidneys harvested and RNA isolated and reverse-transcribed as before. Fig. 4 confirms their genotyping through measurement of Nqo1 expression at protein and mRNA levels, as previously described for the data presented in Fig. 2. The level of Nqo1 protein (Fig. 4A-B) and mRNA (Fig. 4C) was significantly lower in the kidneys of female $Nrf2^{-/-}$ mice, compared with $Nrf2^{+/+}$ counterparts, consistent with loss of Nrf2 function.

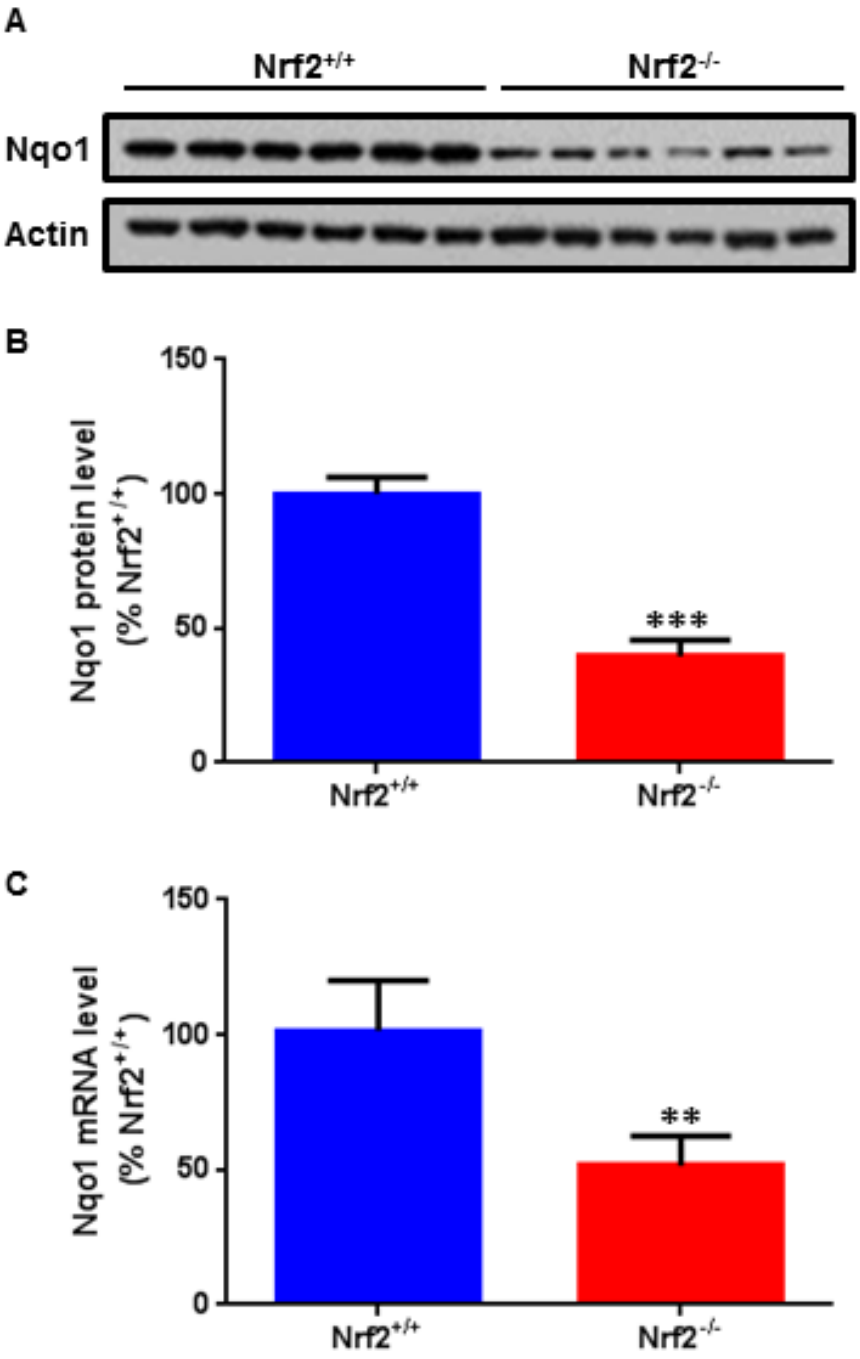

Fig. 4: Differential expression of the Nrf2 target gene Nqo1 in the kidneys of female Nrf2$^{+/+}$ and Nrf2$^{-/-}$ mice. Nqo1 levels were determined by (A-B) immunoblotting and (C) qPCR. (B) Band volumes were quantified by densitometry and normalised against β-actin. (C) Nqo1 mRNA levels were normalised to Gapdh. Data represent mean + S.D. of n=6 animals per treatment group. Statistical analysis was performed with an unpaired T test, ** $P \leq 0.01$; *** $P \leq 0.001$.

qPCR analysis of the selected microRNA species in female mouse kidneys (Fig. 5) showed excellent agreement with both the microRNA array (Table 3) and targeted qPCR (Fig. 3) analysis of male mouse kidneys. miR-466h and miR-3082 expression were significantly reduced in the female Nrf2$^{-/-}$ mouse kidney, as in the male cohort, and the expression of miR-144 and 34b was significantly increased in the female Nrf2$^{-/-}$ mouse kidney. The renal expression of miR-207, miR-466f-3p and 669p-3p did not change significantly in response to genetic inhibition of Nrf2 (Fig. 5), consistent with the targeted PCR analysis of the male cohort (Fig. 3). The expression of miR-574-3p and miR-1187 was significantly upregulated and downregulated, respectively, in the female Nrf2$^{-/-}$ mouse kidney (Fig. 5), despite there being no change in expression in the male cohort (Fig. 3). miR-28c expression was significantly increased in the female Nrf2$^{-/-}$ mouse kidney (Fig. 5), whereas there is no discernible difference in the male cohort; suggesting that the change in miR-28c expression is subtle, or gender specific. miR-146a expression was significantly upregulated in the female Nrf2$^{-/-}$ mouse cohort, as in the male cohort. This data validates a number of microRNAs than can be used in further experimentation to determine their value as novel markers of Nrf2 activity.

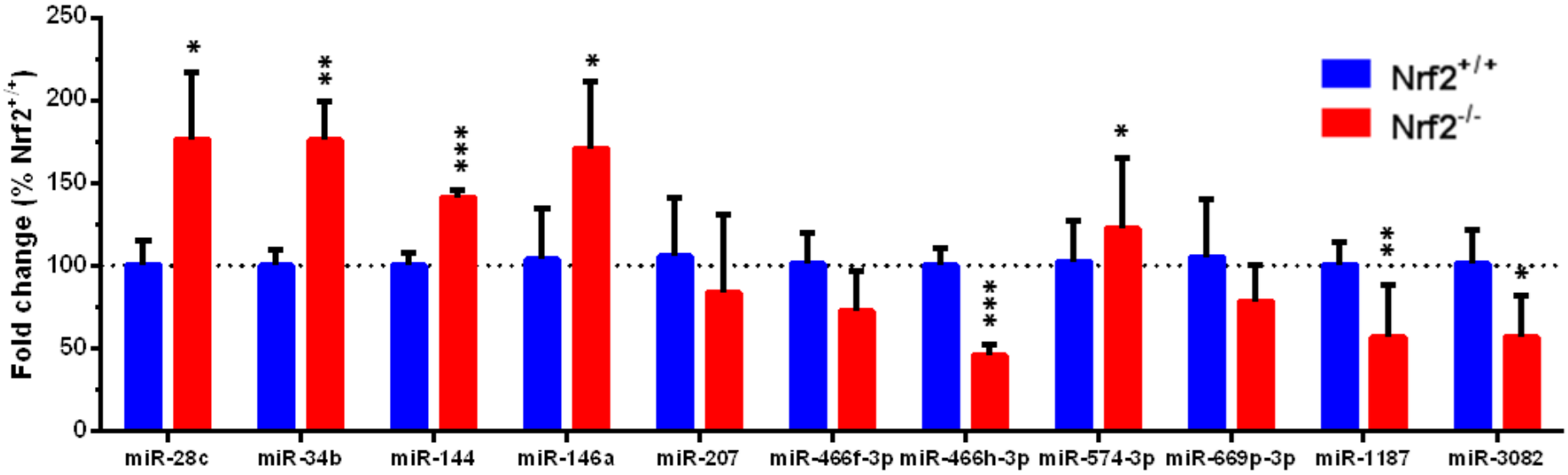

Fig. 5: microRNA species differentially expressed in the female $Nrf2^{-/-}$ mouse kidney. qRT-PCR was performed on cDNA derived from mouse kidney. Data represents mean and S.D of n=6 per group, and are normalised to $Nrf2^{+/+}$. Statistical analysis was performed with an unpaired T test, * $P \leq 0.05$, ** $P \leq 0.01$, *** $P \leq 0.001$.

3.4 Discussion

The transcription factor Nrf2 regulates the expression of multiple defence processes to combat cellular stress (Bryan *et al.*, 2013). Genes and proteins under Nrf2 control in the kidney have been detailed in Chapter 2, and whilst previous work has identified microRNAs that regulate Nrf2 expression, there is a lack of information on microRNAs regulated by Nrf2 itself. This unbiased analysis of renal microRNAs that are altered in response to genetic and pharmacological manipulation of Nrf2 represents the first step into fully characterising the renal microRNA-ome, which could reveal novel mechanisms of Nrf2 function and markers of its activity.

MicroRNAs enable cells to 'fine-tune' translation, and as such changes in microRNA expression are likely to be slight. Nevertheless, the findings of this study demonstrate that following manipulation of Nrf2 in the mouse kidney, the expression of several microRNAs is significantly altered.

MiR-466h is a promising candidate marker of Nrf2 activity in the kidney, being significantly decreased following genetic inhibition of Nrf2, and significantly increased following pharmacological induction of the transcription factor in the microRNA array and targeted qPCR data (Table 3, Fig. 3 and 5). MiR-466h is involved in the oxidative stress response, being upregulated following cerebral ischaemia in rats (Hunsberger *et al.*, 2012), which is consistent with an increase in Nrf2 expression to combat ischaemia-induced ROS generation. MiR-466h has been shown to have a pro-apoptotic role in ovarian cells *in vitro* (Druz *et al.*, 2011) and cerebral ischaemia *in vivo* (Hunsberger *et al.*, 2012), suggesting that regulation of

miR-466h is more complex than simply being a marker of Nrf2 activity. MiR-466h has been described as being upregulated following glucose depletion (Druz *et al.*, 2012), which, taken with the findings of Chapter 2, that proteins involved in energy homeostasis (namely those in the glycolytic and pentose phosphate pathway) are expressed at a lower level in the $Nrf2^{-/-}$ mouse kidney compared to the $Nrf2^{+/+}$ (Fig. 2) it appears that miR-466h, whilst being predictive of Nrf2 activity, also is a marker of the glycolytic state of the cell. To better determine the correlation of miR-466h with Nrf2 activity, an enzyme-linked immunosorbent assay could be performed, linking miR-466h levels with those of Nrf2-regulated proteins defined in Chapter 2. It would also be of interest to use antagomiRs to modulate the level/activity of miR-466h and better define a link between the expression of this microRNA and energy metabolism. Nevertheless, in mouse renal tissue, from the panel of microRNAs selected, miR-466h correlates best with the changes in Nrf2 expression, and as such is a standout candidate for further investigation as a potential marker of Nrf2 activity in relevant biological matrices.

Another strong candidate for use as a marker of Nrf2 activity is miR-28c. Displaying the opposite expression pattern to miR-466h (significantly upregulated in the $Nrf2^{-/-}$ mouse kidney, significantly downregulated in the CDDO-Me treated $Nrf2^{+/+}$ mouse kidney (Fig. 3 and 5)), miR-28c has previously been shown to regulate Nrf2 expression in breast epithelial cells, in a Keap1-independent manner (Yang *et al.*, 2011), with miR-28c expression correlating inversely to Nrf2 expression. Indeed, ectopic expression of miR-28 reduces Nrf2 mRNA and protein expression, whilst removing the miR-28 targeting seed sequence in the 3'UTR of the Nrf2 gene

abrogates the effect of miR-28 (Yang *et al.*, 2011). MiR-28 expression is markedly decreased in renal cell carcinoma (Wang *et al.*, 2015a), a cancer previously described in this thesis as associated with an increase in Nrf2 activity (Chapter 1, Section 1.4.3, (Adam *et al.*, 2011; Ooi *et al.*, 2011; Ooi *et al.*, 2013)). Here we have demonstrated that miR-28c expression is modulated following pharmacological and genetic manipulation of Nrf2 in the mouse kidney. These observations are consistent with a role for miR-28c in the mechanism of action of CDDO-Me as an inducer of Nrf2 although further work is needed to test this directly.

The microRNA array data shows miR-144 to be significantly reduced in the kidneys of CDDO-Me treated $Nrf2^{+/+}$ mice, compared to the vehicle. Targeted analysis of miR-144 expression using qPCR demonstrated less obvious changes following CDDO-Me administration (Fig.3), however miR-144 was shown to be upregulated in the $Nrf2^{-/-}$ mouse kidney, compared to $Nrf2^{+/+}$ in the microRNA array and qPCR data (Fig. 3 and 5). MiR-144 has been characterised elsewhere as a negative regulator of Nrf2 in erythrocytes (Sangokoya *et al.*, 2010), with sickle cell leukaemia patients having high expression of miR-144, and a reduced tolerance for oxidative stress (Sangokoya *et al.*, 2010). Two distinct targeting sites for miR-144 exist in the 3'UTR of Nrf2 mRNA (Sangokoya *et al.*, 2010), suggestive of its role in negatively regulating Nrf2. However, as with miR-28, we found that expression of miR-144 was increased in the $Nrf2^{-/-}$ mouse kidney, suggestive of a feedback loop.

The expression of both miR-28c and miR-144 are induced in the $Nrf2^{-/-}$ mouse kidney, compared to the $Nrf2^{+/+}$, and reduced in the CDDO-Me treated $Nrf2^{+/+}$ mouse kidney, compared to the vehicle. This could potentially be a mechanism for

controlling the strength and/or duration of Nrf2 activation in response to pharmacological stimulation, and they could contribute toward the regulation of Nrf2 target genes (Fig. 6). Further work to ensure the validity of this novel axis could involve determining if CDDO-Me treatment can induce Nrf2 in the presence of a miR-28c antagonist, to define the contribution of miR-28c to Nrf2 signalling.

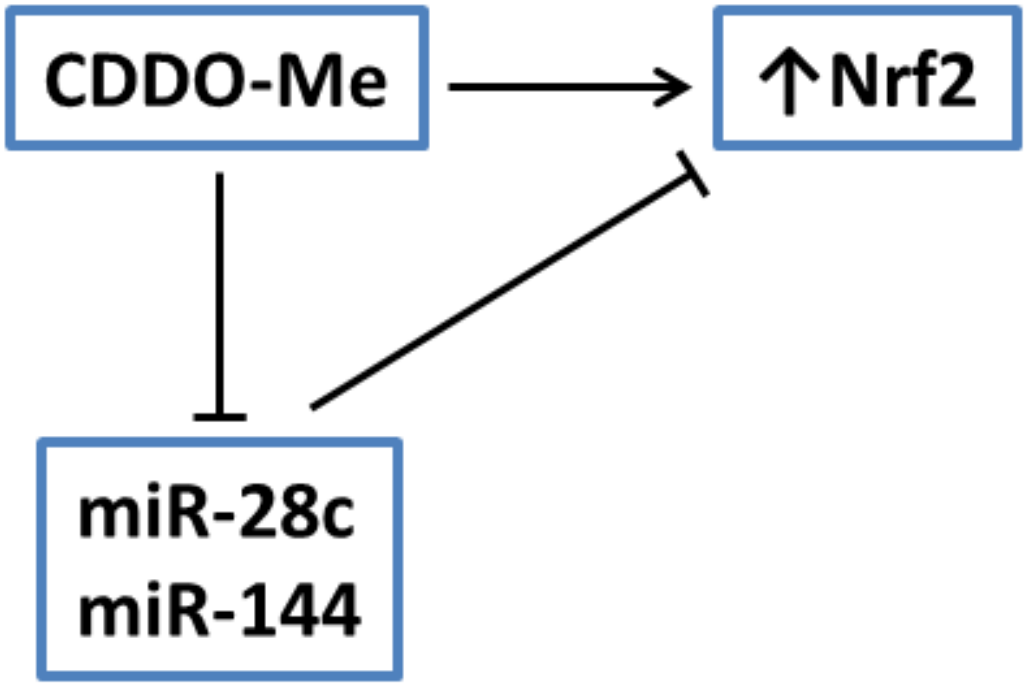

Fig. 6: Schematic overview of the postulated relationship between the Nrf2 inducer CDDO-Me, miR-28c, miR-144 and Nrf2. An increase in Nrf2 activity following CDDO-Me administration is accompanied by a decrease in miR-28c and miR-144 expression, and a corresponding decrease in the ability of these microRNA species to translationally repress Nrf2 mRNA (determined in (Yang *et al.*, 2011)).

Decreased expression of miR-574-3p has been associated with the progression of both gastric (Su *et al.*, 2012) and bladder cancer (Tatarano *et al.*, 2012). Functional studies indicate that miR-574-3p overexpression inhibits the metastatic capabilities of gastric cancer cells (Su *et al.*, 2012), and recent research has suggested a role for this microRNA species in oxidative stress, as it is significantly downregulated in patients with Fragile X syndrome (Alvarez-Mora *et al.*, 2013). The microRNA array data indicates significant changes in the expression of miR-574-3p following genetic inhibition and pharmacological activation of Nrf2 (Table 3), however the qPCR data is less convincing; the only significant difference in expression of miR-574-3p was between CDDO-Me and vehicle treated kidneys of both $Nrf2^{+/+}$ and $Nrf2^{-/-}$ mice (Fig. 3). Since this work was performed, research has been published describing miR-574-3p as a genotoxic stress-responsive microRNA, with expression of both Nrf2 (Xing *et al.*, 2012) and miR-574 induced following X-Ray irradiation (the latter in the A549 lung cancer cell line (Ishikawa *et al.*, 2014)). However, the Nrf2 inducer curcumin was found to decrease the expression of miR-574-3p in a nasal pharyngeal carcinoma cell line (Gao *et al.*, 2014), in contrast to our observation that miR-574-3p is induced in the kidneys of CDDO-Me treated mice. As previously mentioned, microRNA expression profiles differ between organs, and expression profiles of microRNAs change dramatically in cancers (Su *et al.*, 2012). Further work would involve the use of a larger number of $Nrf2^{+/+}$ and $Nrf2^{-/-}$ animals, treated with CDDO-Me or other Nrf2 inducers, in order to fully determine the response of miR-574-3p to changes in renal Nrf2 activity.

The miR-34 family are induced by p53 in response to DNA damage or stress (He *et al.*, 2007), and direct the depletion of cell cycle proteins (He *et al.*, 2007; Yamakuchi *et al.*, 2008), promoting apoptosis. The miR-34 family are also deregulated in cancer (Wang *et al.*, 2014), but not consistently, for example in hepatocellular carcinoma miR-34a has been shown to be both upregulated (Pineau *et al.*, 2010; Wang *et al.*, 2014) and downregulated (Li *et al.*, 2009; Dang *et al.*, 2013). MiR-34b expression was shown here, for the first time, to be induced in the $Nrf2^{-/-}$, compared with the $Nrf2^{+/+}$ mouse kidney in the microRNA array and qPCR data (Table 3, Fig. 3 and 5), consistent with the notion that this microRNA family are induced in situations where cells or tissues may experience different types of stress (He *et al.*, 2007). The induction of miR-34b in the $Nrf2^{-/-}$ mouse kidney may reflect a capacity of this microRNA to determine disease states. As a marker of Nrf2, the miR-34 family may not be the most useful, as it lacks a direct correlation with Nrf2 levels, and it appears that miR-34 deregulation is common in situations where Nrf2 may not necessarily be involved.

The expression of miR-146a has been determined elsewhere to negatively regulate the activation of NF-κB (Saba *et al.*, 2014). The data presented in Fig. 3 and 5 show a significant increase in miR-146a expression in the $Nrf2^{-/-}$ mouse (Fig. 3 and 5). $Nrf2^{-/-}$ mice have an exaggerated Nf-κB response following scratch injury-induced stress (Pan *et al.*, 2012), which suggests that this microRNA is upregulated in response to an increase in NF-κB activity (ostensibly to combat this upregulation of NF-κB signalling), and as such is a good marker of NF-κB signalling, rather than Nrf2. The data presented in Fig. 3 shows a lack of significant downregulation of miR-146a

in the CDDO-Me treated $Nrf2^{+/+}$ mouse kidney, suggesting that this microRNA is not regulated directly by Nrf2.

MiR-207 expression was not significantly altered in either cohort (Fig. 3 and 5), indicative of the robustness of the data. MiR-207 has been shown to be upregulated following exposure to ionising radiation (Tan *et al.*, 2014), enhancing apoptosis in cochlear hair cells (Tan *et al.*, 2014). The upregulation of Nrf2 following ionising radiation has been characterised (McDonald *et al.*, 2010), so perhaps there is a link between miR-207 and Nrf2 which may be more evident in a different cell type.

MiR-1187, which represses Caspase 8 (Yu *et al.*, 2012), has been described elsewhere to be significantly downregulated in mice with acute liver failure, contributing to the induction of hepatic apoptosis (Yu *et al.*, 2012). The microRNA array data (Supplementary Table 2) showed that miR-1187 expression was significantly increased in CDDO-Me treated $Nrf2^{+/+}$ mice, compared to the vehicle, and in the female mouse cohort miR-1187 was significantly reduced in the $Nrf2^{-/-}$ mouse kidney, compared to the $Nrf2^{+/+}$ (Fig. 5). Further work to determine the contribution of this microRNA species toward the enhanced propensity for hepatic injury in the $Nrf2^{-/-}$ mouse (Enomoto *et al.*, 2001) could be examined through the use of microRNA mimics.

Due to the relatively recent discovery of microRNAs, not every species has been 'assigned' a particular role to date. miR-3082 was chosen here as part of the panel for targeted qPCR validation because of the relatively large increase in its expression in the CDDO-Me treated $Nrf2^{+/+}$ mouse kidney, compared to the vehicle

(Supplementary Table 2). There is a target sequence for miR-3082 in the Keap1 gene (www.targetscan.org, v6.2). Therefore the upregulation of miR-3082 in response to CDDO-Me could downregulate the translation of Keap1, contributing to the activation of Nrf2 signalling. MiR-669p-3p was chosen as in the microarray data it was significantly upregulated in the CDDO-Me treated $Nrf2^{+/+}$ mouse kidney (Supplementary Table 2), however a biological function for this microRNA has yet to be determined. There is some suggestion that miR-466f-3p, which was found to be increased in the CDDO-Me treated $Nrf2^{+/+}$ mouse kidney compared to the vehicle (Supplementary Table 2), assists in cell cycle control in bone marrow stem cells (Gong *et al.*, 2014), however further information is lacking. Indeed, more recently discovered microRNAs are still being functionally characterised through use of mimics and antagomiRs, and so the full implications of the data described here are currently unknown.

Previous work by a different group described the expression of miR-27 as being decreased following low micromolar CDDO-Me stimulation in 3 diffferent pancreatic cancer cell lines (Jutooru *et al.*, 2010). However, here miR-27 expression was not significantly altered in $Nrf2^{-/-}$ compared with $Nrf2^{+/+}$ mouse kidney, or in CDDO-Me compared with vehicle-treated $Nrf2^{+/+}$ mouse kidney. It is possible that miR-27 expression may be tissue-specific, or only expressed in certain types of cancer. Additionally, miR-27 may simply be increased in response to relatively high concentrations of CDDO-Me which are known to induce apoptosis (Chapter 4), rather than as a consequence of Nrf2 activation (which is seemingly the case with miR-574-3p, Fig. 3), and so no effect would be seen in the $Nrf2^{-/-}$ mouse. In order to

distinguish the effects of Nrf2 induction from the effects of CDDO-Me, the microRNA expression of Keap1$^{-/-}$ mouse kidneys could be analysed.

Biomarkers by definition must be easy to measure (Starkey Lewis *et al.*, 2012). Therefore, in order to determine the utility of microRNAs as useful markers of Nrf2 activity, future work should determine if the microRNAs shown here to be sensitive to changes in renal Nrf2 activity can be (a) detected and (b) shown to be capable of reporting Nrf2 activity in serum or urine from animals in which the activity of Nrf2 has been modulated. If successful, these findings should be translated to humans, e.g. through the analysis of biofluids from patients receiving Nrf2-inducing drugs such as CDDO-Me or dimethyl fumarate.

Differences in microRNA expression are often transient and relatively small, and because of this they may have a use in determining dynamic changes in Nrf2 activity. One caveat of using microarrays to determine microRNA expression is that the microRNA species reported as having significantly different expression are often the ones that have the highest difference in expression, compared to their relative control. Because of this, targeted qPCR analysis assists in validating the results of the microarray.

One limitation of the experimental design of this study is the use of a single timepoint of exposure to CDDO-Me. MicroRNAs are transient by nature, so it is possible that microRNAs transcribed a short period of time after CDDO-Me administration may have been missed in the current analysis. Moreover, it is possible that the differentially expressed microRNAs reported here reflect systemic changes in Nrf2 activity, and not those that are specific to the kidney. Adaptation

of other pathways to the general loss of Nrf2 function, rather than a loss of direct transcriptional regulation by the transcription factor, may also account for some of the changes in microRNA expression detected in the $Nrf2^{-/-}$ mice. Further analysis of other tissues of $Nrf2^{-/-}$ mice, and $Nrf2^{+/+}$ mice exposed to CDDO-Me would help address this point. Transient and small changes in expression of microRNAs may therefore have been missed, based on the limitations of the assay and experimental design involved.

Using the microRNA array to first determine the expression profiles of 427 mouse microRNAs, and subsequently validating a selection of them using targeted qPCR, this study represents the first mechanistic analysis of Nrf2-regulated microRNA expression in the kidney, and shows for the first time a novel role for Nrf2 in regulating the expression of several microRNAs. This work has identified promising candidates (including miR-28c, miR-144 and miR-466h-3p) for a microRNA-based marker of Nrf2 in the kidney, and has furthered our understanding of the biological roles of Nrf2 in the kidney.

MicroRNA ID	$Nrf2^{-/-}$ vs. $Nrf2^{+/+}$	
	Fold change	P value
miR-455-3p	0.771	0.001
miR-203-3p	0.827	0.029
miR-365-3p	0.829	0.005
miR-455-5p	0.830	0.003
miR-335-5p	0.841	0.005
miR-149-5p	0.850	0.009
miR-196b-5p	0.857	0.002
miR-322-5p	0.867	0.008
miR-92a-3p	0.876	0.016
miR-196a-5p	0.886	0.020
miR-301a-3p	0.894	0.024
miR-3068-3p	0.897	0.017
miR-690	0.902	0.038
miR-192-3p	0.909	0.011
miR-29b-3p	0.909	0.023
miR-26b-5p	0.909	0.030
miR-181b-5p	0.909	0.019
miR-29c-5p	0.910	0.017
miR-20b-5p	0.913	0.048
miR-139-5p	0.914	0.032
miR-9-5p	0.920	0.022
miR-200c-3p	1.104	0.033
miR-30a-5p	1.123	0.003
miR-6378	1.134	0.044
miR-551b-3p	1.145	0.047
miR-143-3p	1.146	0.001
miR-874-3p	1.155	0.001
miR-705	1.160	0.020
miR-146a-5p	1.164	0.001
miR-142-5p	1.165	0.048
miR-1198-5p	1.170	0.006
miR-342-3p	1.180	0.001
miR-6236	1.183	0.010
miR-6351	1.190	0.007
miR-125a-3p	1.197	0.017
miR-6392-3p	1.203	0.046
miR-3081-5p	1.234	0.039
miR-182-5p	1.252	0.000
miR-1931	1.261	0.026
miR-3102-5p	1.282	0.007
miR-133b-3p	1.294	0.022
miR-2861	1.296	0.019

miR-5126	1.296	0.016
miR-211-3p	1.305	0.014
miR-3058-3p	1.349	0.003
miR-1896	1.421	0.001
miR-134-5p	1.443	0.005
miR-3960	1.468	0.016
miR-34a-5p	1.519	0.001
miR-205-5p	1.621	0.027

Supplementary Table 1: MicroRNAs differentially expressed in the $Nrf2^{-/-}$, compared to $Nrf2^{+/+}$ mouse kidney ($P \leq 0.05$, n=5).

MicroRNA ID	CDDO-Me vs. vehicle	
	Fold change	P value
miR-181d-5p	0.744	<0.001
miR-9-5p	0.745	<0.001
miR-34b-5p	0.745	<0.001
miR-10a-3p	0.748	<0.001
miR-33-5p	0.756	<0.001
miR-181c-5p	0.775	0.002
miR-450a-5p	0.792	0.001
miR-30c-2-3p	0.805	<0.001
miR-690	0.812	<0.001
miR-503-5p	0.812	0.004
miR-455-5p	0.812	0.001
miR-3069-3p	0.812	<0.001
miR-144-5p	0.816	0.017
miR-551b-5p	0.819	0.030
miR-5130	0.828	0.016
miR-1839-5p	0.830	<0.001
miR-28c	0.832	0.004
miR-872-5p	0.832	0.003
miR-218-5p	0.836	0.001
miR-203-3p	0.837	0.027
miR-28a-5p	0.838	0.001
miR-1231-5p	0.838	<0.001
miR-301a-3p	0.849	0.001
miR-532-5p	0.850	<0.001
miR-100-5p	0.851	0.008
miR-204-5p	0.852	0.001
miR-140-5p	0.852	0.004
miR-196a-5p	0.855	0.002
miR-9-3p	0.856	0.037
miR-210-3p	0.860	0.016
miR-19a-3p	0.861	0.003
miR-1949	0.862	0.013
miR-32-5p	0.862	0.005
miR-195a-5p	0.862	0.001
miR-26b-5p	0.863	0.001
miR-1940	0.864	0.019
miR-361-5p	0.866	0.001
miR-10b-5p	0.868	<0.001
miR-130a-3p	0.871	0.004
miR-340-5p	0.872	0.001
miR-532-3p	0.873	0.002
miR-322-5p	0.874	0.007

miR-152-3p	0.876	<0.001
miR-30e-3p	0.876	0.004
miR-196b-5p	0.877	0.004
miR-146a-5p	0.878	0.002
miR-335-5p	0.879	0.019
miR-770-3p	0.880	0.007
miR-1264-5p	0.880	0.003
miR-193a-5p	0.881	0.003
miR-10a-5p	0.885	0.001
miR-15a-5p	0.889	0.007
miR-362-3p	0.890	0.016
miR-20b-5p	0.892	0.010
miR-155-5p	0.894	0.049
miR-128-3p	0.894	0.008
miR-374c-5p	0.896	0.009
miR-1839-3p	0.896	0.001
miR-181b-5p	0.897	0.005
miR-5100	0.898	0.005
miR-497-5p	0.898	0.038
miR-350-3p	0.899	0.040
miR-181a-5p	0.900	0.012
miR-425-5p	0.903	0.003
miR-200b-5p	0.903	0.042
miR-484	0.909	0.028
miR-101b-3p	0.912	0.007
miR-1906	0.912	0.011
miR-106b-5p	0.914	0.010
miR-342-3p	0.916	0.042
miR-30a-3p	0.917	0.006
miR-378c	0.918	0.041
miR-29c-5p	0.919	0.020
miR-324-5p	0.922	0.013
miR-30b-5p	0.923	0.009
miR-25-3p	0.928	0.035
miR-200a-3p	0.928	0.017
miR-200b-3p	0.933	0.001
miR-222-3p	0.940	0.017
miR-669a-3-3p	1.155	0.018
miR-466h-5p	1.195	0.022
miR-18b-3p	1.197	0.040
miR-467b-3p	1.200	0.046
miR-6538	1.205	0.038
miR-669e-5p	1.208	0.006
miR-466g	1.226	0.047

miR-877-3p	1.226	0.024
miR-706	1.231	0.005
miR-211-3p	1.239	0.029
miR-3091-5p	1.239	0.022
miR-574-3p	1.241	0.017
miR-669c-3p	1.241	0.004
miR-5620-3p	1.259	0.013
miR-3102-5p	1.272	0.005
miR-1188-3p	1.276	0.006
miR-3473c	1.285	0.019
miR-669p-3p	1.289	0.004
miR-466f-3p	1.304	0.032
miR-466q	1.307	0.023
miR-5132-3p	1.323	0.004
miR-467f	1.339	0.009
miR-466i-3p	1.347	0.014
miR-2861	1.366	0.004
miR-466m-5p	1.375	0.018
miR-669l-5p	1.395	0.001
miR-468-3p	1.398	0.025
miR-466h-3p	1.401	0.003
miR-669n	1.408	0.011
miR-466i-5p	1.447	0.002
miR-1187	1.456	0.006
miR-5126	1.472	0.001
miR-3960	1.480	0.009
miR-32-3p	1.523	0.010
miR-877-5p	1.537	0.001
miR-574-5p	1.547	0.001
miR-3082-5p	1.550	0.005

Supplementary Table 2: MicroRNAs differentially expressed in the CDDO-Me, compared to vehicle treated $Nrf2^{+/+}$ mouse kidney ($P \leq 0.05$, n=5).

Chapter 4

Examination of the relationship between potency towards Nrf2 and cytotoxicity of semi-synthetic triterpenoids and novel mono- and tri-cyclic cyano enones

Contents

4.1 Introduction

Nrf2 regulates the expression of a battery of genes with diverse physiological roles including the antioxidant response, xenobiotic metabolism, lipid metabolism, and the regulation of energy production (Ma, 2013), some of which have been further delineated in Chapter 2. It is therefore evident that Nrf2 plays an important role in cellular homeostasis, which is emphasised by the enhanced susceptibility of $Nrf2^{-/-}$ mice to a number of diseases and chemical toxicities (Copple *et al.*, 2008; Shelton *et al.*, 2013). The converse is also true; induction of Nrf2 has been shown to protect against various pathologies, including kidney injury (Tanaka *et al.*, 2008; Pergola *et al.*, 2011a; Shelton *et al.*, 2013), cancer (Jeong *et al.*, 2006) and diabetes (Li *et al.*, 2014). This has culminated in the recent licensing of the small molecule Nrf2 inducer dimethyl fumarate (DMF) for use in the clinical treatment of multiple sclerosis (Lee *et al.*, 2013).

The triterpenoid Nrf2 inducer CDDO-Me was until recently a promising therapeutic candidate for treatment of chronic kidney disease (CKD). An unexpected side effect of CDDO-Me in a clinical trial designed to assess the capacity of the drug to treat cancer was the improvement of estimated glomerular filtration rate (eGFR, a measure of renal function) (Hong *et al.*, 2012). This knowledge was subsequently used to inform a successful clinical trial seeking to improve the clinical outcome of patients with moderate to severe chronic kidney disease and type II diabetes (Pergola *et al.*, 2011b), which was followed up with a larger, phase III clinical trial in patients with end-stage CKD (de Zeeuw *et al.*, 2013b). The latter clinical trial was, however, prematurely terminated due to a high incidence of adverse events and

deaths in the treatment arm; the causes of which were not clear at the time that the work described here was conducted. One possible reason for the adverse effects of CDDO-Me in end-stage CKD patients is that this patient cohort was inappropriate, given that the induction of Nrf2 signalling has previously been shown to prevent, but not reverse, a number of experimental pathologies (Zhang, 2013). Additionally, no adverse side effects were reported in the clinical trial of CDDO-Me as a cancer therapy (Hong *et al.*, 2012), so it is unclear whether the adverse events were specific to the CKD patient population.

Nrf2 induction hinges on the ability to prevent Keap1 repression of Nrf2, allowing for the transcription of genes under Nrf2 control. It is generally accepted that small molecule Nrf2 inducers modify cysteine residues of Keap1, allowing Nrf2 to evade Keap1 repression (Dinkova-Kostova *et al.*, 2002; Bryan *et al.*, 2013). Thiol reactivity is a common feature of small molecule Nrf2 inducers (Dinkova-Kostova *et al.*, 2002; Bensasson *et al.*, 2010; Dinkova-Kostova, 2012; Bryan *et al.*, 2013). Many existing and withdrawn drugs are known to provoke off-target toxic effects through generation of electrophilic, thiol-reactive metabolites (Park *et al.*, 2011). For example, hepatotoxicity results following acetaminophen overdose due to the generation of a reactive toxic metabolite that depletes intracellular glutathione, inducing oxidative stress (Hinson *et al.*, 2010).

If the adverse events associated with CDDO-Me are not due to induction of Nrf2 *per se*, and instead are due to off-target effects associated with general compound structure (as theorised in (Chin *et al.*, 2014c)), then there is a clear need for the development of second-generation Nrf2 inducers, rationally designed to induce a

lesser degree of toxicity. It is for this reason that TBE-31 and MCE-1, lead compounds from novel tri- and mono-cyclic cyano enone classes are under investigation (Fig. 1).

The aim of this chapter is to elucidate the relationship between thiol reactivity, potency towards Nrf2 and toxicity for triterpenoids and other Nrf2 inducers, to determine if the drive to enhance potency of the triterpenoids (which has culminated in the synthesis of CDDO-Me) has inadvertently produced more toxic molecules. This will inform the ongoing design and development of small molecule Nrf2 inducers, which continue to hold promise as novel drug candidates. Some of the content of this chapter has been published in Toxicological Sciences, '**Chemical tuning enhances both potency toward Nrf2 and *in vitro* therapeutic index of triterpenoids**' (Copple *et al.*, 2014).

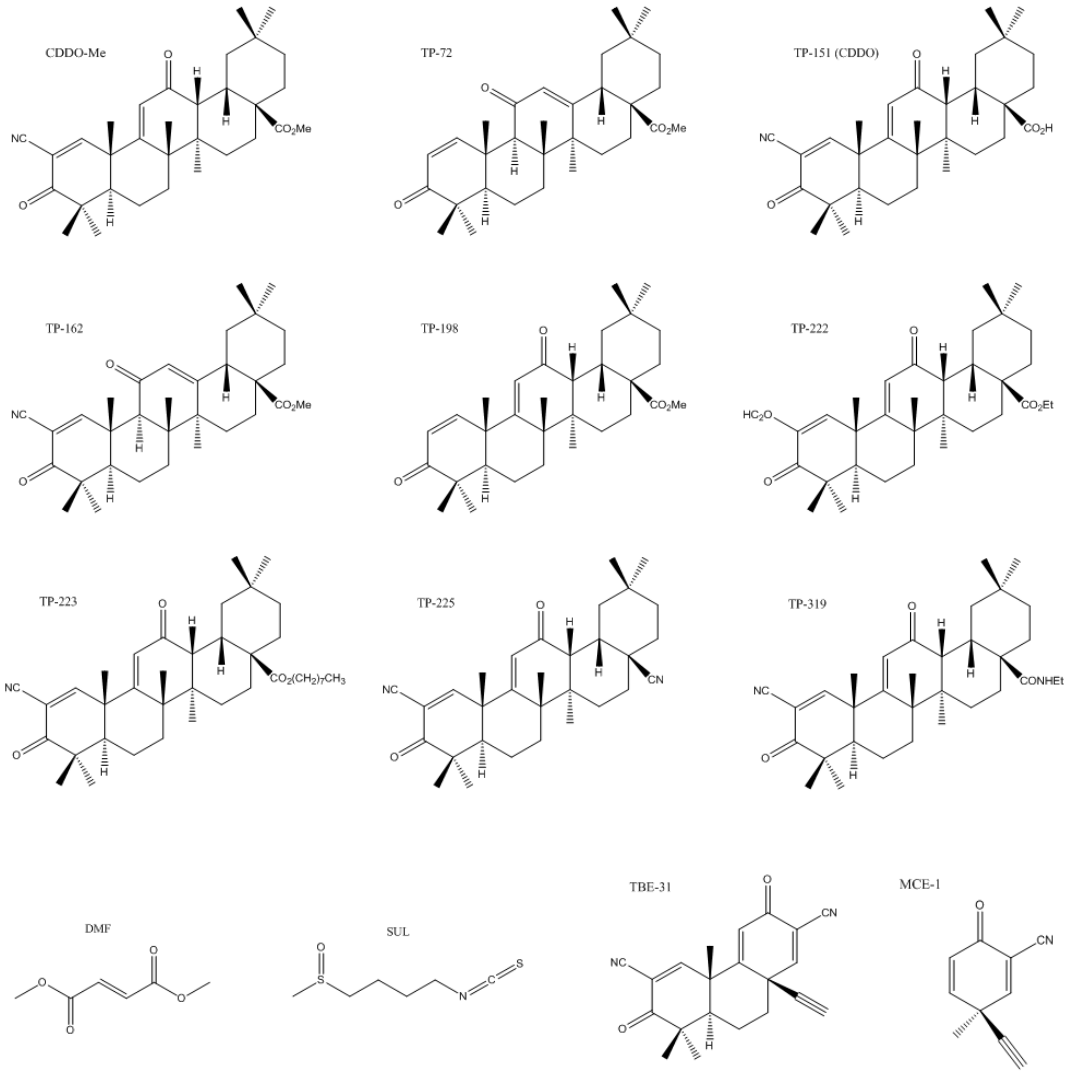

Fig.1: Chemical structures of Nrf2 inducers used in this study. CDDO-Me and related triterpenoid analogues (TP-72 to TP-319), Nrf2 inducers that have entered the clinic (DMF and SUL), the experimental tricyclic and monocyclic cyano enone Nrf2 inducers TBE-31 and MCE-1.

4.2 Methods

***Materials**:* Unless stated, all reagents were obtained from Sigma-Aldrich (Poole, UK).

***Chemistry**:* The synthesis of CDDO-Me and related triterpenoids (Honda *et al.*, 2000; Honda *et al.*, 2002), TBE-31 (Favaloro *et al.*, 2002; Honda *et al.*, 2007) and MCE-1 (Zheng *et al.*, 2012) has been previously described. Compounds were kindly supplied by Dr. Tadashi Honda (Stony Brook University, USA).

***Cell culture**:* Rat H4IIE-ARE8L cells, stably expressing a luciferase reporter regulated by an eight-times repeated antioxidant response element were generated as described (Kratschmar *et al.*, 2012), and kindly provided by Prof. Alex Odermatt (Basel University, Switzerland). Mouse Hepa1c1c7 and human HepG2 cells were obtained from ATCC. Cells were maintained at 37 ^{o}C in a 5 % CO_2 atmosphere in Dulbecco's Modified Eagle's Medium supplemented with 584 mg/L L-glutamine, 10% fetal bovine serum (Life Technologies, Paisley, UK) in Nunc T75 vented flasks (Fisher Scientific). The media for H4IIE-ARE8L cells was supplemented with 1mM HEPES and 1X nonessential amino acids, whereas the media for Hepa1c1c7 and HepG2 cells was further supplemented with 100 U/mL penicillin and 100 µg/mL streptomycin. H4IIE-ARE8L, Hepa1c1c7 or HepG2 cells were plated in Nunc 96 well flat bottomed plates (Fisher Scientific) at 10,000 cells per well. For drug treatments, compounds were dissolved in DMSO, with concentrations of the solvent in the media controlled to <0.5 %.

***Determination of cellular ATP content**:* Following exposure of H4IIE-ARE8L, Hepa1c1c7 or HepG2 cells to the indicated compounds for 24 h, cellular ATP content was quantified using the CellTiter-Glo Luminescent Cell Viability assay (Promega, Southampton, UK) in accordance with manufacturer's instructions. Essentially, 20 µL ATP reagent was added to each well, and the plate was mixed on a plate shaker at 700 RPM for one minute. The plate was subsequently stored in the dark at room temperature for 5 minutes, and then 100 µL of each well content was transferred to a 96 well white luminescence plate (Grenier Bio-One). Luminescence was determined using the Thermo Scientific VarioSkan Flash 3001 device. Data are normalised to the ATP content of vehicle-treated cells.

***Determination of ARE8L reporter activity**:* H4IIE-ARE8L cells were plated as described previously. Following exposure to the indicated compounds for 24 h, reporter assays were performed essentially as described (Kratschmar *et al.*, 2012), using the Bright-Glo Luciferase Assay system (Promega) in accordance with the manufacturer's instructions. Briefly, media was removed from the plate and 100 µL Glo lysis buffer was added. Plate was mixed on a plate shaker at 700 RPM for one minute, and 80 µL per well was added to a 96 well white luminescence plate. 20 µL Bright Glo reporter assay reagent was added, and the plate was subsequently mixed on a plate shaker at 700 RPM for 15 seconds. Luminescence was determined as described previously. Data are normalised to the reporter activity detected in vehicle-treated cells.

***Calculation of* in vitro *therapeutic index*:** The concentrations of each compound that provoked a two-fold increase in the activity of the ARE8L reporter transgene (CD value) and a two-fold decrease in the cellular ATP content (LC50 value) in H4IIE-ARE8L cells was determined by nonlinear regression analysis of the respective concentration-response curves, using GraphPad Prism 6 (GraphPad software). The *in vitro* therapeutic index is expressed as a ratio of LC50 divided by CD.

Total protein determination: Following drug treatment, Hepa1c1c7 cells were washed twice with PBS and lysed with RIPA buffer, and protein content was determined using the Bicinchoninic assay, as described in Chapter 2.

***Immunoblotting*:** Cell lysates (20 µg total protein) were loaded onto NuPAGE 4-12 % Bis-Tris Precast gel (Life Technologies), and immunoblotting performed as described in Chapter 2.

***PI-FACS analysis*:** Propidium iodide (PI) flow cytometry was performed to quantify the population of sub-G_0/G_1 phase cells. Following drug treatment, cells were washed twice with Hank's Buffered Saline Solution (HBSS) and suspended in ice-cold 70 % ethanol overnight at -20^{o}C. Cells were washed once in HBSS, and pelleted at 2000 RPM for 3 min. Pellets were resuspended in HBSS containing 40 µg/ml PI, 0.1 mg/ml RNase, 3.8 mM sodium citrate. Samples were incubated in the dark at 37 ^{o}C for 30 min and subsequently analysed using a Becton-Dickinson FACSCanto II FACS unit. PI fluorescence was measured in the FL-2 channel, with a maximum of 10,000 cells quantified per sample. Samples were mixed after every 3 readings.

4.3 Results

4.3.1 Concept of the in vitro therapeutic index

By calculating the concentrations of a compound that provoke a two-fold increase in the activity of the Nrf2-sensitive ARE8L reporter transgene (CD, concentration of doubling), and a two-fold decrease in cellular ATP content (the LC50) in H4IIE-ARE8L cells, the ratio of LC50 divided by the CD can be used to determine the therapeutic index. Figure 2 depicts examples of hypothetical compounds, with that in A having a large *in vitro* therapeutic index as a result of having a high potency toward Nrf2 (i.e. low CD value) and minimal toxicity (a high LC50 value). The hypothetical compound depicted in B has a low *in vitro* therapeutic index, due to its low potency toward Nrf2 (high CD value) and high toxicity (low LC50). This concept has been used to examine the relationship between Nrf2 induction potency, toxicity and *in vitro* therapeutic index for a number of small molecule inducers of Nrf2.

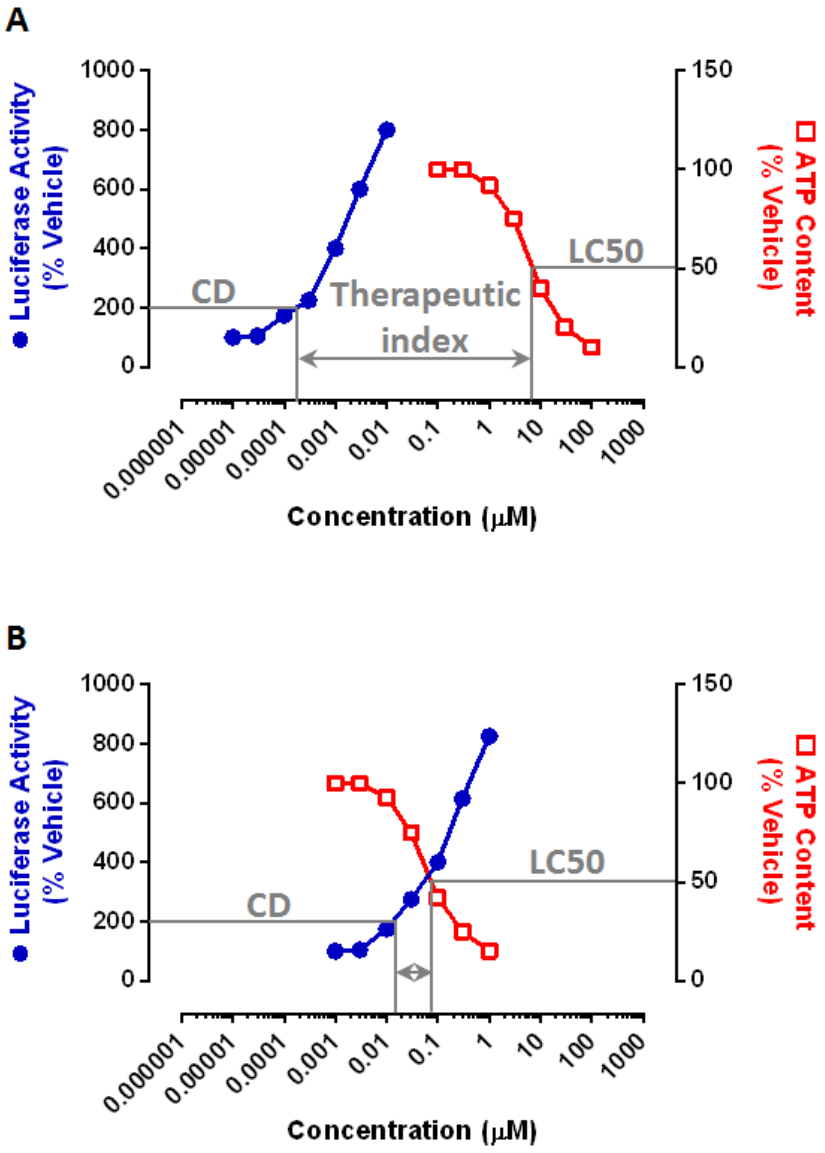

Fig.2: Hypothetical examples of the method used to determine therapeutic index. (A) depicts a compound with a high therapeutic index, with low concentrations needed to provoke a two-fold increase in the activity of ARE8L reporter transgene (CD, blue circles), and high concentrations required to deplete cellular ATP by two-fold (LC50, red squares). (B) depicts a compound with a low therapeutic index, with high concentrations required to provoke a two-fold increase in the ARE8L reporter transgene activity and low concentrations required to induce toxicity.

4.3.2 Therapeutic indices of clinically validated Nrf2 inducers

The relationship between toxicity and potency of Nrf2-inducing compounds was first examined with the clinically validated molecules sulphoraphane (SUL, (Houghton *et al.*, 2013)) and dimethyl fumarate (DMF, (Lee *et al.*, 2013)), alongside CDDO-Me (Fig. 3). H4IIE-ARE8L cells were exposed to the indicated concentrations of CDDO-Me, SUL and DMF. All three compounds were able to induce the activity of the Nrf2 reporter transgene in a concentration-dependent manner. At high concentrations, all three compounds provoked a loss of cell viability, associated with a decrease in ARE8L reporter transgene activity, likely due to the disruption of critical cellular processes, and/or a lack of ATP, which is required for bioluminescence generation.

The calculation of CD values revealed an order of potency for inducing Nrf2 of CDDO-Me>SUL>DMF (Table 2). Calculation of the LC50 values also revealed a rank-order of toxicity of CDDO-Me>SUL>DMF (Table 2). A similar rank-order of toxicity was observed in human HepG2 and mouse Hepa1c1c7 cells, indicating the translational robustness of the data (Fig. 4, Table 1).

Ostensibly, the similar rank orders of CD and LC50 values for CDDO-Me, SUL and DMF indicates that potency towards Nrf2 is inherently related to toxicity. However, it was notable that the CD values of CDDO-Me, SUL and DMF spanned four orders of magnitude, whereas the associated LC50 values spanned just two orders of magnitude. This observation implied that potency and toxicity could be dissociated.

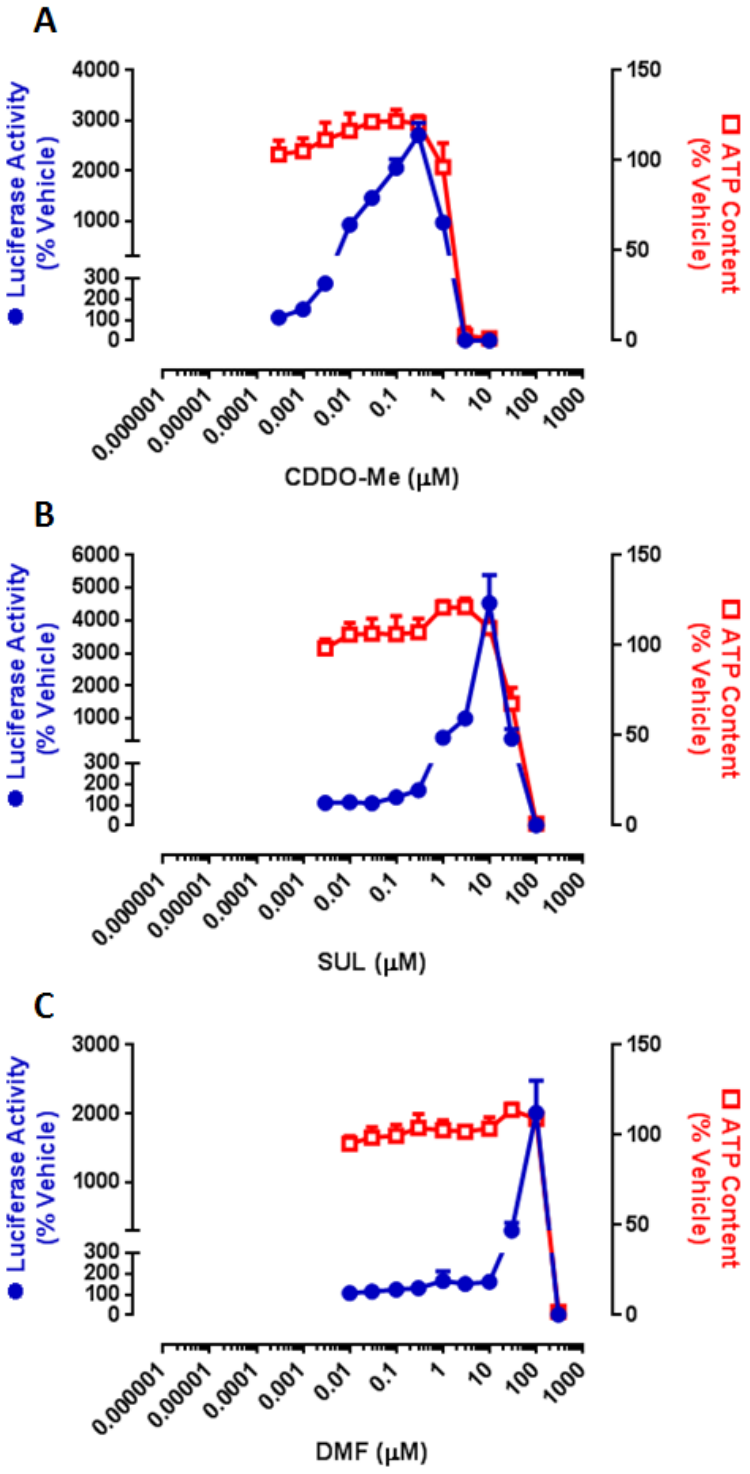

Fig.3: Therapeutic indices of (A) CDDO-Me, (B) SUL and (C) DMF in H4IIE-ARE8L cells. Following 24h exposure to the indicated compound, luciferase reporter activity (blue circles) and ATP content (red squares) were quantified as a measure of Nrf2 induction and toxicity respectively. Data represent the mean and SD (n=3).

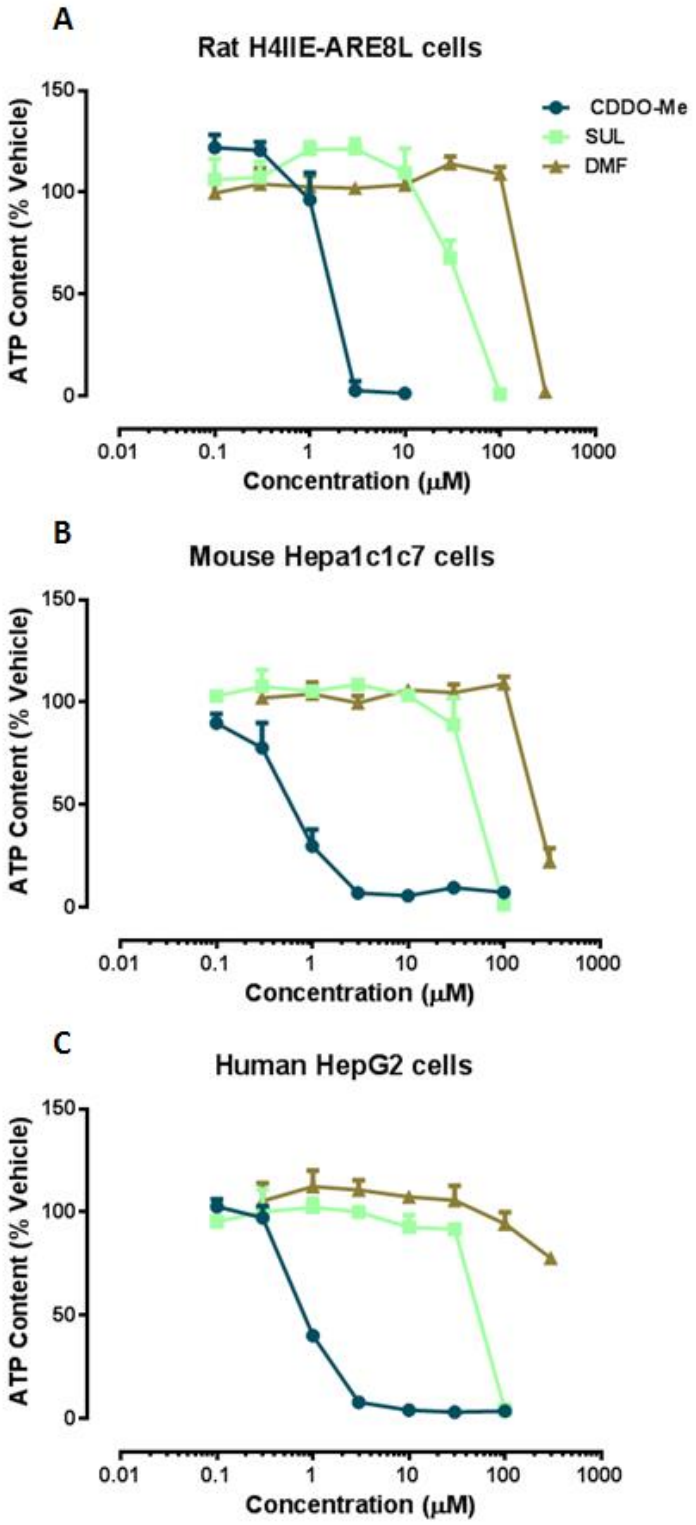

Fig.4: Toxicity of clinically validated Nrf2 inducers in (A) rat H4IIE-ARE8L, (B) mouse Hepa1c1c7 and (C) human HepG2 hepatoma cells. Following 24h exposure to the indicated compound, ATP content was quantified as a measure of toxicity. Data represents the mean and SD (n=3).

	LC50 (μM)		
	CDDO-Me	**SUL**	**DMF**
Rat H4IIE-ARE8L cells	1.4 ± 0.3	35.1 ± 4.1	276.5 ± 14.4
Mouse Hepa1c1c7 cells	0.7 ± 0.2	52.5 ± 15.3	288.0 ± 4.4
Human HepG2 cells	0.9 ± 0.03	60.8 ± 19.2	>300

Table 1: LC50 values of CDDO-Me, SUL and DMF in rat H4IIE-ARE8L cells, mouse Hepa1c1c7 cells and human HepG2 cells. Following 24h exposure to the indicated compound, ATP content was quantified as a measure of toxicity. Data represents the mean and SD (n=3).

4.3.3 Therapeutic indices of triterpenoid Nrf2 inducers

To further examine the relationship between Nrf2 induction potency and toxicity of small molecules within a refined chemical space, eight structurally-related triterpenoid analogues of CDDO-Me were selected based on their reported abilities to induce Nqo1 in Hepa1c1c7 cells (Dinkova-Kostova *et al.*, 2005). Following exposure to H4IIE-ARE8L cells for 24h, TP-72, TP-151, TP-162, TP-198, TP-222, TP-225, TP-233 and TP-319 were shown to evoke concentration-dependent increases in Nrf2 reporter transgene activity (Fig. 5). The potencies of the triterpenoids towards Nrf2 in H4IIE-ARE8L cells were in agreement with their previously reported potencies towards Nqo1 in Hepa1c1c7 cells (Dinkova-Kostova *et al.*, 2005). The triterpenoids induced loss of cell viability at micromolar concentrations, with the exception of TP-72, which at the highest achievable concentration (100 µM) did not deplete ATP (Fig. 5). Calculation of *in vitro* therapeutic indices for each compound confirmed that an increase in potency was associated with a relative enhancement of *in vitro* safety (Fig. 5, Table 2).

Like CDDO-Me, the triterpenoids found to have the highest therapeutic indices (TP-151, TP-162, TP-225 and TP-319) possess a nitrile group at position C-2 on ring A. The nitrile group enhances electrophilicity and imparts reversibility of the Michael acceptor enone group (Honda *et al.*, 2011). Research into novel triterpenoid compounds and derivatives suggests that the reactivity of a Michael acceptor is indicative of biological potency (Zheng *et al.*, 2012). Substitution of the nitrile group at C-2 on the A ring with a carboxyl group (TP-222) produces a compound with 10-100 times lower *in vitro* therapeutic index than TP-151, TP-162, TP-225 and

TP-319, whereas a second nitrile group (C-17 on TP-225), provides the highest therapeutic index of the compounds tested (Table 2). Substitution of a long chain hydrocarbon at C-17 produced one of the least potent Nrf2 inducers (TP-233), and shorter chained compounds tend towards higher therapeutic indices (compare TP-151 and TP-319, Table 2). TP-72 and TP-198 both lack a nitrile group at C-2, but their therapeutic indices still differ, likely due to the positioning of the enone on ring C (Table 2). TP-72 lacks both correct positioning of the enone and a nitrile group on the A ring, and as such has a potency toward Nrf2 that is 30,000 times less than CDDO-Me, and does not induce cell death at the highest possible concentration of 100 μM (Table 2). Taken together, these data serve to emphasise that an increase in potency toward Nrf2 is associated with a relative enhancement of *in vitro* safety (Fig. 5, Table 2).

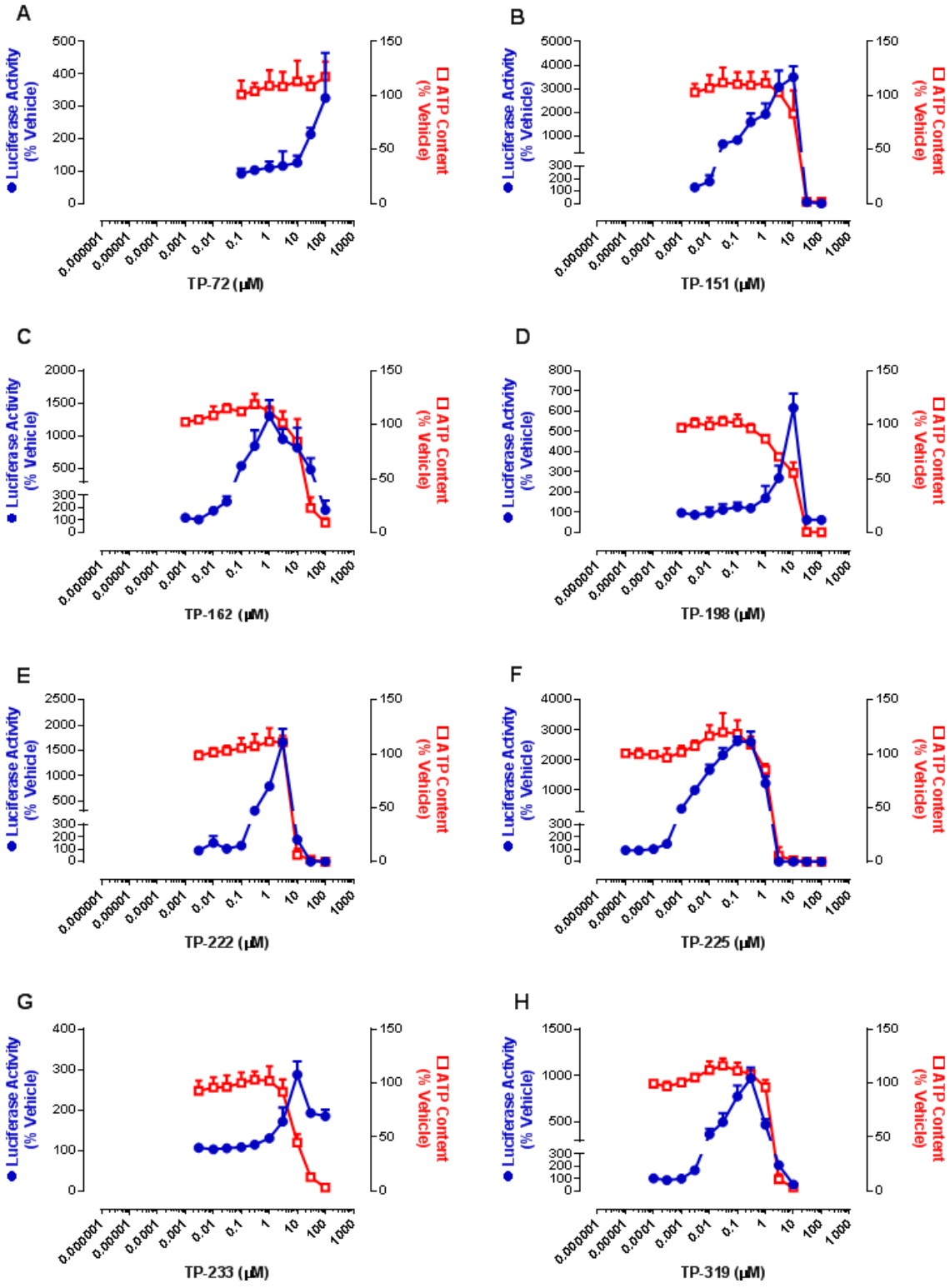

Fig.5: Pharmacological potencies and toxicities of triterpenoids in H4IIE-ARE8L cells. Cells were exposed to the indicated triterpenoids for 24 h. Luciferase reporter activity (blue circles) and ATP content (red squares) were subsequently quantified as measures of Nrf2 induction and toxicity, respectively. Data represent the mean and SD (n=3).

4.3.4 Therapeutic indices of novel tricyclic and monocyclic cyano enone Nrf2 inducers

In light of recent evidence of clinical adverse toxic events associated with CDDO-Me (de Zeeuw *et al.*, 2013b), it is apparent that there is a need for next-generation Nrf2 inducers with comparatively acceptable safety and efficacy. TBE-31 and MCE-1 were selected for investigation because of their established potencies toward Nrf2 *in vitro* and *in vivo* (Honda *et al.*, 2007; Dinkova-Kostova *et al.*, 2010b; Zheng *et al.*, 2012), and as representatives of novel tricyclic and monocyclic cyanoenone classes. H4IIE-ARE8L cells were exposed to the indicated concentrations of TBE-31 and MCE-1 for 24h and the therapeutic indices calculated as before (Fig. 6, Table 2). Both compounds exhibit relatively high therapeutic indices; TBE-31 has a comparable therapeutic index to CDDO-Me, and contains two nitrile groups to modulate enone reactivity. MCE-1, which contains a single nitrile group, has a therapeutic index comparable to sulphoraphane (Table 2). Both TBE-31 and MCE-1 are therefore promising second-generation Nrf2 inducers with relatively good *in vitro* safety and efficacy profiles.

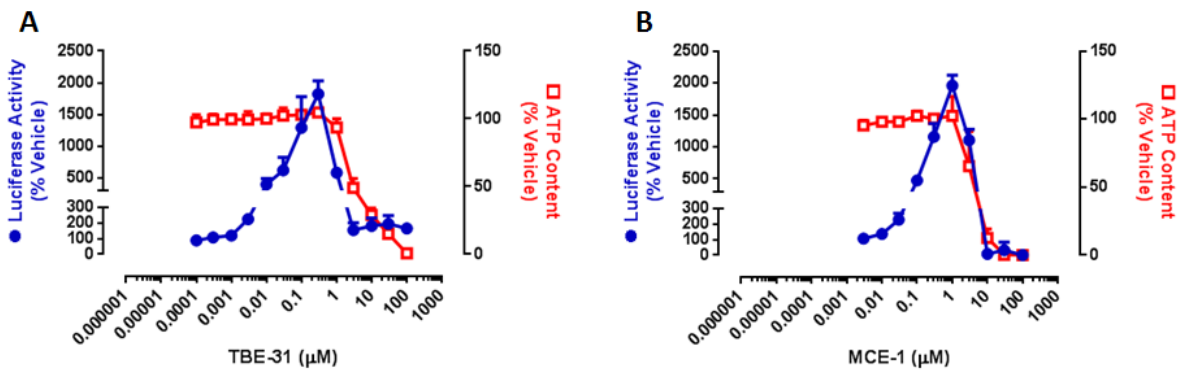

Fig.6: Pharmacological potencies and toxicities of (A) TBE-31 and (B) MCE-1 in H4IIE-ARE8L cells. Cells were exposed to the indicated concentrations of the compounds for 24 h. Luciferase reporter activity (blue circles) and ATP content (red squares) were subsequently quantified as measures of Nrf2 induction and toxicity, respectively. Data represent the mean and SD (n=3).

4.3.5 Correlation of potency towards Nrf2, toxicity and *in vitro* therapeutic index of Nrf2 inducing compounds

Table 2 depicts pharmacological potencies (CD), toxicities (LC50) and resulting *in vitro* therapeutic indices of the 13 compounds studied here. Figure 7 depicts the correlation of potency towards Nrf2 with (A) toxicity and (B) *in vitro* therapeutic index for the compounds. Evidently, with an increase in potency toward Nrf2 there is an increase in toxicity, however this increase is not to the same degree (i.e. not equivalent, Fig. 7A). Indeed, the CD values span four orders of magnitude, whereas the associated LC50 values span just two orders of magnitude. As a result, an increase in potency is associated with an increase in therapeutic index, i.e. a relative enhancement of *in vitro* safety (Fig. 7B).

Compound	CD (µM)	LC50 (µM)	Therapeutic index
TP-225	0.0005 ± 0.0001	1.6 ± 0.2	3448.3 ± 698.2
CDDO-Me	0.001 ± 0.0001	2.1 ± 0.5	1818.1 ± 356.3
TBE-31	0.003 ± 0.001	3.8 ± 0.5	1620.0 ± 652.7
TP-162	0.02 ± 0.009	18.4 ± 4.6	1397.7 ± 415.1
TP-151	0.01 ± 0.004	16.3 ± 3.7	1373.3 ± 201.5
TP-319	0.005 ± 0.001	1.9 ± 0.2	417.7 ± 72.1
MCE-1	0.03 ± 0.01	4.6 ± 2.1	152.4 ± 57.3
SUL	0.4 ± 0.1	51.9 ± 2.6	140.6 ±38.4
TP-222	0.2 ± 0.02	7.2 ± 0.3	33.5 ± 2.1
DMF	20.5 ±8.7	184.4 ± 4.8	10.0 ± 3.7
TP-198	1.6 ± 0.6	8.1 ± 1.4	5.5 ± 1.4
TP-233	4.6 ± 2.1	10.4 ± 2.6	2.6 ± 1.4
TP-72	29.1 ± 2.7	>100	N.D.

Table 2: Pharmacological potencies, toxicities and *in vitro* therapeutic indices of Nrf2 inducers in H4IIE-ARE8L cells. Data represent the mean and SD (n=3), N.D. not determined.

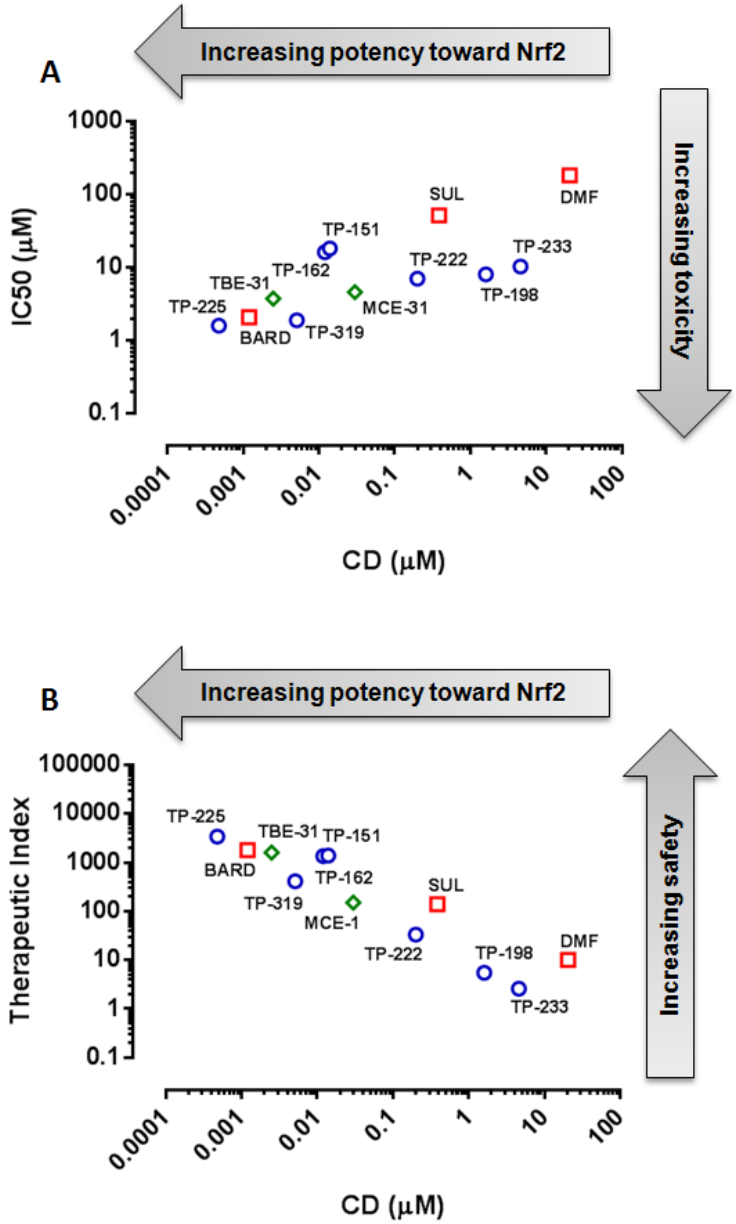

Fig.7: Correlation of potency toward Nrf2, toxicity and *in vitro* therapeutic index of clinically validated (red squares), triterpenoid (blue circles) and novel cyano enone (green diamonds) Nrf2 inducing compounds. Correlation between potency towards Nrf2 and (A) toxicity [Pearson correlation coefficient 0.75, P = 0.005] or (B) *in vitro* therapeutic index [Pearson correlation coefficient -0.93, P = <0.0001]. CD and LC50 values and therapeutic indices for each compound were calculated as described.

4.3.6 Investigation of the mechanism of toxicity of next-generation tricyclic and monocyclic cyano enone compounds

4.3.6.1 Comparable toxicity of TBE-31 and MCE-1 in different cell lines

The relatively high therapeutic indices of TBE-31 and MCE-1 (Fig. 6, Table 2) give an indication of their suitability for future clinical use, however data on their pre-clinical toxicity is lacking. Firstly, the translational robustness of the data generated in rat H4IIE-ARE8L cells was assessed (Fig. 8). Rat H4IIE-ARE8L, mouse Hepa1c1c7 and human HepG2 cells were exposed to the indicated concentrations of TBE-31, MCE-1 and CDDO-Me for 24 h. It was shown that the compounds provoke consistent degrees of toxicity across the different cell lines (Table 3).

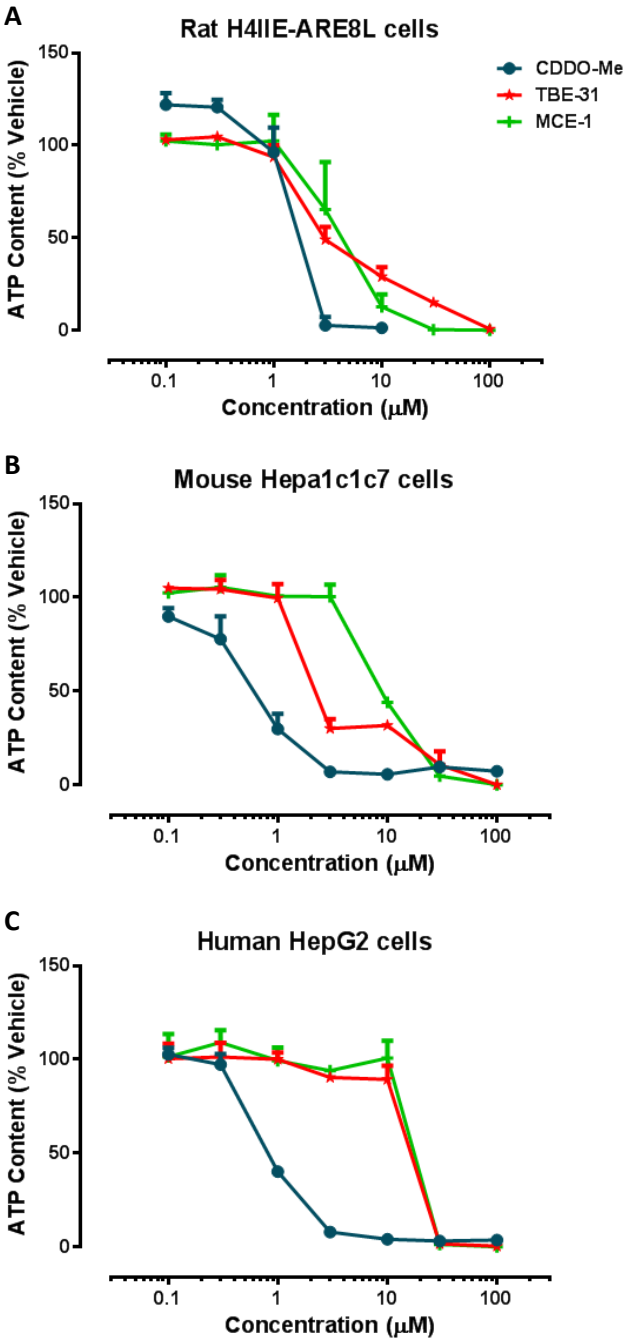

Fig.8: Toxicity of CDDO-Me, TBE-31 and MCE-1 in (A) rat H4IIE-ARE cells, (B) mouse Hepa1c1c7 cells and (C) human HepG2 cells. Following 24 h exposure to the indicated compound, ATP content was quantified as a measure of toxicity. Data represents the mean and SD (n=3).

	LC50 (μM)		
	CDDO-Me	**TBE-31**	**MCE-1**
Rat H4IIE-ARE8L cells	1.4 ± 0.3	3.8 ± 0.9	4.1 ± 1.8
Mouse Hepa1c1c7 cells	0.7 ± 0.2	2.3 ± 0.4	9.3 ± 0.6
Human HepG2 cells	0.9 ± 0.03	16.1 ± 2.6	21.1 ± 6.2

Table 3: LC50 values of CDDO-Me, TBE-31 and MCE-1 in rat H4IIE-ARE8L cells, mouse Hepa1c1c7 cells and human HepG2 cells. Following 24h exposure to the indicated compound, ATP content was quantified as a measure of toxicity. Data represents the mean and SD (n=3).

4.3.6.2 High concentrations of TBE-31 and MCE-1 provoke caspase 3 activation in Hepa1c1c7 cells

Whilst indicative of drug-induced changes in the metabolic activity of cells, assaying ATP content does not give much information on the mechanism of cell death. It has previously been demonstrated that triterpenoids such as CDDO-Me provoke loss of cell viability via the induction of apoptosis (Kim *et al.*, 2002), and so further work was performed to determine the mechanism of cell death induced by TBE-31 and MCE-1. Hepa1c1c7 cells were treated with the indicated concentrations of CDDO-Me, TBE-31 and MCE-1 for 24 h, and lysates subsequently probed for caspase 3 by western blotting. The data in Fig. 9 indicates that all three compounds provoke caspase 3 cleavage from the pro- form to the processed, apoptosis-inducing active form in a concentration-dependent manner. Indeed, the concentrations of each compound that induce caspase 3 processing are close to the LC50 values (Table 3) determined with the ATP assay. These findings indicate that TBE-31 and MCE-1 initiate cell death via apoptosis associated with caspase 3 activation.

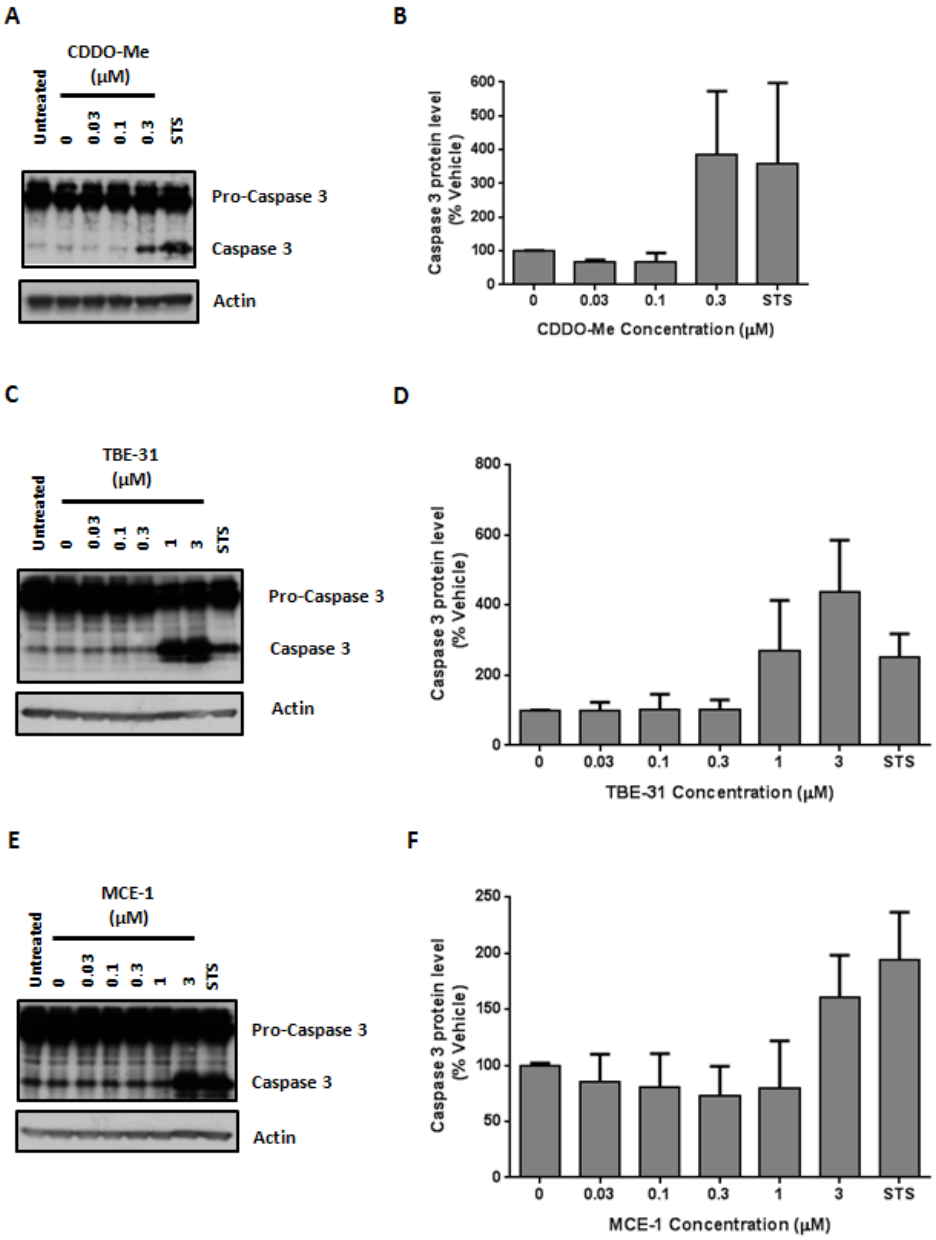

Fig.9: Hepa-1c1c7 cells were exposed to the indicated concentrations of (A,B) CDDO-Me, (C,D) TBE-31 or (E,F) MCE-1 for 24 h. The processing of caspase 3 from its inactive 32 kDa form to its proteolytically active 17 kDa form was determined in whole cell lysates by Western blotting. Staurosporine (STS; 1 μM) was used as a positive control for caspase 3 activation. Actin was probed as a loading control. Active caspase 3, normalised to actin, is expressed as a percentage of the level in vehicle (DMSO)-exposed cells. Blots are representative of n=3 independent experiments. Densitometry data represent the mean and SD (n=3).

4.3.6.3 FACS analysis of TBE-31 and MCE-1-treated Hepa1c1c7 cells demonstrates the induction of apoptosis at high concentrations

To provide further evidence for apoptosis being the major mechanism of cell death induced by TBE-31 and MCE-1, propidium iodide staining and flow cytometry was performed on Hepa1c1c7 cells 24 h after exposure to the compounds, or CDDO-Me (Fig.10). Fig 10A depicts examples of the histograms generated, demonstrating (i) a population of non-apoptotic cells following vehicle treatment, and (ii) a large proportion of cells with hypodiploid/fragmented DNA undergoing apoptosis following exposure to 20 μM CDDO-Me. Fig 10B depicts a concentration-dependent increase in the population of propidium iodide-stained cells, representative of sub G_0/G_1 phase apoptotic cell population. Taken together with our observation of caspase 3 processing (Fig. 9), these data demonstrate that TBE-31 and MCE-1 provoke apoptotic cell death at high concentrations in a similar manner to the triterpenoid CDDO-Me.

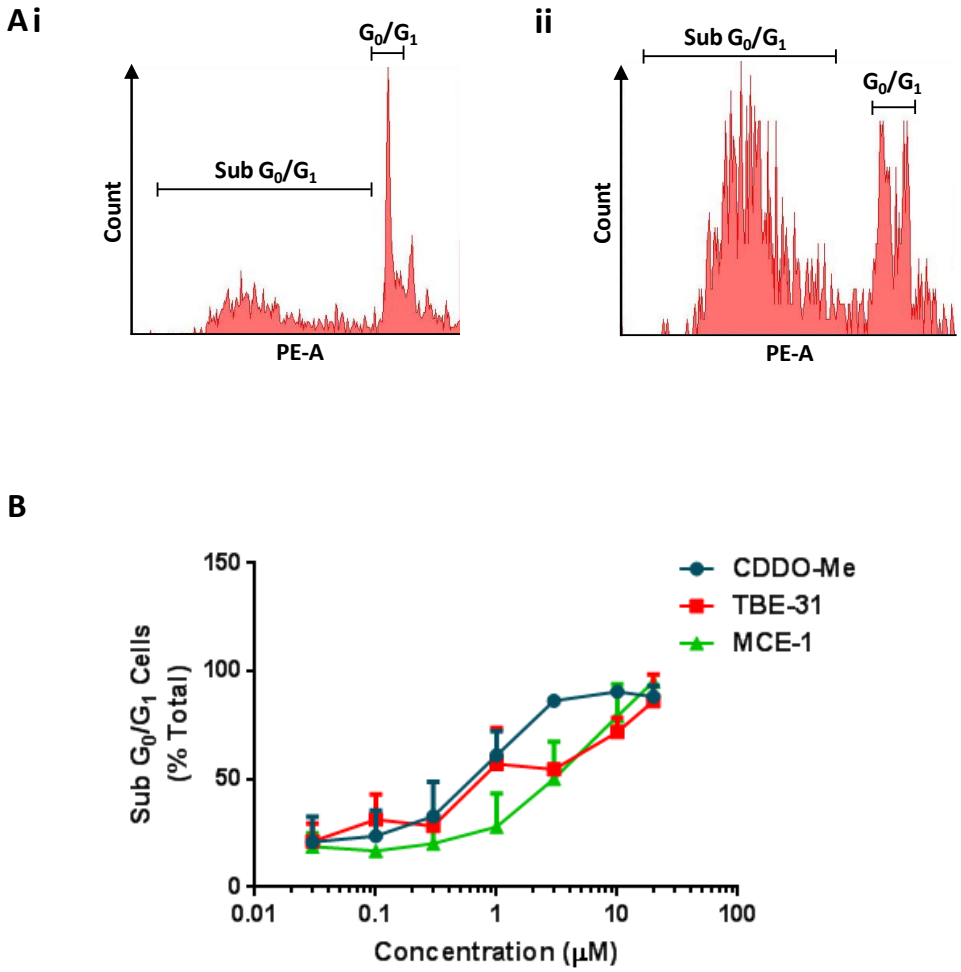

Fig.10: The number of cells in the sub G_0/G_1 phase of the cell cycle were quantified following propidium iodine staining by flow cytometry. Hepa-1c1c7 cells were exposed to the indicated concentrations of CDDO-Me, TBE-31 or MCE-1 for 24 h. (Ai) is a histogram depicting a large proportion of non-apoptotic cells following DMSO treatment; (ii) depicts an apoptotic cell population following 20 μM CDDO-Me treatment. (B) depicts a concentration-dependent increase in apoptotic cells following compound treatment. Data represent mean and SD (n=3).

4.4 Discussion

The pharmacological induction of Nrf2 has shown promise for the treatment of numerous diseases in animal models (Ruiz *et al.*, 2013; Shelton *et al.*, 2013), however the clinical development of one inducer, CDDO-Me, was recently halted due to adverse cardiovascular events in late-stage chronic kidney disease patients (de Zeeuw *et al.*, 2013b). Key properties of Nrf2 inducers include electrophilicity and reactivity towards protein thiols (Bensasson *et al.*, 2010), but reactivity towards unintended targets is known to be a primary trigger of drug toxicity. It is therefore pertinent to address whether therapeutic targeting of Nrf2 could be undermined by the chemical reactivity of small molecule inducers, and to question if the drive to generate more potent and efficacious Nrf2 activators could also inadvertently generate more toxic compounds.

Here, the *in vitro* therapeutic index has been determined for clinically validated Nrf2 inducers (CDDO-Me, SUL and DMF), a selection of triterpenoid analogues of CDDO-Me and the novel tricyclic and monocyclic cyano enones TBE-31 and MCE-1. The data demonstrates an increase in potency toward Nrf2 is associated with a relative increase in *in vitro* safety indicating that it is possible to generate potent Nrf2-inducing small molecules that are not inherently toxic to mammalian cells.

The cessation of the BEACON trial for safety concerns due to 'excess serious events and mortality' provoked a literary response questioning the focus of the trial, and discussing the possible causes of mortality (Tayek *et al.*, 2013; Chin *et al.*, 2014c). The data highlighted heart failure events and death from cardiovascular disease occurring in a higher proportion of patients in the treatment arm (de Zeeuw *et al.*,

2013b). CDDO-Me is known to elevate blood pressure (de Zeeuw *et al.*, 2013b; Chin *et al.*, 2014c), and patients experiencing latter stage (3b, 4) CKD progression treated with CDDO-Me had a propensity toward elevated systolic and diastolic blood pressure, and decreased sodium and water output (de Zeeuw *et al.*, 2013b; Chin *et al.*, 2014c). Whilst in the early stages of investigation, this off-target effect is thought to be due to modification of endothelin signalling (Chin *et al.*, 2014c), highlighting the need for rational design of Nrf2 activating compounds to limit off-target effects. Therefore, a better understanding of the pharmacodynamic actions of Nrf2 inducers is needed to improve the selection or exclusion of certain patient cohorts for future clinical trials. In light of the above, it will be important to determine the effects of next-generation Nrf2 inducers such as TBE-31 and MCE-1 on endothelin signalling prior to any future clinical trials.

Notably, the animal population most closely resembling the BEACON trial clinical population (latter-stage renal failure, 3b, 4), Zucker Diabetic Fatty rats (which spontaneously develop obesity and diabetes linked to enhanced oxidative stress) displayed a similar phenotype to the BEACON trial clinical population (increased blood pressure, weight loss) following exposure to a CDDO-Me analogue (de Zeeuw *et al.*, 2013b; Zoja *et al.*, 2013). These adverse events have been attributed to impurities in the batch of drugs used to treat the animals (Chin *et al.*, 2013), however this rodent group did not experience any of the beneficial effects of CDDO-Me noted in previous animal studies (Aminzadeh *et al.*, 2013b; Chin *et al.*, 2013; Ruiz *et al.*, 2013; Van Laecke *et al.*, 2014). Therefore, Zucker Diabetic Fatty

rats may be a suitable model in which to further examine the mechanisms underlying the adverse effects of CDDO-Me in late-stage CKD patients.

Despite the utility of the *in vitro* therapeutic index as a means to compare the relationship between Nrf2 induction and toxicity in simple cell models, it cannot determine whether a compound will provoke adverse reactions in animals or humans. Indeed, the relatively low *in vitro* therapeutic index of DMF would indicate that it is a poor candidate for clinical use, yet DMF was recently licensed for the management of multiple sclerosis (Lee *et al.*, 2013). Similarly, the relatively high *in vitro* therapeutic index of CDDO-Me would theoretically make it a good candidate for clinical exploration, however the results of the BEACON trial (de Zeeuw *et al.*, 2013b) suggest otherwise, demonstrating the limitations of the controlled *in vitro* system used here, and the complexities of *in vitro* to *in vivo* extrapolation. TP-225 demonstrates the largest *in vitro* therapeutic index of the compounds studied here, indicating it to be a good candidate for clinical use. Indeed, it is known to induce Nrf2 and reduce lesions following topical administration to UV-exposed SKH-1 mice (Dinkova-Kostova *et al.*, 2008), but unpublished data derived from (Dinkova-Kostova *et al.*, 2008) has shown it to have very poor oral bioavailability (Albena Dinkova-Kostova, personal communication), limiting progress in the clinic, a factor which the *in vitro* therapeutic index is not able to predict.

One limitation of using the induction of a luciferase reporter transgene as a marker of potency towards Nrf2 is that it does not indicate the protective effects of the various compounds. A further study in which the the H4IIE-ARE8L cells were

concomitantly exposed to a model toxin and different Nrf2 inducers would provide further information about the protective concentrations of these compounds *in vitro*, which, if linked to subsequent toxicity, would provide mechanistic information about the potential clinical utility of these Nrf2 inducers. This could be further assessed by monitoring the induction of a variety of Nrf2-regulated genes, to understand the relative effectiveness of these Nrf2 inducers at provoking a cytoprotective response.

In conclusion, the data described here indicates that the drive to produce potent small molecule Nrf2 inducers is not associated with the generation of more toxic compounds *in vitro*, suggesting that the cause of the adverse cardiovascular events reported in the BEACON trial is related to poor patient population selection and/or off-target signalling, rather than inherent structural toxicity or the induction of Nrf2 *per se*. Recent work examining the role off-target endothelin signalling may have played in the cessation of the BEACON trial (Chin *et al.*, 2014c) emphasises the need to test other Nrf2 inducing compounds to ensure this effect is structural, rather than Nrf2-mediated. Such studies are vital if next-generation Nrf2 inducers such as TBE-31 and MCE-1 are to enter clinical trials.

The therapeutic promise of CDDO-Me has not been extinguished, as it is currently undergoing a phase II clinical trial assessing its safety and efficacy in patients with pulmonary arterial hypertension (LARIAT, NCT02036970), with the rationale being to capitalise on the anti-inflammatory properties of CDDO-Me by way of suppression of pro-inflammatory mediators in multiple cell types. It is specified that patients enrolled in the trial must have adequate renal function as a result of

the adverse events reported in the BEACON trial. Notably, Chapter 2 delineates the relatively small number of Nrf2 target proteins that are upregulated in the healthy mouse kidney in response to a single acute exposure to CDDO-Me, whilst evidence for the pharmacological induction of Nrf2 in the human kidney, and a role for this in the beneficial effect of CDDO-Me in CKD patients (de Zeeuw *et al.*, 2013b) is currently lacking. This calls into question the rationale of targeting Nrf2 in CKD patients, although more work is needed in this area.

Nevertheless, Nrf2 inducers continue to hold promise as novel treatments for a range of diseases, and the work presented here indicates that enhancement of pharmacological potency is not inherently linked to an increase in toxicity, which will aid the assessment of benefit:risk for Nrf2 inducers in different patient cohorts.

Chapter 5

General Discussion

Introduction

The transcription factor Nrf2 has previously been demonstrated to afford protection against acute kidney injury (Shelton et al., 2013) and chronic disease (Ruiz et al., 2013) in various experimental models, however, at the commencement of the research described here, the physiological and pharmacological roles of Nrf2 in the kidney were relatively poorly understood, compared to other organs. This thesis has sought to address these knowledge gaps through proteomic, transcriptomic and targeted analysis of animal and cell-based models in which Nrf2 is modulated via genetic and/or pharmacological interventions, and through investigation of the relationship between pharmacological potency and toxicity of established and novel Nrf2 inducers.

Role of Nrf2 in protection against acute kidney injury

The investigations described in Chapters 2 and 3 sought to define the molecular processes governed by Nrf2 in the kidney. Whole renal homogenates from $Nrf2^{+/+}$ and $Nrf2^{-/-}$ mice, treated with CDDO-Me or vehicle, were utilised in a multifaceted approach using both iTRAQ proteomics and a microRNA array to define the proteins and microRNAs under Nrf2 control in the kidney.

The key finding of the work presented in Chapter 2 was that the proteins regulated by Nrf2 in the kidney were involved in a wide range of homeostatic processes, including the maintenance of redox balance, the synthesis and conjugation of glutathione, the metabolism and disposition of a wide range of xenobiotics,

pyruvate metabolism, the supply of NADPH and the synthesis and recycling of amino acids (Fig. 1 and 2). That Nrf2 may play an important role in the regulation of these processes has a wide implication for the development of novel Nrf2-targeting drugs, but also in the understanding of the physiological roles of Nrf2 in the kidney.

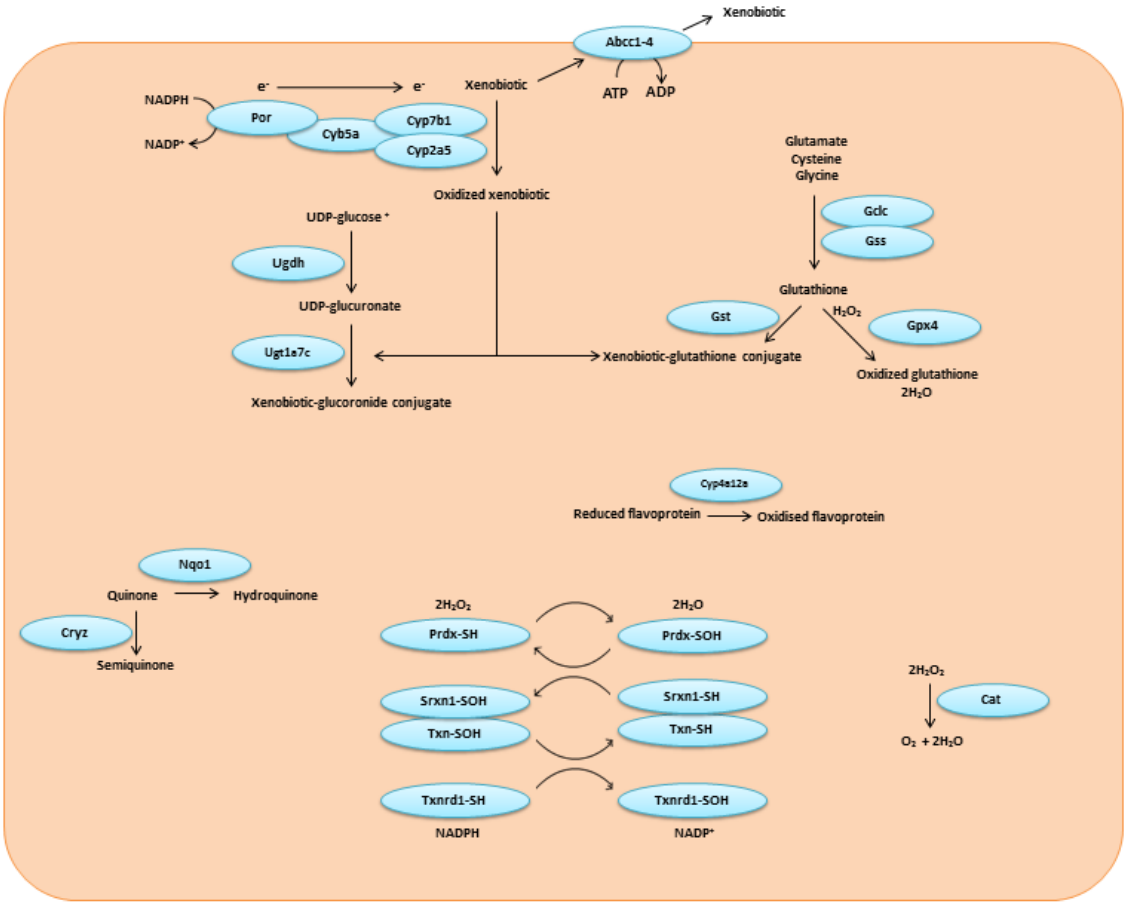

Fig. 1: Schematic of proteins involved in xenobiotic metabolism, the antioxidant pathway and glutathione synthesis shown here to be regulated by Nrf2 at the basal level in the mouse kidney.

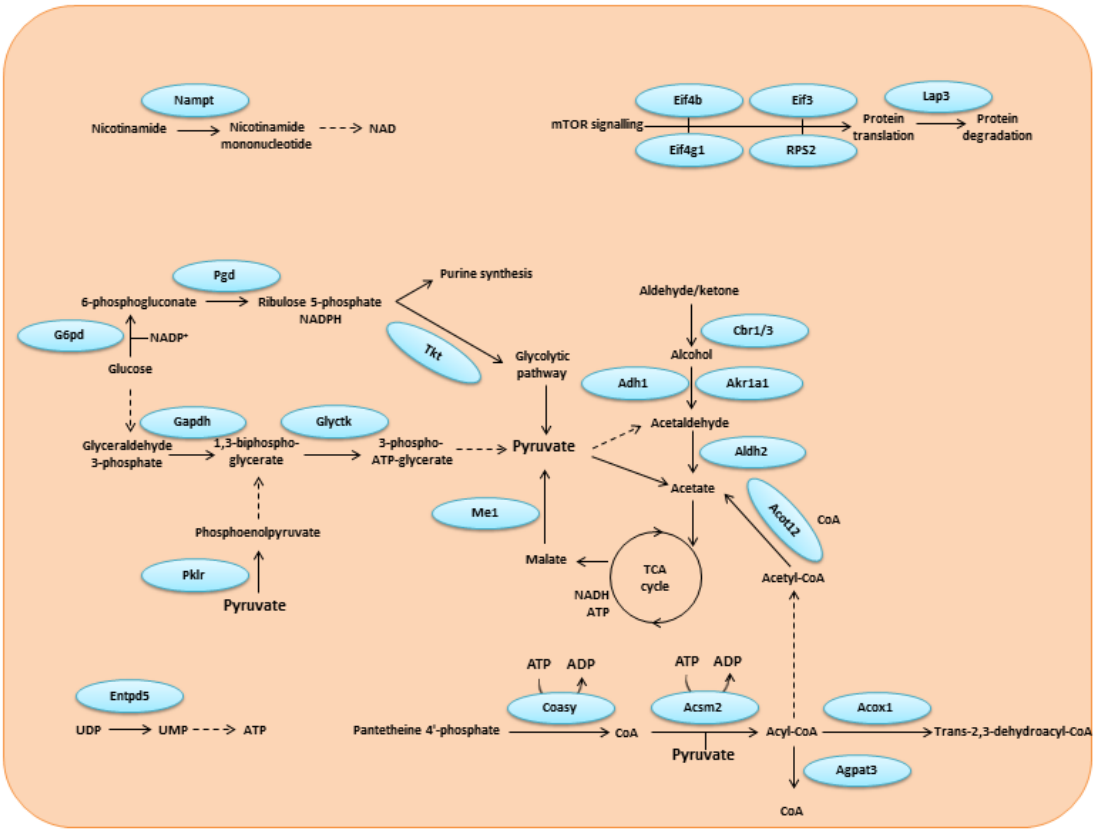

Fig. 2: Schematic of proteins involved in energy homeostasis shown here to be regulated by Nrf2 at the basal level in the mouse kidney.

The involvement of Nrf2 in the regulation of glycolysis and the pentose phosphate pathway is relatively unexplored (Kraft *et al.*, 2004; Heiss *et al.*, 2013; Holmstrom *et al.*, 2013), and determining the impact of Nrf2 on the production of cellular energy is a newly emerging field (Mitsuishi *et al.*, 2012; Hayes *et al.*, 2014). Fig. 2 depicts the renal proteins shown to be positively regulated by Nrf2 in the iTRAQ study within an overall scheme of glycolysis and the pentose phosphate pathway. Additionally, the production of NADPH and FAD has been determined here and elsewhere to be regulated by Nrf2 (Wu *et al.*, 2011a; Holmstrom *et al.*, 2013); consistent with our observation that Nrf2 regulates the expression of Nampt, G6pd

and Pgd, enzymes that controls the production of NADPH (Frederiks *et al.*, 2007; Bowlby *et al.*, 2012).

The enhanced sensitivity to AKI in the Nrf2$^{-/-}$ mouse (Liu *et al.*, 2009; Aleksunes *et al.*, 2010; Shelton *et al.*, 2013) is consistent with the data described in this thesis, in that proteins involved in the maintenance of redox balance and xenobiotic metabolism are decreased in the Nrf2$^{-/-}$ mouse, and increased following CDDO-Me administration. It is likely the cumulative effects of these Nrf2-regulated proteins that reduce the efficiency (or ablate the capacity) of redox balance, xenobiotic metabolism and general ability to cope with stress, such as AKI. Furthermore, an increased ROS burden has been associated with increased cytoskeletal remodelling (Stanley *et al.*, 2014), consistent with the data presented in Chapter 2, Table 5 describing the increase in expression of proteins associated with alterations in epithelial junction signalling and actin cytoskeleton remodelling in the antioxidant-impaired Nrf2$^{-/-}$ mouse. Whether this is a protective response, or is a consequence of reduced antioxidant capacity requires further investigation.

As described in Chapter 3, a number of microRNA species have been found to be differentially expressed in both the Nrf2$^{-/-}$ and CDDO-Me treated Nrf2$^{+/+}$ mouse kidney, and further validation of these findings will (a) provide important insights into the regulatory roles of Nrf2 in the kidney given that a number of these microRNAs as yet do not have an assigned function, and (b) may identify a microRNA-based biomarker of Nrf2 activity.

Given the nature of the negative regulatory role of microRNAs, the general ablation of microRNA biogenesis in a proximal-tubule specific model of IR injury results in

enhanced resistance (Wei *et al.*, 2010). However, podocyte-specific ablation of microRNA biogenesis results in severe renal impairment (Shi *et al.*, 2008), suggesting a complex role for microRNAs in renal physiology that is not cell-specific. Indeed, a number of the microRNAs found here to be regulated by Nrf2 in the kidney do not yet have an assigned function (e.g. miR-3082, miR-669p-3p, miR-466f), emphasising the need for further work to determine the relationship between the increased susceptibility of the $Nrf2^{-/-}$ mouse to AKI, and the role(s) that differential expression of specific microRNA species may have, especially in the context of the different sections of the nephron.

Adverse drug reactions are a significant clinical problem, estimated to cost the NHS 1.6 million bed days and £466 million per year (Pirmohamed *et al.*, 2004), and pose a substantial barrier to the development and use of novel medicines. Nrf2 is known to protect against the adverse reactions associated with exposure to paracetamol (Enomoto *et al.*, 2001), cisplatin (Aleksunes *et al.*, 2010) and bleomycin (Cho *et al.*, 2004) in mice. Inter-individual variation in susceptibility to adverse drug reactions in humans is well documented (Edwards *et al.*, 2000); however, as yet this has not been correlated to variation in Nrf2 activity. Given that disruption of Nrf2 reduces the renal expression of at least 108 proteins in $Nrf2^{-/-}$ compared to $Nrf2^{+/+}$ mice (Chapter 2, Table 2), and the kidney plays an important role in the metabolism of various drugs (Lohr *et al.*, 1998; Perazella, 2009), the potential for inter-individual variation in the activity of the Nrf2 pathway in the kidney, and more generally, should be determined in human populations with respect to susceptibility to adverse drug reactions. Such heterogeneity (for example in expression of renal

transporter and detoxication enzymes), could predispose some individuals to renal diseases or nephrotoxic insults, or render them relatively resistant, and thus may be an informative marker of patient health.

Therapeutic targeting of Nrf2 – potential mechanisms and implications

Following the cessation of the CDDO-Me 'BEACON' clinical trial due to unforeseen adverse clinical events (de Zeeuw *et al.*, 2013b), questions were raised whether the drive to generate more potent and efficacious Nrf2 inducers had inadvertently generated inherently more toxic compounds (Fig. 3). Through examination of cellular responses to a battery of Nrf2-inducing compounds, the work presented in Chapter 4 determined that an increase in potency towards Nrf2 is associated with an increase in *in vitro* therapeutic index, and as such a relative enhancement of *in vitro* safety (Copple *et al.*, 2014).

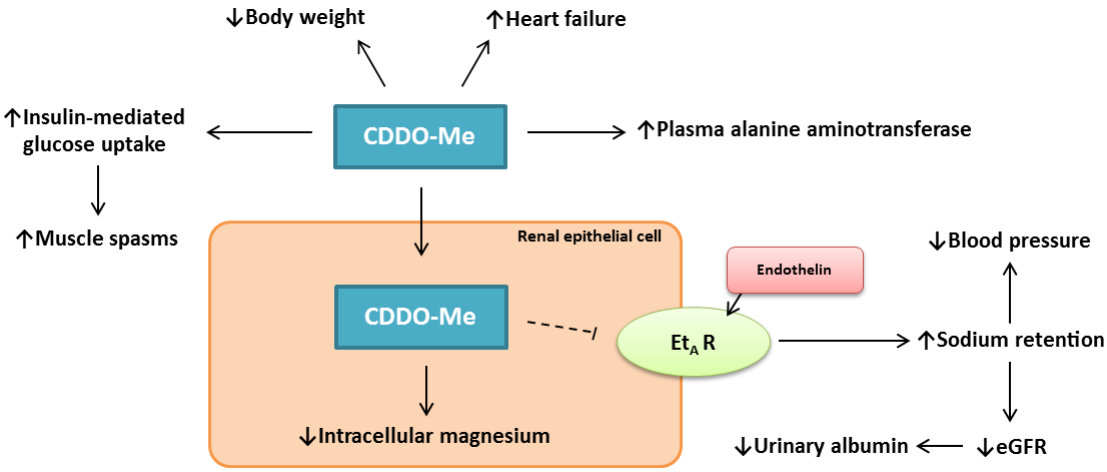

Fig. 3: Overview of adverse effects observed in recent clinical trials of CDDO-Me (Pergola *et al.*, 2011b; de Zeeuw *et al.*, 2013b). Dashed line shows proposed CDDO-Me mediated downregulation of the endothelin A receptor (Et_AR), which leads to a decrease in sodium retention (Camer *et al.*, 2014) and an increase in fluid volume, contributing to an increase in blood pressure and eGFR, at the cost of decreasing filtration capacity and increasing urinary albumin.

The termination of the CDDO-Me 'BEACON' trial can most likely be attributed to poor patient selection and not due to inherent toxicity of CDDO-Me. Since the termination of the trial (and after the work in this thesis was completed), more details about the adverse events have been published, suggesting that patients with a baseline B-type natriuretic peptide (BNP, a peptide secreted by the heart functioning to decrease systemic vascular resistance and increase natriuresis, the excretion of Na^+ at the kidney) of ≥200 pg/mL had an increased risk of heart failure when treated with CDDO-Me, compared to the placebo (Chin *et al.*, 2014b). Renal failure is associated with an increase in BNP, and a corresponding increase in fluid volume (Cowie *et al.*, 2002). BNP levels were increased in the CDDO-Me group, compared to the placebo in the 'BEACON' study (de Zeeuw *et al.*, 2013b), likely as a result of an off-target effect of CDDO-Me in modulating the renal endothelin system (Chin *et al.*, 2014c). The role of Nrf2 in the modulation of endothelin signalling by CDDO-Me has not been examined. Because the patients enrolled in the 'BEACON' study already had higher than usual fluid retention, it seems likely that the effect of CDDO-Me on endothelin signalling compounded this issue, and resulted in the adverse cardiac events (Camer *et al.*, 2014; Chin *et al.*, 2014a; Chin *et al.*, 2014c; Chin *et al.*, 2014b). Converse to the renal system, suppression of the cardiac endothelin signalling is protective against hypertension and heart failure (Nasser *et al.*, 2014), therefore the tissue-specificity of this off-target effect of CDDO-Me must be investigated; emphasising the need to consider whole animal physiology when determining the pharmacological effects of CDDO-Me and alternative Nrf2-inducing drugs.

To our knowledge, the mechanism behind the improvement of eGFR by CDDO-Me (Hong *et al.*, 2012) has yet to be shown to be Nrf2-dependent, and our immunohistochemical analysis (Chapter 2, Fig. 11) did not reveal particularly intense staining of Nrf2 and Nqo1 on the glomerular podocytic membrane. Likewise, the mechanism of action of dimethyl fumarate (licensed as a treatment for multiple sclerosis (Lee *et al.*, 2013)) has also yet to be determined as Nrf2-dependent. The contribution of Nrf2 induction to the beneficial effects of CDDO-Me in CKD and other diseases requires further investigation, especially given that CDDO-Me targets other cellular signalling pathways (Fig. 4), albeit generally at higher concentrations than those required to induce Nrf2. In particular, the role of NF-κB inhibition in the therapeutic effects of CDDO-Me, DMF and other Nrf2 inducers is a key knowledge gap that will inform the utility of such drugs in the treatment of different diseases. Therefore, further work is needed to define the pharmacological and toxicological consequences of targeting Nrf2 in renal and other diseases.

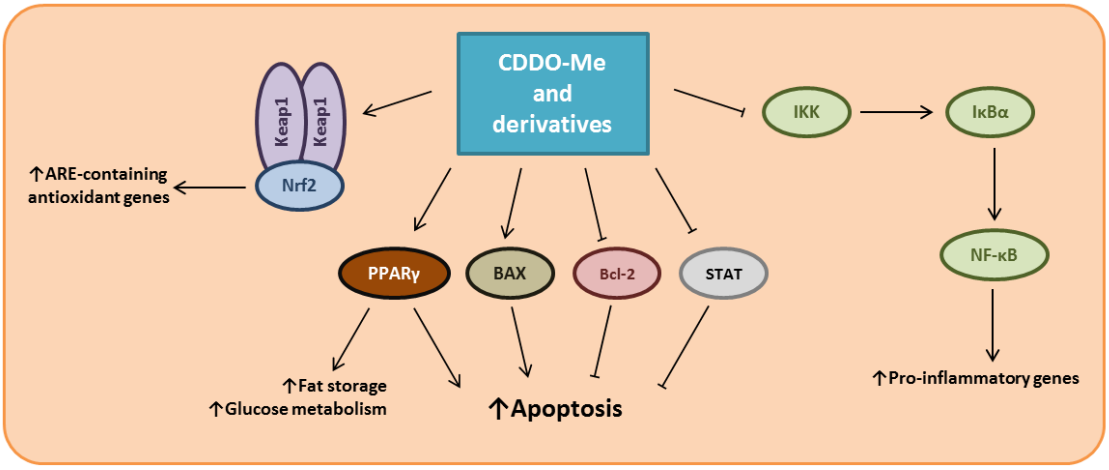

Fig. 4: Known pharmacological targets of CDDO-Me and its derivatives. In addition to activating the Nrf2 pathway, CDDO-Me has also been shown to induce PPARγ expression resulting in an increase in fat storage and glucose metabolism in both normal physiological conditions and in acute kidney injury (Wu *et al.*, 2011b). CDDO-Me mediated induction of PPARγ, and BAX (Konopleva *et al.*, 2002), and inhibition of Bcl-2 (Wang *et al.*, 2015b) and STAT (Liby *et al.*, 2006) are pro-apoptotic. Finally, inhibition of the NF-κB pathway reduces the expression of pro-inflammatory genes (Shanmugam *et al.*, 2014). The relative contributions of these pharmacological effects to the ability of CDDO-Me to improve eGFR in CKD patients is not known.

CDDO-Me is currently being investigated in a trial ('LARIAT', NCT02036970) for patients with pulmonary arterial hypertension (but not elevated BNP or renal dysfunction), based on the proposed beneficial reduction of cardiac endothelin signalling highlighted in the 'BEACON' trial (Chin *et al.*, 2014b), and the compound's known anti-inflammatory activity (Shanmugam *et al.*, 2014) and ability to improve metabolic function (Chapter 2, (Reisman *et al.*, 2012)), via Nrf2-regulation of energy metabolism. Additionally, the Japanese pharmaceutical company Kyowa Hakko

Kirin have recently restarted a Phase II clinical trial treating CKD patients with CDDO-Me, but with the proviso that these patients have a BNP of <200 pg/mL. This highlights that lessons have been learned from the CDDO-Me 'BEACON' trial.

The induction of Nrf2 by CDDO-Me has been associated with significant weight loss in cynomolgus monkeys (Reisman *et al.*, 2012), and induction of Nrf2 in mouse astrocytes has been shown to upregulate a number of genes involved in glycolysis (Kraft *et al.*, 2004) consistent with the data presented here indicating that Nrf2 positively regulates the expression of proteins that contribute to glycolysis and energy metabolism. Sulphoraphane treatment has been reported to reduce weight gain in a mouse model of diabetic nephropathy (Zheng *et al.*, 2011), whilst dimethyl fumarate prevents weight gain in a mouse Huntington's Disease model (Ellrichmann *et al.*, 2011). Furthermore, the induction of traumatic haemorrhage injury in rats results in a decrease in Nrf2 protein activity and energy production, which was rescued with resveratrol treatment (Jian *et al.*, 2014). These observations suggest that the modulation of Nrf2 may be a novel strategy for stimulating weight loss. However, pharmacological activation of Nrf2 may also carry the potential to adversely affect energy metabolism and weight in certain disease states. This aspect of patient safety should be considered during the development of novel Nrf2-inducing drugs.

The clinical future of Nrf2 inducing compounds is not as bleak as first thought at the termination of the 'BEACON' trial. RTA-408, a derivative of CDDO, is currently undergoing eight clinical trials for a wide range of diseases including combatting advanced solid tumours (NCT02029729), in patients with melanoma (NCT02259231)

and mitochondrial myopathy (NCT02255422). These clinical trials have exclusion criteria for patients with a baseline BNP of >200 pg/mL and for patients with a history of specific cardiac disorders. The exclusion criteria have highlighted the possibility of using CDDO derivatives in treating a much wider range of diseases. Better understanding of patient selection and the physiological and pharmacological roles of Nrf2 suggest that CDDO-Me and other Nrf2 inducing compounds may still hold promise as novel treatments for disease.

Biomarkers of Nrf2 activity

Due to the lack of available biomarkers of Nrf2 activity, multiple methods, both *in vitro* and *in vivo*, have been established to determine the value of monitoring Nrf2 activity for the detection of pharmacological and toxicological events. The use of the reporter cell line detailed in Chapter 4 (H4IIE-ARE8L, (Copple *et al.*, 2014)), and cell lines expressing fluorescent-tagged Nrf2 or its target genes (Wink *et al.*, 2014) represent a step towards deriving an easily-measureable Nrf2 response. In addition, the KeratinoSens^{TM} assay is now recommended by the OECD as part of a panel of *in vitro* tests for identifying skin sensitising compounds based on the induction of a ARE-luciferase reporter construct (Emter *et al.*, 2010). Similarly, transcriptomic signatures have been used to define responses to toxicity and identify novel renal biomarkers of injury in the non-transformed human proximal tubule cell line RPTEC/TERT1 following exposure to a variety of nephrotoxins (Aschauer *et al.*, 2014). Analysis of primary cells would allow for the consolidation of key markers of Nrf2 activity, which would aid the continuing drive to utilise cell

models to predict toxicity of new drugs, and define the contribution of Nrf2 to such responses.

Whilst *in vitro* work has utility, due to the limited physiological relevance of cell lines and the rapid dedifferentiation of primary cells (Van der Hauwaert *et al.*, 2013) these cells are often only proximal tubule-like, and the physiological response in context with the whole organism is therefore not accurate, and translational markers of Nrf2 activity are unable to be analysed. The development of Nrf2-luc reporter mice (OKD48-luc, producing bioluminescence measureable through whole animal or *ex vivo* organ imaging upon activation of the Nrf2 response (Oikawa *et al.*, 2012)) has enabled the measurement of Nrf2 activity in real time *in vivo*, and therefore provides an excellent route to examine the relationship between drug disposition, organ toxicity and the activation of the Nrf2 response. However, the translational value of Nrf2-luc mice is likely to be limited, as drug metabolism varies between species, and may not accurately reflect the Nrf2 pathway response in humans.

Patient peripheral blood mononuclear cells (PBMCs) represent one avenue of investigation for utilisation of a clinical biomarker of Nrf2 activity. NQO1 mRNA was reported to be increased 5-fold in the PBMCs of patients administered CDDO-Me as a treatment for solid tumours and lymphomas (Hong *et al.*, 2012). Aldo-keto reductase activity in PBMCs was shown to be increased following Nrf2 induction, representing a promising translational marker of Nrf2 activity (Jung *et al.*, 2013). Currently it is unclear whether NQO1 and aldo-keto reductase measurement in PBMCs represents the status of Nrf2 activation in the whole body or in target

organs, and therefore the lack of a measureable biomarker of Nrf2 activity is hindering the detailed assessment of the response of the Nrf2 pathway in humans. Additionally, HO-1 has been detected in the urine and plasma of patients with acute kidney injury (Zager *et al.*, 2012), however this protein is known to be regulated by multiple mechanisms other than Nrf2 (Alam *et al.*, 2003), and was not detected in the iTRAQ study in Chapter 2, therefore its utility as a generic biomarker of Nrf2 activity is questionable.

Monitoring Nrf2 activity in patients would aid in understanding the functional consequences of Nrf2 manipulation. The lack of appropriate markers of Nrf2 activity leads to problems in determining both the basal state and the extent of inter-individual variation in expression of Nrf2 in patients. Quantifying the basal expression of Nrf2 could assist in the personalisation of drug regimens. Indeed, measurement of the basal state of Nrf2 in patients enrolled in the CDDO-Me 'BEACON' clinical trial could have provided new knowledge about the contribution of Nrf2 towards the adverse effects, and about the pathological changes in the patient population following CDDO-Me administration.

Current clinical biomarkers of renal disease in humans include the use of proteins and mRNA (for example, detection of nephrin mRNA in podocytic injury (Wang *et al.*, 2007), and albumin following albuminuria), however more accurate next-generation biomarkers of renal disease are required as current ones are often unreliable (Nayak *et al.*, 2013). Circulating microRNAs represent a largely unexplored resource of potential biomarkers of disease that may be more effective than current protein or mRNA-based biomarkers, in part due to their transient

nature that is well suited to dynamic measurement. In the case of paracetamol hepatotoxicity, miR-122 expression is detectable in plasma at levels above normal earlier than typical markers of hepatic injury (Starkey Lewis *et al.*, 2011).

Impaired Nrf2 activity is associated with chronic kidney disease (Kim *et al.*, 2010; Aminzadeh *et al.*, 2013a), and therefore the measurement of microRNAs and proteins responsive to Nrf2 activity in an easily available biofluid could provide insights into disease state and/or prognosis. Whether the proteins (e.g. Gstm1, Nqo1, Cat) and microRNAs (e.g. miR-28c, miR-144 and miR-466h) shown here to be regulated by Nrf2 can accurately reflect the activity of Nrf2 in a manner befitting of a biomarker should be investigated by triangulating suitable *in vitro* and *in vivo* models with clinical data. A possible route could involve the correlation of a protein or microRNA known to be regulated by Nrf2 with a biomarker of renal disease (such as Kim-1) through the use of in-situ hybridisation and the subsequent correlation of trends in expression of this particular biomarker of renal disease in an easily accessible biofluid from patients with CKD. The identification of such a biomarker would allow the relevance of Nrf2 as a therapeutic target and critical node in the toxicological response to drugs to be examined in humans.

References

Adam J, Hatipoglu E, O'Flaherty L, Ternette N, Sahgal N, Lockstone H*, et al.* (2011). Renal cyst formation in Fh1-deficient mice is independent of the Hif/Phd pathway: roles for fumarate in KEAP1 succination and Nrf2 signaling. *Cancer Cell* 20**:** 524-537.

Adams J, Kelso R, Cooley L (2000). The kelch repeat superfamily of proteins: propellers of cell function. *Trends Cell Biol* 10**:** 17-24.

Ahmad MK, Naqshbandi A, Fareed M, Mahmood R (2012). Oral administration of a nephrotoxic dose of potassium bromate, a food additive, alters renal redox and metabolic status and inhibits brush border membrane enzymes in rats. *Food Chem* 134**:** 980-985.

Ahmad R, Raina D, Meyer C, Kharbanda S, Kufe D (2006). Triterpenoid CDDO-Me blocks the NF-kappaB pathway by direct inhibition of IKKbeta on Cys-179. *J Biol Chem* 281**:** 35764-35769.

Alam J, Cook JL (2003). Transcriptional regulation of the heme oxygenase-1 gene via the stress response element pathway. *Curr Pharm Des* 9**:** 2499-2511.

Aleksunes LM, Goedken MJ, Rockwell CE, Thomale J, Manautou JE, Klaassen CD (2010). Transcriptional regulation of renal cytoprotective genes by Nrf2 and its potential use as a therapeutic target to mitigate cisplatin-induced nephrotoxicity. *J Pharmacol Exp Ther* 335**:** 2-12.

Alvarez-Mora MI, Rodriguez-Revenga L, Madrigal I, Torres-Silva F, Mateu-Huertas E, Lizano E*, et al.* (2013). MicroRNA expression profiling in blood from fragile X-associated tremor/ataxia syndrome patients. *Genes Brain Behav* 12**:** 595-603.

Aminzadeh MA, Nicholas SB, Norris KC, Vaziri ND (2013a). Role of impaired Nrf2 activation in the pathogenesis of oxidative stress and inflammation in chronic tubulo-interstitial nephropathy. *Nephrol Dial Transplant* 28**:** 2038-2045.

Aminzadeh MA, Reisman SA, Vaziri ND, Khazaeli M, Yuan J, Meyer CJ (2014). The synthetic triterpenoid RTA dh404 (CDDO-dhTFEA) restores Nrf2 activity and attenuates oxidative stress, inflammation, and fibrosis in rats with chronic kidney disease. *Xenobiotica* 44**:** 570-578.

Aminzadeh MA, Reisman SA, Vaziri ND, Shelkovnikov S, Farzaneh SH, Khazaeli M*, et al.* (2013b). The synthetic triterpenoid RTA dh404 (CDDO-dhTFEA) restores endothelial function impaired by reduced Nrf2 activity in chronic kidney disease. *Redox Biol* 1**:** 527-531.

Antoine DJ, Mercer AE, Williams DP, Park BK (2009). Mechanism-based bioanalysis and biomarkers for hepatic chemical stress. *Xenobiotica* 39**:** 565-577.

Apopa PL, He X, Ma Q (2008). Phosphorylation of Nrf2 in the transcription activation domain by casein kinase 2 (CK2) is critical for the nuclear translocation and transcription activation function of Nrf2 in IMR-32 neuroblastoma cells. *J Biochem Mol Toxicol* 22**:** 63-76.

Aschauer L, Limonciel A, Wilmes A, Stanzel S, Kopp-Schneider A, Hewitt P*, et al.* (2014). Application of RPTEC/TERT1 cells for investigation of repeat dose nephrotoxicity: A transcriptomic study. *Toxicol In Vitro*.

Ayodele OE, Alebiosu CO, Salako BL (2004). Diabetic nephropathy--a review of the natural history, burden, risk factors and treatment. *J Natl Med Assoc* 96**:** 1445-1454.

Bakris GL, Fonseca VA, Sharma K, Wright EM (2009). Renal sodium-glucose transport: role in diabetes mellitus and potential clinical implications. *Kidney Int* 75**:** 1272-1277.

Bandyopadhyay S, Gronostajski RM (1994). Identification of a conserved oxidation-sensitive cysteine residue in the NFI family of DNA-binding proteins. *J Biol Chem* 269**:** 29949-29955.

Banning A, Deubel S, Kluth D, Zhou Z, Brigelius-Flohe R (2005). The GI-GPx gene is a target for Nrf2. *Mol Cell Biol* 25**:** 4914-4923.

Bartel DP (2004). MicroRNAs: genomics, biogenesis, mechanism, and function. *Cell* 116**:** 281-297.

Bartel DP (2009). MicroRNAs: Target Recognition and Regulatory Functions. *Cell* 136**:** 215-233.

Bensasson RV, Zoete V, Berthier G, Talalay P, Dinkova-Kostova AT (2010). Potency ranking of triterpenoids as inducers of a cytoprotective enzyme and as inhibitors of a cellular inflammatory response via their electron affinity and their electrophilicity index. *Chem Biol Interact* 186**:** 118-126.

Benson AM, Hunkeler MJ, Talalay P (1980). Increase of NAD(P)H:quinone reductase by dietary antioxidants: possible role in protection against carcinogenesis and toxicity. *Proc Natl Acad Sci U S A* 77**:** 5216-5220.

Biswas M, Chan JY (2010). Role of Nrf1 in antioxidant response element-mediated gene expression and beyond. *Toxicol Appl Pharmacol* 244**:** 16-20.

Blank V (2008). Small Maf proteins in mammalian gene control: mere dimerization partners or dynamic transcriptional regulators? *J Mol Biol* 376**:** 913-925.

Bokenkamp A, Ludwig M (2011). Disorders of the renal proximal tubule. *Nephron Physiol* 118**:** p1-6.

Bowlby SC, Thomas MJ, D'Agostino RB, Jr., Kridel SJ (2012). Nicotinamide phosphoribosyl transferase (Nampt) is required for de novo lipogenesis in tumor cells. *PLoS One* 7**:** e40195.

Brater DC (2000). Pharmacology of diuretics. *Am J Med Sci* 319**:** 38-50.

Bryan HK, Olayanju A, Goldring CE, Park BK (2013). The Nrf2 cell defence pathway: Keap1-dependent and -independent mechanisms of regulation. *Biochem Pharmacol* 85**:** 705-717.

Bui CB, Shin J (2011). Persistent expression of Nqo1 by p62-mediated Nrf2 activation facilitates p53-dependent mitotic catastrophe. *Biochem Biophys Res Commun* 412**:** 347-352.

Busauschina A, Schnuelle P, van der Woude FJ (2004). Cyclosporine nephrotoxicity. *Transplant Proc* 36**:** 229S-233S.

Calderon J, Ortiz-Perez D, Yanez L, Diaz-Barriga F (2003). Human exposure to metals. Pathways of exposure, biomarkers of effect, and host factors. *Ecotoxicol Environ Saf* 56**:** 93-103.

Camer D, Huang XF (2014). The endothelin pathway: a protective or detrimental target of bardoxolone methyl on cardiac function in patients with advanced chronic kidney disease? *Am J Nephrol* 40**:** 288-290.

Castrop H (2007). Mediators of tubuloglomerular feedback regulation of glomerular filtration: ATP and adenosine. *Acta Physiol (Oxf)* 189**:** 3-14.

Cavin C, Delatour T, Marin-Kuan M, Fenaille F, Holzhauser D, Guignard G*, et al.* (2009). Ochratoxin A-mediated DNA and protein damage: roles of nitrosative and oxidative stresses. *Toxicol Sci* 110**:** 84-94.

Cavin C, Delatour T, Marin-Kuan M, Holzhauser D, Higgins L, Bezencon C*, et al.* (2007). Reduction in antioxidant defenses may contribute to ochratoxin A toxicity and carcinogenicity. *Toxicol Sci* 96**:** 30-39.

Chan JY, Kwong M (2000). Impaired expression of glutathione synthetic enzyme genes in mice with targeted deletion of the Nrf2 basic-leucine zipper protein. *Biochimica Et Biophysica Acta* 1517**:** 19-26.

Chan JY, Han XL, Kan YW (1993). Isolation of cDNA encoding the human NF-E2 protein. *Proc Natl Acad Sci U S A* 90**:** 11366-11370.

Chan K, Han XD, Kan YW (2001). An important function of Nrf2 in combating oxidative stress: detoxification of acetaminophen. *Proc Natl Acad Sci U S A* 98**:** 4611-4616.

Chan K, Lu R, Chang JC, Kan YW (1996). NRF2, a member of the NFE2 family of transcription factors, is not essential for murine erythropoiesis, growth, and development. *Proc Natl Acad Sci U S A* 93**:** 13943-13948.

Chen J, Shaikh ZA (2009). Activation of Nrf2 by cadmium and its role in protection against cadmium-induced apoptosis in rat kidney cells. *Toxicology and Applied Pharmacology* 241**:** 81-89.

Cheng X, Ku CH, Siow RC (2013). Regulation of the Nrf2 antioxidant pathway by microRNAs: New players in micromanaging redox homeostasis. *Free Radic Biol Med* 64**:** 4-11.

Chevillard G, Blank V (2011). NFE2L3 (NRF3): the Cinderella of the Cap'n'Collar transcription factors. *Cell Mol Life Sci* 68**:** 3337-3348.

Chin M, Lee CY, Chuang JC, Bumeister R, Wigley WC, Sonis ST*, et al.* (2013). Bardoxolone methyl analogs RTA 405 and dh404 are well tolerated and exhibit efficacy in rodent models of Type 2 diabetes and obesity. *Am J Physiol Renal Physiol* 304**:** F1438-1446.

Chin MP, Meyer CJ (2014a). Response to Letter to the Editor: Risk Factors for Heart Failure in Patients with Type 2 Diabetes Mellitus and Stage 4 Chronic Kidney Disease Treated with Bardoxolone Methyl. *J Card Fail*.

Chin MP, Wrolstad D, Bakris GL, Chertow GM, de Zeeuw D, Goldsberry A*, et al.* (2014b). Risk Factors for Heart Failure in Patients with Type 2 Diabetes Mellitus and Stage 4 Chronic Kidney Disease Treated with Bardoxolone Methyl. *Journal of Cardiac Failure*.

Chin MP, Reisman SA, Bakris GL, O'Grady M, Linde PG, McCullough PA*, et al.* (2014c). Mechanisms contributing to adverse cardiovascular events in patients with type 2 diabetes mellitus and stage 4 chronic kidney disease treated with bardoxolone methyl. *Am J Nephrol* 39**:** 499-508.

Cho HY, Reddy SP, Yamamoto M, Kleeberger SR (2004). The transcription factor NRF2 protects against pulmonary fibrosis. *FASEB J* 18**:** 1258-1260.

Chorley BN, Campbell MR, Wang X, Karaca M, Sambandan D, Bangura F*, et al.* (2012). Identification of novel NRF2-regulated genes by ChIP-Seq: influence on retinoid X receptor alpha. *Nucleic Acids Res* 40**:** 7416-7429.

Choudhury D, Ahmed Z (2006). Drug-associated renal dysfunction and injury. *Nat Clin Pract Nephrol* 2**:** 80-91.

Cooley ME, Davis LE, DeStefano M, Abrahm J (1994). Cisplatin: a clinical review. Part I--Current uses of cisplatin and administration guidelines. *Cancer Nurs* 17**:** 173-184.

Copple IM (2012). The Keap1-Nrf2 cell defense pathway--a promising therapeutic target? *Adv Pharmacol* 63**:** 43-79.

Copple IM, Goldring CE, Kitteringham NR, Park BK (2008). The Nrf2-Keap1 defence pathway: role in protection against drug-induced toxicity. *Toxicology* 246**:** 24-33.

Copple IM, Goldring CE, Kitteringham NR, Park BK (2010a). The keap1-nrf2 cellular defense pathway: mechanisms of regulation and role in protection against drug-induced toxicity. *Handb Exp Pharmacol***:** 233-266.

Copple IM, Lister A, Obeng AD, Kitteringham NR, Jenkins RE, Layfield R*, et al.* (2010b). Physical and functional interaction of sequestosome 1 with Keap1 regulates the Keap1-Nrf2 cell defense pathway. *J Biol Chem* 285**:** 16782-16788.

Copple IM, Shelton LM, Walsh J, Kratschmar DV, Lister A, Odermatt A*, et al.* (2014). Chemical tuning enhances both potency toward nrf2 and in vitro therapeutic index of triterpenoids. *Toxicol Sci* 140**:** 462-469.

Corney DC, Flesken-Nikitin A, Godwin AK, Wang W, Nikitin AY (2007). MicroRNA-34b and MicroRNA-34c are targets of p53 and cooperate in control of cell proliferation and adhesion-independent growth. *Cancer Res* 67**:** 8433-8438.

Cowie MR, Mendez GF (2002). BNP and congestive heart failure. *Prog Cardiovasc Dis* 44**:** 293-321.

Crampton N, Kodiha M, Shrivastava S, Umar R, Stochaj U (2009). Oxidative stress inhibits nuclear protein export by multiple mechanisms that target FG nucleoporins and Crm1. *Mol Biol Cell* 20**:** 5106-5116.

Cui W, Li B, Bai Y, Miao X, Chen Q, Sun W*, et al.* (2013). Potential role for Nrf2 activation in the therapeutic effect of MG132 on diabetic nephropathy in OVE26 diabetic mice. *Am J Physiol Endocrinol Metab* 304**:** E87-99.

D'Agati VD, Kaskel FJ, Falk RJ (2011). Focal segmental glomerulosclerosis. *N Engl J Med* 365**:** 2398-2411.

Dang Y, Luo D, Rong M, Chen G (2013). Underexpression of miR-34a in hepatocellular carcinoma and its contribution towards enhancement of proliferating inhibitory effects of agents targeting c-MET. *PLoS One* 8**:** e61054.

Dantzler WH (2003). Regulation of renal proximal and distal tubule transport: sodium, chloride and organic anions. *Comp Biochem Physiol A Mol Integr Physiol* 136**:** 453-478.

de Haan JB (2011). Nrf2 activators as attractive therapeutics for diabetic nephropathy. *Diabetes* 60**:** 2683-2684.

de Souza CG, Sattler JA, de Assis AM, Rech A, Perry ML, Souza DO (2012). Metabolic effects of sulforaphane oral treatment in streptozotocin-diabetic rats. *J Med Food* 15**:** 795-801.

de Zeeuw D, Akizawa T, Agarwal R, Audhya P, Bakris GL, Chin M*, et al.* (2013a). Rationale and trial design of Bardoxolone Methyl Evaluation in Patients with Chronic Kidney Disease and Type 2 Diabetes: the Occurrence of Renal Events (BEACON). *Am J Nephrol* 37**:** 212-222.

de Zeeuw D, Akizawa T, Audhya P, Bakris GL, Chin M, Christ-Schmidt H*, et al.* (2013b). Bardoxolone methyl in type 2 diabetes and stage 4 chronic kidney disease. *N Engl J Med* 369**:** 2492-2503.

Dinkova-Kostova AT (2012). The Role of Sulfhydryl Reactivity of Small Molecules for the Activation of the KEAP1/NRF2 Pathway and the Heat Shock Response. *Scientifica (Cairo)* 2012**:** 606104.

Dinkova-Kostova AT, Talalay P (2010a). NAD(P)H:quinone acceptor oxidoreductase 1 (NQO1), a multifunctional antioxidant enzyme and exceptionally versatile cytoprotector. *Arch Biochem Biophys* 501**:** 116-123.

Dinkova-Kostova AT, Holtzclaw WD, Cole RN, Itoh K, Wakabayashi N, Katoh Y*, et al.* (2002). Direct evidence that sulfhydryl groups of Keap1 are the sensors regulating induction of phase 2 enzymes that protect against carcinogens and oxidants. *Proc Natl Acad Sci U S A* 99**:** 11908-11913.

Dinkova-Kostova AT, Talalay P, Sharkey J, Zhang Y, Holtzclaw WD, Wang XJ*, et al.* (2010b). An exceptionally potent inducer of cytoprotective enzymes: elucidation of the structural features that determine inducer potency and reactivity with Keap1. *J Biol Chem* 285**:** 33747-33755.

Dinkova-Kostova AT, Liby KT, Stephenson KK, Holtzclaw WD, Gao X, Suh N*, et al.* (2005). Extremely potent triterpenoid inducers of the phase 2 response: correlations of protection against oxidant and inflammatory stress. *Proc Natl Acad Sci U S A* 102**:** 4584-4589.

Dinkova-Kostova AT, Jenkins SN, Wehage SL, Huso DL, Benedict AL, Stephenson KK*, et al.* (2008). A dicyanotriterpenoid induces cytoprotective enzymes and reduces multiplicity of skin tumors in UV-irradiated mice. *Biochem Biophys Res Commun* 367**:** 859-865.

Dominguez JH, Camp K, Maianu L, Garvey WT (1992). Glucose transporters of rat proximal tubule: differential expression and subcellular distribution. *Am J Physiol* 262**:** F807-812.

Dounousi E, Papavasiliou E, Makedou A, Ioannou K, Katopodis KP, Tselepis A*, et al.* (2006). Oxidative stress is progressively enhanced with advancing stages of CKD. *Am J Kidney Dis* 48**:** 752-760.

Druz A, Betenbaugh M, Shiloach J (2012). Glucose depletion activates mmu-miR-466h-5p expression through oxidative stress and inhibition of histone deacetylation. *Nucleic Acids Res* 40**:** 7291-7302.

Druz A, Chu C, Majors B, Santuary R, Betenbaugh M, Shiloach J (2011). A novel microRNA mmu-miR-466h affects apoptosis regulation in mammalian cells. *Biotechnol Bioeng* 108**:** 1651-1661.

Eades G, Yang M, Yao Y, Zhang Y, Zhou Q (2011). miR-200a regulates Nrf2 activation by targeting Keap1 mRNA in breast cancer cells. *J Biol Chem* 286**:** 40725-40733.

Edwards IR, Aronson JK (2000). Adverse drug reactions: definitions, diagnosis, and management. *Lancet* 356**:** 1255-1259.

Eggler AL, Small E, Hannink M, Mesecar AD (2009). Cul3-mediated Nrf2 ubiquitination and antioxidant response element (ARE) activation are dependent on the partial molar volume at position 151 of Keap1. *Biochem J* 422**:** 171-180.

Eladari D, Chambrey R, Peti-Peterdi J (2012). A new look at electrolyte transport in the distal tubule. *Annu Rev Physiol* 74**:** 325-349.

Elangovan S, Hsieh TC (2008). Control of cellular redox status and upregulation of quinone reductase NQO1 via Nrf2 activation by alpha-lipoic acid in human leukemia HL-60 cells. *Int J Oncol* 33**:** 833-838.

Ellrichmann G, Petrasch-Parwez E, Lee DH, Reick C, Arning L, Saft C*, et al.* (2011). Efficacy of fumaric acid esters in the R6/2 and YAC128 models of Huntington's disease. *PLoS One* 6**:** e16172.

Emter R, Ellis G, Natsch A (2010). Performance of a novel keratinocyte-based reporter cell line to screen skin sensitizers in vitro. *Toxicol Appl Pharmacol* 245**:** 281-290.

Enomoto A, Itoh K, Nagayoshi E, Haruta J, Kimura T, O'Connor T*, et al.* (2001). High sensitivity of Nrf2 knockout mice to acetaminophen hepatotoxicity associated with decreased expression of ARE-regulated drug metabolizing enzymes and antioxidant genes. *Toxicol Sci* 59**:** 169-177.

Fan W, Tang Z, Chen D, Moughon D, Ding X, Chen S*, et al.* (2010). Keap1 facilitates p62-mediated ubiquitin aggregate clearance via autophagy. *Autophagy* 6.

Favaloro FG, Jr., Honda T, Honda Y, Gribble GW, Suh N, Risingsong R*, et al.* (2002). Design and synthesis of tricyclic compounds with enone functionalities in rings A and C: a novel class of highly active inhibitors of nitric oxide production in mouse macrophages. *J Med Chem* 45**:** 4801-4805.

Favreau LV, Pickett CB (1991). Transcriptional regulation of the rat NAD(P)H:quinone reductase gene. Identification of regulatory elements controlling basal level expression and inducible expression by planar aromatic compounds and phenolic antioxidants. *J Biol Chem* 266**:** 4556-4561.

Filipowicz W, Bhattacharyya SN, Sonenberg N (2008). Mechanisms of post-transcriptional regulation by microRNAs: are the answers in sight? *Nat Rev Genet* 9**:** 102-114.

Frederiks WM, Kummerlin IP, Bosch KS, Vreeling-Sindelarova H, Jonker A, Van Noorden CJ (2007). NADPH production by the pentose phosphate pathway in the zona fasciculata of rat adrenal gland. *J Histochem Cytochem* 55**:** 975-980.

Gang GT, Kim YH, Noh JR, Kim KS, Jung JY, Shong M*, et al.* (2013). Protective role of NAD(P)H:quinone oxidoreductase 1 (NQO1) in cisplatin-induced nephrotoxicity. *Toxicol Lett* 221**:** 165-175.

Gao W, Chan JY, Wong TS (2014). Curcumin exerts inhibitory effects on undifferentiated nasopharyngeal carcinoma by inhibiting the expression of miR-125a-5p. *Clin Sci (Lond)* 127**:** 571-579.

Gong Y, Xu F, Zhang L, Qian Y, Chen J, Huang H*, et al.* (2014). MicroRNA expression signature for Satb2-induced osteogenic differentiation in bone marrow stromal cells. *Mol Cell Biochem* 387**:** 227-239.

Greger R (2000). Physiology of renal sodium transport. *Am J Med Sci* 319**:** 51-62.

Grimson A, Farh KK, Johnston WK, Garrett-Engele P, Lim LP, Bartel DP (2007). MicroRNA targeting specificity in mammals: determinants beyond seed pairing. *Mol Cell* 27**:** 91-105.

Hamer RA, El Nahas AM (2006). The burden of chronic kidney disease. *BMJ* 332**:** 563-564.

Harvey CJ, Thimmulappa RK, Singh A, Blake DJ, Ling G, Wakabayashi N*, et al.* (2009). Nrf2-regulated glutathione recycling independent of biosynthesis is critical for cell survival during oxidative stress. *Free Radic Biol Med* 46**:** 443-453.

Hayes JD, Dinkova-Kostova AT (2014). The Nrf2 regulatory network provides an interface between redox and intermediary metabolism. *Trends Biochem Sci* 39**:** 199-218.

Hayes JD, McMahon M, Chowdhry S, Dinkova-Kostova AT (2010). Cancer chemoprevention mechanisms mediated through the Keap1-Nrf2 pathway. *Antioxid Redox Signal* 13**:** 1713-1748.

Hayes JD, Chanas SA, Henderson CJ, McMahon M, Sun C, Moffat GJ*, et al.* (2000). The Nrf2 transcription factor contributes both to the basal expression of glutathione S-transferases in mouse liver and to their induction by the chemopreventive synthetic antioxidants, butylated hydroxyanisole and ethoxyquin. *Biochem Soc Trans* 28**:** 33-41.

He L, He X, Lowe SW, Hannon GJ (2007). microRNAs join the p53 network--another piece in the tumour-suppression puzzle. *Nat Rev Cancer* 7**:** 819-822.

Heiss EH, Schachner D, Zimmermann K, Dirsch VM (2013). Glucose availability is a decisive factor for Nrf2-mediated gene expression. *Redox Biol* 1**:** 359-365.

Hinson JA, Roberts DW, James LP (2010). Mechanisms of acetaminophen-induced liver necrosis. *Handb Exp Pharmacol***:** 369-405.

Holmstrom KM, Baird L, Zhang Y, Hargreaves I, Chalasani A, Land JM*, et al.* (2013). Nrf2 impacts cellular bioenergetics by controlling substrate availability for mitochondrial respiration. *Biol Open* 2**:** 761-770.

Honda T, Rounds BV, Gribble GW, Suh N, Wang Y, Sporn MB (1998). Design and synthesis of 2-cyano-3,12-dioxoolean-1,9-dien-28-oic acid, a novel and highly active inhibitor of nitric oxide production in mouse macrophages. *Bioorg Med Chem Lett* 8**:** 2711-2714.

Honda T, Honda Y, Favaloro FG, Jr., Gribble GW, Suh N, Place AE*, et al.* (2002). A novel dicyanotriterpenoid, 2-cyano-3,12-dioxooleana-1,9(11)-dien-28-onitrile, active at picomolar concentrations for inhibition of nitric oxide production. *Bioorg Med Chem Lett* 12**:** 1027-1030.

Honda T, Sundararajan C, Yoshizawa H, Su X, Honda Y, Liby KT*, et al.* (2007). Novel tricyclic compounds having acetylene groups at C-8a and cyano enones in rings A and C: highly potent anti-inflammatory and cytoprotective agents. *J Med Chem* 50**:** 1731-1734.

Honda T, Rounds BV, Bore L, Finlay HJ, Favaloro FG, Jr., Suh N*, et al.* (2000). Synthetic oleanane and ursane triterpenoids with modified rings A and C: a series of highly active inhibitors of nitric oxide production in mouse macrophages. *J Med Chem* 43**:** 4233-4246.

Honda T, Yoshizawa H, Sundararajan C, David E, Lajoie MJ, Favaloro FG, Jr.*, et al.* (2011). Tricyclic compounds containing nonenolizable cyano enones. A novel class of highly potent anti-inflammatory and cytoprotective agents. *J Med Chem* 54**:** 1762-1778.

Hong DS, Kurzrock R, Supko JG, He X, Naing A, Wheler J*, et al.* (2012). A phase I first-in-human trial of bardoxolone methyl in patients with advanced solid tumors and lymphomas. *Clin Cancer Res* 18**:** 3396-3406.

Houghton CA, Fassett RG, Coombes JS (2013). Sulforaphane: translational research from laboratory bench to clinic. *Nutr Rev* 71**:** 709-726.

Hu Q, Zhang DD, Wang L, Lou H, Ren D (2012). Eriodictyol-7-O-glucoside, a novel Nrf2 activator, confers protection against cisplatin-induced toxicity. *Food Chem Toxicol* 50**:** 1927-1932.

Hummel CS, Lu C, Loo DD, Hirayama BA, Voss AA, Wright EM (2011). Glucose transport by human renal Na+/D-glucose cotransporters SGLT1 and SGLT2. *Am J Physiol Cell Physiol* 300**:** C14-21.

Hunsberger JG, Fessler EB, Wang Z, Elkahloun AG, Chuang DM (2012). Post-insult valproic acid-regulated microRNAs: potential targets for cerebral ischemia. *Am J Transl Res* 4**:** 316-332.

Ishikawa K, Ishikawa A, Shoji Y, Imai T (2014). A genotoxic stress-responsive miRNA, miR-574-3p, delays cell growth by suppressing the enhancer of rudimentary homolog gene in vitro. *Int J Mol Sci* 15**:** 2971-2990.

Itoh K, Wakabayashi N, Katoh Y, Ishii T, O'Connor T, Yamamoto M (2003). Keap1 regulates both cytoplasmic-nuclear shuttling and degradation of Nrf2 in response to electrophiles. *Genes Cells* 8**:** 379-391.

Itoh K, Wakabayashi N, Katoh Y, Ishii T, Igarashi K, Engel JD*, et al.* (1999). Keap1 represses nuclear activation of antioxidant responsive elements by Nrf2 through binding to the amino-terminal Neh2 domain. *Genes Dev* 13**:** 76-86.

Itoh K, Chiba T, Takahashi S, Ishii T, Igarashi K, Katoh Y*, et al.* (1997). An Nrf2 small Maf heterodimer mediates the induction of phase II detoxifying enzyme genes through antioxidant response elements. *Biochem Biophys Res Commun* 236**:** 313-322.

Jain A, Lamark T, Sjottem E, Larsen KB, Awuh JA, Overvatn A*, et al.* (2010). p62/SQSTM1 is a target gene for transcription factor NRF2 and creates a positive feedback loop by inducing antioxidant response element-driven gene transcription. *J Biol Chem* 285**:** 22576-22591.

Jaloszynski P, Murata S, Shinkai Y, Takahashi S, Kumagai Y, Nishimura S*, et al.* (2007). Dysfunction of Nrf2 decreases KBrO3-induced oxidative DNA damage in Ogg1-null mice. *Biochem Biophys Res Commun* 364**:** 966-971.

Jaramillo MC, Zhang DD (2013). The emerging role of the Nrf2-Keap1 signaling pathway in cancer. *Genes Dev* 27**:** 2179-2191.

Jeong WS, Jun M, Kong AN (2006). Nrf2: a potential molecular target for cancer chemoprevention by natural compounds. *Antioxid Redox Signal* 8**:** 99-106.

Jian B, Yang S, Chaudry IH, Raju R (2014). Resveratrol restores sirtuin 1 (SIRT1) activity and pyruvate dehydrogenase kinase 1 (PDK1) expression after hemorrhagic injury in a rat model. *Mol Med* 20**:** 10-16.

Jiang T, Huang Z, Lin Y, Zhang Z, Fang D, Zhang DD (2010). The protective role of Nrf2 in streptozotocin-induced diabetic nephropathy. *Diabetes* 59**:** 850-860.

Jung KA, Choi BH, Nam CW, Song M, Kim ST, Lee JY*, et al.* (2013). Identification of aldo-keto reductases as NRF2-target marker genes in human cells. *Toxicol Lett* 218**:** 39-49.

Jutooru I, Chadalapaka G, Abdelrahim M, Basha MR, Samudio I, Konopleva M*, et al.* (2010). Methyl 2-cyano-3,12-dioxooleana-1,9-dien-28-oate decreases specificity protein transcription factors and inhibits pancreatic tumor growth: role of microRNA-27a. *Mol Pharmacol* 78**:** 226-236.

Kang SJ, You A, Kwak MK (2011). Suppression of Nrf2 signaling by angiotensin II in murine renal epithelial cells. *Arch Pharm Res* 34**:** 829-836.

Kanki K, Umemura T, Kitamura Y, Ishii Y, Kuroiwa Y, Kodama Y*, et al.* (2008). A possible role of nrf2 in prevention of renal oxidative damage by ferric nitrilotriacetate. *Toxicol Pathol* 36**:** 353-361.

Kaspar JW, Jaiswal AK (2010). An autoregulatory loop between Nrf2 and Cul3-Rbx1 controls their cellular abundance. *J Biol Chem* 285**:** 21349-21358.

Kim DH, Saetrom P, Snove O, Jr., Rossi JJ (2008). MicroRNA-directed transcriptional gene silencing in mammalian cells. *Proc Natl Acad Sci U S A* 105**:** 16230-16235.

Kim HJ, Vaziri ND (2010). Contribution of impaired Nrf2-Keap1 pathway to oxidative stress and inflammation in chronic renal failure. *Am J Physiol Renal Physiol* 298**:** F662-671.

Kim HJ, Sato T, Rodriguez-Iturbe B, Vaziri ND (2011). Role of intrarenal angiotensin system activation, oxidative stress, inflammation, and impaired nuclear factor-erythroid-2-related factor 2 activity in the progression of focal glomerulosclerosis. *J Pharmacol Exp Ther* 337**:** 583-590.

Kim HJ, Na JI, Min BW, Na JY, Lee KH, Lee JH*, et al.* (2014). Evaluation of Protein Expression in Housekeeping Genes across Multiple Tissues in Rats. *Korean J Pathol* 48**:** 193-200.

Kim JH, Yu S, Chen JD, Kong AN (2012). The nuclear cofactor RAC3/AIB1/SRC-3 enhances Nrf2 signaling by interacting with transactivation domains. *Oncogene*.

Kim KB, Lotan R, Yue P, Sporn MB, Suh N, Gribble GW*, et al.* (2002). Identification of a novel synthetic triterpenoid, methyl-2-cyano-3,12-dioxooleana-1,9-dien-28-oate, that potently induces caspase-mediated apoptosis in human lung cancer cells. *Mol Cancer Ther* 1**:** 177-184.

Kim YC, Masutani H, Yamaguchi Y, Itoh K, Yamamoto M, Yodoi J (2001). Hemin-induced activation of the thioredoxin gene by Nrf2. A differential regulation of the antioxidant responsive element by a switch of its binding factors. *J Biol Chem* 276**:** 18399-18406.

Kitteringham NR, Abdullah A, Walsh J, Randle L, Jenkins RE, Sison R*, et al.* (2010). Proteomic analysis of Nrf2 deficient transgenic mice reveals cellular defence and lipid metabolism as primary Nrf2-dependent pathways in the liver. *J Proteomics* 73**:** 1612-1631.

Kobayashi A, Kang MI, Watai Y, Tong KI, Shibata T, Uchida K*, et al.* (2006). Oxidative and electrophilic stresses activate Nrf2 through inhibition of ubiquitination activity of Keap1. *Mol Cell Biol* 26**:** 221-229.

Kobayashi A, Ito E, Toki T, Kogame K, Takahashi S, Igarashi K*, et al.* (1999). Molecular cloning and functional characterization of a new Cap'n' collar family transcription factor Nrf3. *J Biol Chem* 274**:** 6443-6452.

Kobayashi A, Kang MI, Okawa H, Ohtsuji M, Zenke Y, Chiba T*, et al.* (2004). Oxidative stress sensor Keap1 functions as an adaptor for Cul3-based E3 ligase to regulate proteasomal degradation of Nrf2. *Mol Cell Biol* 24**:** 7130-7139.

Kobayashi M, Sugiyama H, Wang DH, Toda N, Maeshima Y, Yamasaki Y*, et al.* (2005). Catalase deficiency renders remnant kidneys more susceptible to oxidant tissue injury and renal fibrosis in mice. *Kidney Int* 68**:** 1018-1031.

Komatsu M, Kurokawa H, Waguri S, Taguchi K, Kobayashi A, Ichimura Y*, et al.* (2010). The selective autophagy substrate p62 activates the stress responsive transcription factor Nrf2 through inactivation of Keap1. *Nat Cell Biol* 12**:** 213-223.

Komlosi P, Fintha A, Bell PD (2004). Current mechanisms of macula densa cell signalling. *Acta Physiol Scand* 181**:** 463-469.

Konopleva M, Tsao T, Ruvolo P, Stiouf I, Estrov Z, Leysath CE*, et al.* (2002). Novel triterpenoid CDDO-Me is a potent inducer of apoptosis and differentiation in acute myelogenous leukemia. *Blood* 99**:** 326-335.

Kraft AD, Johnson DA, Johnson JA (2004). Nuclear factor E2-related factor 2-dependent antioxidant response element activation by tert-butylhydroquinone and sulforaphane occurring preferentially in astrocytes conditions neurons against oxidative insult. *J Neurosci* 24**:** 1101-1112.

Kratschmar DV, Calabrese D, Walsh J, Lister A, Birk J, Appenzeller-Herzog C*, et al.* (2012). Suppression of the Nrf2-dependent antioxidant response by glucocorticoids and 11beta-HSD1-mediated glucocorticoid activation in hepatic cells. *Plos One* 7**:** e36774.

Kwak MK, Itoh K, Yamamoto M, Sutter TR, Kensler TW (2001). Role of transcription factor Nrf2 in the induction of hepatic phase 2 and antioxidative enzymes in vivo by the cancer chemoprotective agent, 3H-1, 2-dimethiole-3-thione. *Mol Med* 7**:** 135-145.

Lee BH, Hsu WH, Chang YY, Kuo HF, Hsu YW, Pan TM (2012a). Ankaflavin: a natural novel PPARgamma agonist upregulates Nrf2 to attenuate methylglyoxal-induced diabetes in vivo. *Free Radic Biol Med* 53**:** 2008-2016.

Lee CK, Park KK, Chung AS, Chung WY (2012b). Ginsenoside Rg3 enhances the chemosensitivity of tumors to cisplatin by reducing the basal level of nuclear factor erythroid 2-related factor 2-mediated heme oxygenase-1/NAD(P)H quinone oxidoreductase-1 and prevents normal tissue damage by scavenging cisplatin-induced intracellular reactive oxygen species. *Food Chem Toxicol* 50**:** 2565-2574.

Lee DH, Stangel M, Gold R, Linker RA (2013). The fumaric acid ester BG-12: a new option in MS therapy. *Expert Review of Neurotherapeutics* 13**:** 951-958.

Lee HW, Lee EH, Ha SY, Lee CH, Chang HK, Chang S*, et al.* (2012c). Altered expression of microRNA miR-21, miR-155, and let-7a and their roles in pulmonary neuroendocrine tumors. *Pathol Int* 62**:** 583-591.

Lee Y, Kim M, Han J, Yeom KH, Lee S, Baek SH*, et al.* (2004). MicroRNA genes are transcribed by RNA polymerase II. *EMBO J* 23**:** 4051-4060.

Lee Y, Ahn C, Han J, Choi H, Kim J, Yim J*, et al.* (2003). The nuclear RNase III Drosha initiates microRNA processing. *Nature* 425**:** 415-419.

Legrand M, Mik EG, Johannes T, Payen D, Ince C (2008). Renal hypoxia and dysoxia after reperfusion of the ischemic kidney. *Mol Med* 14**:** 502-516.

Leonard MO, Kieran NE, Howell K, Burne MJ, Varadarajan R, Dhakshinamoorthy S*, et al.* (2006). Reoxygenation-specific activation of the antioxidant transcription factor Nrf2 mediates cytoprotective gene expression in ischemia-reperfusion injury. *Faseb Journal* 20**:** 2624-2626.

Levonen AL, Landar A, Ramachandran A, Ceaser EK, Dickinson DA, Zanoni G*, et al.* (2004). Cellular mechanisms of redox cell signalling: role of cysteine modification in controlling antioxidant defences in response to electrophilic lipid oxidation products. *Biochem J* 378**:** 373-382.

Li H, Zhang L, Wang F, Shi Y, Ren Y, Liu Q*, et al.* (2011a). Attenuation of glomerular injury in diabetic mice with tert-butylhydroquinone through nuclear factor erythroid 2-related factor 2-dependent antioxidant gene activation. *Am J Nephrol* 33**:** 289-297.

Li N, Muthusamy S, Liang R, Sarojini H, Wang E (2011b). Increased expression of miR-34a and miR-93 in rat liver during aging, and their impact on the expression of Mgst1 and Sirt1. *Mech Ageing Dev* 132**:** 75-85.

Li N, Fu H, Tie Y, Hu Z, Kong W, Wu Y*, et al.* (2009). miR-34a inhibits migration and invasion by down-regulation of c-Met expression in human hepatocellular carcinoma cells. *Cancer Lett* 275**:** 44-53.

Li W, Khor TO, Xu C, Shen G, Jeong WS, Yu S*, et al.* (2008a). Activation of Nrf2-antioxidant signaling attenuates NFkappaB-inflammatory response and elicits apoptosis. *Biochem Pharmacol* 76**:** 1485-1489.

Li W, Yu S, Liu T, Kim JH, Blank V, Li H*, et al.* (2008b). Heterodimerization with small Maf proteins enhances nuclear retention of Nrf2 via masking the NESzip motif. *Biochimica Et Biophysica Acta* 1783**:** 1847-1856.

Li Z, Geng YN, Jiang JD, Kong WJ (2014). Antioxidant and anti-inflammatory activities of berberine in the treatment of diabetes mellitus. *Evid Based Complement Alternat Med* 2014**:** 289264.

Liby K, Voong N, Williams CR, Risingsong R, Royce DB, Honda T*, et al.* (2006). The synthetic triterpenoid CDDO-Imidazolide suppresses STAT phosphorylation and induces apoptosis in myeloma and lung cancer cells. *Clin Cancer Res* 12**:** 4288-4293.

Liby K, Hock T, Yore MM, Suh N, Place AE, Risingsong R*, et al.* (2005). The synthetic triterpenoids, CDDO and CDDO-imidazolide, are potent inducers of heme oxygenase-1 and Nrf2/ARE signaling. *Cancer Res* 65**:** 4789-4798.

Limonciel A, Wilmes A, Aschauer L, Radford R, Bloch KM, McMorrow T*, et al.* (2012). Oxidative stress induced by potassium bromate exposure results in altered tight junction protein expression in renal proximal tubule cells. *Arch Toxicol* 86**:** 1741-1751.

Liu J, Wu KC, Lu YF, Ekuase E, Klaassen CD (2013). NRF2 Protection against Liver Injury Produced by Various Hepatotoxicants. *Oxid Med Cell Longev*.

Liu M, Grigoryev DN, Crow MT, Haas M, Yamamoto M, Reddy SP*, et al.* (2009). Transcription factor Nrf2 is protective during ischemic and nephrotoxic acute kidney injury in mice. *Kidney Int* 76**:** 277-285.

Liu M, Reddy NM, Higbee EM, Potteti HR, Noel S, Racusen L*, et al.* (2014). The Nrf2 triterpenoid activator, CDDO-imidazolide, protects kidneys from ischemia-reperfusion injury in mice. *Kidney Int* 85**:** 134-141.

Liu Y (2006). Renal fibrosis: new insights into the pathogenesis and therapeutics. *Kidney Int* 69**:** 213-217.

Lohr JW, Willsky GR, Acara MA (1998). Renal drug metabolism. *Pharmacol Rev* 50**:** 107-141.

Lote CJ, Harper L, Savage CO (1996). Mechanisms of acute renal failure. *Br J Anaesth* 77**:** 82-89.

Louhelainen M, Merasto S, Finckenberg P, Lapatto R, Cheng ZJ, Mervaala EM (2006). Lipoic acid supplementation prevents cyclosporine-induced hypertension and nephrotoxicity in spontaneously hypertensive rats. *J Hypertens* 24**:** 947-956.

Luo ZF, Qi W, Feng B, Mu J, Zeng W, Guo YH*, et al.* (2011). Prevention of diabetic nephropathy in rats through enhanced renal antioxidative capacity by inhibition of the proteasome. *Life Sci* 88**:** 512-520.

Ma Q (2013). Role of nrf2 in oxidative stress and toxicity. *Annu Rev Pharmacol Toxicol* 53**:** 401-426.

Maher JM, Cheng X, Slitt AL, Dieter MZ, Klaassen CD (2005). Induction of the multidrug resistance-associated protein family of transporters by chemical activators of receptor-mediated pathways in mouse liver. *Drug Metab Dispos* 33**:** 956-962.

Malhotra D, Portales-Casamar E, Singh A, Srivastava S, Arenillas D, Happel C*, et al.* (2010). Global mapping of binding sites for Nrf2 identifies novel targets in cell survival response through ChIP-Seq profiling and network analysis. *Nucleic Acids Res* 38**:** 5718-5734.

Marin-Kuan M, Nestler S, Verguet C, Bezencon C, Piguet D, Mansourian R*, et al.* (2006). A toxicogenomics approach to identify new plausible epigenetic mechanisms of ochratoxin a carcinogenicity in rat. *Toxicol Sci* 89**:** 120-134.

McBride MW, Brosnan MJ, Mathers J, McLellan LI, Miller WH, Graham D*, et al.* (2005). Reduction of Gstm1 expression in the stroke-prone spontaneously hypertension rat contributes to increased oxidative stress. *Hypertension* 45**:** 786-792.

McDonald JT, Kim K, Norris AJ, Vlashi E, Phillips TM, Lagadec C*, et al.* (2010). Ionizing radiation activates the Nrf2 antioxidant response. *Cancer Res* 70**:** 8886-8895.

McMahon M, Itoh K, Yamamoto M, Hayes JD (2003). Keap1-dependent proteasomal degradation of transcription factor Nrf2 contributes to the negative regulation of antioxidant response element-driven gene expression. *J Biol Chem* 278**:** 21592-21600.

McMahon M, Thomas N, Itoh K, Yamamoto M, Hayes JD (2004). Redox-regulated turnover of Nrf2 is determined by at least two separate protein domains, the redox-sensitive Neh2 degron and the redox-insensitive Neh6 degron. *J Biol Chem* 279**:** 31556-31567.

McMahon M, Itoh K, Yamamoto M, Chanas SA, Henderson CJ, McLellan LI*, et al.* (2001). The Cap'n'Collar basic leucine zipper transcription factor Nrf2 (NF-E2 p45-related factor 2) controls both constitutive and inducible expression of intestinal detoxification and glutathione biosynthetic enzymes. *Cancer Res* 61**:** 3299-3307.

Meijer HA, Smith EM, Bushell M (2014). Regulation of miRNA strand selection: follow the leader? *Biochem Soc Trans* 42**:** 1135-1140.

Mitsuishi Y, Taguchi K, Kawatani Y, Shibata T, Nukiwa T, Aburatani H*, et al.* (2012). Nrf2 redirects glucose and glutamine into anabolic pathways in metabolic reprogramming. *Cancer Cell* 22**:** 66-79.

Moi P, Chan K, Asunis I, Cao A, Kan YW (1994). Isolation of NF-E2-related factor 2 (Nrf2), a NF-E2-like basic leucine zipper transcriptional activator that binds to the tandem NF-E2/AP1 repeat of the beta-globin locus control region. *Proc Natl Acad Sci U S A* 91**:** 9926-9930.

Molina-Jijon E, Tapia E, Zazueta C, El Hafidi M, Zatarain-Barron ZL, Hernandez-Pando R*, et al.* (2011). Curcumin prevents Cr(VI)-induced renal oxidant damage by a mitochondrial pathway. *Free Radic Biol Med* 51**:** 1543-1557.

Morozova N, Zinovyev A, Nonne N, Pritchard LL, Gorban AN, Harel-Bellan A (2012). Kinetic signatures of microRNA modes of action. *RNA* 18**:** 1635-1655.

Nakamura M, Shirai A, Yamazaki O, Satoh N, Suzuki M, Horita S*, et al.* (2014). Roles of renal proximal tubule transport in acid/base balance and blood pressure regulation. *Biomed Res Int* 2014**:** 504808.

Narasimhan M, Patel D, Vedpathak D, Rathinam M, Henderson G, Mahimainathan L (2012). Identification of novel microRNAs in post-transcriptional control of Nrf2 expression and redox homeostasis in neuronal, SH-SY5Y cells. *Plos One* 7**:** e51111.

Nash K, Hafeez A, Hou S (2002). Hospital-acquired renal insufficiency. *Am J Kidney Dis* 39**:** 930-936.

Nasser SA, El-Mas MM (2014). Endothelin ETA receptor antagonism in cardiovascular disease. *Eur J Pharmacol* 737**:** 210-213.

Nayak R, Annigeri RA, Vadamalai V, Seshadri R, Balasubramanian S, Rao BS*, et al.* (2013). Accuracy of spot urine protein creatinine ratio in measuring proteinuria in chronic kidney disease stage 3 and 4. *Indian J Nephrol* 23**:** 428-433.

Nielsen S, Smith BL, Christensen EI, Knepper MA, Agre P (1993). CHIP28 water channels are localized in constitutively water-permeable segments of the nephron. *J Cell Biol* 120**:** 371-383.

Nielsen S, Frokiaer J, Marples D, Kwon TH, Agre P, Knepper MA (2002). Aquaporins in the kidney: from molecules to medicine. *Physiol Rev* 82**:** 205-244.

Nioi P, Nguyen T, Sherratt PJ, Pickett CB (2005). The carboxy-terminal Neh3 domain of Nrf2 is required for transcriptional activation. *Mol Cell Biol* 25**:** 10895-10906.

Nioi P, McMahon M, Itoh K, Yamamoto M, Hayes JD (2003). Identification of a novel Nrf2-regulated antioxidant response element (ARE) in the mouse NAD(P)H:quinone oxidoreductase 1 gene: reassessment of the ARE consensus sequence. *Biochem J* 374**:** 337-348.

Niture SK, Jain AK, Jaiswal AK (2009). Antioxidant-induced modification of INrf2 cysteine 151 and PKC-delta-mediated phosphorylation of Nrf2 serine 40 are both required for

stabilization and nuclear translocation of Nrf2 and increased drug resistance. *J Cell Sci* 122**:** 4452-4464.

Nottrott S, Simard MJ, Richter JD (2006). Human let-7a miRNA blocks protein production on actively translating polyribosomes. *Nat Struct Mol Biol* 13**:** 1108-1114.

Oh CJ, Kim JY, Choi YK, Kim HJ, Jeong JY, Bae KH*, et al.* (2012). Dimethylfumarate attenuates renal fibrosis via NF-E2-related factor 2-mediated inhibition of transforming growth factor-beta/Smad signaling. *Plos One* 7**:** e45870.

Oh GS, Kim HJ, Choi JH, Shen A, Choe SK, Karna A*, et al.* (2013). Pharmacological activation of NQO1 increases NAD levels and attenuates cisplatin-mediated acute kidney injury in mice. *Kidney Int*.

Oikawa D, Akai R, Tokuda M, Iwawaki T (2012). A transgenic mouse model for monitoring oxidative stress. *Sci Rep* 2**:** 229.

Okamura K, Liu N, Lai EC (2009). Distinct mechanisms for microRNA strand selection by Drosophila Argonautes. *Mol Cell* 36**:** 431-444.

Ooi A, Dykema K, Ansari A, Petillo D, Snider J, Kahnoski R*, et al.* (2013). CUL3 and NRF2 mutations confer an NRF2 activation phenotype in a sporadic form of papillary renal cell carcinoma. *Cancer Res* 73**:** 2044-2051.

Ooi A, Wong JC, Petillo D, Roossien D, Perrier-Trudova V, Whitten D*, et al.* (2011). An antioxidant response phenotype shared between hereditary and sporadic type 2 papillary renal cell carcinoma. *Cancer Cell* 20**:** 511-523.

Palsamy P, Subramanian S (2011). Resveratrol protects diabetic kidney by attenuating hyperglycemia-mediated oxidative stress and renal inflammatory cytokines via Nrf2-Keap1 signaling. *Biochimica Et Biophysica Acta* 1812**:** 719-731.

Pan H, Wang H, Wang X, Zhu L, Mao L (2012). The absence of Nrf2 enhances NF-kappaB-dependent inflammation following scratch injury in mouse primary cultured astrocytes. *Mediators Inflamm* 2012**:** 217580.

Papp D, Lenti K, Modos D, Fazekas D, Dul Z, Turei D*, et al.* (2012). The NRF2-related interactome and regulome contain multifunctional proteins and fine-tuned autoregulatory loops. *FEBS Lett* 586**:** 1795-1802.

Park BK (1986). Metabolic basis of adverse drug reactions. *J R Coll Physicians Lond* 20**:** 195-200.

Park BK, Boobis A, Clarke S, Goldring CE, Jones D, Kenna JG*, et al.* (2011). Managing the challenge of chemically reactive metabolites in drug development. *Nat Rev Drug Discov* 10**:** 292-306.

Park HM, Cho JM, Lee HR, Shim GS, Kwak MK (2008). Renal protection by 3H-1,2-dithiole-3-thione against cisplatin through the Nrf2-antioxidant pathway. *Biochem Pharmacol* 76**:** 597-607.

Perazella MA (2009). Renal vulnerability to drug toxicity. *Clin J Am Soc Nephrol* 4**:** 1275-1283.

Pergola PE, Krauth M, Huff JW, Ferguson DA, Ruiz S, Meyer CJ*, et al.* (2011a). Effect of bardoxolone methyl on kidney function in patients with T2D and Stage 3b-4 CKD. *Am J Nephrol* 33**:** 469-476.

Pergola PE, Raskin P, Toto RD, Meyer CJ, Huff JW, Grossman EB*, et al.* (2011b). Bardoxolone methyl and kidney function in CKD with type 2 diabetes. *N Engl J Med* 365**:** 327-336.

Petrik J, Zanic-Grubisic T, Barisic K, Pepeljnjak S, Radic B, Ferencic Z*, et al.* (2003). Apoptosis and oxidative stress induced by ochratoxin A in rat kidney. *Arch Toxicol* 77**:** 685-693.

Pieczenik SR, Neustadt J (2007). Mitochondrial dysfunction and molecular pathways of disease. *Exp Mol Pathol* 83**:** 84-92.

Pietsch EC, Chan JY, Torti FM, Torti SV (2003). Nrf2 mediates the induction of ferritin H in response to xenobiotics and cancer chemopreventive dithiolethiones. *J Biol Chem* 278**:** 2361-2369.

Pineau P, Volinia S, McJunkin K, Marchio A, Battiston C, Terris B*, et al.* (2010). miR-221 overexpression contributes to liver tumorigenesis. *Proc Natl Acad Sci U S A* 107**:** 264-269.

Pirmohamed M, James S, Meakin S, Green C, Scott AK, Walley TJ*, et al.* (2004). Adverse drug reactions as cause of admission to hospital: prospective analysis of 18,820 patients. *British Medical Journal* 329**:** 15-19.

Plafker KS, Nguyen L, Barneche M, Mirza S, Crawford D, Plafker SM (2010). The ubiquitin-conjugating enzyme UbcM2 can regulate the stability and activity of the antioxidant transcription factor Nrf2. *J Biol Chem* 285**:** 23064-23074.

Prabu SM, Muthumani M (2012). Silibinin ameliorates arsenic induced nephrotoxicity by abrogation of oxidative stress, inflammation and apoptosis in rats. *Mol Biol Rep* 39**:** 11201-11216.

R-Programming-Environment (2005). R: A language and environment for statistical computing. In: *R Foundation for Statistical Computing*.

Rana TM (2007). Illuminating the silence: understanding the structure and function of small RNAs. *Nat Rev Mol Cell Biol* 8**:** 23-36.

Reisman SA, Chertow GM, Hebbar S, Vaziri ND, Ward KW, Meyer CJ (2012). Bardoxolone methyl decreases megalin and activates nrf2 in the kidney. *J Am Soc Nephrol* 23**:** 1663-1673.

Ren Y, Garvin JL, Liu R, Carretero OA (2007). Possible mechanism of efferent arteriole (Ef-Art) tubuloglomerular feedback. *Kidney Int* 71**:** 861-866.

Rodriguez-Mulero S, Errasti-Murugarren E, Ballarin J, Felipe A, Doucet A, Casado FJ*, et al.* (2005). Expression of concentrative nucleoside transporters SLC28 (CNT1, CNT2, and CNT3) along the rat nephron: effect of diabetes. *Kidney Int* 68**:** 665-672.

Ross D (2004). Quinone reductases multitasking in the metabolic world. *Drug Metab Rev* 36**:** 639-654.

Ross PL, Huang YN, Marchese JN, Williamson B, Parker K, Hattan S*, et al.* (2004). Multiplexed protein quantitation in Saccharomyces cerevisiae using amine-reactive isobaric tagging reagents. *Mol Cell Proteomics* 3**:** 1154-1169.

Ruiz S, Pergola PE, Zager RA, Vaziri ND (2013). Targeting the transcription factor Nrf2 to ameliorate oxidative stress and inflammation in chronic kidney disease. *Kidney Int* 83**:** 1029-1041.

Rushmore TH, Pickett CB (1990). Transcriptional regulation of the rat glutathione S-transferase Ya subunit gene. Characterization of a xenobiotic-responsive element controlling inducible expression by phenolic antioxidants. *J Biol Chem* 265**:** 14648-14653.

Saba R, Sorensen DL, Booth SA (2014). MicroRNA-146a: A Dominant, Negative Regulator of the Innate Immune Response. *Front Immunol* 5**:** 578.

Sahin K, Tuzcu M, Sahin N, Ali S, Kucuk O (2010a). Nrf2/HO-1 signaling pathway may be the prime target for chemoprevention of cisplatin-induced nephrotoxicity by lycopene. *Food Chem Toxicol* 48**:** 2670-2674.

Sahin K, Tuzcu M, Gencoglu H, Dogukan A, Timurkan M, Sahin N*, et al.* (2010b). Epigallocatechin-3-gallate activates Nrf2/HO-1 signaling pathway in cisplatin-induced nephrotoxicity in rats. *Life Sci* 87**:** 240-245.

Sahin K, Orhan C, Tuzcu M, Muqbil I, Sahin N, Gencoglu H*, et al.* (2014). Comparative in vivo evaluations of curcumin and its analog difluorinated curcumin against cisplatin-induced nephrotoxicity. *Biol Trace Elem Res* 157**:** 156-163.

Sangokoya C, Telen MJ, Chi JT (2010). microRNA miR-144 modulates oxidative stress tolerance and associates with anemia severity in sickle cell disease. *Blood* 116**:** 4338-4348.

Schafer FQ, Buettner GR (2001). Redox environment of the cell as viewed through the redox state of the glutathione disulfide/glutathione couple. *Free Radic Biol Med* 30**:** 1191-1212.

Schanen BC, Li X (2011). Transcriptional regulation of mammalian miRNA genes. *Genomics* 97**:** 1-6.

Schwanhausser B, Busse D, Li N, Dittmar G, Schuchhardt J, Wolf J*, et al.* (2011). Global quantification of mammalian gene expression control. *Nature* 473**:** 337-342.

Sekhar KR, Rachakonda G, Freeman ML (2010). Cysteine-based regulation of the CUL3 adaptor protein Keap1. *Toxicol Appl Pharmacol* 244**:** 21-26.

Shanmugam MK, Dai X, Kumar AP, Tan BK, Sethi G, Bishayee A (2014). Oleanolic acid and its synthetic derivatives for the prevention and therapy of cancer: preclinical and clinical evidence. *Cancer Lett* 346**:** 206-216.

Shelby MK, Klaassen CD (2006). Induction of rat UDP-glucuronosyltransferases in liver and duodenum by microsomal enzyme inducers that activate various transcriptional pathways. *Drug Metab Dispos* 34**:** 1772-1778.

Shelton LM, Park BK, Copple IM (2013). Role of Nrf2 in protection against acute kidney injury. *Kidney Int* 84**:** 1090-1095.

Shi S, Yu L, Chiu C, Sun Y, Chen J, Khitrov G*, et al.* (2008). Podocyte-selective deletion of dicer induces proteinuria and glomerulosclerosis. *J Am Soc Nephrol* 19**:** 2159-2169.

Shibutani S, Takeshita M, Grollman AP (1991). Insertion of specific bases during DNA synthesis past the oxidation-damaged base 8-oxodG. *Nature* 349**:** 431-434.

Shin DH, Park HM, Jung KA, Choi HG, Kim JA, Kim DD*, et al.* (2010). The NRF2-heme oxygenase-1 system modulates cyclosporin A-induced epithelial-mesenchymal transition and renal fibrosis. *Free Radic Biol Med* 48**:** 1051-1063.

Singh A, Ling G, Suhasini AN, Zhang P, Yamamoto M, Navas-Acien A*, et al.* (2009). Nrf2-dependent sulfiredoxin-1 expression protects against cigarette smoke-induced oxidative stress in lungs. *Free Radic Biol Med* 46**:** 376-386.

Singh B, Ronghe AM, Chatterjee A, Bhat NK, Bhat HK (2013). MicroRNA-93 regulates NRF2 expression and is associated with breast carcinogenesis. *Carcinogenesis* 34**:** 1165-1172.

Spizzo R, Nicoloso MS, Lupini L, Lu Y, Fogarty J, Rossi S*, et al.* (2010). miR-145 participates with TP53 in a death-promoting regulatory loop and targets estrogen receptor-alpha in human breast cancer cells. *Cell Death Differ* 17**:** 246-254.

Stachurska A, Ciesla M, Kozakowska M, Wolffram S, Boesch-Saadatmandi C, Rimbach G*, et al.* (2013). Cross-talk between microRNAs, nuclear factor E2-related factor 2, and heme oxygenase-1 in ochratoxin A-induced toxic effects in renal proximal tubular epithelial cells. *Mol Nutr Food Res* 57**:** 504-515.

Stanley A, Thompson K, Hynes A, Brakebusch C, Quondamatteo F (2014). NADPH oxidase complex-derived reactive oxygen species, the actin cytoskeleton, and Rho GTPases in cell migration. *Antioxid Redox Signal* 20**:** 2026-2042.

Star RA (1998). Treatment of acute renal failure. *Kidney Int* 54**:** 1817-1831.

Starkey Lewis PJ, Merz M, Couttet P, Grenet O, Dear J, Antoine DJ*, et al.* (2012). Serum microRNA biomarkers for drug-induced liver injury. *Clin Pharmacol Ther* 92**:** 291-293.

Starkey Lewis PJ, Dear J, Platt V, Simpson KJ, Craig DG, Antoine DJ*, et al.* (2011). Circulating microRNAs as potential markers of human drug-induced liver injury. *Hepatology* 54**:** 1767-1776.

Su Y, Ni Z, Wang G, Cui J, Wei C, Wang J*, et al.* (2012). Aberrant expression of microRNAs in gastric cancer and biological significance of miR-574-3p. *Int Immunopharmacol* 13**:** 468-475.

Taganov KD, Boldin MP, Chang KJ, Baltimore D (2006). NF-kappaB-dependent induction of microRNA miR-146, an inhibitor targeted to signaling proteins of innate immune responses. *Proc Natl Acad Sci U S A* 103**:** 12481-12486.

Taguchi K, Motohashi H, Yamamoto M (2011). Molecular mechanisms of the Keap1-Nrf2 pathway in stress response and cancer evolution. *Genes Cells* 16**:** 123-140.

Taguchi K, Fujikawa N, Komatsu M, Ishii T, Unno M, Akaike T*, et al.* (2012). Keap1 degradation by autophagy for the maintenance of redox homeostasis. *Proc Natl Acad Sci U S A* 109**:** 13561-13566.

Tan PX, Du SS, Ren C, Yao QW, Zheng R, Li R*, et al.* (2014). MicroRNA-207 enhances radiation-induced apoptosis by directly targeting Akt3 in cochlea hair cells. *Cell Death Dis* 5**:** e1433.

Tanaka Y, Aleksunes LM, Goedken MJ, Chen C, Reisman SA, Manautou JE*, et al.* (2008). Coordinated induction of Nrf2 target genes protects against iron nitrilotriacetate (FeNTA)-induced nephrotoxicity. *Toxicol Appl Pharmacol* 231**:** 364-373.

Tatarano S, Chiyomaru T, Kawakami K, Enokida H, Yoshino H, Hidaka H*, et al.* (2012). Novel oncogenic function of mesoderm development candidate 1 and its regulation by MiR-574-3p in bladder cancer cell lines. *Int J Oncol* 40**:** 951-959.

Tayek JA, Kalantar-Zadeh K (2013). The extinguished BEACON of bardoxolone: not a Monday morning quarterback story. *Am J Nephrol* 37**:** 208-211.

Thompson A, Schafer J, Kuhn K, Kienle S, Schwarz J, Schmidt G*, et al.* (2003). Tandem mass tags: a novel quantification strategy for comparative analysis of complex protein mixtures by MS/MS. *Anal Chem* 75**:** 1895-1904.

Tian H, Zhang B, Di J, Jiang G, Chen F, Li H*, et al.* (2012). Keap1: one stone kills three birds Nrf2, IKKbeta and Bcl-2/Bcl-xL. *Cancer Lett* 325**:** 26-34.

Tirmenstein MA, Nicholls-Grzemski FA, Schmittgen TD, Zakrajsek BA, Fariss MW (2000). Glutathione-dependent regulation of nitric oxide production in isolated rat hepatocyte suspensions. *Antioxid Redox Signal* 2**:** 767-777.

Tong KI, Katoh Y, Kusunoki H, Itoh K, Tanaka T, Yamamoto M (2006). Keap1 recruits Neh2 through binding to ETGE and DLG motifs: characterization of the two-site molecular recognition model. *Mol Cell Biol* 26**:** 2887-2900.

Tong KI, Padmanabhan B, Kobayashi A, Shang C, Hirotsu Y, Yokoyama S*, et al.* (2007). Different electrostatic potentials define ETGE and DLG motifs as hinge and latch in oxidative stress response. *Mol Cell Biol* 27**:** 7511-7521.

Tsai PY, Ka SM, Chao TK, Chang JM, Lin SH, Li CY*, et al.* (2011). Antroquinonol reduces oxidative stress by enhancing the Nrf2 signaling pathway and inhibits inflammation and sclerosis in focal segmental glomerulosclerosis mice. *Free Radic Biol Med* 50**:** 1503-1516.

Tsuda M, Sekine T, Takeda M, Cha SH, Kanai Y, Kimura M*, et al.* (1999). Transport of ochratoxin A by renal multispecific organic anion transporter 1. *J Pharmacol Exp Ther* 289**:** 1301-1305.

Umemura T, Sai K, Takagi A, Hasegawa R, Kurokawa Y (1990). Oxidative DNA damage, lipid peroxidation and nephrotoxicity induced in the rat kidney after ferric nitrilotriacetate administration. *Cancer Lett* 54**:** 95-100.

Ungvari Z, Tucsek Z, Sosnowska D, Toth P, Gautam T, Podlutsky A*, et al.* (2013). Aging-induced dysregulation of dicer1-dependent microRNA expression impairs angiogenic capacity of rat cerebromicrovascular endothelial cells. *J Gerontol A Biol Sci Med Sci* 68**:** 877-891.

Unwin RD (2010). Quantification of proteins by iTRAQ. *Methods Mol Biol* 658**:** 205-215.

Van der Hauwaert C, Savary G, Gnemmi V, Glowacki F, Pottier N, Bouillez A*, et al.* (2013). Isolation and characterization of a primary proximal tubular epithelial cell model from human kidney by CD10/CD13 double labeling. *PLoS One* 8**:** e66750.

Van Laecke S, Van Biesen W, Vanholder R (2014). The paradox of bardoxolone methyl: a call for every witness on the stand? *Diabetes Obes Metab*.

Vermeulen A, Behlen L, Reynolds A, Wolfson A, Marshall WS, Karpilow J*, et al.* (2005). The contributions of dsRNA structure to Dicer specificity and efficiency. *RNA* 11**:** 674-682.

Wakabayashi N, Dinkova-Kostova AT, Holtzclaw WD, Kang MI, Kobayashi A, Yamamoto M*, et al.* (2004). Protection against electrophile and oxidant stress by induction of the phase 2 response: fate of cysteines of the Keap1 sensor modified by inducers. *Proc Natl Acad Sci U S A* 101**:** 2040-2045.

Waldman SA, Terzic A (2008). MicroRNA signatures as diagnostic and therapeutic targets. *Clin Chem* 54**:** 943-944.

Walsh J, Jenkins RE, Wong M, Olayanju A, Powell H, Copple I*, et al.* (2014). Identification and quantification of the basal and inducible Nrf2-dependent proteomes in mouse liver: biochemical, pharmacological and toxicological implications. *J Proteomics* 108**:** 171-187.

Wang C, Hu J, Lu M, Gu H, Zhou X, Chen X*, et al.* (2015a). A panel of five serum miRNAs as a potential diagnostic tool for early-stage renal cell carcinoma. *Sci Rep* 5**:** 7610.

Wang G, Lai FM, Lai KB, Chow KM, Li KT, Szeto CC (2007). Messenger RNA expression of podocyte-associated molecules in the urinary sediment of patients with diabetic nephropathy. *Nephron Clin Pract* 106**:** c169-179.

Wang HE, Muntner P, Chertow GM, Warnock DG (2012). Acute kidney injury and mortality in hospitalized patients. *Am J Nephrol* 35**:** 349-355.

Wang L, Yu J, Xu J, Zheng C, Li X, Du J (2014). The analysis of microRNA-34 family expression in human cancer studies comparing cancer tissues with corresponding pericarcinous tissues. *Gene* 554**:** 1-8.

Wang YY, Yang YX, Zhao R, Pan ST, Zhe H, He ZX*, et al.* (2015b). Bardoxolone methyl induces apoptosis and autophagy and inhibits epithelial-to-mesenchymal transition and stemness in esophageal squamous cancer cells. *Drug Des Devel Ther* 9**:** 993-1026.

Wasserman WW, Fahl WE (1997). Functional antioxidant responsive elements. *Proc Natl Acad Sci U S A* 94**:** 5361-5366.

Wei Q, Bhatt K, He HZ, Mi QS, Haase VH, Dong Z (2010). Targeted deletion of Dicer from proximal tubules protects against renal ischemia-reperfusion injury. *J Am Soc Nephrol* 21**:** 756-761.

Wiesen JL, Tomasi TB (2009). Dicer is regulated by cellular stresses and interferons. *Mol Immunol* 46**:** 1222-1228.

Wink S, Hiemstra S, Huppelschoten S, Danen E, Niemeijer M, Hendriks G*, et al.* (2014). Quantitative high content imaging of cellular adaptive stress response pathways in toxicity for chemical safety assessment. *Chem Res Toxicol* 27**:** 338-355.

Wu J, Liu X, Fan J, Chen W, Wang J, Zeng Y*, et al.* (2014a). Bardoxolone methyl (BARD) ameliorates aristolochic acid (AA)-induced acute kidney injury through Nrf2 pathway. *Toxicology* 318**:** 22-31.

Wu KC, Cui JY, Klaassen CD (2011a). Beneficial Role of Nrf2 in Regulating NADPH Generation and Consumption. *Toxicological Sciences* 123**:** 590-600.

Wu L, Fan J, Belasco JG (2006). MicroRNAs direct rapid deadenylation of mRNA. *Proc Natl Acad Sci U S A* 103**:** 4034-4039.

Wu QQ, Wang Y, Senitko M, Meyer C, Wigley WC, Ferguson DA*, et al.* (2011b). Bardoxolone methyl (BARD) ameliorates ischemic AKI and increases expression of protective genes Nrf2, PPARgamma, and HO-1. *Am J Physiol Renal Physiol* 300**:** F1180-1192.

Wu T, Ye Y, Min SY, Zhu J, Khobahy E, Zhou J*, et al.* (2014b). Prevention of murine lupus nephritis by targeting multiple signaling axes and oxidative stress using a synthetic triterpenoid. *Arthritis Rheumatol* 66**:** 3129-3139.

Xing X, Zhang C, Shao M, Tong Q, Zhang G, Li C*, et al.* (2012). Low-dose radiation activates Akt and Nrf2 in the kidney of diabetic mice: a potential mechanism to prevent diabetic nephropathy. *Oxid Med Cell Longev* 2012**:** 291087.

Xue M, Qian Q, Adaikalakoteswari A, Rabbani N, Babaei-Jadidi R, Thornalley PJ (2008). Activation of NF-E2-related factor-2 reverses biochemical dysfunction of endothelial cells induced by hyperglycemia linked to vascular disease. *Diabetes* 57**:** 2809-2817.

Yamakuchi M, Ferlito M, Lowenstein CJ (2008). miR-34a repression of SIRT1 regulates apoptosis. *Proc Natl Acad Sci U S A* 105**:** 13421-13426.

Yamamoto T, Suzuki T, Kobayashi A, Wakabayashi J, Maher J, Motohashi H*, et al.* (2008). Physiological significance of reactive cysteine residues of Keap1 in determining Nrf2 activity. *Mol Cell Biol* 28**:** 2758-2770.

Yang L, Calingasan NY, Thomas B, Chaturvedi RK, Kiaei M, Wille EJ*, et al.* (2009). Neuroprotective effects of the triterpenoid, CDDO methyl amide, a potent inducer of Nrf2-mediated transcription. *Plos One* 4**:** e5757.

Yang M, Yao Y, Eades G, Zhang Y, Zhou Q (2011). MiR-28 regulates Nrf2 expression through a Keap1-independent mechanism. *Breast Cancer Res Treat* 129**:** 983-991.

Yates MS, Kwak MK, Egner PA, Groopman JD, Bodreddigari S, Sutter TR*, et al.* (2006). Potent protection against aflatoxin-induced tumorigenesis through induction of Nrf2-regulated pathways by the triterpenoid 1-[2-cyano-3-,12-dioxooleana-1,9(11)-dien-28-oyl]imidazole. *Cancer Res* 66**:** 2488-2494.

Yates MS, Tauchi M, Katsuoka F, Flanders KC, Liby KT, Honda T*, et al.* (2007). Pharmacodynamic characterization of chemopreventive triterpenoids as exceptionally potent inducers of Nrf2-regulated genes. *Mol Cancer Ther* 6**:** 154-162.

Yoh K, Itoh K, Enomoto A, Hirayama A, Yamaguchi N, Kobayashi M*, et al.* (2001). Nrf2-deficient female mice develop lupus-like autoimmune nephritis. *Kidney Int* 60**:** 1343-1353.

Yoh K, Hirayama A, Ishizaki K, Yamada A, Takeuchi M, Yamagishi S*, et al.* (2008). Hyperglycemia induces oxidative and nitrosative stress and increases renal functional impairment in Nrf2-deficient mice. *Genes Cells* 13**:** 1159-1170.

Yoon HY, Kang NI, Lee HK, Jang KY, Park JW, Park BH (2008). Sulforaphane protects kidneys against ischemia-reperfusion injury through induction of the Nrf2-dependent phase 2 enzyme. *Biochem Pharmacol* 75**:** 2214-2223.

Yoshida Y, Miyazaki K, Kamiie J, Sato M, Okuizumi S, Kenmochi A*, et al.* (2005). Two-dimensional electrophoretic profiling of normal human kidney glomerulus proteome and construction of an extensible markup language (XML)-based database. *Proteomics* 5**:** 1083-1096.

Yu DS, An FM, Gong BD, Xiang XG, Lin LY, Wang H*, et al.* (2012). The regulatory role of microRNA-1187 in TNF-alpha-mediated hepatocyte apoptosis in acute liver failure. *Int J Mol Med* 29**:** 663-668.

Zager RA, Johnson AC, Becker K (2012). Plasma and urinary heme oxygenase-1 in AKI. *J Am Soc Nephrol* 23**:** 1048-1057.

Zhang DD (2013). Bardoxolone brings Nrf2-based therapies to light. *Antioxid Redox Signal* 19**:** 517-518.

Zhang DD, Hannink M (2003). Distinct cysteine residues in Keap1 are required for Keap1-dependent ubiquitination of Nrf2 and for stabilization of Nrf2 by chemopreventive agents and oxidative stress. *Mol Cell Biol* 23**:** 8137-8151.

Zhang DD, Lo SC, Cross JV, Templeton DJ, Hannink M (2004). Keap1 is a redox-regulated substrate adaptor protein for a Cul3-dependent ubiquitin ligase complex. *Mol Cell Biol* 24**:** 10941-10953.

Zhang L, Zhu Z, Liu J, Hu Z (2014). Protective effect of N-acetylcysteine (NAC) on renal ischemia/reperfusion injury through Nrf2 signaling pathway. *J Recept Signal Transduct Res*.

Zheng H, Whitman SA, Wu W, Wondrak GT, Wong PK, Fang D*, et al.* (2011). Therapeutic potential of Nrf2 activators in streptozotocin-induced diabetic nephropathy. *Diabetes* 60**:** 3055-3066.

Zheng S, Santosh Laxmi YR, David E, Dinkova-Kostova AT, Shiavoni KH, Ren Y*, et al.* (2012). Synthesis, chemical reactivity as Michael acceptors, and biological potency of monocyclic cyanoenones, novel and highly potent anti-inflammatory and cytoprotective agents. *J Med Chem* 55**:** 4837-4846.

Zhou H, Huang C, Xia XG (2008). A tightly regulated Pol III promoter for synthesis of miRNA genes in tandem. *Biochim Biophys Acta* 1779**:** 773-779.

Zhu H, Itoh K, Yamamoto M, Zweier JL, Li Y (2005). Role of Nrf2 signaling in regulation of antioxidants and phase 2 enzymes in cardiac fibroblasts: protection against reactive oxygen and nitrogen species-induced cell injury. *FEBS Lett* 579**:** 3029-3036.

Zipper LM, Mulcahy RT (2002). The Keap1 BTB/POZ dimerization function is required to sequester Nrf2 in cytoplasm. *J Biol Chem* 277**:** 36544-36552.

Zoja C, Corna D, Nava V, Locatelli M, Abbate M, Gaspari F*, et al.* (2013). Analogs of bardoxolone methyl worsen diabetic nephropathy in rats with additional adverse effects. *Am J Physiol Renal Physiol* 304**:** F808-819.